# Particle engineered inhalable dry powders of rifampicin

**Dissertation**

zur

Erlangung des Doktorgrades (Dr. rer. nat.)

der

Mathematisch-Naturwissenschaftlichen Fakultät

der

Rheinischen Friedrich-Wilhelms-Universität Bonn

vorgelegt von

**Kai Wilfried August Berkenfeld**

aus

Köln

**Bonn 2019**

Angefertigt mit Genehmigung der Mathematisch-Naturwissenschaftlichen
Fakultät der Rheinischen Friedrich-Wilhelms-Universität Bonn

Promotionskommission:

Erstgutachter: Prof. Dr. Alf Lamprecht
Zweitgutachter: Prof. Dr. Jason T. McConville
Fachnahes Mitglied: Prof. Dr. Matthias Wüst
Fachfremdes Mitglied: Prof. Dr. Valentin Stein

Tag der Promotion: 27.02.2019
Erscheinungsjahr: 2019

**In Gedenken an Oswald Mainka**

Acknowledgements

I would like to thank my parents for supporting me in all endeavors and decisions I took, not only with regard to the past years but also throughout my entire life. They always provided a sheltered space for development by gaining my own experiences and encouraged me to go beyond and explore what was to be found. Also, I would like to thank my family for showing great interest in and appreciation for what I do.

I would like to express my gratitude to Prof. Alf Lamprecht for giving me the opportunity to work on this interesting and challenging topic. I highly appreciate that I was given room to develop the project into a direction I thought was reasonable, but also was provided guidance and support, where needed. Also, I would like to thank Prof. Jason McConville for co-supervizing my work and hosting me at the University of New Mexico during the first year of my studies. I would like to thank Prof. Linda Felton, Prof. Pavan Muttil, and Prof. Pamela Hall with their teams for their support and the interesting discussions we had. I was also very lucky to meet Elena Macchi and Alaa Elmaoued and many other friends who made Albuquerque a home for me. Staying at UNM was a wonderful experience with regard to too many aspects to be listed here.

Not only at UNM, but also at the University of Bonn I met many people who aided making the last years an enjoyable and intense period of my life. Firstly, I would like to thank Prof. Karl Wagner for his support, encouragement, and mentoring as well as for giving me the opportunity to participate in additional interesting projects. Especially, I would like to thank Martina Gerlitz, who always is a great support with all administrative issues. And of course, I want to thank my colleagues who provided an interesting community for discussions and other enjoyable events - not only in the lab, but also during many other occasions. Traveling to Madrid with Alvaro Lopez Marmol and Tugrul Mert Serim, wakeboarding with Stefan Wanning, climbing with Pia Steinlein, or the Andalusia trip is just an incomplete list of events and people that I will always remember with pleasure.

## Abstract

Tuberculosis (TB) is an infectious disease caused by *Mycobacterium tuberculosis*. Main site of infection are the lungs, but infection of other organs can occur in later stages. First line therapy includes antibiotic therapy using a combination of three out of four drugs (rifampicin, isoniazid, ethambutol, and pyrazinamide), for a period of at least 26 weeks. In the case of rifampicin, fairly high daily doses of 10 mg/KGBW (600 mg max.) are to be administered, which often times is accompanied by unwanted side effects that might not only affect the patient´s overall status, but could also compromise compliance and adherence to the therapeutic regimen. In order to achieve therapeutically effective concentrations at the site of infection (the lungs) whilst minimizing systemic exposure to avoid unwanted side effects, inhalable antibiotic therapy is desirable. Much effort has already been made to develop respirable dry powder dosage forms of rifampicin, and spray drying was shown as suitable method to produces rifampicin particles with favorable aerosol performance. Two solvent free polymorphs as well as several solvates are described in literature. This work systematically investigated aerosol properties of formulations spray dried from solutions and suspension of rifampicin in common solvents, in order to assess if different (pseudo-) polymorphs show suitability for a potential aerosol therapy. In a first study, formulations spray dried from ethanol, methanol, isopropyl alcohol, acetone, dichloromethane, and water were manufactured and assessed for their aerodynamic (NGI), as well as their solid state (XRPD) properties. Suitable candidates were found in samples spray dried from ethanol, methanol, and water, yielding three crystalline and one amorphous formulation. Additionally an amorphous reference formulation showing the characteristic shape of collapsed spheres, often seen when spray drying solutions, was manufactured. Selected formulations were repeated and investigated more closely with special focus on crystallographic properties or mechanism of particle formation in the case of crystalline, or amorphous formulations respectively. All formulations investigated in the second study showed good aerosol properties with fine particle fractions (FPF, being the fraction of the dose with an aerodynamic diameter ≤ five µm, which is indicative for lung deposition) of about 40%, but one formulation spray dried from aqueous solutions of rifampicin in water showed excellent aerosol properties with FPFs as high as 90%. Crystallographic studies showed that suspensions spray dried from water are most likely a member of an isostructural series of solvates that was firstly described as rifampcin pentahydrate. Contrary, samples spray dried from ethanol and methanol were

shown to be members of a common isostructural series, but could not clearly be allocated to other (pseudo-) polymorphs already reported in literature. In order to investigate the mechanism of particle formation when spray drying samples from watery or isopropylalcoholic solutions, drying kinetics of individual droplets were investigated using an acoustic levitator. It was found that in watery solution rifampicin displays early crust formation, which detaches from the liquid core that eventually is removed from the system. As a consequence remaining particles consist of the highly collapse shell only, creating a powder of low density with excellent aerosol properties.

For efficient formulation design, it is highly desirable to develop suitable *in vitro* tools being predictive of *in vivo* performance of the formulation. It is known from literature that aerodynamic diameters smaller than five µm are indicative for lung deposition, but standard *in vitro* test methods as for example the NGI, which are designed to provide a suitable test system in an QC environment, fail to provide accuracy in full dose assessment necessary. Amongst others, lack of physiological relevance of the NGIs induction port, has been identified as a reason for this. Much effort has already been made to develop more biorelevant deposition models, but limited information on the impact of modifications of the IP on aerosol data using the NGI is available. Additionally, approaches most intensely investigated represent idealized physiological conditions of an averaged patient collective, which is a reasonable approach in many applications, but a more dynamic model might be desirable to investigate lung deposition in special patient populations (e.g. children or patients with pathophysiological alterations) or to investigate fundamental mechanisms of particle deposition in the relevant regions. In this study we presented a modified induction port to be used with the NGI that was manufactured based on geometries (trachea) derived from a computer tomographic scan of a patient, and 3D printed using FDM technique. In a first study it was investigated which types of aerosol formulations are critical in terms of tracheal deposition, by assessing the aerodynamic properties of preparations of salbutamol, formulated as pressurized metered dose inhaler (pMDI), dry powder inhaler, and solution for nebulization, respectively. Additionally, the impact of using a valved holding chamber was investigated. It was found that using the modified induction port offered no additional information in the case of the dry powder, and nebulizer formulation. Contrary, the pMDI formulation showed increased deposition, which consequently translated into a lower FPF, which was found to correlate better to *in vivo* data reported in literature. In a second study,

additional pMDI formulations, which were selected on availability of *in vivo* data of lung deposition in literature, were assessed and results of *in vitro / in vivo* (IVIVC) correlation were found more accurate than ones obtained using the regular induction port, which is monographed in the European and United States pharmacopoeia. Additionally, another modified induction port was manufactured to get a more accurate understanding of the factors responsible for increased tracheal deposition in certain formulations, and it was confirmed that adding physiologically more accurate geometries to the induction port is beneficial for IVIVC. It was concluded that besides a physiologically relevant trachea, the next model should also include more biorelevant mouth/throat region, as this was found relevant in certain formulations.

The novel induction port was also used to estimate *in vivo* performance of the rifampicin formulations investigated. Though increased deposition in the induction port, which correlated to a decrease in expected lung deposition, was found, differences were found at a magnitude, which probably cannot be resolved in an *in vivo* setting. Thus good to excellent aerosol performance achieved could translate into good performance *in vivo*.

**TABLE OF CONTENT:**

# 1 Introduction and theoretical background

## 1.1 Physiology of the respiratory tract

Similarly, to most other terrestrial vertebrate species, humans regulate their blood oxygen and carbon dioxide level by proactive exchange of the atmospheric gas phase over a perfused, permeable membrane. Due to this constant exchange, a gradient of gas concentrations in blood and atmosphere is maintained, which facilitates passive diffusion of oxygen and carbon dioxide molecules into, or from blood circulation respectively. Gas exchange occurs in a distinct organ called the lungs, which are part of the respiratory tract. The respiratory tract can be subdivided into the upper and the lower respiratory tract. The upper respiratory tract is formed by oral and nasal cavities, pharynx, and larynx. The lower respiratory tract consists of the trachea, bronchi, and lungs. Main function of the upper respiratory tract is to condition the air inspired, which includes adaptation of gas to body temperature, as well as humidification, and purification by removal of e.g. dust or other particles. Moving to the lower respiratory tract, inspired gas firstly passes the trachea, which is a tubular membrane surrounded by cartilaginous rings, connecting larynx and the lungs. At its proximal end, the trachea subdivides into the primary bronchi, which are two branches supplying the left and right lung respectively. The bronchial system divides another 22 times until bronchioles terminate into alveolar sacs. Based on its physiological function, the bronchial system can be subdivided into two zones. The main physiological purpose of the conducting zone, which comprises of the first 16 generations of bronchi and terminal bronchioles, is to conduct gases inspired to the deep lungs. In the respiratory zone, which comprises of the remaining 7 generations of respiratory bronchioles as well as alveolar ducts and alveoli, gas exchange occurs. Alveoli are terminal cavities, where mainly type I pneumocytes and endothelial cells of the supplying capillary system form a thin barrier between the ambient atmospheric gas and the blood (the blood-gas-barrier), which typically is as low as 500 nm thick. Other cell types present in the alveolar epithelium include type II (= granular) pneumocytes whose main function is the secretion of surfactant, as well alveolar macrophages, lymphocytes, and mast cells, which are part of the immune system. Due to the high number of subdivisions in the bronchial system, about 3 x $10^8$ alveoli are present, this gives rise to a high surface area of about 70 $m^2$,

available for gaseous diffusion. The lungs are located inside the pleural sac in the chest. They are passively inflated by contraction of muscles of respiration (mainly the diaphragm, which divides thoracic and abdominal cavities), expanding the volume of the thoracic cavity, which is connected to the parietal pleura of the pleural sac. Upon relaxation of the muscles, exhalation occurs passively. Forced exhalation is facilitated by contraction of abdominal wall muscles. The total volume of the lungs is about 6000 mL, the tidal volume is the volume exchanged during a regular breathing cycle; approximately 500 mL. As a typical breathing frequency at rest would be 0.2 Hz (i.e. 12 cycles per min.), the total volume of the lungs is exchanged once each minute. If needed, the inspirational volume can be increased by another 3000 mL (= inspiratory reserve volume) and 1200 mL can be exhaled upon forced expiration (expiratory reserve volume) [1,2].

## 1.2 Pathophysiology of the respiratory tract

Most common pathophysiological conditions of the respiratory tract are associated with infections of the upper airways that are usually caused by virus infections, sometimes with the occurrence of secondary bacterial infections. Though having a high prevalence, these infections do not often require causal therapeutic intervention and so will not be discussed further here. Following, selected indications for inhalable therapy as well as general approaches for treatment will be briefly discussed.

### 1.2.1 **Asthma**

Asthma is an inflammatory disease of the respiratory tract that is characterized by hyper reactivity of the bronchial system. Typically, patients suffer from reoccurring episodes of dyspnoea, which is related to bronchoconstriction, oedema in the airways, increased secretion of viscous mucus, or in most cases a combination of these causes. According to its genesis, it can be classified as allergic or intrinsic asthma. In allergic asthma, hyper reaction is triggered by exogenous stimuli (e.g. pollen) that causes an allergic reaction, which in many cases is immunoglobulin E (IgE) mediated. With disease progression, asthma inducing stimuli might become unspecific, which is related to a general proceeding of hyper reactivity and might be amplified by a positive feedback mechanism involving the vagus nerve. In contrast, intrinsic

asthma is not initially based on specific exogenous stimuli, but rather shows the unspecific, vagus mediated, mechanism. Intrinsic asthma attacks can be triggered by several factors including, for example: cold air, tobacco smoke, exercise, or dust [2]. Besides training and education as well as precise assessment and monitoring of the patient's state, control of environmental factors, and control of comorbid conditions affecting the asthma, pharmacotherapy is important to successfully treat asthma. Substances used in pharmacotherapeutic treatment can be divided into two distinct classes: Long term control medications, which are used to maintain control and prevent exacerbations, and immediate relief medications, which are used to treat acute symptoms occurring. Table 1 gives an overview on drug classes used in asthma therapy. Depending on the severity of the asthma, different combinations of aforementioned drug classes can be applied according to an escalation scheme [3]. Due to the complexity of the disease, detailed information on interventions and escalation stages will not be provided here and the reader is kindly referred to the relevant guidelines.

Table 1. Overview on drug classes used in asthma therapy.

| | **Substance class** | **Example substance** |
|---|---|---|
| **Long - term mediction** | Corticosteroids | Budesonide |
| | | Beclomethasone dipropionate |
| | | Fluticasone propionate |
| | | Mometasone furoate |
| | | Ciclesonide |
| | Long acting $\beta_2$ agonists | Salmeterol xinafoate |
| | | Formoterol fumarate dihydrate |
| | Immunomodulators | Methotrexate |
| | | Omalizumab |
| | Leukotriene modifiers | Montelukast |
| | | Zafirlukast |
| | Methylxanthines | Theophylline |
| | Mast cell stabilizers | Cromolyn sodium |
| | | Nedocromil |
| **Quick - relief medication** | Anticholinergics | Ipratropium bromide |
| | Short acting $\beta_2$ agonists | Salbutamol sulfate |

### 1.2.2 **Chronic obstructive pulmonary disease (COPD)**

COPD is a chronic disease of the respiratory tract that is mainly characterized by restricted airflow caused by abnormalities of (small) airways and/or alveoli (emphysema). Other symptoms associated with COPD are dyspnoea, hypoxia, chronic cough, inflammation, and sputum production. The main causes for COPD are reported as exposure to noxious gases and particles (e.g. tobacco smoke, as well as indoor or outdoor air pollution), genetic predisposition, or comorbidity (e.g. asthma, bronchitis), and infections [4]. Clinically, persistent airflow restrictions are assessed by means of spirometry and a forced expiratory volume as a one second ($FEV_1$)/forced vital capacity (FVC) ratio, and a value of <0.7 post bronchdilatator exposition is understood as confirmative for COPD. For effective COPD therapy, smoking cessation is essential. Pharmacotherapeutic interventions may provide reduction of symptoms (at rest or upon exercise), as well as frequency and severity of exacerbations. However, as of now, there is little supporting positive evidence of pharmacotherapeutics affecting the long-term decline of lung function. Table 2 gives an overview on drug classes used in COPD treatment. Additionally, depending on degree of severity of hypoxia, oxygen therapy might be indicated for use. Similarly to asthma, COPD is a highly complex disease and the reader is kindly referred to the respective guideline, for example “The Global Initiative for Chronic Obstructive Lung Disease” [5], that provides additional information for dosing regimen, escalation stages etcetera.

Table 2. Overview on drug classes used in COPD therapy.

| **Substance class** | **Example substance** |
|---|---|
| Corticosteroids | Budesonide |
| | Beclomethasone dipropionate |
| | Fluticasone propionate |
| | Mometasone furoate |
| | Ciclesonide |
| Long acting $\beta_2$ agonists | Salmeterol xinafoate |
| | Formoterol fumarate dihydrate |
| Short acting $\beta_2$ agonists | Salbutamol sulfate |
| | Fenoterol hydrobromide |
| Anticholinergics | Ipratropium bromide |
| | Aclidinium bromide |
| | Tiotropium |
| Methylxanthines | Theophylline |
| | Aminophylline |
| Phosphodiesterase four inhibitors | Roflumilast |

### 1.2.3 **Infectious diseases**

As previously mentioned, viral infections of the upper airways with or without bacterial co-infections are the most common pathophysiological condition and usually require no causal therapy. In more severe cases, systemic antibiotic therapy can be indicated if bacterial co-infections can be confirmed. In contrast, infections (bacterial or viral) of the lower respiratory tract may cause severe complications with a broad variety of clinical symptoms, for example, inflammation of the lung tissue (oedema), respiratory distress, or sepsis. In case of bacterial infections of the lungs, inhalable antibiotic therapy is desirable but as of now, only a few formulations have been approved. Most antibiotics available as inhalable formulations, i.e. aztreonam (monobactam antibiotic) and tobramycin (aminoglycoside antibiotic) are approved only for the treatment of cystic fibrosis associated *pseudomonas aeruginosa* infections. Additionally, colistin (ploymyxin E) is approved for treatment of acute or chronic pulmonary infections with gram-negative bacteria, but its clinical use is mainly limited to treatment of chronic cystic fibrosis associated *pseudomonas* infections. Aztreonam is available as solution for nebulization only; only in recent years have dry powder formulations of colistin

(Colobreathe®, Turbospin® DPI) and tobramycin (TOBI®, Podhaler® DPI) become available. Besides formulations approved for the pulmonary route, several injectable antibiotic (amikacin, amphotericin B, ceftazidime, gentamicin) formulations applied using nebulizers have been used "off-label" in clinical practice [6], which highlights the need of a higher number of commercially available inhalable antibiotics.

### 1.2.4 **General considerations**

Delivery of active pharmaceutical agents to the respiratory system is not only appropriate for local treatment of respiratory diseases such as asthma, COPD, or infections, but may also be suitable for systemic drug delivery, for example in the delivery of peptides or proteins such as insulin [7], or rescue medication for e.g. pain therapy [8]. Due to the high surface area available and the small dimensions of the diffusion barrier, rapid and complete absorption of the drug administered is possible. Additionally, the absence of degrading enzymes (e.g. proteases) and systemic distribution (without the first-pass effect of the liver) is likely to result in higher bioavailabilities, when compared to oral administration of active pharmaceutical ingredients (APIs) [9]. To ensure deposition in the desired target area, therapeutic aerosol particles must fulfill certain requirements. Most relevant here is the aerodynamic diameter. It is defined as the equivalent diameter of the unit density sphere showing the same settling velocity as the particle of interest. Equation 1 shows the most general case of the relationship of aerodynamic diameter ($d_{ae}$) and geometric diameter ($d_{geo}$), particle ($\rho_p$) and reference particle density ($\rho_{ae}$), Cunningham slip correction factors for sample ($C_p$) and reference ($C_{ae}$) particle diameters, and a shape correction factor ($\chi$).

$$d_{ae} = d_{geo}\sqrt{\frac{\rho_p C_p}{\chi \rho_{ae} C_{ae}}}$$

Equation 1. Relation of $d_{ae}$ to $d_{geo}$ [10].

In the case of a density unit sphere per definition $\rho_p$= 1 g/cm$^3$, $\chi$= 1, and $C_p/C_{ae}$= 1 is true. Cunningham slip correction factors are used to compensate for non-continuum effects occurring at high Knudsen numbers. Knudsen numbers are dimensionless factors relating the particle diameter to its mean free path length in the system [11]. Equation 1 implies that $d_{ae}$ of a particle can effectively be manipulated by changing its geometrical diameter, density, or

shape. It is generally assumed that particles showing an aerodynamic diameter of one to five µm are suitable for deposition in the lower respiratory tract [12,13]. Five distinct mechanisms triggering particle deposition can be identified: impaction, sedimentation, diffusion, interception, and electrostatic precipitation [14]. Impaction describes separation of the aerosol particle from the air stream upon changes in the motion vector of the airflow field. Due to the particle's momentum it undergoes radial acceleration and might separate from the airflow and impact onto the walls of the flow path defining structure (e.g. trachea or bronchi). Sedimentation of particles occurs due to gravitational pull and becomes more effective in the lower respiratory tract, where particle velocities are low. Diffusion of particles predominantly occurs in the lower respiratory tract as well and is caused by Brownian motion of sub-micron particles. Thus, sedimentation and diffusion are competing processes, and predominance of one over the other is mainly depending on particle mass. At settling velocities lower than 0.001 cm/s, which is equivalent to a unit density sphere equivalent diameter of about 0.5 µm, diffusion becomes predominant. Interception describes particle surface interactions of fibrous particles and the extent of deposition by interception depends on the length of the fiber. As therapeutical aerosols usually exhibit a more spherical morphology, deposition by interception in this context plays a negligible role. Importantly, this mechanism is highly relevant for toxicological evaluation of those fibrous materials (e.g. asbestos). Electrostatic precipitation might occur if particles demonstrate high electric mobility. Charged particles induce image charges on the airway surfaces, which triggers separation from the air stream. This effect occurs, for example upon *in situ* formation of dry particles from aqueous droplets, but has low relevance in equilibrated systems [14]. Figure 1 gives an overview on the extent of particle deposition via impaction, sedimentation, and diffusion as a function of particle diameter of unit density spheres. This figure illustrates that particle deposition of pharmaceutical aerosols in the lungs only appears in the size range of about one to five µm. The upper limit is defined by the maximum $d_{ae}$ suitable for passing the upper airways and the lower limit is defined by deposition efficiency of the particles. If particles do not deposit, their exhalation is to be assumed. It is also shown that deposition efficiency increases at $d_{ae}$ lower than 0.1 µm. However, these low diameter powders are extremely cohesive and, as of now, of little relevance when considering deposition mechanisms. Figure 2 depicts typical sites of deposition, related to $d_{ae}$.

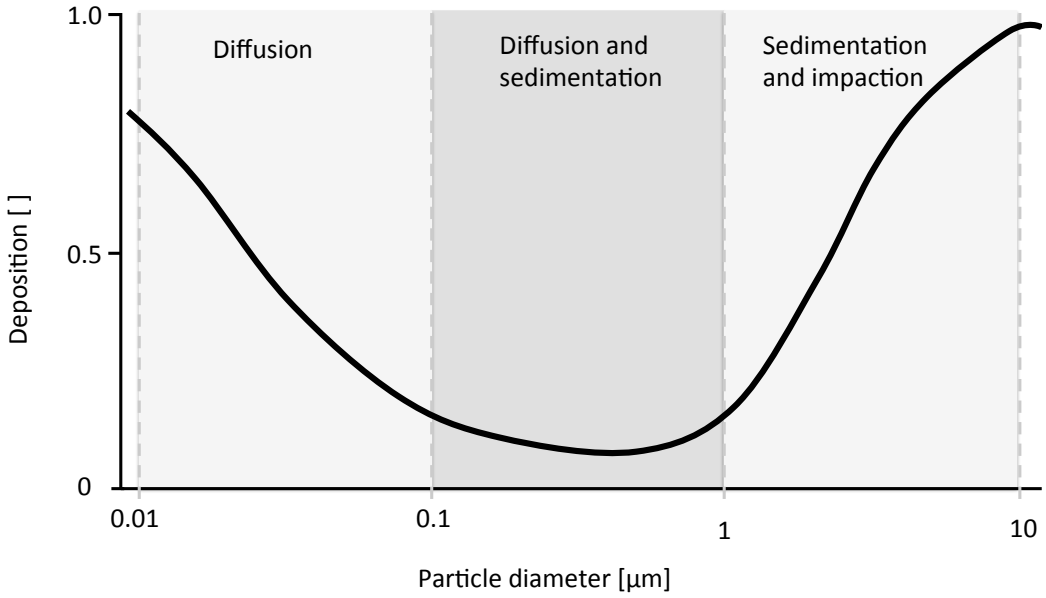


Figure 1. Deposition frequencies as function of $d_{ae}$. Modified from [15].

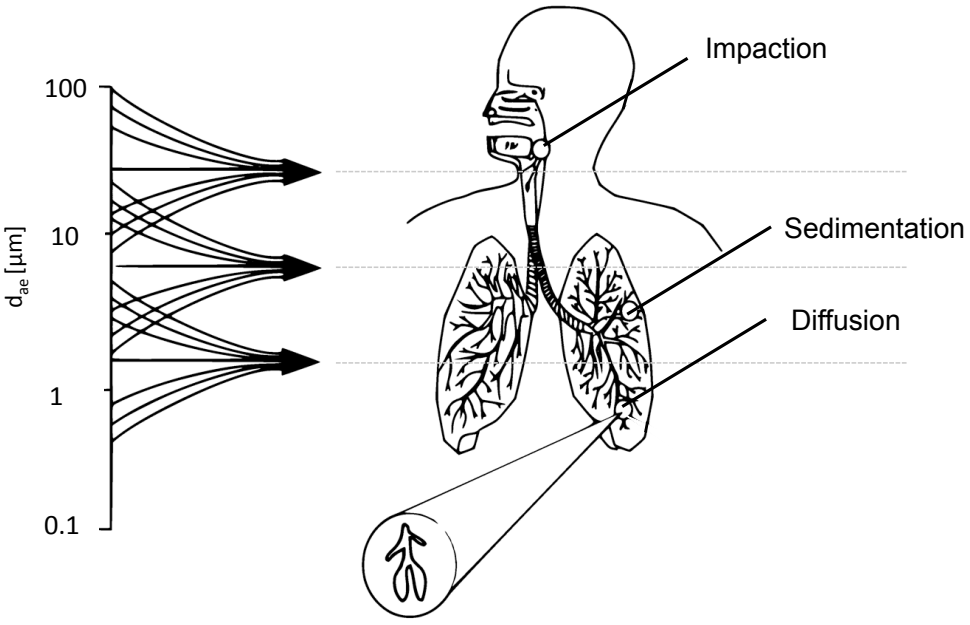


Figure 2. Sites of deposition related to $d_{ae}$. Modified from [16].

Since the site of deposition in the airways is related to $d_{ae}$, aerosols for different indications might have different requirements. For example for asthma therapy, targeting to the bronchi and bronchioles is desired; In this case larger particles could be needed compared to those for systemic treatment, where particles need to be targeted to alveoli (in order to be absorbed across a high surface area).

## 1.3 Aerosol therapy

### 1.3.1 Dry powder inhalation devices

Dry powder inhalers (DPIs) are designed to reproducibly deliver a predefined dose of a drug to the small airways and alveolar region of the lung. It is well reported that particles with a mass median aerodynamic diameter (MMAD) of one to five μm are effectively deposited at aforementioned sites [17]. The MMAD of a particle depends on its geometrical diameter, density, and morphology with these properties generally being manipulated during the manufacturing process [18]. Due to interparticulate forces (i.e. mechanical interlocking, capillary, electrostatic, and van der Waals forces [19]) micronized powders are very adhesive/cohesive; spontaneously forming agglomerates. The extent of the partial and consequently of the combined forces is dependent on powder properties such as: particle size, morphology, shape, and chemical properties [20], as well as environmental factors like relative humidity [21]. Since the extent of agglomeration negatively affects the fraction of the inhaled powder, which is within the respirable range [22], these agglomerates must be effectively deagglomerated prior to or during the processes of aerosolization and inhalation [23]. DPIs that utilize a patient's inspiratory airflow to provide the required energy to overcome the aforementioned interparticulate forces are known as *passive* devices, whereas those that utilize other sources of energy are referred to as *active* devices. One advantage of utilizing a patient's inspiratory airflow as the main source of energy is that such devices are breath actuated; this inherently avoids the need to synchronize the actuation and inspiration maneuver by the patient. The downside of this approach is that devices currently available show a device-specific airflow resistance, and this often demands a relatively high inspiratory effort [24], which might be a potential hurdle for patient populations suffering from obstructive airway diseases such as asthma or COPD, the elderly, or very young [25]. The extent of lung deposition is also dependent on the individual patient's inspiratory flow rate

causing a potential inter-patient variability in the dose effectively delivered [26]. Another critical factor affecting the reproducibility of doses delivered by multidose inhalers is dose metering. While single dose and multi-unit dose devices use pre-metered powders packed into blisters or capsules, bulk powder bed multidose inhalers use powder reservoirs so that the dose to be delivered has to be separated from the bulk material prior to actuation [27]. For both types of devices, suitable powder flow properties are essential, either for accurate dosing or emptying of the single-dose container entirely. Since flow properties of micronized powders are often poor, most formulations consist of physical blends of drug particles with larger carrier particles such as lactose (30-90 μm), to aid de-agglomeration and powder flow [28]. In light of the aforementioned considerations, the ideal DPI would reproducibly deliver an accurate dose, regardless of a patient's condition. Clinically, it may also be advantageous if the device is breath actuated, easy, and safe to use, offers some type of control feedback mechanism (related to efficacy), and has an accurate dose counter. The dose counting mechanism is a standardized requirement that serves to help patients to track whether doses have been administered appropriately, and when to replace the device at a suitable time [29,30]. Single use disposable DPIs have to meet different requirements than reusable ones. But the need for an effective dose metering system is however, negated. Since the disposable DPI itself can be packed and sealed, it is therefore not exposed to direct environmental conditions such as humidity, so there may be no need to ensure a high level of protection of the drug within the DPI. Patients potentially using disposable DPIs cannot be expected to be familiar with medical inhalation devices, so it is preferable to keep operation of the device as simple as possible. Visible or audible control feedback mechanisms would be a great benefit to naive patients. Of course, it is compulsory for disposable devices to meet all the requirements necessary to ensure a safe therapy (i.e., dose accuracy and reproducibility) [31]. Figure 3 shows a schematic drawing of a typical single unit dose DPI.

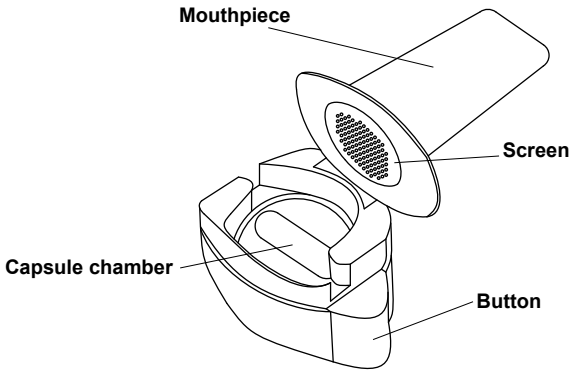


Figure 3. Schematic diagram of a DPI device of the Aerolizer type (Breezhaler).

### 1.3.2 **Pressurized metered dose inhaler (pMDI)**

In contrast to passive DPI devices, pMDIs utilize propellant gases as main source of energy to form a respirable aerosol. As minimal requirements, they consist of an aluminum container that holds the drug formulation, a metering valve, and an actuator [32]. The active ingredient is typically formulated as solution, or suspension of micronized particles in a liquefied propellant. Over a relevant temperature range, propellants must liquefy at moderate pressures, which are typically less than 500 kPa for a pure propellant, or mixtures of propellants. Additionally, they are required to be physically and chemically compatible with the API and other excipients, nonflammable, and nontoxic [33].

Starting from the mid 1990s, chlorofluorocarbon (CFC) propellants, previously used in pMDI formulation design, were replaced by non ozone layer depleting hydrofluoroalkanes (HFA); as requested in the Montreal Protocol of 1987 [34]. Besides re-formulating already approved products, this transition also demanded modifications of the pMDI parts used, as HFA propellants show different physicochemical properties, such as polarity and vapor pressure, when compared CFCs [34,35]. The change to use HFAs instead of CFC propellants also offered new opportunities, leading to a new generation of pMDI products that exhibited better performance in terms of fine particle fractions (FPF) generated, when compared to their CFC containing predecessors. Besides the active ingredient and the propellant, HFA pMDI formulations may include surfactants and solubilizing excipients such as ethanol [35]. By

design, the drug containing HFA formulation is stored within an aluminum canister, onto which the metering valve is crimped. Aluminum is the material of choice as it fulfills all requirements that need to be met since it is sufficiently robust to hold the propellant system pressure, impervious, light protective, and chemically inert. Additionally, surface modifications can be used to chemically and physically stabilize the formulation, thereby minimizing container/drug interactions [36]. As reproducible dose delivery is essential, the metering valve is one of the most critical parts of the pMDI assembly. Doses metered are in the range of 25 - 100 µL and shaking of the devices prior to actuation by the patient is required to ensure accurate and reproducible metering and drug delivery. Consequently, applicable doses are limited to about 200 µg per actuation for suspension based inhalers whereas investigational solution based pMDIs are reported to deliver up to 1.5 mg per actuation [37,38]. The basic principle of operation is that prior to actuation the metering chamber displays an open orifice, establishing a connection to the reservoir so that it can be filled gravimetrically. Upon actuation, this connection closes and another valve, establishing a connection to an expansion chamber, opens. Now exposed to atmospheric pressure, the metered dose of the API containing propellant formulation flash evaporates, creating the therapeutic aerosol when exiting from the actuator nozzle [39]. Comparably to DPI formulations, suspension based pMDI formulations must de-agglomerate prior to (shaking) or during actuation, to ensure that the aerodynamic particle size distribution (aPSD) is within the desired range. APSDs of solution based pMDIs are correlated to the PSD of the initial droplets generated, which can be effectively influenced by the geometry of the nozzle used and the dimensions of the actuator nozzle path [35,40]. Expansion of the propellant and evaporation of other included liquid excipients (e.g. EtOH) does not occur isothermically, thus decreasing the temperature of the aerosol plume. This reduction in temperature phenomenon, known as “Freon effect” was reported to induce bronchoconstriction in some patients, which compromises their compliance [41]. Additionally, synchronization of the actuation and inhalation maneuver has been shown to be challenging to certain patient sub-populations [29,39]. The use of valved holding chambers (VHC), spacer devices extending the distance from the actuator nozzle to the patient, addresses both issues, but suffers from diminished therapeutically effective doses due to electrostatic interactions of the aerosol particles with the wall of the spacer, as well as somewhat unwieldy and erroneous handling by the patient [42]. Another approach to overcome the need to actuate and inspire simultaneously is the addition of breath actuated valves to the pMDI assembly. The Autohaler® (3M

Pharmaceuticals, St. Paul, MN, USA) for example, must be primed prior to inhalation by lifting a leaver and actuates automatically upon detection of inspiratory flow as low as 30 L/min. Actuation of the airflow triggered valve creates a clicking sound, which serves as positive feedback control that the dose was inhaled correctly [43]. Modern pMDI devices also incorporate an accurate dose counter, which enables the patient to keep track on when to discard and replace the prescribed medication [39]. Since pMDIs as well as multi use DPIs, are intended for everyday patient use, equivalent requirements are important for an "ideal" device. These criteria include: accurate and reproducible delivery of a predefined dose, audible or visible feedback mechanisms and a robust mode of application (e.g. breath actuation) to verify and assure that the dose was inhaled correctly, as well as a reliable dose counting mechanism. Figure 4 shows a schematic diagram of a pMDI.

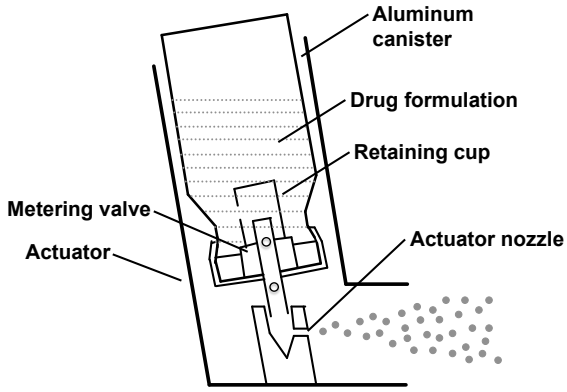


Figure 4. Schematic diagram of a pMDI. Modified from [31].

### 1.3.3 **Nebulizer**

Nebulizer devices are capable of aerosolizing a drug containing formulation (a solution, an emulsions, or suspensions) in order to create a therapeutic mist that can be inspired by a patient [44]. Since nebulizers are active devices, correct inhalation requires only little inspiratory effort when compared to DPIs. Another benefit is that no complex actuation/inhalation maneuver is necessary, making nebulizers the first choice for patients with impaired function: physically restricted patients (such as the elderly or very young patients), or those with obstructed airways [45]. Commercially available nebulizers can be assigned into two general categories for aerosol generation. In the first instance, jet nebulizers

utilize compressed air or oxygen, which is provided by a compressor unit, to aerosolize the drug containing formulation in a two fluid atomizer [45]. Product feed occurs passively utilizing Bernoulli´s principle, whereby a gas flow is applied through a small orifice and a negative pressure is created in an adjacent feed tube that provides a pressure gradient sufficiently high to convey the formulation to the atomization zone where droplets are broken down by turbulent rupture and secondary decay [45,46]. In contrast, ultrasonic nebulizers (or vibrating mesh nebulizers) operate independently from a compressed air source using a piezoelectric crystal oscillating at high frequencies (1-3 MHz) to generate the aerosol [46]. In comparison to pMDI or DPI formulations, formulations for jet nebulization usually are more facile in development and a wide range of drug substances have been investigated, so nebulized formulations may provide quicker access and higher stability of investigational therapies in clinical testing [47–50]. However, performance of most nebulizers used is considerably lower than that achieved by pMDI or DPI devices, often not exceeding a $FPF_{total}$ of about 10% as the majority of the dose is retained within the device itself [51,52]. It is also problematic that deposition rates are highly influenced by the patient´s breathing pattern [53,54], and that a large fraction of the dose is lost when exhaling [51]. To address this issue so called breath enhanced nebulizers (see Figure. 5) have been introduced. The enhanced nebulizer uses the patient´s inspirational airflow to create a negative pressure which aids in promoting aerosol generation and reduces losses upon expiration thus generating higher FPFs [55]. Another approach to address this problem is to couple vibrating mesh nebulizers to diagnostic tools and microprocessors. Smart nebulizers determine the patient´s individual breathing pattern and actuate only during the early phases of inspiration. Additionally formulation specific characteristics can be incorporated which can lead to an improved aerosol generation characteristics [56], consequently generating higher FPFs.

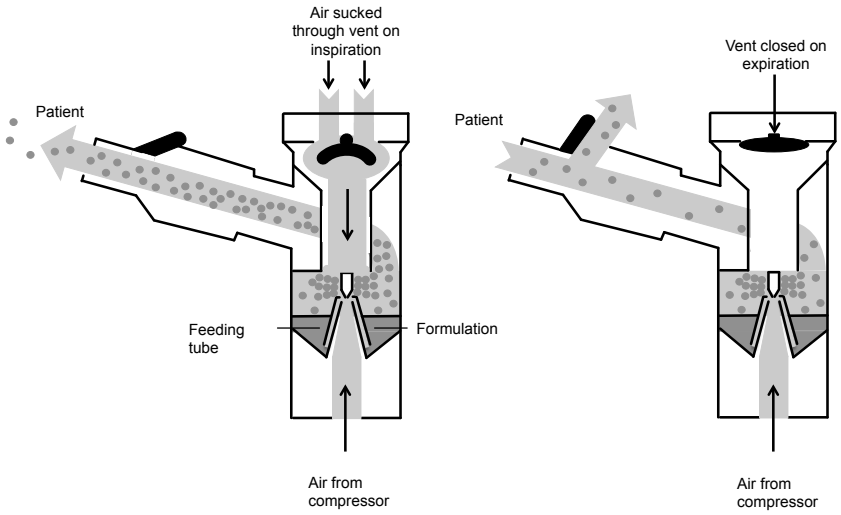


Figure 5. Schematic diagram of a breath enhanced jet nebulizer. Modified from [57].

### 1.3.4 **Overview on approved inhalable drugs in Germany**

A broad range of different inhalable preparations are approved and marketed in Germany. Main indications are asthma and COPD. Table 3 gives an overview on dry powder preparations and Table 4 gives an overview of pMDIs approved in Germany. These lists are based on online research using the Gelbe Liste Pharmindex database [58], and searching for the respective dosage form. Since nebulized formulations are not the focus area of the research presented in these studies, they will not be discussed further.

Table 3. Overview on DPIs approved in Germany.

| Substance | Product name | Manufacturer | $m_{drug}$/dose [$\mu$g] | DPI | Indication |
|---|---|---|---|---|---|
| **Salbutamol sulfate** | Salbu Easyhaler | Orion Pharma | (200 / 400) | Easyhaler | COPD |
| | Ventilastin | MEDA | 100 | Novolizer | Asthma / COPD |
| | Cyclocaps Salbutamol | PB Pharma | 400 | Cyclohaler | COPD |
| **Salmeterol xinafoate** | Serevent | GSK | 50 | Diskus | Asthma |
| **Salmeterol xinafoate** | Seretide | GSK | 50 / (250 / 500) | Diskus | Asthma |
| **Fluticasone propionate** | Rolenium | Elpen Pharma | 50 / (250 / 500) | Elpenhaler | Asthma / COPD |
| | Atmadisc | GSK | 50 / (100 / 250 / 500) | Diskus | Asthma |
| **Tiotropium bromide** | Spiriva | BI | 18 | Handihaler | COPD |
| | Braltus | TEVA | 10 | Zonda | COPD |
| **Umeclidinium bromide** | Incruse | GSK | 50 | Ellipta | COPD |
| **Umeclidinium bromide** | Anoro | GSK | 50 / 22 | Ellipta | COPD |
| **Vilanterol** | | GSK | | | |
| **Aclidinium bromide** | Bretaris | Astra Zeneca | 322 | Genuair | COPD |
| **Aclidinium bromide** | Eklira | Astra Zeneca | 322 | Genuair | COPD |
| **Aclidinium bromide** | Brimica | Astra Zeneca | 322 / 12 | Genuair | COPD |
| **Formoterol fumarate** | Duaklir | Astra Zeneca | 322 / 12 | Genuair | COPD |
| **Beclometasone dipropionate** | Cyclocaps Beclometason | PB Pharma | (100 / 200 / 400) | Cyclohaler | Asthma |
| | Beclomet Easyhaler | Orion Pharma | (100 / 200 / 400) | Easyhaler | Asthma |
| **Beclometasone dipropionate** | Kantos | Chiesi | 100 / 6 | Nexthaler | Asthma |
| **Formoterol hemifumarate** | Foster | Chiesi | 100 / 6 | Nexthaler | Asthma |
| **Budesonide** | Cyclocaps Budesonid | PB Pharma | 100 / 200 / 400 / 600 / 800 | Cyclohaler | Asthma / COPD |
| | Budesonid Easyhaler | Orion Pharma | 100 / 200 / 400 | Easyhaler | Asthma |
| | Miflonide | Novartis | 200 / 400 | Cyclohaler | Asthma |
| | Budecort | MEDA | 200 / 400 | Novolizer | Asthma |
| | Novopulmon | MEDA | 200 / 400 | Novolizer | Asthma |
| | Pulmicort | Astra Zeneca | 200 / 400 | Turbohaler | Asthma |
| **Budesonide** | Duoresp | TEVA | (160 / 320) / (4.5 / 9) | Spiromax | Asthma |
| **Formoterol hemifumarate** | Symbicort | Astra Zeneca | (80 / 160 / 320) / (4.5 / 9) | Turbohaler | Asthma |
| **Fluticasone propionate** | Flutide | GSK | 50 / 100 / 250 / 500 | Diskus | Asthma |
| **Fluticasone furoate** | Relvar | GSK | 50 / 100 / 250 / 500 | Diskus | Asthma |
| **Vilanterol** | | | | | |
| **Formoterol hemifumarate** | Cyclocaps Formoterol | PB Pharma | 12 | Cyclohaler | Asthma |
| | Foradil | Hexal | 12 | Cyclohaler | Asthma / COPD |
| | Oxis | Astra Zeneca | 12 | Turbohaler | Asthma / COPD |
| | Formatris | MEDA | (6 / 12) | Novolizer | Asthma / COPD |
| | Formotop | MEDA | (6 / 12) | Novolizer | COPD |
| **Glycopyrronium bromide** | Seebri | Novartis | 44 | Breezehaler | COPD |
| | Tovanor | Novartis | 44 | Breezehaler | COPD |
| **Glycopyrronium bromide** | Ultibro | Novartis | 44 / 85 | Breezehaler | COPD |
| **Indacaterol** | Ulunar | UCB | 44 / 85 | Breezehaler | COPD |
| | Xoterna | Kohl Pharma | 44 / 85 | Breezehaler | COPD |
| **Indacaterol** | Onbrez | Novartis | 150 / 300 | Breezehaler | COPD |
| **Mometasone furoate** | Asmanex | MSD | 200 / 400 | Twisthaler | Asthma |
| **Tobramycin** | TOBI | Novartis | 2800 | Podhaler | Cystic fibrosis with P. Aeruginosa infection |

Table 4. Overview on pMDIs approved in Germany.

| Substance | Product name | Manufacturer | $m_{drug}$/dose [$\mu$g] | Formulation | Indication |
|---|---|---|---|---|---|
| **Beclometasone propionate** | Beclohexal | Hexal | 100 | solution | Asthma |
| | Beclo Sandoz | Hexal | 100 | solution | Asthma |
| | Berotec N | BI | 100 | solution | Asthma |
| | Junik | Infectopharm | 100 | solution | Asthma / COPD |
| | Junik Autohaler | Infectopharm | (50 / 100) | solution | Asthma / COPD |
| | Ventolair Autohaler | TEVA | (50 / 100 / 250) | solution | Asthma / COPD |
| | Sanasthmax | Chiesi | (50 / 250) | solution | Asthma / COPD |
| | Arobec | IVAX Pharma | (50 / 100) | solution | Asthma |
| | Beclometason CT | TEVA | (50 / 100 / 200) | solution | Asthma |
| | Beclometason | Ratiopharm | (50 / 100 / 250) | solution | Asthma |
| **Beclometasone propionate** | Foster | Chiesi | (100 / 200) / 6 | solution | Asthma / COPD |
| **Formoterol hemifumarate** | Formodual | Kohlpharma | 100 / 6 | solution | Asthma / COPD |
| | Inuvair | Chiesi | 100 / 6 | solution | Asthma / COPD |
| | Kantos | Chiesi | (100 / 200) / 6 | solution | Asthma / COPD |
| **Budesonide** | Budiair | Chiesi | 200 | solution | Asthma / COPD |
| **Ciclesonide** | Alvesco | Astra Zeneca | (80 / 160) | solution | Asthma |
| **Fenoterol HBr** | Dosberotec | Kohlpharma | 100 | solution | Asthma / COPD |
| **Fluticasone dipropionate** | Flutihexal | Hexal | (125 / 250) | suspension | Asthma |
| | Flutide | GSK | (50 / 125) | suspension | Asthma / COPD |
| **Fluticasone dipropionate** | Flutiform | Mundipharma | (50 / 150) / 5 / not reported | solution | Asthma |
| **Formoterol hemifumarate** | Affera | Mundipharma | 250 / 10 / not reported | solution | Asthma |
| **Na-Cromoglicate** | | | | | |
| **Formoterol hemifumarate** | Foradil | Hexal | 12 | solution | Asthma |
| | Forair | Chiesi | 12 | solution | Asthma |
| **Ipratropium Br** | Atrovent N | Axicorp | 20 | solution | Asthma / COPD |
| **Ipratropium Br** | Ipratropiumbr. Hexal | Axicorp | 20 | solution | Asthma / COPD |
| **Reproterol** | Aarane N | Sanofi | (500)/(1000) | suspension | Allergic Asthma |
| **Na-Cromoglicate** | Allergospasmin N | MEDA | (500)/(1000) | suspension | Allergic Asthma |
| **Salbutamol sulfate** | Bronchospray novo | Infectopharm | 100 | suspension | Asthma / COPD |
| | Bronchospray Autohaler | Infectopharm | 100 | suspension | Asthma / COPD |
| | Salbuhexal | Hexal | 100 | suspension | Asthma / COPD |
| | Salbutamol Sandoz | Hexal | 100 | suspension | Asthma / COPD |
| | Salbulair N Autohaler | TEVA | 100 | suspension | Asthma / COPD |
| | Salbulair N Easi-Breathe | TEVA | 100 | suspension | Asthma / COPD |
| | Sultanol | GSK | 100 | suspension | Asthma / COPD |
| | Salbutamol | 1A | 100 | suspension | Asthma / COPD |
| | | AL | | | |
| | | Ratiopharm | | | |
| | | Stada | | | |
| **Salmeterol xinafoate** | Salmeterol Hexal | Hexal | 25 | suspension | Asthma |
| | Serevent | GSK | 25 | suspension | Asthma |
| **Salmeterol** | Seretide | GSK | (25) / (125 / 250) | suspension | Asthma |
| **Fluticasone dipropionate** | Serkep | Mylan | (25) / (125 / 250) | suspension | Asthma |
| | Atmadisc | GSK | (25) / (50 / 125) | suspension | Asthma |
| | Viani | GSK | (50) / (250) | suspension | Asthma |

## 1.4 Aerosol analysis

### 1.4.1 The Cascade impactor (CI)

As described in the previous sections, knowledge of aerodynamic aerosol properties is essential to evaluate the performance of an inhalable product. Aerosol impactor analysis continues to be the most important method for characterizing inhalable formulations. The United States Pharmacopoeial (USP) Convention and the European Pharmacopoeia (Ph.Eur.) describe four different types of impaction methods: Andersen Cascade Impactor (Apparatus 1/3/D), Marple-Miller Impactor (Apparatus 2), Multi-stage Liquid Impinger (Apparatus 4/C) , and Next Generation Pharmceutical Impactor (NGI, Apparatus 5/E). Additionally, the Ph.Eur. describes a simple twin stage impinger test (Apparatus A). Each test method is designed to provide quality assurance for industrial manufacturing environments by providing highly standardized and robust tests to assess aerosol characteristics [59].

Shortly after the commercial distribution of the first pMDI in 1955 by Riker Laboratories (Loughborough, Leicestershire, UK), the first particle sizing method was introduced to assure reproducible quality. Here, scattering of an incident light beam on the test aerosol was used to calculate the PSD [60]. This method, which is still in use today, shows fundamental limitations; since it is not the aerodynamic, but the geometric diameter of the particles that was determined. As discussed earlier, not only the geometric diameter, but also particle density and shape are crucial for its aerodynamic behavior. Thus, this method can be helpful in providing quality control (QC) data on batch-to-batch variability, if the particles assessed show identical solid-state properties. In 1958, the first cascade impaction device was designed by Andersen to collect and sample viable airborne particles. It featured a six stage vertical design that allowed particle collection by inertial deposition. In this device, the test aerosol is supplied into the inlet of the cascade impactor and classified in six consecutive stages. Each stage consists of a plate, showing perforations that from stage to stage differ in size and number, and a petri dish holding an agar gel, onto which the particles (in this case bacterial spores) impact. Particle classification occurs by inertial impaction, which is facilitated by increasing acceleration of the particles due to increasing jet velocities generated in the nozzles [61]. As characteristic aerodynamic cut-off sizes can be attributed to each stage, this device is capable of determining the aPSD of an aerosol sample. The first application of CI analysis on pharmaceutical aerosols was reported by Polli et al. in 1969 [62]. Two years later in 1971, an

eight stage version of the Andersen cascade impactor (ACI Mark I) was introduced for pharmaceutical aerosol analysis by Riker Laboratories. Over the years, several different designs of CIs including the Multi-stage Liquid impinger or the Marple-Miller impactor were developed and described. They were designed specifically for pharmaceutical applications, providing higher resolution in the relevant size range with simplified product recovery. In the 1990s, a consortium comprising of representatives of all major laboratories associated with inhalable product testing was recruited in order to develop a novel cascade impaction device based on experience gained using earlier models, which was intended to provide a highly standardized, versatile, and reproducible test method [10]. Table 5 shows essential requirements for this device (NGI), as defined by the consortium.

Table 5. Requirements defined as essential characteristics for the NGI. From [10].

| | **Essential requirement** |
|---|---|
| **1** | Automatable, but suitable for manual operation |
| **2** | Operates over a range of flow rates 30 - 100 L/min |
| **3** | Calibration data for the flow rates of 30 - 100 L/min are available |
| **4** | Capable of fully characterizing the "less than 10 $\mu$m" cloud size range |
| **5** | Needs right number of stages at right cut-offs (independent of flow rate); minimum of 5 stages 0.5 - 5 $\mu$m, one stage between 5 and 10 $\mu$m plus high capacity stage at 10 $\mu$m or higher (pre-separator) |
| **6** | The stages will be followed by a micro-orifice collector that is 90% efficient for particles larger than or equal to 0.2 mm aerodynamic diameter |
| **7** | Efficiency curves for stages must be appropriate; GSD for all stages similar; overlap between stages is minimized |
| **8** | Deposition profile unaffected by stage loadings (up to 10 mg) |
| **9** | Operates using defined entry conditions |
| **10** | The empty volume of the impactor must be no more than 1.5 L, measured from the inlet of the USP/EP inlet to the exit of the impactor body, including the pre-separator |
| **11** | Low wall losses; not more than 5% on any stage and not more than 5% total on all stages |
| **12** | Good drug recovery (mass balance) |
| **13** | No bounce/re-entrainment |
| **14** | Capable of being grounded; unaffected by static |
| **15** | Physically robust |
| **16** | Constructed using inert/robust materials (can use common solvents) |
| **17** | Good accuracy and precision (65%) |
| **18** | Operator independent (no statistical difference between results between independent laboratories) |
| **19** | Acceptable to regulators/Pharmacopoeia |
| **20** | Designed and manufactured to ISO 9000 or equivalent |
| **21** | Applicable to all single shot inhaled delivery systems (MDIs, DPIs, aqueous inhalers) |
| **22** | Easy to qualify and validate in the laboratory |
| **23** | Fast; cycle time of less than 30 min for manual determinations |

Not all requirements discussed are critical to the performance of the NGI, and focus was also put on user convenience and cost efficiency. At the end of the development phase, the consortium presented a CI with a horizontal design, comprising of seven stages and a terminal high efficiency collector (Micro orifice collector, MOC). It also includes an USP/Ph.Eur. compliant induction port (IP), as well as a preseparator unit to remove coarse carrier particles, if needed. To ensure narrow distributions around the nominal stage cut off, nozzles were designed in a way that they would fulfil requirements, which had been investigated empirically [63–66] with the following specifications: a) exhibiting a Reynolds number of 500-3000, b) a nozzle to plate distance should be between 1-10 times the dimension of the nozzle diameter, and c) limited cross flow (i.e. limiting the interaction of airflow traversing from the inner most nozzles across flow paths of the outer nozzles). Each impaction stage particle size cut off was designed to be equally distant on a logarithmic scale [10]. Circular stage nozzles and flow paths connecting the stages are arranged in a horizontal alignment and are incorporated into the lid of the device. Particles deposit into individual cups, which are inserted into a tray in the bottom part of the device, which facilitates easy removal for product recovery and subsequent quantification (Figure. 6).

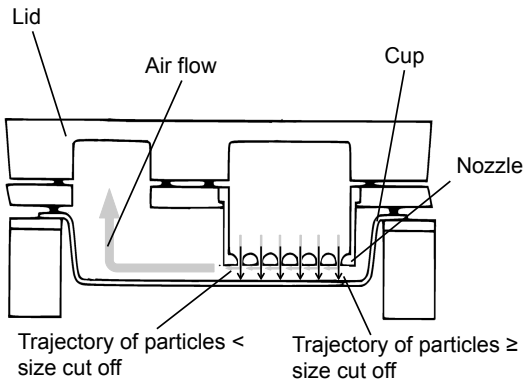


Figure 6. Schematic drawing of one NGI stage. Modified from [67].

Due to the function of the MOC, a terminal filter stage is redundant in most cases. Initially, the NGI was calibrated for functionality over the airflow range of 30-100 L/min, this was later was extended to operate from 15-100 L/min in order to make it suitable for analysis of nebulized formulations. Figure 7 shows a schematic picture of the NGI in open and closed position.

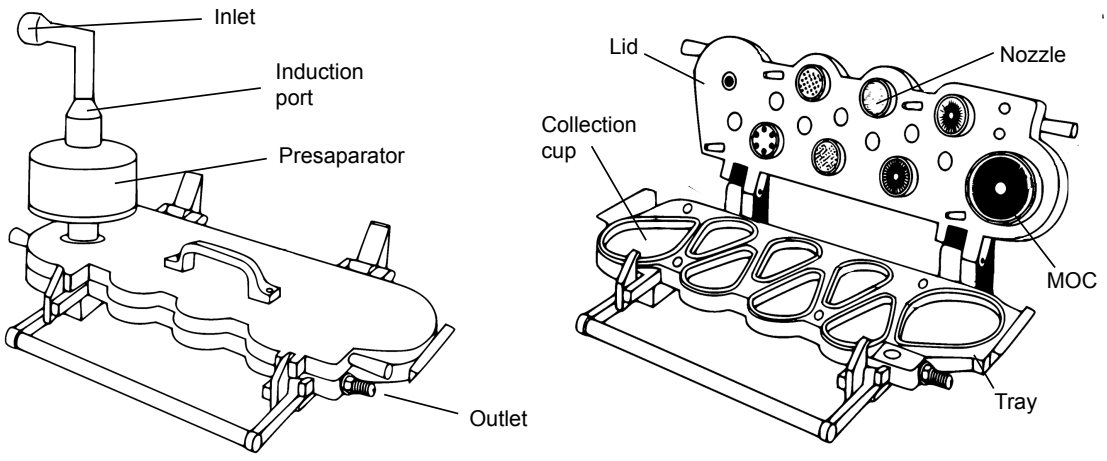


Figure 7. Schematic drawing of the NGI. Modified from [67].

Below is a brief description of the experimental procedure for aerosol characterization for a typical DPI formulation:

1. Determination of the flow rate to generate a pressure drop of 4 kPa across the DPI.
2. Optional coating of collection cups with typically silicone oil or glycerol (in order to minimize potential particle reentrainment).
3. Filling 15 mL of recovery solvent into the preseparator.
4. Assembling the cascade impactor.
5. Adjustment of flow rate through the impactor inlet (e.g. USPIP) to flow rate determined in Step 1, above.
6. DPI priming.
7. Connection of the DPI using a suitable mouthpiece (premanufactured generally using an airtight silicone material).
6. Actuation of the DPI into the CI for the duration it takes to draw 4 L of gas through the device.
7. Confirmation of sonic flow over the device.
8. If necessary, repetition of Steps 4-6 until a quantifiable dose is deposited, but max. n= 10.
9. Disassembly of the device and recovery of impacted powders following actuation of the DPI using a suitable solvent, as well as collection of the solution from the preseparator and washing using a suitable solvent.

10. Determination of the mass of powder deposited at the individual stages, preseparator, IP, and the DPI device.
11. Statistical evaluation of the results including:
11.1. Plotting relative frequencies of powder deposition over stages.
11.2. Plotting cumulative frequencies of MOC to S1 over in-stage cut off values at the given flow rate used. If determined at the inlet of the device, flow rate must be corrected according to Equation 2, as pressure drops over the DPI and the impactor change the actual total flow over the system.

$$Q_{out} = \frac{Q_{in} p_0}{p_0 - \Delta p}$$

Equation 2. Correction of flow rate over the test system with: $Q_{out}$= mass flow at outlet, $Q_{in}$= mass flow at inlet, $p_0$= atmospheric pressure, and $\Delta p$= pressure drop over the test system.

11.3. Linearization of cumulative distribution by probit transformation of y axis (i.e. cumulative frequency).
11.4.1. Linear regression model of the data set obtained in Step 11.3.
11.4.2. Evaluation if assumption of log-normal distribution is valid.
11.5. Determination of MMAD and GSD using the linear regression model obtained in 11.4.
11.6. Determination of FPFs and ED.

A detailed description of the experimental procedure can be found in the USP General Chapters <601> [68], or Ph.Eur. 2.9.18 [67].

### 1.4.2 **Modified induction ports for CI analysis**

As discussed in the previous section, CI experiments as monographed in USP and Ph.Eur. provide highly standardized testing for QC and industrial manufacture. However, each test fails to make precise predictions of *in vivo* behavior of formulations tested. From the clinical and basic science perspective it is highly desirable to develop test systems that deliver a high grade of *in vitro*/*in vivo* correlation (IVIVC). Along with other considerations, the following limitations for impactors have been identified: simplification of the patient's breathing behavior [69], simulation of poor device utilization [70], and particle bounce [71]. Furthermore, simplification of physiological conditions found in the upper respiratory tract [72] has been identified as major issue for IVIVC. The IP monographed in the USP and

Ph.Eur. is a simple tube of uniform cross sectional diameter with a 90° bend, which is intended to represent the throat and upper airways [73]. It is commonly assumed that large particles as well as large agglomerates can impact in the upper regions of the human respiratory tract. This being the case, this already 'removed' fraction of the dose would not be available to become therapeutically effective in the deep lung. Depending on the nature of the API used, it is possible that an increase in the occurrence of unwanted side effects could result from this upper airway deposition. Much effort has been made to improve IVIVC by replacing the standard USP IP with an IP that better represents physiological conditions. Advanced mouth/throat (MT) models have been generated from casts [74–76] or through the use of magnetic resonance/computer tomographic (MRT/CT) imaging techniques [77,78]. Prototype models have been prepared using resin, rubber, or fiber glass [75–77], as well as rapid prototyping techniques, such as fused deposition modeling (FDM) [78]. Most of these studies offer fundamental mechanistic insight, but provide little information on how alteration of the IP influences the outcome of cascade impaction experiments, which are considered as method of choice in formulation and device development [79]. Specifically, these studies have not highlighted which characteristics make a given formulation susceptible to divergent results. As benchtop size 3D printing devices have become more readily accessible, 3D printing technologies have gained great attention over the past few years. In the pharmaceutical field, an interesting area of research has grown involving 3D printing related to personalized medicine. In this area, 3D printers have been used to manufacture highly customized dosage forms [80]. Development of a novel modified IP (mIP) based on CT scans using 3D printing FDM technology will be presented in Chapter 3. This chapter also includes an evaluation of the mIP and will discuss it in context of the previous work conducted on this topic.

### 1.4.3 **Additional tests to characterize inhalable pharmaceutical preparations**

Additional tests to ensure quality of inhalable products include determination of dose stability over the life cycle of a device or stress tests under non-standardized conditions (e.g. elevated RH or temperature), as well as performance testing after storage. As these tests are predominantly relevant for commercial development and manufacture, they will not be discussed here.

## 1.5 Systematic review on experimental tuberculosis therapy using inhalable dry powders of RF

### 1.5.1 Introduction

Tuberculosis (TB) is an infectious disease caused by *Mycobacterium tuberculosis*. *M. tuberculosis* is a gram-negative bacterial species of the ubiquitous mycobacteriaceae family, showing slow growth (generation time is typically about 24 hours), complex cell envelopes, and intracellular pathogenesis. Depending on the patient's immune status, it may remain dormant for several years, which leads to delayed development of clinical symptoms [81]. Main site of infection are the lungs, though infections can secondarily spread to other organs (e.g. liver), and eventually generalize. Characteristic symptoms after lung infection, which typically occurs after exposition to bacteria conveying aerosols, include cough, fever, and hemoptysis, as well as anorexia and weight loss [82]. In 2016, approximately 10 million cases of TB were registered, making it the 9th leading cause of death globally and the leading cause of death from a single infectious agent [83]. Standard therapies of drug susceptible strains include administration of four first line antibiotics i.e. rifampicin (Rifampin, RF), isoniazid, ethambutol, and pyrazinamide over a period of at least 26 weeks [84]. In case of RF the recommended daily dose is per oral administration of 10 mg per kilogram bodyweight (KGBW), but 600 mg maximum. Continuous administration of high doses of RF is often accompanied with unwanted side effects, including: rash, pruritus, urticaria, induction of transaminases, as well as more severe incidents as thrombocytopenia, or kidney failure [85]. Due to the therapeutic burden, and since the regimen has to be followed strictly over a long period of time, patient's adherence is often poor - especially when it comes to the treatment of latent (i.e. clinically inapparent) tuberculosis [86]. Due to the high volume of distribution of approximately 1 L/KGBW [85], application of high doses is necessary to achieve concentrations at the site of infection which are sufficiently high to become therapeutically effective. Additionally, *M. tuberculosis* survives and replicates after phagocytosis. Phagocytosis actually protects the bacteria from antibacterial drugs present in the lung tissue; a compound problem that is exacerbated by cellular encapsulation [87]. So, in addition of delivering a drug dose that is sufficiently high to efficiently inhibit free bacteria, it would also be advantageous to demonstrate proactive targeting to phagocytes [88]. To limit the total drug

exposure and therefore the therapeutic burden it is desirable to develop a dosage form that is suitable for direct application to the site of infection, i.e. the lungs.

RF is a semi-synthetic antibiotic drug that was first reported in 1966 by Maggi et al. In this original publication, it was synthesized by reacting 3-formyl rifamycin SV with 1-amino-4-methylpiperazine, yielding an orange to red crystalline powder, when recrystallized from acetone. RF is described as slightly soluble in water at pH higher than six, with increased solubility at lower pHs. Additionally, it is soluble in most organic solvents [89]. Two solvent-free polymorphs (F-I and F-II) as well as numerous stoichiometric hydrates and solvates are reported in literature [90–96]. F-II is a metastable form that transitions into F-I by consecutive melting and recrystallization at a temperature of about 190 °C [90,97]. RF is reported to be fairly stable at neutral pH but tends to oxidize to RF-quinone in basic environments, which can effectively be prevented by adding ascorbic acid. In acidic environments, hydrolysis to 3-formyl-rifamycin SV occurs, which tends to precipitate [89]. *In vivo,* RF is mainly metabolized by cytochrome P-450 (CYP) mediated deacetylation to 25-deacetyl-RF and shows induction of the CYP superfamily enzymes, which lowers its oral bioavailability from about 90% to 70% after three weeks of therapy [85].

In order to successfully develop a pulmonary therapeutic form of RF, not only the general requirements for inhalable dosage forms as discussed in Section 1.3.1 must be met (i.e. aerosolizability, reliability of dosing etc.), the unique physicochemical properties of RF mean that there has to be an increased focus on long term stability, related to chemical and solid state properties. Additional requirements depend on the therapeutic strategy intended and might demand utilization of sophisticated manufacturing techniques and excipients, if for example, alveolar macrophage targeting is desired. However, since most high TB burden countries are of low income, or developing countries [83], therapy cost effectiveness is paramount. Thus, estimated production costs for the formulation, the DPI device type, and cold-chain transportation must be considered when evaluating novel formulation approaches. These additional aspects will not be elaborated further in this review; being beyond its scope. The focus of this review is to give an overview of RF pulmonary dry powder formulations developed and tested, as well as a presentation of the device types used in these studies, this will provide an in-depth evaluation of aerosol properties reported.

### 1.5.2 **Results**

A literature search of the PubMed [98] database was conducted on 05-10-18 and returned 228 results. Figure 8 gives an overview on processing of primary results in a modified PRISMA scheme [99]. Figure 9 gives an overview on articles reporting formulation development with and without aerosol testing per year. Figure 10 provides an overview on formulation strategies investigated per year.

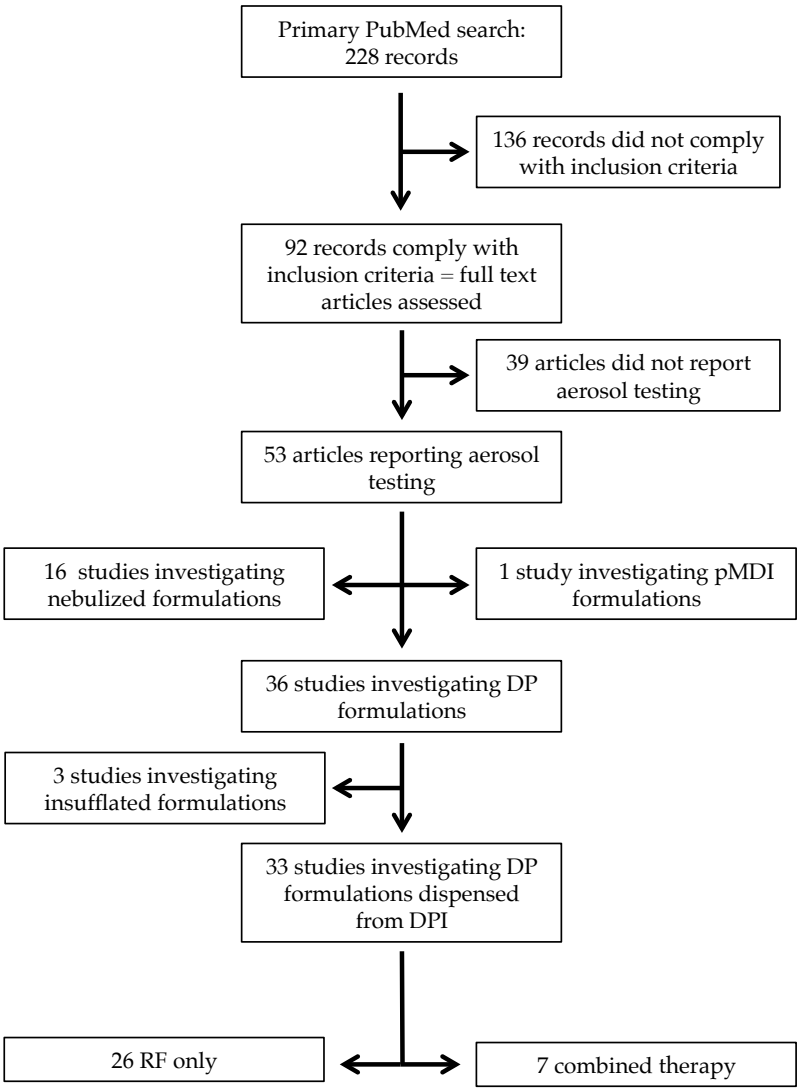


Figure 8. Overview on data processing using a modified PRISMA scheme.

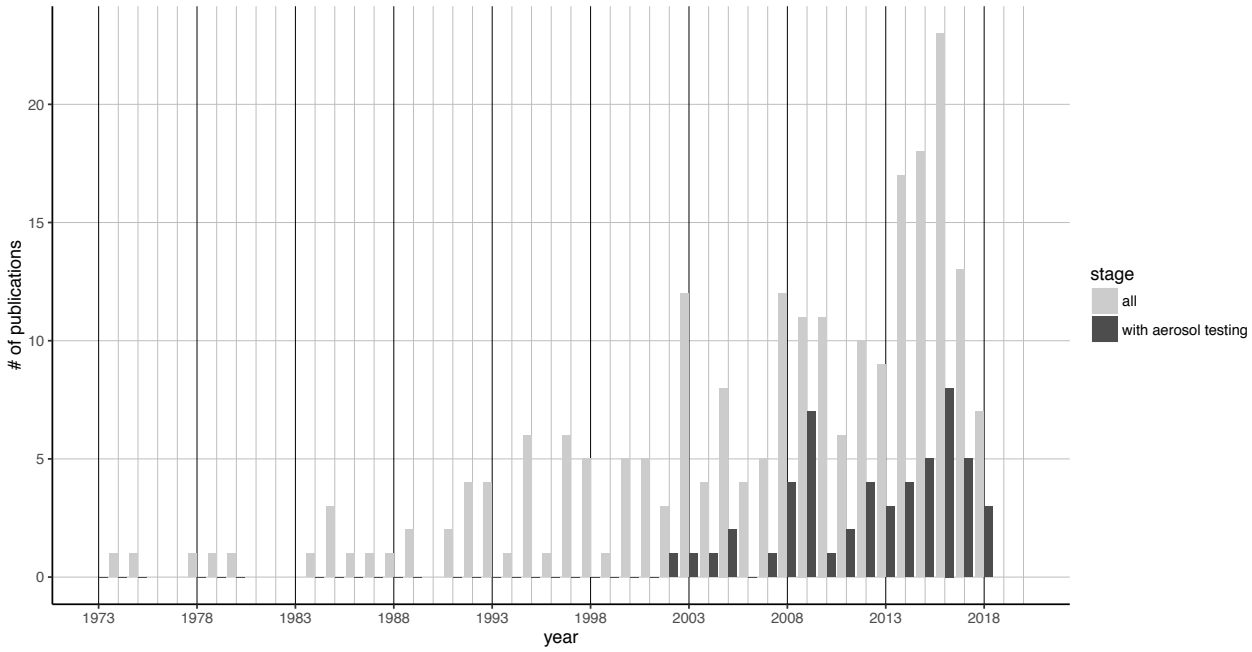


Figure 9. Overview of publications with and without aerosol testing per year.

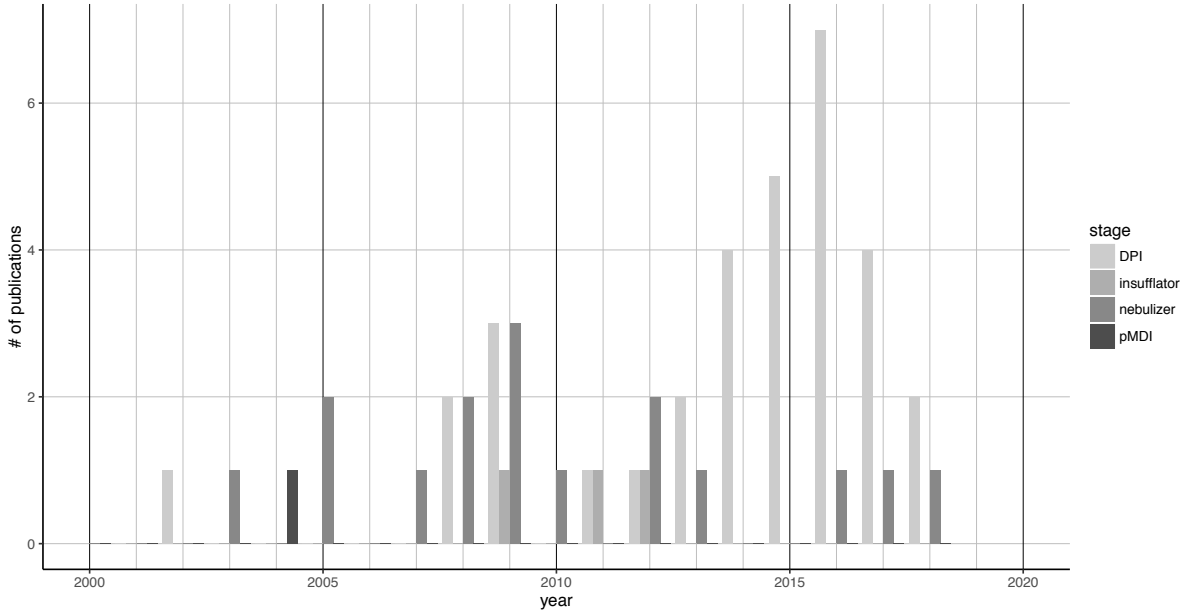


Figure 10. Overview of publications per year sorted by drug delivery system.

### 1.5.3 **Discussion**

#### 1.5.3.1 Utilized Dry powder inhalation devices

Various dry powder inhalation devices used in these studies are reviewed here. Each of the capsule based single unit dose inhalers used in the studies, will be briefly summarized.

Handihaler®

The Handihaler (Boehringer Ingelheim, Ingelheim am Rhein, Germany) is a capsule based DPI device showing high intrinsic resistance of $5.1 \times 10^{-2}(\sqrt{kPa} * min)/L$ [100]. For dose application, the mouthpiece must be tilted back and a size three capsule is to be inserted into the capsule compartment. Prior to inhalation, the device must be primed by pushing in a button, which triggers the puncture of the capsule by two pins. Upon inhalation, the capsule assumes a spinning motion, which facilitates ejection and de-agglomeration of the dry powder from the capsule. The capsule is kept within its compartment (see Figure 11) by a metal grid that is inserted in the bottom end of the mouthpiece. Upon inhalation, the capsule makes a whirring sound that serves as positive feedback control for correct inhalation.

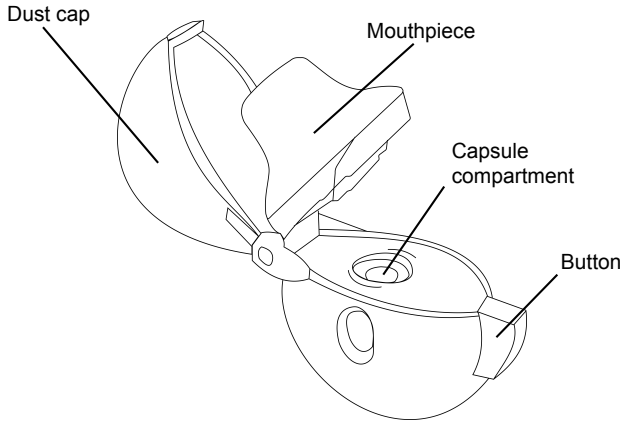


Figure 11. Schematic drawing of the Handihaler.

Aerolizer® / Lupihaler® / Plastiape RS01 / Osmohaler® / Cyclohaler®

The Aerolizer (Novartis, Basel, Switzerland), Lupihaler (Lupin Ltd., Mumbai, India), RS01 (Plastiape, Sirone, Italy), Osmohaler (Pharmaxis Ltd, New South Wales, Australia), and the Cyclohaler (PB Pharma, Meerbusch, Germany) devices are members of a DPI device family with highly similar designs using the same de-agglomeration technology. Note that Plastiape is not a pharmaceutical company but is specialized in the production of plastic packaging, medicinal devices, and nonpackaging based products. Two different makes showing different intrinsic resistances of the device are marketed: one low resistance make with a nominal airflow of 100 L/min which is reported to correspond to an intrinsic resistance of $1.8 \times 10^{-2} (\sqrt{kPa} * min)/L$ [101] and another intermediate resistance make, generating the pressure drop of 4 kPa at 65 L/min, which corresponds to an intrinsic resistance of $3.1 \times 10^{-2} (\sqrt{kPa} * min)/L$ [102]. Similarly to the Handihaler, for dose application the mouthpiece must be tilted back and a size three capsule is inserted (see Figure 12). Additionally, the capsule orientation in this device family is horizontal, whereas it is kept in vertical position in the Handihaler device. To prime the device, two buttons located opposite and on each side of the device are pushed, this triggers capsule puncture by either two opposing single pins, or opposing four pin configurations. Upon inhalation air is drawn through tangential slits in the device housing causing the capsule to spin; facilitating ejection and de-agglomeration of the dry powder. Similarly to the Handihaler, a plastic mesh holds the capsule in place. A whirring sound created by the swirling capsule also serves as audible feedback control.

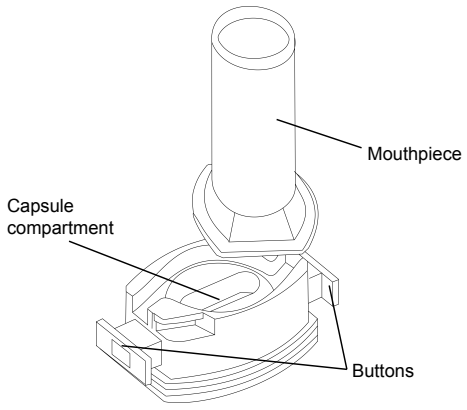


Figure 12. Schematic drawing of the Cyclohaler.

Rotahaler®

The Rotahaler device (currently Cipla, Mumbai, India, developed by Glaxo, London, UK) shows a distinct release mechanism of the powder from the capsule, when compared to the Handihaler or Aerolizers. Capsules are not punctuated. Instead, the bottom and top part of the capsule are separated, releasing the dry powder. Separation of capsule halves is triggered by consecutive insertion of the capsule into the device and twisting of its lower part. A flap that is connected firmly to the bottom part of the device, hits the lower half of the capsule upon rotation, opening it up by the shear force applied. Upon inhalation a vortex is created in the main compartment of the inhaler, facilitating de-agglomeration and aerosolization of the powder. A mesh is located in the lower part of the mouthpiece in order to retain the capsule within the compartment. The inhaler is made out of transparent plastic, so that correct inhalation can be confirmed visually. Pressure drop of 4 kPa is achieved at an airflow rate of 45 L/min [103], which corresponds to an intrinsic resistance of $4.4 \times 10^{-2} (\sqrt{kPa} * min)/L$. A schematic drawing of the Rotahaler can be found in Figure 13.

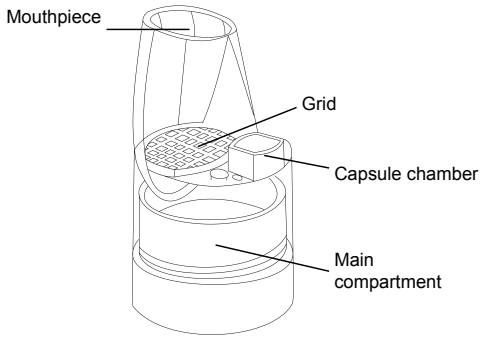


Figure 13. Schematic drawing of the Rotahaler.

Revolizer®

The Revolizer device is another single unit dose DPI marketed by Cipla. Its engine resembles the one used in the Handihaler. Similarly, a size three capsule is inserted into a vertical capsule compartment and a grid is inserted into the lower part of the inhalation channel in order to retain the capsule within the chamber. Upon inhalation, the capsule spins, ejecting and aerosolizing the dry powder. Significant differences are observed, compared to previously described designs. Priming of the device does not occur by pushing a button in order to puncture the capsule, but the punctuation mechanism is connected to the mouthpiece, which is to be tilted back in order to insert the capsule (see Figure 14). When placing the mouthpiece in the closed position, two pins that are triggered by a spring mechanism automatically pierce the capsule. Similar to the Rotahaler it has a high airflow resistance generating a pressure drop of 4 kPa at 44 L/min [103], which corresponds to an intrinsic resistance of $4.5 \times 10^{-2} (\sqrt{kPa} * min)/L$.

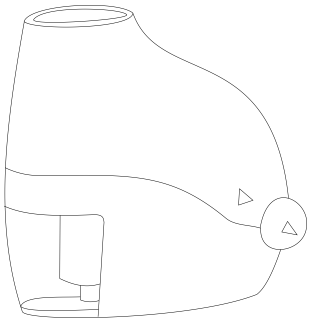

Figure 14. Schematic drawing of the Revolizer.

Jethaler®

The Jethaler (Unisia Jecs Corp. (Hitachi), Isesaki, Japan) (see Figure 15) is another single unit dose capsule-based device with a distinct engine for powder de-agglomeration. Priming of the device occurs by pushing in a button in order to pierce the capsule using two pins. Upon inhalation, the powder is ejected from the size two capsule and the subsequently generated aerosol plume is directed into a mixing chamber that resembles a jet-mill. Here, particles

collide, which is thought to aid de-agglomeration, before being released into the inhalation channel. Unfortunately, since only limited information about this device is available, no further description can be provided.

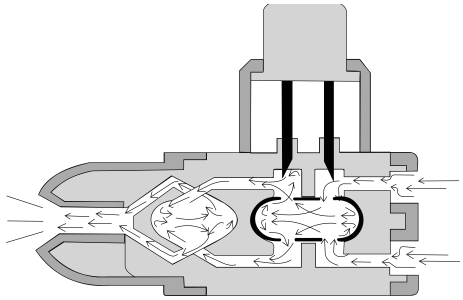

Figure 15. Schematic drawing of flow paths inside the Jethaler device. Redrawn from [104].

Turbospin®

Developed and marketed by PH&T (Milan, Italy) this single unit dose inhaler is based on the Spinhaler device, which was launched by Fisons (Ipswich, UK) in 1969. This inhalation device is distinctively different from the Spinhaler, though the principle of operation, i.e. ejection and aerosolization of the dry powder from a spinning capsule, as well as the overall design was maintained. In the Spinhaler device, the capsule holder was found on top of a rotor, which set the capsule into spinning motion upon inhalation [105]. In contrast, the capsule spinning in the Turbospin device is induced by airflow path design (see Figure 16). To apply a dose, the patient is required to unscrew the mouthpiece, insert a size two capsule into the capsule chamber, and re-attach the mouthpiece. The capsule is primed by depressing a plunger at the rear end of the device, which triggers puncturing of the capsule by two pins. Upon inhalation, air is drawn through tangential slits, causing the capsule to spin. Whilst spinning, the capsule produces a whirring noise that again serves as control for correct inhalation. The same technology has also been applied to the Podhaler ® device (also PH&T), which is an optimized version of the Turbospin. A pressure drop of 4 kPa is achieved at a flow rate of about 71 L/min, which corresponds to an intrinsic resistance of $2.8 \times 10^{-2} (\sqrt{kPa} * min)/L$ [106].

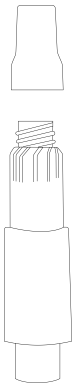

Figure 16. Schematic drawing of the Turbospin device.

### 1.5.3.2 Dry powder formulations of Rifampicin

Different approaches to formulate RF into respirable dry powders have been investigated and reported over the past 15 years. In the next part of this overview, studies published that include aerosol testing will be briefly discussed and presented for excipient classes and are laid out chronologically within the respective sections. Table 6 gives an overview of studies discussed in this chapter, as well as $FPF_{total}$s achieved in each respective study.

Table 6. Overview on studies discussed.

| | Author | Year | DPI used | Test system (flow rate) | FPF | Reference |
|---|---|---|---|---|---|---|
| **RF only formulations** | [ ] | [ ] | [ ] | [L/min] | [%] | [ ] |
| **PLGA (/ PLA)** | Sethuraman and Hickey | 2002 | Handihaler | ACI (60 / 90) | 45 | [110] |
| | Coowanitwong et al. | 2008 | Cyclohaler | ACI (28.3) | 23 - 68 | [111] |
| | Sung et al. | 2009 | Plastiape | ACI (28.3) | 36 - 68 | [112] |
| | Ohashi et al. | 2009 | Jethaler | ACI (28.3) | 35 | [113] |
| | Son and McConville | 2012 | Aerolizer | NGI (60) | 24 - 45 | [114] |
| **Lipids** | Changsan et al | 2008 | unknown | ACI (60) | 32 - 67 | [117, 118] |
| | Kumar et al. | 2013 | Rotahaler | ACI (28.3) | 68 | [119] |
| | Manca et al. | 2014 | Turbospin | NGI (70) | 50 | [120] |
| | Patil et al. | 2015 | unknown | ACI (60) | 26 | [121] |
| | Singh et al. | 2015 | Turbospin | NGI (70) | 50 | [122] |
| | Maretti et al. | 2016 | Plastiape | ACI (60) | 9 - 70 | [123, 124] |
| | Srichana et al. | 2016 | novel DPI | ACI (60) | 37 | [125] |
| **Chitosan** | Kundawala et al. | 2014 | unknown | ACI (60) | 55 - 62 | [127] |
| | Pai et al. | 2016 | Lupihaler | ACI (28.3) | > 25 | [128] |
| | Rawal et al. | 2017 | unknown | ACI (unknown) | 33 | [129] |
| **Carbohydrates** | Mizoe et al. | 2007 | Jethaler | ACI (28.3) | about 35 | [130] |
| | Vadakkan et al. | 2015 | unknown | ACI (60) | 63 - 78 | [131] |
| | Goyal et al. | 2015 / 16 | unknown | ACI (5) | not reported | [132, 133] |
| | Garg et al. | 2015 | unknown | ACI (5) | not reported | [134] |
| **Mesoporous silica** | Mohseni et al. | 2015 | Cyclohaler | ACI (50) | 46 | [135] |
| **Excipient free** | Son and McConville | 2011 | Aerolizer / Handihaler | NGI (60) | 37 - 64 | [91] |
| | Parikh, Patel, and Dalwadi | 2014 | unknown | ACI (unknown) | 46 | [136] |
| | Rawal et al. | 2017 | Turbospin | ACI (30) | 23 - 29 | [137] |
| **Combined formulations** | | | | | | |
| **RF, isoniazid, pyrazinamide** | Chan et al. | 2013 | Aerolizer | MSLI (100) | 46 | [138] |
| **RF, colistin** | Zhou et al. | 2014 | Aerolizer | MSLI (100) | 80 - 90 | [139] |
| | Wang et al. | 2016 | Osmohaler | NGI (100) | 69 - 73 | [140] |
| **RF, colistin, meropenem, tigecycline** | Lee et al. | 2016 | Aerolizer | NGI (60) | 54 - 68 | [141] |
| **RF, isoniazid** | Kadota et al. | 2017 | Aerolizer | ACI (28.3 / 60) | 3 - 53 | [142] |
| **RF, kanamycin** | Momin et al. | 2018 | Aerolizer | NGI (100) | 69 - 78 | [143, 144] |

RF formulations including poly-(D,L-lactic-co-glycolic acid) (PLGA) and poly-(D,L-lactic acid) (PLA).

PLGA is a synthetic, yet biocompatible and biodegradable copolymer, which has been widely used as structural polymer in micro- and nanoparticle preparation and is approved for human therapy by the US Food and Drug Administration (FDA) [107]. Different qualities of PLGA vary in monomer ratio, where lactic to glycolic acid ratios of 50:50 and 75:25 are most commonly used. Kinetic of hydrolytic degradation in biological relevant environment is strongly depending on the monomer ratio, and higher lactic acid content leads to slower degradation [108]. Also depending on the monomer ratio, PLGA shows differing degrees of crystallinity, where PLA homopolymers tend to be more crystalline than PGA ones. In the amorphous state, copolymers show a glass transition in the range of 36-68 °C [109].

Sethuraman and Hickey were the first to investigate aerosol performance of RF/PLGA microparticles (MPs) in 2002 [110]. In this study, PLGA (75:25) microspheres were prepared by a solvent evaporation technique, jet milled, and blended with lactose monohydrate or maltodextrin carrier particles. As a control, RF was jet milled and blended with carrier particles. Dry powder blends were dispensed from the Handihaler device and aerosol properties were assessed using an 8-stage MKII ACI at flow rates of 60 and 90 L/min. The main focus of the study was assessment of surface properties of the active and carrier particles in order to deduce a descriptive factor that would allow prediction of dispersibility/aerosol properties from surface energies. FPFs of jet milled RF-PLGA particles were found in the range of three to 13% and the best aerosol performance was achieved using sieved lactose monohydrate at a flow rate of 90 L/min. Control formulations were found to perform significantly better, yielding FPFs of about 45%, determined at 90 L/min. It should be mentioned that the Handihaler is a high resistance device, and that USP/Ph.Eur. compliant testing would have required lower flow rates of about 40 L/min, so it is to be expected that FPFs reported would not be achieved in an *in vivo* setting.

Another study, published by Coowanitwong et al., reported the preparation of PLGA and PLA MPs using a spray drying method, in order to achieve modified release [111]. Different ratios of RF with PLA and PLGA, as well as a control formulation containing RF only were dissolved in dichloromethane (DCM) and subsequently spray dried. Besides characterization of aerosol properties, resultant powders were tested for *in vitro* dissolution characteristics, *in vitro* macrophage toxicity, and *in vivo* pharmacokinetic profiles. Dry powders were dispensed from a Cyclohaler device and tested using a 28.3 L/min 8-stage MKII ACI. Resulting FPFs were found to be 55-68% and 23-34% for PLA and PLGA microparticles, respectively. Interestingly, powders were not filled into size three capsules but placed in the capsule chamber of the device, allowing higher doses per actuation to be dispersed. Also in this study, non-ideal aerosol testing conditions were applied, as testing was conducted using the 28.3 L/min ACI, which is more suitable for pMDI than DPI testing; especially when taking into account that the Cyclohaler generates a pressure drop of 4 kPa at about 65 or 110 L/min, depending on which model had been used. Additionally, the system actuation occurred for one minute, which is an about five-fold time increase compared to USP/Ph.Eur. standards. Furthermore, there was no stage coating in the study, serving to decrease the comparability

between test runs. However, FPFs of more than 60% are notably high. On the other hand, incomplete drug release from the MPs, especially at higher polymer concentrations, as well as limited drug loading, lower the dose effectively to be delivered. Interestingly, relative bioavailability of PLA MPs after intratracheal instillation in rats showed a strong decrease (compared to RF only MPs), which might be indicative of macrophage uptake. However, no additional experiments to exclude other mechanisms discussed were conducted.

A study published in 2009 by Sung et al. [112] investigated *in vitro* and *in vivo* performance of PLGA (50:50) nanoparticles (NPs) incorporated into leucine MPs. Porous MPs of RF in leucine were prepared as control formulation. NPs were prepared by emulsification/solvent evaporation and subsequently spray dried with leucine and additional RF. The reference formulation was prepared by co-dissolving RF and leucine in EtOH/water with subsequent spray drying. Particles obtained showed spherical NP agglomerates or corrugated porous particles respectively. Aerosol testing was performed after dispensing from an unspecified Plastiape device using the 28.3 L/min 8-stage ACI. Nano- in microparticle formulations were found to yield FPFs of 36-45% whereas the control formulation showed a fairly high FPF of 68%. However, drug loading of the reference formulation was only determined to be approximately 40%. *In vitro* dissolution studies showed fast but incomplete release. *In vivo* studies investigating pharmacokinetic profiles of inhalable, as well as i.v. and p.o. administered reference formulations showed fast onset and prolonged RF exposition in the case of inhalable formulations assessed. Additionally, it was shown that the RF NP formulations were effectively retained within the lungs.

Another study investigating nano- in microparticular formulations of RF was released in 2009 by Ohashi et al. [113]. Here, nanoparticles composed of RF and PLGA (50:50) were incorporated into mannitol MPs, using a spray drying method facilitating one step *in situ* preparation and encapsulation of NPs by means of a four fluid nozzle. Additionally, another microparticulate formulation of RF and mannitol was prepared for *in vivo* uptake studies. As a reference, RF/PLGA MPs were prepared using a two-fluid nozzle. Particles obtained show spherical morphology with a smooth, or corrugated surface for nano- in micro- and microparticles respectively. For aerosol testing (RF/mannitol microparticles were not assessed in this study), powder samples were dispensed from a Jethaler device and analyzed using a 28.3 L/min 8-stage ACI, and both formulations tested showed FPFs of approximately 35%. *In*

*vitro* macrophage uptake of nanoparticles was shown in a cell culture study, using NR8383 rat macrophage cells. *In vivo* deposition and macrophage uptake was investigated after intratracheal insufflation of test formulations, in which RF was substituted by indocyanine green, by fluorescence imaging. It was shown that PLGA microparticles were removed from the lower regions of the lung within one hour, which was attributed to mucociliary clearance. Contrary, microcarriers of mannitol were shown to dissolve and release PLGA NPs, which were found to be persistent in the lungs and were taken up by macrophages.

A different approach was reported by Son and McConville in 2012 [114]. In this study PLGA and PLA were not used as matrix forming polymer but to coat RF MPs, which had been recrystallized from EtOH, in order to achieve sustained release. Coating was achieved by co spray drying suspensions of RF in EtOH and solutions of PLA or PLGA (75:25) in DCM using a three-fluid nozzle. Reference formulations of RF dihydrate (suspension in EtOH, also see section discussing excipient free formulations) and amorphous RF/PLGA or PLA (dissolved in DCM) matrix MPs were produced by spray drying, using a two-fluid nozzle. For aerosol testing, powders were aerosolized using the Aerolizer DPI and classified by NGI at 60 L/min. Formulations containing polymer yielded FPFs in the range from 24-45%, whereas the crystalline, uncoated reference performed significantly better yielding 70% of fine particles. It is to be mentioned that the Aerolizer device generates a pressure drop of 4 kPa at about 110 L/min, which limits comparability of the results to other studies and might actually underestimate powder performance in an *in vivo* setting. Dissolution studies confirmed sustained release for polymeric formulations, and extent of retardation was found more pronounced in the case of PLA, when compared to the PLGA particles. In case of the PLGA particles, coated formulations showed slower release, whereas PLA coated MPs showed opposite behavior. Crystalline formulations prepared were found stable upon storage for six months, whereas amorphous formulation showed certain degradation.

Lipid formulations of RF

Another class of excipients that has widely been used to produce micro- and nano- carrier systems, are lipids. The term ‘lipid’ includes a wide range of hydrophobic biomolecules e.g. mono-, di-, and triglycerides, fatty acids, steroids, and waxes [115]. Phospholipids, e.g.

phosphatidylcholine, display the ability to form bilayers in aqueous environment, which is due to polar and non-polar entities within the molecule. This can be utilized to form uni-, oligo-, or multilamellar liposomes, and number of lamellae can effectively be controlled during manufacture. Here, phospholipid bilayers form spherical vesicles that encapsulate an aqueous core. Hydrophilic drugs can be incorporated into the liquid core while hydrophobic drugs can be incorporated into the bilayers. In order to modify properties such as membrane fluidity, other lipid excipients, e.g. cholesterol, can be incorporated into the membrane [116]. Solid lipid micro-/nanoparticles can be obtained by using solid lipids, e.g. Na-stearate, and may offer certain advantages for the formulation including sustained release [115]. Excipients used commonly are of biological origin but fully synthetic qualities are available in many cases.

The first study investigating aerosol properties of RF loaded liposomes was published in 2008 by Changsan et al. [117]. Blank liposomes, which consisted of different ratios of cholesterol and phosphatidylcholine, were prepared using a film rehydration method and loaded with RF. Liposomes produced were in the size range of 220-260 nm and showed drug encapsulation efficiencies of 30-50%. To generate aerosolizable powders, the selected liposome formulation was freeze dried, and included the addition of different carbohydrates (trehalose, lactose, and mannitol) that acted as cryoprotecting and matrix forming excipients. Six week storage stability of RF was investigated for the liposome powders and suspensions, as well as a control solution of RF at 4 °C and ambient temperature. Unless subjected to cooling, freeze dried test formulations were found to be unstable, with an approximate 20% reduction in drug content. All other formulations showed significant decrease in drug content regardless the storage conditions. Aerosol testing was conducted by dispensing the dry powder formulations from an unspecified DPI device, analyzing the resulting aerosol using a 60 L/min ACI. Unfortunately, not only the DPI specifications, but also the exact make of the ACI remain unclear, as size cut-offs reported and stage set up do not match expectations, assuming device manufacture according to critical dimensions as specified in USP or Ph.Eur. FPFs achieved are reported as 32, 28, and 67% for formulations containing trehalose, lactose, and mannitol respectively. A single dose for each formulation assessed, was reported to deliver 50 µg of RF, which might be insufficient for effective TB treatment. In a second publication by this group, liposomes previously described were investigated in terms of lung epithelial and

alveolar macrophage cell toxicity, using an *in vitro* cell culture model [118]. It was concluded that the liposomes produced were non-inflammatory and non-toxic.

In 2013, Kumar et al. reported manufacture and assessment of cationic lipopolymeric nanomicelles composed of RF and stearic acid, which was covalently conjugated with polyethylenimine (SABPEI) [119]. RF and SABPEI were dissolved in DCM/MeOH and spray dried under an inert nitrogen atmosphere, using a two-fluid nozzle. Amongst other tests, resultant powders were assessed for physical characteristics, *in vitro* drug release, loading efficiency, and aerosol properties. Aerosol properties were determined using an 8-stage ACI at a flow rate of 28.3 L/min. Dry powders were dispensed from a Rotahaler device and the assembly was actuated for one minute. It was reported that only particles deposited on the stages were included for determination of the FPF, which was defined as the relative deposition on S2-S5. FPF of the test formulation was reported as 68%, which was probably over estimated, due to the fact that only an unspecified fraction of the bulk sample was considered for analysis. It should be mentioned that SEM images also showed a binary blend of the spray dried product with lactose monohydrate carrier particles, and lactose monohydrate is listed in the materials section but was never referred to again in any method. Unfortunately, due to poor methodology, the aerosol testing reported was impossible to evaluate. Drug loading efficiency of the spray dried powders was found to be 99% yielding particles with approximately 50% w/w API content. Dissolution studies showed a more rapid release from the test formulation, when compared to bulk RF control powder. However, it should be noted that dissolution experiments were carried out in non-sink conditions, so this may have affected the overall drug release characteristics.

A different approach to increase aerosolizability of RF loaded liposomes was reported by Manca et al. in 2014 [120]. Here, liposomal vesicles composed of phosphatidylcholine, hydrogenated phosphatidylcholine, and cholesterol were hydrated in an aqueous dextrose solution, sonicated using an ultrasonic probe, and surface modified with chitosan and carrageenan. Suspensions of liposomes obtained were then spray dried with lactose and calcium carbonate to produce inhalable dry powders. For aerosol testing, doses of 3 mg of dry powders were filled into size two gelatine capsules and aerosolized using the Turbospin device. Aerosol assessment was conducted using the NGI at a flow rate of 70 L/min. Uncoated liposomes showed insufficient aerosol properties, whereas surface modified

formulations were found to perform significantly better, yielding FPFs of about 50%. Additionally, cell uptake and toxicity of liposomal formulations was assessed in an *in vitro* cell culture model, using A549 alveolar epithelial cells. It was found that liposomes were less toxic (MTT assay) to this cell line when compared to suspensions of free RF and were internalized by the cells, which was assessed by fluorescence labelling and confocal laser scanning microscopy (CLSM).

In 2015, another study investigating RF loaded liposomes for pulmonary delivery was published by Patil et al. [121]. In this study, different liposomal formulations were freeze dried using sucrose as a cryoprotectant and analyzed for aerosol properties, *in vitro* drug release, *in vitro* anti-microbial activity, solid state properties, and *in vivo* pharmacokinetics after intratracheal or peroral instillation. Liposomes consisting of cholesterol and lecithin were prepared using a thin film hydration method. Aerosol assessment of the optimized formulation is reported, but unfortunately it is unclear what exact method was used, as description indicates consecutive use of a 60 L/min ACI and an unspecified three stage glass impinger. It is also unclear which device was used for dry powder aerosolization. However, it is reported that the optimized formulation yielded a FPF of 26%, which is fairly low in comparison to FPFs achieved in other studies already discussed that use liposomal formulations. *In vitro* activity testing indicated higher efficiency than free RF but lower efficiency than control groups (free ciprofloxacin 10.0 µg/mL and free streptomycin 7.5 µg/mL). *In vivo* data suggests an increase in bioavailability after administration via the pulmonary route. It is to be mentioned that interpretation of results presented in this study is highly compromised by inaccurate description of the methods as well as poor data presentation.

Manufacture and assessment of RF loaded lipid microspheres was reported by Singh et al. in 2015 [122]. RF and soybean phospholipids (Lipoid S75, Lipoid, Ludwigshafen, Germany) were dissolved in DCM, spray dried, and then analyzed for physicochemical and aerosol properties as well as *in vivo* pharmacokinetics at the target organ, and deposition. Aerosol testing was conducted using an 8-stage ACI, operated at 28.3 L/min. Powders were aerosolized from an unknown, apparently capsule based, DPI. FPF, defined as the cumulative mass recovered from S2-S7 divided by the mass initially loaded into the capsule, was reported as 78%, which is somewhat confusing, as cumulative device (determined indirectly via

emitted fraction (EF) of 80%), s0 (approx. 5%), and s1 (approx. 8%) deposition are reported as approx. 33%. EF was defined as relative mass in the capsule prior to and after actuation, which actually over predicts the EF, as powder adhering to the device was ignored. Additionally, IP and preseparator deposition were not reported, which compromises evaluation of the data presented. In animal experiments using rats, test (lipid microspheres suspended in saline) and reference formulations (RF suspended in saline) were applied using a jet nebulizer and selected organs (lungs, heart, liver, kidneys, spleen) were harvested at pre-set time points. The authors concluded an eightfold increase in relative RF lung deposition for the lipid microsphere formulations, which was based on evaluation of the AUC determined in lung tissue. However, this method of extraction from the recovered tissues was not reported and one might suspect that not only the amount of RF released was analyzed, but also RF still entrapped within the microspheres, which would not be subject to systemic distribution and elimination. Neither *in vitro* drug release nor *in vitro* cell uptake was determined, so the only valid conclusion drawn from this experimental setup was that the lipid microspheres persisted in the lungs. Transferability of this study to a proposed dry powder application is limited, as surface properties of hydrated microparticles are expected to differ significantly from dry microparticles, which would need time for equilibration at the site of action.

The first study investigating aerosol performance of formulations comprising solid lipid nanoparticles (SLNP) was reported in 2016 by Maretti et al. [123]. SLNPs were manufactured by dissolving RF in stearic acid with the application of heat and emulsifying the lipid phase in an aqueous solution of sodium taurocholate using ultra sonification. The resultant particles were purified by dialysis and subsequently freeze dried, using mannitol or trehalose as a cryoprotectant. A two level full factorial design of experiments (DoE) approach was conducted to investigate and optimize formulation and process characteristics. Aerosol testing was conducted using an abbreviated ACI setup (fast screening imapctor, Copley scientific, Nottingham, UK) consisting of two stages separating aerosols into two, i.e. coarse and fine, particle fractions. The CI was operated at 60 L/min. Powders where filled into size three HPMC capsules and aerosolized using the Plastiape RS01 device. It is unclear, if the 100 L/min or 65 L/min make of the device was used, so this experimental setup might actually underestimate *in vivo* aerosol performance. Using this experimental setup, FPFs of 9-70% were achieved. The main conclusion after evaluation of the DoE data was that rapid freezing in combination with sample dilution provides process conditions that permit omission of the

cryoprotectant. Omission of the cryoprotectant was considered to be beneficial for the feasibility in pulmonary therapy. Another study, published by the same group in 2017, investigated mannosylated SLNP with a slightly different composition [124]. Here, cholesteryl myristate mixed with either palmitic acid or tripalmitin was melted with RF and emulsified into aqueous solutions of either sodium taurocholate or sodium taurocholate with methyl α-D-mannopyranoside. Resulting SLNP suspensions were then freeze dried using optimized conditions determined in the previous study. Amongst other tests, formulations investigated were assessed for *in vitro* cell toxicity and particle uptake (J774 murine macrophage cells), and aerosol properties. Aerosol properties were determined using the NGI. Dry powders were filled into size three capsules and dispensed from the Plastiape RS01 device, which required a flow rate of 60 L/min to generate the required pressure drop of 4 kPa in order to comply with USP and Ph.Eur. requirements. One might assume that this make of the DPI was also used in the previous study. Though achieving high EFs (>89%) for all formulations, FPFs in this study were found to be fairly low (3-25%), which was attributed to the cohesiveness of the formulations. Furthermore, functionalized SLNPs were found to be taken up more rapidly by macrophages, though the overall extent, after 6 hours was found to be identical to the control group.

A highly interesting study published by Srichana et al. in 2016 reports human *in vivo* toxicological data after administration of RF loaded lipid microparticles using a novel DPI device [125]. To manufacture respirable particles, soy bean lecithin and cholesterol were dissolved in a mixture of ethanol and water (2:1). After lecithin/cholesterol dissolution, mannitol spheres of 2 µm as well as RF were added, which yielded a suspension of the mannitol spheres in the hydroalcoholic solution. The suspension was then spray dried. Powders were filled into size three capsules and dispensed from a novel low intrinsic resistance $1.0 \times 10^{-2}(\sqrt{kPa} * min)/L$ DPI device. Not much information is provided about the device but apparently it utilized a capsule opening mechanism similar to that of the Rotahaler, and its design included a mesh at the inlet of the mouthpiece. Aerosol testing was conducted using an 8-stage ACI at a flow rate of 60 L/min. The FPF for the RF formulation was determined as 37% and the MMAD was approximately three µm. During *in vivo* assessment of the formulation using data gathered from 39 participants, no intervention related adverse effects were observed. Also, blood marker levels were comparable for all groups, indicating good short-term tolerability of inhaled RF.

RF formulations including chitosan

Chitosan is a biopolymer that is obtained after the hydrolytic deacetylation of chitin (poly-(N-acetyl-D-glucosamine)), which can be extracted from, e.g. crustacean shells. Depending on the degree of deacetylation as well as molecular weight, different chitosan properties can be obtained (e.g. viscosity, acidity, or solubility). With the protonation of free amino groups, chitosan shows increased solubility in acidic environments and is capable of forming salts. Thus, aqueous solubility is also strongly depending on the ion strength of the solvent [126]. Nanoparticles formed from chitosan typically show a positive zeta potential.

The first study providing aerosol data with chitosan containing microparticles was published in 2014 by Kundawala et al. [127]. Particles were manufactured as follows: RF was dissolved in EtOH before adding a watery solution of ascorbic acid and chitosan, which was precipitated by adding pentasodiumtriphosphate (TPP). Leucin and lactose were added as structural excipients before spray drying the suspension obtained. Resultant powders were characterized by determination of solid-state properties, drug loading/encapsulation efficiency, particle sizing, aerosol testing, and *in vitro* dissolution. Additionally, pharmacokinetics was studied post intratracheal insufflation into rats. Particles produced, showed a corrugated spherical shape, when analyzed using a scanning electron microscope (SEM). Aerosol testing was conducted using an 8 stage ACI at a flow rate of 60 L/min and powders were dispensed from an unspecified, capsule based DPI. FPFs reported are in the range of 55-62%. In this publication, FPF was determined by relating the cumulative mass recovered from all stages to the total mass recovered, which was likely to over predict actual aerosol performance. As only characteristic numbers (i.e. MMAD, GSD, FPF, and EF) were reported, evaluation of results presented is somewhat compromised. However, low MMADs of about three µm indicate the potential to obtain suitable aerosol properties. *In vitro* release studies conducted in pH 7.4 phosphate buffer showed sustained release for all formulations. It should be mentioned that the solubility of chitosan is pH dependant, so different release kinetics might be expected upon release at the target site. *In vivo* studies assessing RF blood levels after peroral or pulmonary application, verified delayed onset and longer plasma half-life for the test formulations, which was attributed to sustained release from the delivery system.

Pai et al. published another study investigating respirable chitosan particles in 2016 [128]. Chitosan MPs were prepared in a similar way as previously discussed but were not incorporated into leucine/lactose particles, but formulated as binary blend with lactose monohydrate. To briefly summarize, chitosan and RF were dissolved in 0.1 N acetic acid and chitosan was cross-linked/precipitated using TPP. Resultant suspension was then spray dried, and the dry powder obtained was blended with lactose carriers. Characterization included solid state and aerosol characterization, *in vitro* dissolution testing, *in vitro* macrophage uptake, and *in vivo* toxicity studies of MP suspensions. Aerosol characterization was carried out using a 28.3 L/min ACI. Dry powders were dispensed using the Lupihaler device. FPFs obtained were found to be below 25%, which might partially be attributed to the low operational flow rate of the ACI, which is insufficient for the Lupihaler to perform properly. *In vitro* dissolution studies showed modified release for some formulations but proper evaluation of the release properties was compromised by the premature termination of the experiment. *In vivo* toxicity assessment showed good short-term tolerability of the MPs.

In 2017 Rawal et al. investigated *in vitro* and *in vivo* performance of chitosan nanoparticles [129]. In this study, chitosan nanoparticles were prepared using a method similar to the ones previously described, involving dissolution of chitosan and RF in acetic acid, followed by chitosan crosslinking and precipitation using TPP. In contrast to previous studies, inhalable particles were obtained by freeze drying the resulting suspensions, and lactose was used as cryoprotectant. Formulations were optimized in terms of size and drug loading. The optimized formulation was then blended with coarse lactose carriers. Characterization included determination of solid state properties as well as *in vitro* dissolution, aerosol, stability, and cell toxicity testing using J774 murine macrophages. Additionally, *in vitro* acute toxicity and pulmonary pharmacokinetic studies were conducted, using rats. Aerosol testing was conducted using an ACI of unknown specification. Also the DPI device used, remains unclear. Aerosol data of one optimized formulation only was reported with a FPF of 33%. Due to the fact that not much information about the device and operating conditions, as well as only MMAD, FPF, and GSD are provided, proper evaluation of the aerosol performance is compromised, but the results presented appear to align with studies previously discussed. Also, results from dissolution and cell culture studies are in line with previous publications showing sustained release and low cell toxicity. *In vivo* studies comparing the test formulation

to a binary blend of micronized RF and a perorally instilled RF solution, showed prolonged persistence of RF in the lungs in the case of the NPs. However, the method of pulmonary application is not reported and application of more than 300 mg/KGBW seems fairly high, but probably was found necessary due to the low drug loading of 13% w/w.

Carbohydrates

Besides sugars, carbohydrates used in the studies presented include a wide variety of mono-oligo-, or polymeric sugar derived excipients like sugar alcohols, cyclodextrins, or alginate. Sugars and sugar alcohols typically have applications as matrix forming excipients to incorporate free drug or for example, nanoparticles. In contrast, cyclodextrins are used as solubility enhancers that also might act as structural excipients. Another interesting field of application investigated is the utilization of carbohydrate excipients, such as mannan or guar gum, to proactively target microparticles to alveolar macrophages by means of mannose receptor mediated internalization.

Co spray drying of RF and mannitol solutions, using a four fluid nozzle, was investigated by Mizoe et al. in 2008 [130], and presented a one step approach to incorporate RF into mannitol microspheres. It should be mentioned that this study was conducted by the same group that later had published another study, previously discussed in the PLGA section [113]. Manufacture of MPs was executed by dissolving RF in a mixture of acetone and ethylacetate, which was then co spray dried with a solution of mannitol in water. Both feed solutions were supplied to different channels of the four-fluid nozzle. In order to achieve sustained release from the particles additional batches containing lipids were prepared. However, the sustained release batches were not subjected to aerosol or solid-state characterization and were only used for *in vivo* experiments. SEM images probably show collapsed spheres, but in depth evaluation is compromised by insufficient image quality. Aerosol testing was conducted using an eight stage ACI at a flow rate of 28.3 L/min and dry powders were dispensed using the Jethaler device. Samples characterized showed moderate to low inhaler, and moderate preseparator deposition. IP deposition was found to be fairly high (about 30-35%). S2-S7 deposition was in the range of 35-43% indicating acceptable overall performance. *In vivo* studies investigating pharmacokinetics after intratracheal administration showed rapid onset and elimination of RF from the blood, which was attributed to a low residence time of RF-

mannitol MPs in the lungs. To overcome this issue, additional formulations containing lipids were investigated but this altered strategy was found to have little effect on the outcome. The second study of that group [113] mentioned earlier in this paragraph was conducted to overcome this issue by adding PLGA to the microspheres.

An interesting study on the synthesis, characterization, and toxicological evaluation of a novel lipopolysaccharide, intended for use as matrix forming polymer for inhalable MPs, was published by Vadakkan et al. in 2015 [131]. Stearyl amine was grafted onto dextran with two different degrees of substitution, and resulting lipopolysaccharides, were formulated into RF loaded MPs, using a spray drying method. One formulation with unmodified dextran was sprayed as reference. Distribution and toxicity of the grafted polymers was investigated *in vivo* using rats as well as in *in vitro* cell culture studies using THP-1 (human monocytic) cells. Aerosol testing was conducted using an eight stage ACI at a flow rate of 60 L/min. Powders were dispensed from an unknown inhaler. FPFs were determined as 63%, 75%, and 78% for the dextran and low and high degree of substitution particles, respectively. Unfortunately, the authors fail to provide full deposition data including DPI and IP deposition (use of a preseparator unit is not mentioned), which would have been desirable to strengthen the excellent results reported. Interestingly, drug loading was limited to 25% and it would have been highly interesting to see how the particles might have performed at higher drug loading. *In vitro* and *in vivo* toxicity experiments indicated biocompatibility but divergent results regarding toxicity were obtained from *in vivo* and *in vitro* experiments. *In vivo* studies showed a certain degree of pathological alteration of the target issue, which was attributed to the long residence time of the particles in the lungs. However, these results could not be confirmed *in vitro*.

In 2015 and 2016, Goyal et al. published results of two studies investigating chitosan, mannan, guar gum, and guar gum decorated chitosan nanoparticles that were incorporated into mannitol/leucine MPs by spray drying, in order to obtain a respirable formulation [132]. Firstly, chitosan, guar gum, and mannan nanoparticles loaded with RF were prepared using the ionic gelation method, already described in the chitosan section above, antisolvent precipitation, or spray drying respectively. In an additional second step, mannitol and leucin were added to the nanoparticulate suspension, which was subsequently spray dried. Samples were characterized for their solid state properties, *in vitro* dissolution, aerosol performance,

and AJ774 macrophage toxicity and uptake, as well as *in vivo* lung deposition and pharmacokinetics. Additionally, efficacy of the formulations was tested using an *in vivo* infection model (2016 study [133]). It should be mentioned that all experiments were also carried out using isoniazid, but these results are not discussed here as they are outside the scope of this text. Aerosol testing was conducted using an ACI that was coupled to a jet mill collection vessel at a flow rate of 5 L/min, dispensing 2 g of sample from an unknown device. The method reported is not easily understood and obviously deviates from the standard procedure of aerosol characterization using cascade impactors, which may have highly compromised evaluation of the results, if they were presented. Only MMADs (i.e. missing FPF, GSD, and ED) being in the range of 1.2-1.9 µm were reported, this was found to be insufficient for valid scientific evaluation. Nonetheless, *in vivo* γ-scintigraphic studies showed inhomogenous lung deposition, since different formulations applied seem to accumulate at different locations. This was evaluated as beneficial in the 2015 publication, as one 'target' spot was identified as region with the highest prevalence of lesions associated with TB, but targeting could not be confirmed in the 2016 study, where a similar formulation accumulated elsewhere. *In vitro* macrophage cell uptake assay showed equivalence in uptake of chitosan, guar gum, and guar gum decorated chitosan nanoparticles after eight hours, whereas mannan nanoparticles showed slightly lower uptake, over the same period. Interestingly, uptake after eight hours was found significantly lower than after 2 or 4 hours in the case of mannan nanoparticles, which had not been commented. Decorated chitosan, guar gum and mannan nanoparticles were found to be taken up more rapidly, which was associated to receptor mediated phagocytosis. Minor increase in the uptake of guar gum decorated nanoparticles over chitosan nanoparticles was found in the 2016 study. *In vitro* dissolution studies showed sustained release at a similar degree of retention for all formulations. *In vivo* infectious disease model indicated superior performance of guar gum decorated chitosan nanoparticles over chitosan nanoparticles and free drugs respectively.

In 2015, Garg et al. investigated feasibility of RF loaded alginate nanoparticles for pulmonary application [134]. Alginate particles, prepared by an ionotropic gelation technique, were loaded with RF or isoniazid and subsequently spray dried, incorporating mannitol and leucine as structural excipients. Samples were characterized for their solid state properties, *in vitro* dissolution, aerosol testing, and cell toxicity, as well as *in vivo* lung distribution and organ pharmacokinetics. Aerosol testing was carried out using an ACI coupled to a jet mill

collection vessel at a flow rate of 5 L/min. The DPI device used was not reported, but the sample size was 2 g. Limitations of this type of experimental setup have already been discussed in the previous paragraph. MMADs of test formulations were found to be "ranging from 1 to 2 μm", from which the authors deduced preferred deposition in the posterior part of the lungs. *In vitro* dissolution studies confirmed sustained release for both formulations. *In vivo* lung deposition studies showed accumulation of the formulation in a specific lung location, which is in accordance with other results already discussed (see previous paragraph, 2016 study). *In vitro* toxicity studies showed good tolerability of alginate nanoparticles. *In vivo* pharmacokinetic studies showed sustained release and increased bioavailability for both nanoparticulate formulations.

Mesoporous silica

One study published in 2015 by Mohseni et al. reported the investigation of mesoporous silica aggregates as a potential carrier system for RF [135]. Here, in-house synthesized mesoporous particles were passively loaded with RF and spray dried under various conditions, using a half factorial design DoE approach. Particles were assessed for solid state characteristics, as well as *in vitro* dissolution, and aerosol performance. Aerosol performance was determined using the ACI at 50 L/min after dispensing dry powders from the Cyclohaler device. It should be mentioned that using the ACI a 50 L/min flow rate is unusual and does not comply with the USP or Ph.Eur., as calibration at that flow rate is not fully established. MMAD of all formulations investigated were used as responses in the DoE, which must be considered as inadequate as MMAD is not always correlated to deagglomeration and aerosolization of a given formulation, and can give no information about the actual efficiency of said formulation. Particles of small geometric diameter might display very small MMADs for example, but might be highly cohesive and so may not be easily deagglomerated, which could lead to impaction in the upper airways. Bearing in mind that one of the main reasons for inhalable RF therapy development is to reduce systemic exposure in order to avoid unwanted side effects, FPF would have been the more appropriate response parameter. Unfortunately, incomplete aerosol data was reported for only one formulation (which should be expected to be the optimized formulation); indicating an FPF of 46% and an EF of 83%. Despite this being a decent result, one might assume that the actual potential of the formulation might not

have been realized, and that using the Cyclohaler at a standardized flow rate equivalent to a pressure drop of 4 kPa for the device could have yielded higher FPFs. On the other hand, higher airflow velocities could induce higher triboelectric charges, so one must conclude that this study could have been more meaningful, if data acquired would have been processed in a more adequate way.

Excipient free formulations

The following section describes formulation strategies that do not involve the use of excipients, and are aimed at maximizing drug loading of a respirable formulation. Since drug dose quantities that can effectively be aerosolized are limited, high potency formulation approaches (i.e. high API loading) may be desirable unless efficient drug targeting to the site of infection (e.g. alveolar macrophages) is involved. Excipients often times are found to be necessary to produce fine powders that are easily de-agglomerated, or might aid proactive uptake of the API by macrophages. Excipient free approaches usually involve effective particle engineering by for example, spray drying or other suitable techniques.

The first study reporting an excipient free formulation of inhalable RF MPs was published by Son and McConville in 2011 [91]. RF was recrystallized from anhydrous ethanol and the resulting suspension was subsequently spray dried, using a two fluid nozzle. As a reference, another formulation yielding amorphous RF particles was spray dried from a solution of RF in DCM. Samples were assessed for solid state properties and stability, as well as *in vivo* dissolution and aerosol testing. SEM images showed flake like crystals and corrugated spheres for the test and reference formulations respectively. Aerosol testing was carried out using the NGI at a flow rate of 60 L/min. Dry powders were aerosolized using either the Handihaler, or Aerolizer device. FPFs of test formulation dispensed from the Handihaler device at capsule loading of 7, 15, and 30 mg were found to be 59%, 64%, and 60% respectively. Performance with the Aerolizer device was slightly higher, generating a FPF of 69%. The control formulation showed FPFs of 51% and 37% using the Handihaler and Aerolizer devices, respectively. It should be mentioned that the aerosol analysis at a flow rate of 60 L/min was a deviation from standard USP and Ph.Eur protocol, as the Handihaler and Aerolizer devices generate a pressure drop of 4 kPa at flow rates of about 40 L/min and 110 L/min respectively. Interestingly the test formulation was found to perform better on the

Aerolizer, whereas the reference formulation displayed better performance on the Handihaler, which was due to pronounced powder retention within the capsule. It was hypothesized that, being a high resistance device, more energy was imparted to aid de-agglomeration using the Handihaler at given flow rate, which suited better de-agglomeration in the case of the reference formulation. Contrary, larger apertures in the capsule after punctuation with the Handihaler would facilitate premature ejection of powder agglomerates, in case of the test formulation. Dissolution testing was conducted using a novel test method for aerosols, which had previously been developed by the same group, where powder samples are recovered from the NGI stages (particularly S3) and subjected to dissolution experiments, and immediate release was shown for both formulations. Crystals obtained were characterized as RF-dihydrate, which was based on thermogravimetric analysis. Formation of a co-crystalline system was also indicated by XRPD and DSC analyses. However, no identifying assay (e.g. Karl Fisher titration) was conducted to confirm that loss on drying observed was actually caused by evaporation of water from the crystals. Stability studies conducted at ambient conditions over a period of 9 months confirmed chemical stability of the test sample, whereas the reference was found to show pronounced degradation.

Another study conducted by Parikh, Patel, and Dalwadi in 2014 reported *in vivo* assessment of the amorphous reference formulation of the study previously discussed [136]. Manufacture of amorphous RF particles was facilitated by spray drying solutions of RF from DCM. Samples were characterized for *in vitro* dissolution and aerosol properties, as well for *in vivo* pharmacokinetics after intratracheal and peroral administration. Aerosol characterization was carried out using an 8-stage ACI at unknown flow rate. Also unknown was the device that was used to aerosolize the dry powders. The test formulation showed a FPF of 78% and an EF of 59%. As the FPF reported is higher than the actual fraction emitted it is to be assumed that the FPF reported is related to the emitted fraction, rather than the whole sample. Thus, the adjusted $FPF_{total}$ would be 46%, which is in reasonable agreement with the study conducted by Son and McConville (2011). *In vitro* dissolution studies using simulated gastric (pH 1.2) and phagosomal (pH 4.5) fluid showed pH dependent drug release, exhibiting more rapid release in the more acidic environment, which is in good agreement with literature. *In vivo* pharmacokinetic studies showed higher bioavailability and shorter onset time, if the formulation is administered through the pulmonary route, which also is in good agreement with literature.

In a study published by Rawal et al. in 2017, *in vitro* and *in vivo* performance of an optimized binary blend of micronized RF with lactose carrier particles was reported [137]. Using a DoE approach, the authors determined the most appropriate drug/coarse and fine lactose ratio and besides flow properties and blend and content uniformity, FPFs yielded were the primary responses. Unfortunately, the method of micronization was not reported. Aerosol testing was conducted using an 8-stage ACI at a flow rate of 30 L/min and dry powders were dispensed using the Rotahaler device. Operating the ACI at 30 L/min is somewhat unusual and additionally probably underestimates aerosol performance, as the pressure drop of 4kPa is generated at a flow rate of about 45 L/min. All formulations assessed yielded FPFs in the range of 23-29% and MMADs from 4.1-5.7 µm. *In vivo* lung pharmacokinetic studies administering the respirable dry powder through an unknown device or a perorally instilled solution of RF, showed comparable results to another study by the same group investigating chitosan nanoparticles, which has already been discussed in the appropriate section above.

#### 1.5.3.2.1 DPI formulations with combined therapy approaches

The first study reporting aerosol testing of a formulation combining multiple antibiotic APIs was published in 2013 by Chan et al. [138]. In this study, RF, pyrazinamide, and isoniazid were dissolved in EtOH/water 50:50 and spray dried in order to produce respirable MPs. As a reference, formulations containing the individual antibiotics only were produced in the same manner. Formulations were characterized for solid state properties, as well as *in vitro* aerosol and dissolution testing. SEM images of formulations including all antibiotics showed spherical particles of different size, displaying a smooth surface. SEM images of control formulations showed large, thin walled, and highly collapsed (RF), agglomerated spherical (isoniazid), and agglomerated brick like (pyrazinamide) particles. Aerosol testing was conducted using a MSLI at a flow rate of 100 L/min. Powder samples were dispensed using the Aerolizer device. Unfortunately, only data of the test formulation is reported showing an FPF of 46%, and a MMAD of 3.5 µm. Interestingly, higher relative concentrations of RF were found in the lower stages of the impactor, which was attributed to inhomogenous distribution and particle fragmentation, which was confirmed using time of flight-secondary ion mass spectrometry (ToF-SIMS). Dissolution studies showed immediate release from the single antibiotic samples. Triple antibiotic samples showed a similar profile, but RF dissolved

at a slightly slower rate. It was concluded that dissolution rates in the triple antibiotic formulation were too high for effective macrophage uptake.

Investigation of another combined drug formulation was published by Zhou et al. in 2014 [139]. In this study, a similar technique was used to formulate RF and colistin, which were spray dried combined and individually from an EtOH/water 50:50 mixture. Analytical methods applied included: solid state characterization, x-ray photoelectron spectroscopy (XPS), ToF-SIMS, and *in vitro* aerosol testing, as well as an evaluation of the antimicrobial activity of isolated, and combined APIs. Aerosol characterization was carried out using a MSLI that was operated at a flow rate of 100 L/min, and powders were aerosolized using the Aerolizer device. SEM images of the formulations showed corrugated spherical and highly collapsed thin walled particles for colistin and RF samples, respectively. The morphology of the combination formulation was similar to that of the RF particles. Aerosolization of test formulations yielded high FPFs of approximately 80%, 90%, and 90% for the colistin, RF, and combination formulations, respectively. As already reported in a previous study, ToF-SIMS and XPS analyses showed that RF predominantly forms the particle shell, and the desirable aerosol properties observed were attributed to the hygrophobicity of RF [138]. Additionally, the impact of relative humidity on aerosol performance was investigated; but only in the case of pure colistin, pronounced differences in FPFs were found. It was hypothesized that RF being present at the particle surface effectively protects the colistin within combined API particles. Administartion of a combined therapy of RF and colistin was found to be more effective against *A. baumannii* bacteria than the individual drugs, and a synergistic effect of both antibiotics was hypothesized.

Another study focusing on the effects of different surface compositions of aforementioned particles was published in 2016 [140]. In order to generate particles with different surface properties, different ratios of RF and colistin were spray dried from EtOH/water 50:50. Analytical procedures reported included: characterization of solid-state properties, XPS, ToF-SIMS, and *in vitro* aerosol testing. Evaluation of the antimicrobial activity of isolated, and combined APIs was conducted using *P. aeruginosa.* SEM images of particles obtained displayed an identical morphology to the particles obtained in the studies presented in the previous paragraphs [138,139]. Aerosol assessment was conducted using the NGI at a flow

rate of 100 L/min and aerosols were dispensed using the Osmohaler device, which is highly similar to the Aerolizer device used in the aforementioned previous studies. FPFs generated using this setup were significantly lower than ones previously reported but still showed excellent performance yielding 69%, 65%, 73%, and 80% for pure RF particles and combined particles at a colistin/RF ratio of 4:1, 1:1, and 1:4, respectively. Lower FPFs generated were attributed to the difference in capsule punctuation mechanism of the respective inhalers: the Aerolizer used in the previous study was a design using 2x4 pins, whereas the Osmohaler used in the present study had a 2x1 pin configuration. XPS and ToF-SIMS confirmed that RF was predominantly present at any colistin to RF ratio, which aligns with conclusions drawn in the previous study. Furthermore, all other results presented in this study were consistent with the previous results.

A study, investigating a combination of three different antibiotic drugs in one respirable formulation, was published by Lee et al. in 2016 [141]. RF, colistin, meropenem, and tigecycline were spray dried individually and in different ternary combinations using a Büchi (Flawil, Switzerland) B-90 nano-spray dryer. Powders were characterized for solid state properties as well as *in vitro* aerosol performance. Additionally, antimicrobial activity was assessed by determination of minimal inhibitory concentrations using antibiotics sensitive and multi drug resistant strains of *P. aeruginosa, E. coli, K. pneumonia, and A. baumanii*. Aerosol testing was conducted using the NGI at a flow rate of 60 L/min and powder samples were dispensed from an Aerolizer device of unknown resistance. Aerosolized dry powders showed a FPF of 55, 54, and 68 for RF, colistin/meropenem/RF, and colistin/tigecycline/RF, respectively.

Another study published in 2017 by Kadota et al. focused on the applicability of different carbohydrates in manufacture of combined RF and isoniazid (INH) MPs using a spray drying process [142]. Briefly summarized, RF and INH as well as carbohydrates (i.e. lactose, sucrose, maltose, β-cyclodextrin, methyl-β-cyclodextrin, and highly branched β-cyclodextrin (HBβCD)) were dissolved in EtOH and water, respectively. Solutions were premixed at a ratio of 3:10 and then spray dried using a two fluid nozzle. Particles obtained were characterized for their solid-state properties, as well as *in vitro* aerosol testing. SEM images show larger agglomerates of highly collapsed nanospheres and only the sample including HBβCD with RF showed individual collapsed spherical particles, which were larger in size.

Aerosol testing was conducted using an ACI at a flow rate set at either 28.3 L/min or 60 L/min. Dry powder samples were filled into HPMC capsules and aerosolized using the Jethaler device. Different formulations investigated yielded FPFs in the range of 3% (INH) to 38% (RF) for single drug formulations with HBβCD, and 25% (sucrose) to 51% (HBβCD) for combined formulations with different sugars. Additionally the combined HBβCD formulation was tested at a flow rate of 60 L/min and yielded a FPF of 53%. FPFs of the best performing formulation assessed did not differ strongly when investigated at different flow rates, which indicated that the Jethaler device provided stable performance across a wide range of flow rates.

In 2018, Momin et al. published two publications investigating a combined dosage form that incorporated RF and kanamycin into one respirable formulation [143,144]. The study design was similar to studies published by Chan et al. [138], Zhou et al. [139], and Wang et al. [140] by investigating surface enrichment of RF. The approach was extended by using a DoE approach to optimize formulation designs: the RF to Kanamycin ratio, the EtOH to water ratio, and process parameters (i.e. inlet temperature), [143]. Kanamycin was chosen as hygroscopic model drug, which was shown to be difficult to formulate into aerosolizable dry powders. Spray drying with RF was utilized to improve particle properties due to its hydrophobicity and shell accumulation propensity; as found in several studies discussed earlier. Surface composition was analysed using ToF-SIMS and XPS, and aerosol testing was conducted using the NGI at 100 L/min after dispensing powder samples from an Aerolizer device. Results of the DoE study included only truncated aerosol data, since only FPFs and EFs were reported. However, but full characterization was provided for the optimized formulation, as well as reference formulations of kanamycin and RF (separately spray dried under optimized conditions). $FPF_{emitted}$s reported were in the range of 82-85% for different batches prepared, which translates to $FPF_{total}$s of 69-78%. $FPF_{emitted}$s were found equivalent, but reference formulations achieved lower EFs (84-85%) than the test formulation (91-92%). All other results presented in this study incl. XPS, ToF-SIMS, solid-state characterization, and *in* vitro cell toxicity were in line with previous studies.

#### 1.5.3.3 Conclusion

A variety of therapeutic strategies to, for example facilitate proactive drug targeting to macrophages, or manufacture high drug load formulations have been investigated. Studies discussed present results from all stages of preclinical to early clinical development, ranging from pre-formulation development to human *in vivo* toxicity studies. Many of the studies described report innovative therapeutic and technological approaches and show high data quality and conclusive evaluation. On the other hand, it was also found that certain studies display poor methodology, data quality, and evaluation. These studies have not been excluded, but their limitations, especially focusing on aerosol testing, have been discussed critically. In general, it was noted that little focus was placed on the long-term stability of the formulations, which actually might be highly critical with respect to the amorphous formulations presented; since amorphous materials have been shown to be prone to degradation. On the other hand, the stability of amorphous active ingredients may be positively influenced by incorporation into a matrix, as has been described in several of the studies. As of now, it is not clear which formulation strategy or therapeutic approach is the most suitable for a more efficient TB therapy, but many promising attempts are in the pipeline. Interestingly, only one study investigating PLGA or PLA formulations was published after 2010, and this study did not utilize the polymers as matrix excipients in order to prepare nano- or microparticles, but as a sustained release coating for an excipient free, particle engineered formulation. From this observation one might conclude that nano- or microparticulate formulation approaches involving PLGA/PLA have been appropriately investigated on a pre-clinical level, but have failed to leap into clinical testing. This stagnation may be due to a variety of reasons that could include: high excipient/manufacturing costs, non-scalability of the processes involved, or even a lack of innovation and intellectual property generated to attract investors. Other formulation strategies, including the use of different excipient classes, multiple drug combinations, or excipient free formulations are still under active investigation and more interesting results are to be expected in the near future.

## 1.6 Aim and scope of the thesis

Aim of this thesis was to develop inhalable and excipient free dry powder particles of the antibiotic drug rifampicin, which is used in first line tuberculosis therapy. The manufacturing

technique to be investigated was spray drying of suspensions and solutions of rifampicin from various solvents. Special focus was set on the determination of the crystallographic properties, aerosol properties, as well as physical and chemical stability of the particles. Additionally, another aim was to investigate the feasibility of using FDM 3D printing to generate a modified induction port to be used with the NGI, in order to provide more biorelevant aerosol testing for the formulations developed.

Chapter one aimed to give a general introduction to aerosol therapy, covering physiological and pathophysiological conditions of the human respiratory tract as well as an introduction to formulation strategies for pulmonary therapeutics and aerosol testing. Special focus was set on experimental tuberculosis therapy using dry powder inhalation devices, which provided the framework of the work presented.

Cascade impactor analysis is an important tool not only to compare different inhalable formulations, but it can also be utilized to predict the performance of a given formulation/device system *in vivo*. In order to provide a more biorelevant testing system for pulmonary formulations, the aim of the studies reported in chapter three was to show the feasibility of applying a rapid prototype technique (fused deposition modeling 3D printing) in combination with patient based 3D imaging, in order to generate a more physiologically relevant induction port, which was based on actual patient data obtained from a computer tomographic scan. The modified induction ports were tested with different, commercially available formulations to a) investigate, which types of formulation are susceptible to tracheal deposition (section 3.1) and b) estimate the quality of the IVIVC. Thus, based on the results obtained in section 3.1, additional commercial formulations were selected based on availability of *in vivo* lung deposition data in literature, so that the quality of the *in vitro* prediction of *in vivo* lung deposition could be assessed (section 3.2).

Chapter four reports the development of respirable rifampicin particles, manufactured using different spray drying methods. Suspensions and solutions of rifampicin in a variety of organic solvents as well as water were investigated and assessed for their suitability to produce particles of distinct shape, aerodynamic performance, or polymorph. In a second study, the most promising candidates from this exploratory trial were investigated more detailed. Special interest in this set of studies was to get a deeper understanding of the mechanism of particle formation and crystallographic behavior of amorphous and crystalline particles obtained respectively. Formulations showing the best aerosol performance were also investigated, using a low performance, disposable inhalation device surrogate in order to

show that these formulations demand low requirements from the DPI only, as well as to use a more discriminating approach to evaluate the quality of suchlike formulations. Additionally, it was of interest to investigate the aerodynamic behavior of the test formulations using the modified cascade impaction experiment developed in chapter three in order to estimate, how the formulations developed would perform *in vivo*.

# 2 Materials and methods

## 2.1 Materials

### 2.1.1 **Active ingredients used**

Chemical structures of the Active ingredients used are shown in Figure 17.

#### 2.1.1.1 Rifampicin

Rifampicin for manufacture of microparticles was obtained from TCI (Tokyo, Japan). Rifampicin as reference material for analytical purposes was obtained from Sigma Aldrich (Saint Louis, MO, USA).

#### 2.1.1.2 Salbutamol sulfate

Salbutamol (SAL, in USA: Albuterol) sulfate was obtained from Alfa Aesar (Thermo Fisher GmbH, Karlsruhe, Germany).

#### 2.1.1.3 Corticosteroids

Beclometasone dipropionate was obtained from TCI (Tokyo, Japan). Fluticasone propionate and Ciclesonide were obtained from Swanpnroop drugs and pharmaceuticals (Maharashtra, India).

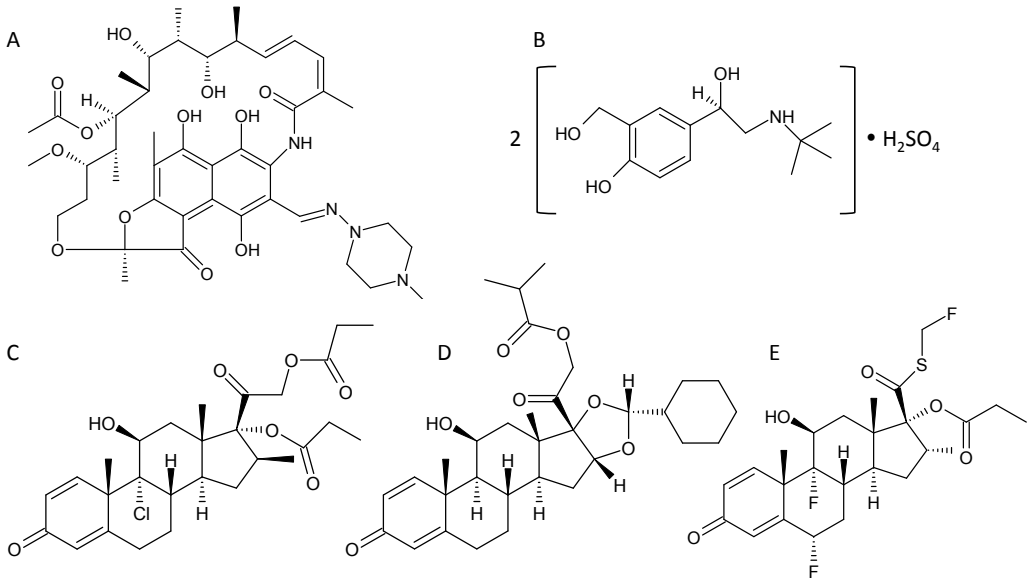


Figure 17. Chemical structures of APIs used: rifampicin (A), salbutamol sulfate (B), ciclesonide (C), beclometasone dipropionate (D), and fluticasone propionate (E).

### 2.1.2 **Commercial formulations**

Table 7 shows an overview on all commercial formulations used. All products were purchased from a local pharmacy.

Table 7. Overview on commercial formulations used.

| **Substance** | **Product name** | **Formulation** | **$m_{drug}$/dose [$\mu$g]** | **Excipients used** | **Manufacturer** |
|---|---|---|---|---|---|
| **Salbutamol sulfate** | Sultanol | pMDI, suspension | 100 | HFA134a | GSK (London, UK) |
| | Sultanol forte | solution for nebulizer | 5000 | Sulfuric acid<br>Benzalkonium chloride<br>Water | |
| | Cyclocaps Cyclohaler | DPI | 400 | Lactose monohydrate | PB Pharma (Meerbusch, Germany) |
| **Beclometasone dipropionate** | Beclohexal | pMDI, solution | 100 | HFA134a<br>Ethanol | Hexal (Holzkirchen, Germany) |
| | Foster (+ Formoterol) | pMDI, solution | 100 | HFA134a<br>Ethanol<br>HCl | GSK (London, UK) |
| **Fluticasone propionate** | Flutide forte | pMDI, suspension | 250 | HFA134a | GSK (London, UK) |
| **Ciclesonide** | Alvesco | pMDI, solution | 160 | HFA134a<br>Ethanol | AstraZeneca (Wedel, Germany) |

### 2.1.3 Additional materials and chemicals

A Pari (Starnberg, Germany) Vortex valved holding chamber (VHC) was purchased from a local pharmacy. PLA filament 3 mm was obtained from Kiboplast (Kirchheimbolanden, Germany). Polyvinylalcohol (PVA, Mowiol® 4-88) and ascorbic acid was obtained from Sigma Aldrich (St. Louis, MO, USA). Dibasic potassiumhydrogenphosphate (Carl Roth GmbH, Karlsruhe, Germany), monobasic sodiumhydrogenphosphate, anhydrous magnesium chloride 99% (both Alfa Aesar, Haverhill, MA, USA), Apura™ Combi Titrant 2 mg/mL, and sodiumtartrate dihydrate (Merck kGaA, Darmstadt, Germany) was obtained from VWR. Water used was purified in house using a purification system (Merck-Millipore, Burlington, MA, USA). Isopropyl alcohol (IPA) and all other solvents used were HPLC grade. Handihaler dry powder inhalers were a kind gift from Boehringer Ingelheim (Ingelheim am Rhein, Germany). Breezhaler dry powder inhalers were a kind gift from a local hospital (Marien-Hospital, Bochum, Germany). Actitube charcoal filters (Berlin, Germany) were obtained from a local source.

## 2.2 Methods

### 2.2.1 Systematic review of publications on inhalable formulations of Rifampicin

Systematic literature review was conducted using the PubMed database [98]. Search term used for primary research was: “(rifampicin) AND (inhalable OR pulmonary delivery OR inhalation OR dry powder OR respirable)”. Primary results were pre- selected as follows: Exclusion of review articles, case studies, epidemiological studies, and experimental studies investigating other routes of applications than the pulmonary one. The data subset acquired was classified for publications reporting and missing aerosol testing respectively. Publications with aerosol testing were finally classified according to the formulation strategy used: i.e. application via DPI, pMDI, nebulizer, or insufflator. All articles reporting dry powder (DPI) aerosol testing were discussed.

### 2.2.2 Manufacture of 3D printed objects

A 3D model of a human trachea was retrieved from a CT dataset from the Gene Expression Omnibus database [58]. Digital Imaging and Communications in Medicine files were

reconstructed, cropped, cleaned up, and exported using ImageJ [145] with BoneJ [146] plugin. The final model was merged with adaptor fittings modeled with OpenSCAD [147] using Blender [148] (mIP). The model file for a 3D printed version of the USP IP (USPIP, USP3DIP) was generated according to USP specifications using OpenSCAD. Additionally, another modified USP IP (USP3DSEIP) showing an increased inner surface area, matching the one of the mIP but maintaining the basic geometry of the USPIP, was generated using the Blender software. Surface area of the model was determined using a computational approach by removing vertices not participating in the inner surface of the model and calculating the surface area of the remnants. To generate the USP3DSEIP model, a cylinder was inserted into the lower segment of the USP3DIP model. Gcode was generated using Slic3r [149]. Another modification of the mIP was introduced by replacing the distal section of the IP by its USPIP counterpart, thus generating a model with physiological relevant trachea and idealized MT section (mIPext). All models were 3D printed using a X400 3D printer (GermanRepRap, Feldkirchen, Germany), equipped with two 0.5 mm nozzles. The printed model was fine-tuned to fit, using sand paper (type kk114F, G80 G600, VSM AG; Hannover, Germany) and polishing paste (grade for acryl glasses and plastics, Mellerud Chemie GmbH, Brüggen (Niederrhein), Germany). The 3D printing parameters were set as follows: extruder temperature= 200 °C, bed temperature= 50 °C, layer height= 0.3 mm. To achieve optimum printout adhesion, the print bed was coated with 0.5 % w/v PVA solution.

### 2.2.3 **Assessment of air tightness of 3D printed objects**

Prior to use, all 3D printed models were tested for air tightness. The outlet of each test object was connected to a Dosage Unit Sampling Apparatus for DPIs (Copley scientific, Nottingham, UK), and the inlet was sealed, and the pressure drop at maximum pump capacity was recorded. Intrinsic resistance of all test objects and the USPIP was determined using the same setup. To evaluate the quality of the connecting elements, airflow consistency over the test objects was evaluated by following procedure: (1) the NGI was assembled (as used in a standard cascade impactor experiment) with the USPIP and an airflow meter (DFM 2000, Copley scientific, Nottingham, UK) was connected using a modified mouthpiece adapter. (2) The flow rate was then adjusted, sequentially, to predefined rates: 10, 20, 30, 40, 50, 60, 70, 80, 90, and 100 L/min. with the IP being replaced with the test object at each flow rate. (3)

Deviation from each airflow rate at the inlet was noted (n= 1).

### 2.2.4 **Computational fluid dynamics (CFD)**

Airflow velocities over the USPIP and mIP that would have occurred during NGI assessment (below) at given conditions (i.e. pMDI setup), as well as airflow fields over the disposable inhaler model (ACT), were simulated using an OpenFOAM 3.01 linux distribution [150]. An additional simulation for the USP3DIP was omitted as it is identical to the USPIP. 3D meshes were generated from lithography files using SnappyHexMesh. PimpleFoam, a transient large time-step solver for incompressible fluids using a PISO based algorithm, was used to numerically solve the Navier-Stokes-Equations. Additionally, a standard k-ω turbulence model at a turbulence level of 5%, as proposed by [151] was implied. Results were visualized using ParaView. All software tools used are included in the OpenFOAM 3.01 toolbox. Figure 18 illustrates the workflow of computational fluid dynamics studies.

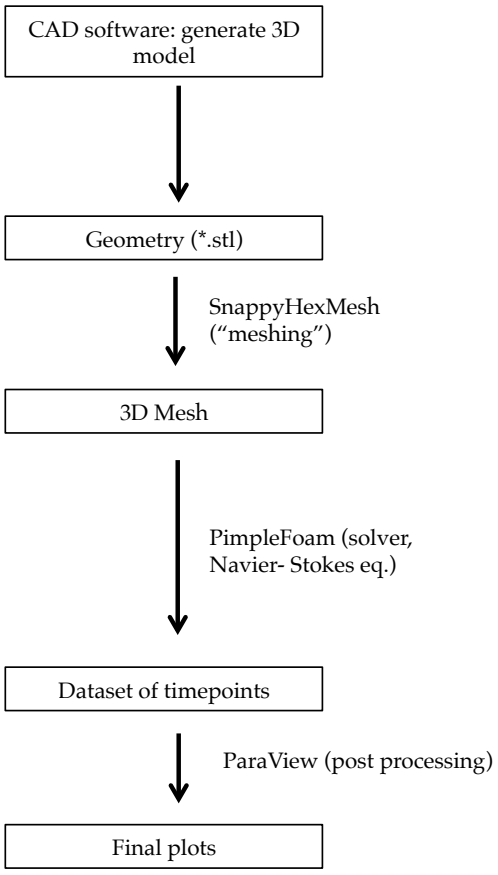


Figure 18. Work flow of CFD studies.

### 2.2.5 **Manufacture of RF particles**

RF was added to predefined (see Tables 8 and 9) amounts of solvent while being exposed to ultrasound using an ultrasonic bath (Typ 106, Bandelin electronic, Berlin, Germany). After adding, samples were sonicated for 10 minutes at controlled temperature of 25 ±1 °C. Temperature was maintained by constant water exchange using a thermostat (DC 10, Haake Technik GmbH, Vreden, Germany). Solutions obtained were filtered through a suitable 0.22 µm filter unit and stored in light protected 2.5 L glass bottles. Suspensions were stirred constantly and processed as obtained after recrystallization. Solutions and suspensions were spray dried using a Buchi B-290 (Flawil, Switzerland) spray dryer equipped with a modified three fluid nozzle (inner channel blocked, 0.7 mm nozzle tip, 1.5 mm screw cap), a high performance cyclone, an inert loop B-295, a dehumidifier B-296 (all Buchi) and an anemometer (model AF89-AD1AA13C0AA, Fluid components Intl. San Marcos, CA, USA). Process parameters were set as follows: Feed rate= 7.4 mL/min; outlet temperature= 60 ±3 °C; nozzle flow: 0.01 NCMH, system flow: 15 NCMH. To asses the impact of the drying method applied, another aqueous solution of RF (RFaqexp1 was spray freeze dried using an in-house built spray freeze dryer [152]. In brief: the solution was sprayed into cold (−200 °C, cooled with liquid nitrogen) atmospheric gas, leading to rapid freezing of the droplets. Frozen particles were collected and subsequently freeze dried using a Lyovac GT 2 (Steris, GmbH, Hürth, Germany) freeze dryer. Nozzle used and atomization parameters were as applied in the spray drying process. After manufacture, all samples were equilibrated and stored at 32% RH (saturated magnesium chloride slurry). Batch size for all formulations was 10 g, except of RFaqexp1, RFaqexp2, and RFaqexp3 as well as RFaqAm1 and RFaqAm2, where the batch size was 9 g. Exact amount of RF dissolved and suspended was determined using a validated HPLC method, where needed. Tables 8 and 9 give an overview on sample composition in the exploratory and main study respectively.

Table 8. Overview on formulations manufactured in the exploratory study.

| Sample name | Solvent | Conc. diss [mg/mL] | Conc. susp. [mg/mL] | Sample vol. [mL] | Method used [ ] |
|---|---|---|---|---|---|
| RFaqexp1 | water | 1.6 | 0.0 | 4950 | SFD |
| RFaqexp2 | | 1.9 | 0.0 | 4950 | SD/FD |
| RFaqexp3 | | 0.8 | 0.0 | 4950 | SD |
| RFaqexp4 | | 1.6 | 0.2 | 3667 | |
| RFaqexp5 | | 0.1 | 5.3 | 1833 | |
| RFIPAexp1 | IPA | 11.9 | 0.0 | 794 | |
| RFIPAexp2 | | 9.6 | 9.4 | 528 | |
| RFIPAexp3 | | 9.4 | 28.7 | 262 | |
| RFMeOHexp1 | MeOH | 9.5 | 0.0 | 901 | |
| RFMeOHexp2 | | 13.5 | 3.4 | 595 | |
| RFMeOHexp3 | | 5.5 | 28.2 | 297 | |
| RFEtOHexp1 | EtOH | 0.6 | 0.0 | 14092 | |
| RFEtOHexp2 | | 0.8 | 1.1 | 9394 | |
| RFEtOHexp3 | | 0.5 | 1.7 | 4697 | |
| RFEtOHexp4 | | 0.5 | 29.9 | 333 | |
| RFACexp1 | acetone | 6.3 | 0.0 | 1332 | |
| RFACexp2 | | 9.7 | 1.7 | 880 | |
| RFACexp3 | | 10.6 | 12.1 | 440 | |
| RFDCMexp2 | DCM | 132.2 | 0.0 | 44 | |
| RFDCMexp3 | | 56.4 | 284.8 | 29 | |

Table 9. Overview on formulations manufactured in the main study.

| Sample name | Solvent | Conc. diss. [mg/mL] | Conc. susp. [mg/mL] | Sample vol. [mL] |
|---|---|---|---|---|
| RFaqCryst1 | water | 0.2 | 4.0 | 1833 |
| RFaqAm1 | | 0.6 | 0.0 | 4950 |
| RFaqAm2 | | 1.2 | 0.0 | 4950 |
| RFaqAm3 | | 1.7 | 0.1 | 3667 |
| RFIPAAm1 | IPA | 12.6 | 0.0 | 804 |
| RFMeOHCryst1 | MeOH | 10.4 | 19.9 | 298 |
| RFEtOHCryst1 | EtOH | 0.4 | 1.8 | 4698 |
| RFEtOHCryst2 | EtOH | 0.6 | 29.4 | 333 |

### 2.2.6 **Cascade impactor analysis**

#### 2.2.6.1 Characterization of the low cost/disposable DPI surrogate

Charcoal pipe filters (Actitubes) were modified and used as surrogate for a low performance, low cost, and disposable DPI (= ACT). They consist of a simple cardboard tube, which is filled with charcoal pellets. Ends are capped with either a ceramic, or plastic stopper, which are perforated with 7 and 12 holes respectively. For using it as inhaler surrogate, caps and charcoal filling of individual tubes were removed, the cardboard tube was cleaned by blowing out with compressed air, filled with the sample, and re-capped. Resistance of the empty inhaler was determined by adjusting to predefined flow rates (5, 10, 15, 20, 25, 30, 35, 40, 45, 50 L/min) and recording the pressure drop using a critical flow control unit (Copley scientific, Nottingham, UK), n= 5. To visualize the airflow characteristics of the ACT, a CFD model (see Section 2.15.) was implied. Critical dimensions of the holes in the stoppers were determined by evaluation of SEM images of the stoppers (n= 5 each) resulting in individual distributions of orifice diameters for both, the plastic (n= 60) and the ceramic (n= 35) end. All other dimensions were determined using a caliper.

#### 2.2.6.2 Cascade impactor analysis of RF samples

Aerodynamic properties of spray dried formulations were assessed using a Next Generation

Pharmaceutical Impactor (MSP Co., Shoreview, MN, USA) coupled to two serial HCP5 aspirators and a critical flow control unit (both Copley scientific, Nottingham, UK), equipped with either the USPIP, USP3DIP, or the mIP, as well as a preseparator unit containing 15 mL of MeOH. RF samples were filled into size three HPMC capsules and aerosolized using the Handihaler (Boehringer Ingelheim, Ingelheim am Rhein, Germany) or Breezhaler (Novartis, Basel Switzerland) dry powder inhalers, or filled into and aerosolized from the ACT. All samples were analyzed at flow rates generating pressure drops of four kPa over the inhaler, being 43.3 L/min, 100.0 L/min, and 20.0 L/min for the Handihaler, Breezhaler, and the ACT respectively. Prior to use, all samples were equilibrated at 32% RH. Samples were recovered using 0.05% ascorbic acid in MeOH and evaluated using HPLC. RH was set to 50 ±2% by placing the DPI in a polyacrylate housing and purging with a nitrogen flow of desired RH, at a flow rate equivalent to the one over the NGI. RH adjustment was achieved by mixing dry and wet nitrogen in appropriate proportions. To investigate the stability of the aerodynamic performance over time, abbreviated NGI (aNGI) experiments were conducted at the respective time points of the stability study, as described in an earlier study [59]. An A/E type glass fiber filter (Pall Corporation, Ann Arbor, MI, USA) was cut to size and inserted upstream of stage four, generating a NGI setup comprising of three classes (i.e. inhaler (and capsule), induction port-S3, and filter). All experiments were carried out in triplicate.

#### 2.2.6.3 Cascade impactor analysis in mIP trials

Different inhalable formulations were evaluated using a Next Generation Pharmaceutical Impactor (MSP Co., Shoreview, MN, USA) coupled to two serial HCP5 aspirators and a critical flow control unit (Copley scientific, Nottingham, UK), equipped with either the USPIP, USP3DIP, mIP, mIPext, or USP3DSEIP. Deviating from standard USP/Ph.Eur. procedure, a preseparator unit was used when analyzing pMDI and nebulizer formulations to increase comparability to the setup used characterizing the DPI formulation, which requires use of a preseparator. PMDI and nebulized formulations were analyzed at 30.0 L/min and 15.0 L/min respectively. Sultanol forte inhalable solution was nebulized using a PARI LC sprint R jet nebulizer with blue insert (PARI GmbH, Starnberg, Germany). To analyze formulations dispensed from the Cyclohaler (the DPI) the flow rate was, as required by USP and Ph.Eur., set to 100.0 L/min, as the required pressure drop of four kPa over the device is achieved at approx. 110 L/min, which is beyond the calibrated airflow range of the NGI. Additionally, 15 mL of recovery solvent was added to the preseparator. Salbutamol samples

were recovered using MeOH/potassiumdihydrogenphosphate solution 0.0014 M, 50/50 and evaluated using HPLC. Beclometasone dipropionate, fluticasone propionate, and ciclesonide samples were recovered using MeOH. For nebulizer and DPI experiments, the relative humidity was set to 50 ±2% by placing the DPI in a polyacrylate housing and purging with a nitrogen flow of desired RH, at a flow rate equivalent to the one through the NGI. RH adjustment was achieved as described in the previous paragraph. For nebulizer experiments all inlets of the device and compressor unit were provided with nitrogen flow at desired rate and RH, as described above. PMDI experiments were carried out at ambient conditions. Prior to assessment of the nebulized formulation, independence of the method used from environmental influences (i.e. RH and temperature) was shown by comparison of deposition patterns with ones obtained with the NGI cooled to about 4 °C by submerging the device in an ice bath. To investigate reproducibility of the 3D printing process two additional mIP copies were manufactured and assessed in an aNGI [59] experiment comparing IP deposition of the pMDI formulation. A type A/E glass fiber filter (Pall Corporation, Ann Arbor, MI, USA) was cut to size and inserted upstream of S2, generating a NGI setup comprising of five classes (i.e. actuator, IP, preseparator, S1, and filter). The aNGI was operated at 30 L/min. Experiments were carried out n= 3, unless otherwise stated

### 2.2.7 **High performance liquid chromatography (HPLC) analysis**

#### 2.2.7.1 HPLC analysis of salbutamol samples

Samples were analyzed using a Waters (Milford, MA, USA) HPLC 2695 separations module equipped with either a 996 photodiode array detector or a 2487 dual wave-length detector (USP3DSE study only) using a method modified from [153]: Chromatography was carried out on a 250 mm RP-18 column (Lichrospher 100 RP 18-5µm EC, Merck), at a flow rate of 1.5 mL/min and an injection volume of 100 µL. Mobile phase consisted of MeOH/phosphate buffer 3.0/triethylamine 50/49.9/0.1. Column temperature was set to 45 °C. Absorption was determined at 275 nm. The HPLC method was calibrated in the range of 0.25-20.0 µg/mL.

#### 2.2.7.2 HPLC analysis of beclometasone dipropionate samples

Chromatography was carried out using aforementioned setup. Mobile phase consisted of MeOH/water 95/5, flow rate was set to 1 mL/min, and injection volume was 20 µl. Column temperature was kept constant at 25 °C. Samples were analyzed at a wavelength of 239 nm. HPLC method was calibrated in the range of 0.25-20.0 µg/mL.

#### 2.2.7.3 HPLC analysis of fluticasone propionate samples

Chromatography was carried out using the setup previously reported. Mobile phase consisted of MeOH/water 90/10, column temperature was kept at 25 °C, and injection volume was 20 µL. Samples were analyzed at 250 nm. HPLC method was calibrated in the range of 0.25-20.0 µg/mL.

#### 2.2.7.4 HPLC analysis of ciclesonide samples

Chromatography was carried out using aforementioned setup. Mobile phase consisted of MeOH at a flow rate of 1 mL/min and injection volume was 20 µL. Column temperature was kept constant at 25 °C. Samples were analyzed at a wavelength of 245 nm. HPLC method was calibrated in the range of 0.25-20.0 µg/mL.

#### 2.2.7.5 HPLC analysis of rifampicin samples

Samples were analyzed on an aforementioned system using a method modified from [91]: Chromatography was carried out on a 250 mm RP-18 column (Lichrospher 100 RP 18-5 µm EC, Merck), at a flow rate of 1.0 mL/min and an injection volume of 20 µL. Mobile phase consisted of phosphate buffer pH 5.2/MeOH/acetonitrile 50/33/17. Column temperature was set to 25 °C. Absorption was determined at 337 nm. The HPLC method was calibrated in the range of 1-200 µg/mL (NGI), and 50-150 µg/mL (purity).

### 2.2.8 **Analysis of residual water by Karl Fisher titration**

Water content of spray dried samples was analyzed using a V30S volumetric titrator coupled to a Stromboli headspace sampler (Mettler Toledo, Columbus, OH, USA). Samples were dried at 150 °C and the resultant vapor was quantified by re-dissolving in MeOH and titrating with a 2 mg/mL combined titrant (Apura Combi Titrant). The potency of the titrant was determined and corrected for each experiment using a sodium tartrate dihydrate standard [154].

### 2.2.9 **Analysis of residual solvents using headspace gas chromatography (GC)**

Analysis of residual solvents was performed on a Focus GC with TriPlus headspace autosampler (Thermo Scientific, Waltham, MA, USA). Chromatography was carried out on a FS-CS-624 (CS Chromatographie service GmbH, Langerwehe, Germany) quartz capillary column with an inner diameter of 0.32 mm and a length of 30 m. Inner walls were coated with 6% poly-(cyanopropyl) phenylsiloxane and 94% poly-(dimethyl) siloxane. Gradient program parameters were set as follows: 1) 6 min isothermic elution at 40 °C, 2) ramp to 150 °C at 120 °C / min, and 3) 4 min at 150 °C. Headspace incubator temperature was set to 80 °C, and incubation time before sampling was 10 min. Sampling volume was 1 mL and split ratio was 1:7.

### 2.2.10 **Thermogravimetric analysis (TGA)**

Loss on drying (LOD) was determined using a TGA-7 thermobalance (PerkinElmer, Waltham, MA) in the temperature range from 30-200 °C. After 5 minutes of equilibration at 30 °C, a temperature ramp of 10 °C/min was applied to the samples.

### 2.2.11 **Scanning electron microscopy**

Samples were mounted onto SEM stubs using double adhesive tape and sputter coated with gold for two cycles of two minutes each. Images were taken using a Hitachi S-2460N scanning electron microscope (Hitachi Ltd., Tokyo, Japan) in high vacuum. Acceleration voltage was 10 kV, working distance was set as needed and is reported on the individual pictures.

### 2.2.12 **X-ray powder diffractometry (XRPD)**

Powders were analyzed in a 5-40° 2θ range with a PANalytical X´pert X-ray diffractometer (PANalytical, Almelo, the Netherlands) using nickel filtered CuKα radiation at a wavelength of 1.5406 Å, which was generated at an acceleration voltage and current of 45 kV and 40 mA respectively. Samples were placed in circular stainless steel sample holder and kept in spinning motion during measurement.

For humidity and temperature trials, the aforementioned system was equipped with a THC (Anton Paar, Graz, Austria) temperature/humidity chamber. $N_2$ was used as purge gas, and sample temperature was kept constant at 25 °C. Samples were subjected to two cycles of 0-20-40-60-80-97-80-60-40-20-0% RH with each stage held for 150 minutes, after the RH in the chamber had stabilized. X-ray diffractograms were recorded every hour so that a minimum of two data points per step was recorded. After completing the second cycle, samples were sequentially heated up to predefined temperatures of 40, 60, 80, 100, and 120 °C, and equilibrated for 15 min before recording the diffractogram.

### 2.2.13 **Differential scanning calorimetry (DSC)**

Samples were placed into non-hermetic sealed, punctured 40 µL aluminum pans, and analyzed at a temperature range from 30-200 °C, using a DSC2 differential scanning calorimeter (Mettler Toledo, Greifensee, Switzerland). Samples were analyzed under $N_2$ purge in standard mode, applying a heat rate of 10 °C/min.

### 2.2.14 **Acoustic levitation (AL) experiments**

To get a deeper understanding of the mechanism behind the formation of the spray dried particles, single droplets of solvents (IPA, MeOH, water) and solutions of RF therein were dried in an experimental acoustic levitator, which is described in detail here [155]. In brief: A standing sound wave was being formed between an emitting piezo transducer and a concave reflector. A liquid droplet of 1 ±0.01 µL of volume was placed below one of the pressure nodes, which generates a stable levitation of the droplet. Drying of the back illuminated droplet was observed with a CCD camera (Basler scA1390, Germany) coupled to a long-distance microscope (Navitar Zoom 6000, USA). Magnification of the microscope was

calibrated using a high precision microscale. In the acoustic field the droplet was exposed to a dry nitrogen flow of 0.5 L/min (n= 10).

#### 2.2.14.1 Contact angle measurements

Contact angle measurements were conducted by drop shape analysis (DSA) using a FM 40 (Krüss, Hamburg, Germany) drop shape analyzer (n= 5).

#### 2.2.14.2 Viscosity

Viscosity of solutions used in the acoustic levitation experiments was determined using an Ubbelohde type viscometer 501 03/ 0c (SI analytics GmbH, Mainz, Germany), which was placed into a water bath providing exact temperature control. Temperature was adjusted to 25.0 °C. Hagenbach correction was applied to the results (n= 5).

#### 2.2.14.3 Surface tension

Surface tension of plain solvents and solutions of RF therein was determined using a model 13356 (Krüss, Hamburg, Germany) ring tensiometer. Temperature was adjusted to 25.0 °C (n= 5).

#### 2.2.14.4 Solutions density

Density of RF solutions in EtOH, IPA, and $H_2O$ as well as control pure solvents was determined using a Gay-Lussac type pycnometer (ISO 3507 compliant model, Brand, Wertheim, Germany). Equilibration temperature was 25 °C (n= 5).

#### 2.2.14.5 Dynamic vapor sorption (DVS)

DVS experiments were carried out on a DVS 1 (Surface Measurement Systems, Middlesex, UK) placed in a temperature controlled cabinet (t= 25 °C) using in-house made quartz pans. Prior to experiments, samples were dried at 0% RH until a *dm/dt* stability of 0.002 %/min was reached. Then samples were exposed to increasing humidity at a ramp of 10% RH/h before being equilibrated at 97% RH using aforementioned endpoint (= half cycle). Two consecutive full cycles were performed during each experiment.

### 2.2.15 Stability testing

Stability testing of the formulations was performed on RFaqCryst1, RFEtOHCryst1, RFMeOHCryst1, RFaqAm1, and RFIPAAm1 in accordance to the International Conference

on Harmonization (ICH) guideline Q1A(R2) “Stability Testing of New Drug Substances and Products” [156]. As refrigerated storage was proposed for RF bulk powder, samples were stored in a climate cabinet (Type 9120-0040, Binder GmbH, Tuttlingen, Germany) at accelerated conditions for refrigerated products, i.e. 25 ±2 °C and 60 ±5% RH. Samples were analyzed at predefined time points of one, three, and six months using HPLC, XRPD, DSC, and aNGI analyses. Additionally, another set of samples was stored in the refrigerator (4 °C) and analyzed after six months.

### 2.2.16 **Data processing and statistical analysis**

NGI overview plots show relative stage deposition. Error bars indicate one SD. Cumulative undersize plots including S1-MOC were generated and linearized by log-transforming stage cutoffs and probit-transforming relative frequencies. A linear regression model was used to calculate the MMAD, FPFs related to the emitted ($FPF_{emitted}$) or total ($FPF_{total}$) dose, and geometric standard deviation (GSD), as described in USP <601>. Emitted fraction (EF) is the mass fraction of particles emitted from the DPI, pMDI, or nebulizer. Groups in mIP studies were compared using one-way ANOVA followed by Bonferroni adjusted two sample t-test at a family error rate of 0.05, if group means were found significantly different ($p < 0.05$). Statistical analyses were performed using R 3.3.1 [157] with chemCal and ggplot2 packages.

Acoustic levitator data was standardized by relating to the first time point acquired. Axis ratio and diameter of the backlight area equivalent sphere ($d_{eq}$(area)) were calculated from images acquired and plotted over time, error bars indicate one SD. Plotting was conducted using R 3.3.1 with ggplot2 package.

TGA data was analyzed using Pyris (PerkinElmer) software.

Data from contact angle measurements was processed using Drop Shape Analysis 1.92.1.1 software (Krüss, Hamburg, Germany).

XRPD overview plots were generated from unmodified data using R. Datasets from studies using the humidity control chamber were corrected for baseline offset and Kα reflections using X´pert Highscore (PANalytical, Almelo, the Netherlands) software and plotted using R 3.3.1 with ggplot2 package.

DSC data was analyzed using STAR (Mettler Toledo) software. Overview plots were generated using R 3.3.1 with ggplot2 package.

Chemical stability of feed solution used for manufacture of RFaqexp3 was evaluated testing for normality using Shapiro-Wilk test using R 3.3.1.

# 3 Investigating Next Generation Pharmaceutical Impactor performance using modified 3D printed induction ports

## 3.1 Results and discussion of induction port design, manufacture, and formulation screening

### 3.1.1 Results

#### 3.1.1.1 Cascade impactor analysis using model salbutamol formulations

A trachea model for use with the NGI, a USP IP replica, and a model based on USP IP geometry but with an inner surface equivalent to the trachea model were manufactured and assessed. The test objects are shown in Figure 19. Table 10 provides an overview on the test objects and formulations assessed. The maximum operating pressure drop of sealed test objects was determined as 95.0 kPa, 94.5 kPa, 94.6 kPa, and 94.1 kPa for the USPIP, USP3DIP, mIP, and the USP3DSEIP respectively. If measurable, intrinsic resistance of test objects was found to be lower than $0.005$ $(\sqrt{kPa} * min)/L$. Deviations from airflow adjusted using the USPIP were determined as 1.2 ±1.1%, 0.2 ±0.5 %, and 1.3 ±1.0 % for the USP3DIP, mIP, and the USP3DSEIP respectively. Two additional copies of the mIP were manufactured and assessed using an aNGI setup. Test objects were found to show statistically equivalent (p= 0.27871) SAL deposition of 62.6 ±3.0%, 62.9 ±2.8%, and 64.4 ±2.1% respectively.

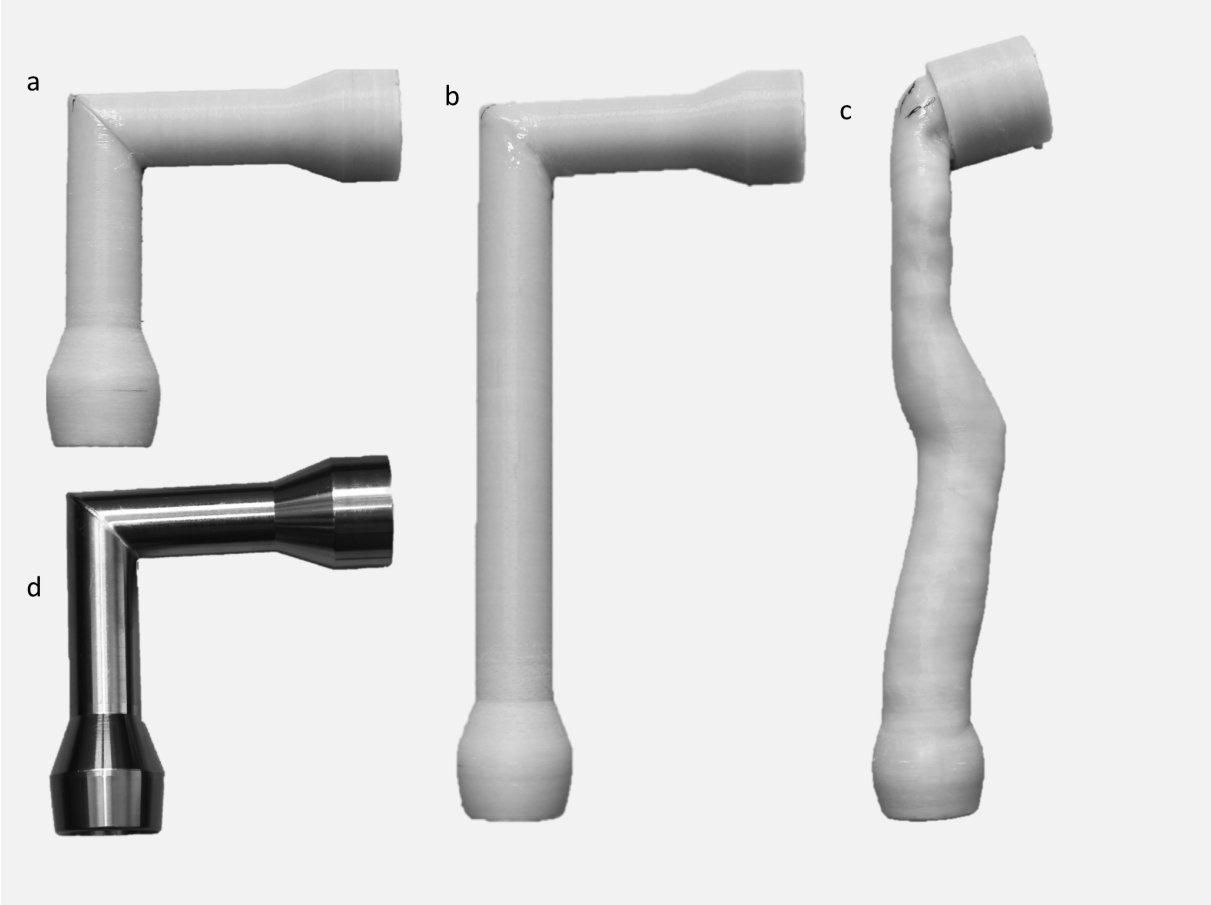


Figure 19. Photographs of the USP3DIP (a), USP3DSEIP (b), mIP (c), and USPIP (d).

Table 10. Overview on test objects and formulations tested.

| | | Formulation tested | | | |
|---|---|---|---|---|---|
| IP | Description | pMDI | pMDI + VHC | DPI | Nebulizer |
| USPIP | Standard USP IP | + | + | + | + |
| mIP | Trachea model IP | + | + | + | + |
| USP3DIP | 3D printed copy of USPIP | + | - | + | + |
| USP3DSEIP | 3D printed copy of USPIP with surface area of mIP | + | - | - | - |

NGI experiments of SAL formulated as pMDI using the USPIP show high IP deposition, little preseparator deposition, and a fairly narrow particle size distribution (see Figure 20, Table

11). USPIP and USP3DIP were found to perform statistically equivalent. Statistically different results were obtained comparing the USPIP to the mIP, as experiments showed an increase in IP deposition. GSD increase was statistically significant (p= 0.04148), whereas the MMAD remained equivalent. Increased mIP deposition was found to have a strong impact on $FPF_{total}$, which decreased significantly (p= 0.00218), when compared to the USPIP.

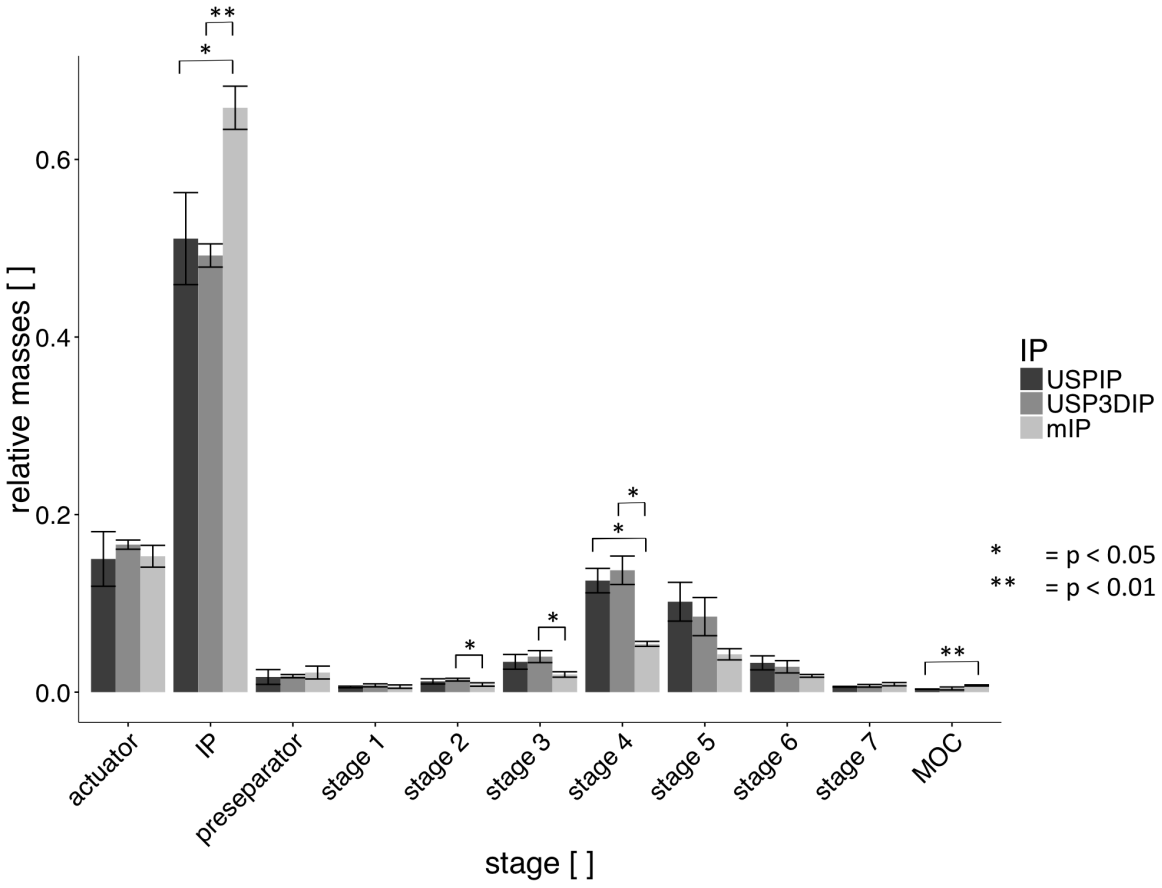


Figure 20. Results of NGI experiments analyzing the Sultanol pMDI, comparing USPIP, USP3DIP, and mIP (n= 9).

Table 11. Overview on aerosol characteristics of formulations and IPs tested.

| | | | IP tested | | |
|---|---|---|---|---|---|
| Formulation | | USPIP | USP3DIP | mIP | USP3DSEIP |
| pMDI | **MMAD** [$\mu$m] | 2.47 ±0.12 | 2.58 ±0.11 | 2.32 ±0.08 | 2.48 ±0.09 |
| | **GSD** [] | 1.76 ±0.03 | 1.81 ±0.02 | 2.11 ±0.10 | 1.77 ±0.05 |
| | $\mathbf{FPF_{total}}$ [%] | 28.82 ±1.99 | 28.21 ±1.49 | 14.15 ±1.19 | 29.84 ±2.45 |
| | $\mathbf{FPF_{emitted}}$ [%] | 33.99 ±3.63 | 33.83 ±1.68 | 16.72 ±1.60 | 34.92 ±2.45 |
| | $\mathbf{F_{emitted}}$ [%] | 85.00 ±3.08 | 83.38 ±0.52 | 84.69 ±1.23 | 85.50 ±0.91 |
| DPI | **MMAD** [$\mu$m] | 3.03 ±0.12 | 3.03 ±0.12 | 2.72 ±0.32 | |
| | **GSD** [] | 3.20 ±0.19 | 3.06 ±0.08 | 3.08 ±0.12 | |
| | $\mathbf{FPF_{total}}$ [%] | 21.62 ±1.48 | 23.17 ±1.95 | 20.44 ±2.22 | |
| | $\mathbf{FPF_{emitted}}$ [%] | 27.18 ±0.87 | 28.50 ±1.87 | 25.36 ±2.72 | |
| | $\mathbf{F_{emitted}}$ [%] | 79.50 ±3.33 | 81.25 ±1.74 | 80.67 ±2.18 | |
| nebulizer | **MMAD** [$\mu$m] | 3.46 ±0.07 | 3.23 ±0.76 | 3.00 ±0.13 | |
| | **GSD** [] | 2.31 ±0.12 | 2.61 ±0.41 | 2.32 ±0.03 | |
| | $\mathbf{FPF_{total}}$ [%] | 26.46 ±3.04 | 26.63 ±2.24 | 27.06 ±1.82 | |
| | $\mathbf{FPF_{emitted}}$ [%] | 60.72 ±3.26 | 60.37 ±6.31 | 61.09 ±1.34 | |
| | $\mathbf{F_{emitted}}$ [%] | 43.50 ±2.91 | 44.19 ±1.37 | 44.30 ±2.77 | |
| pMDI + VHC | **MMAD** [$\mu$m] | 2.28 ±0.08 | | 2.23 ±0.05 | |
| | **GSD** [] | 1.76 ±0.08 | | 1.73 ±0.09 | |
| | $\mathbf{FPF_{total}}$ [%] | 23.25 ±5.20 | | 24.37 ±3.03 | |
| | $\mathbf{FPF_{emitted}}$ [%] | 82.41 ±2.83 | | 75.47 ±4.83 | |
| | $\mathbf{F_{emitted}}$ [%] | 28.14 ±5.80 | | 32.22 ±2.30 | |

Aerodynamic characterization of SAL formulated as binary dry powder blend for inhalation showed only moderate USPIP deposition, but high deposition in the preseparator unit (see Figure 21). USP3DIP was found to perform equivalently to the USPIP. The mIP showed a significantly increased deposition, when compared to the USPIP, and preseparator deposition decreased slightly, but not significantly. Comparison of these IPs, did not result in statistically significant differences in MMAD, GSD, or FPF (see Table 11).

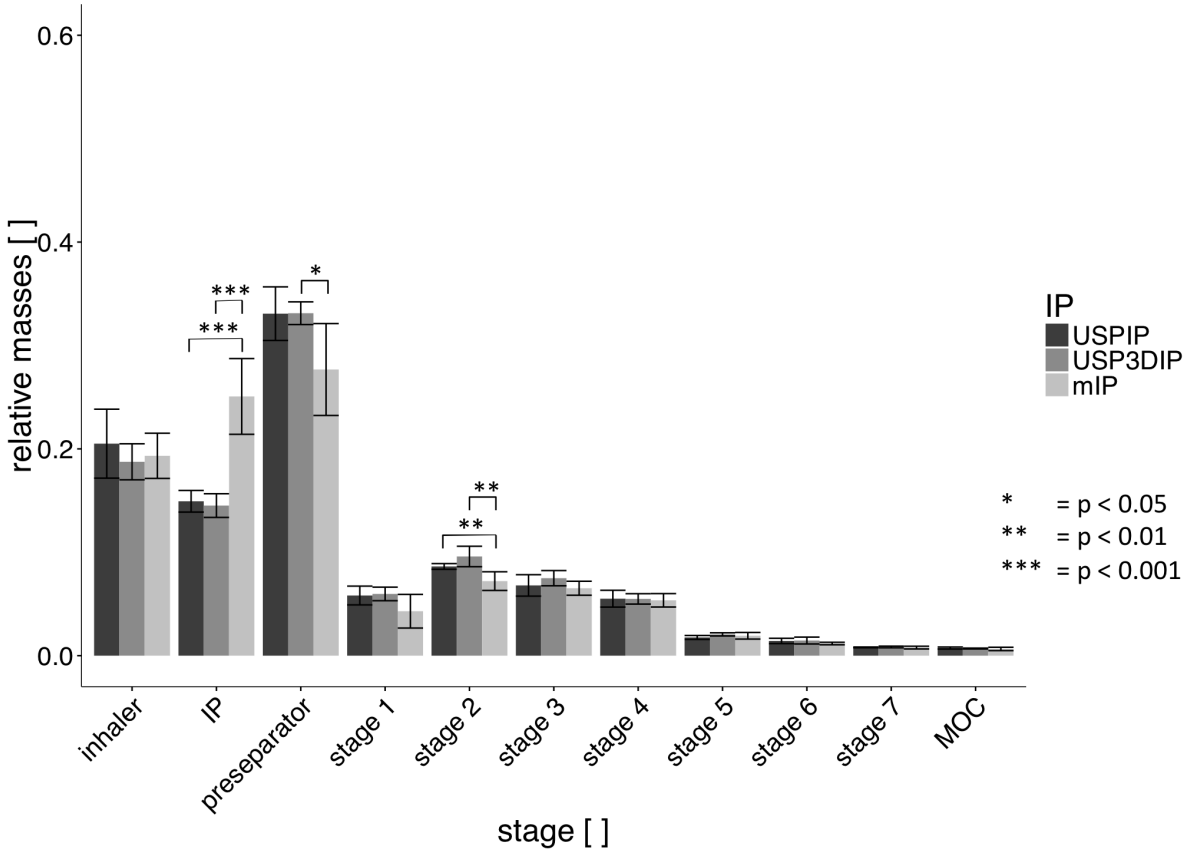


Figure 21. Results of NGI experiments analyzing the Cyclocaps Cyclohaler DPI, comparing the USPIP, USP3DIP (n= 6), and mIP (n= 9).

NGI experiments assessing the deposition of SAL formulated as solution for nebulization showed a broad distribution over all NGI stages (see Figure 22). Little mass was retained in the IP and preseparator. The major deposition was found within the nebulizer itself. Characteristics determined using the USPIP were statistically equivalent to that using the USP3DIP and the mIP (see Table 11). A statistical difference in deposition was found in the USPIP, when compared to the USP3DIP.

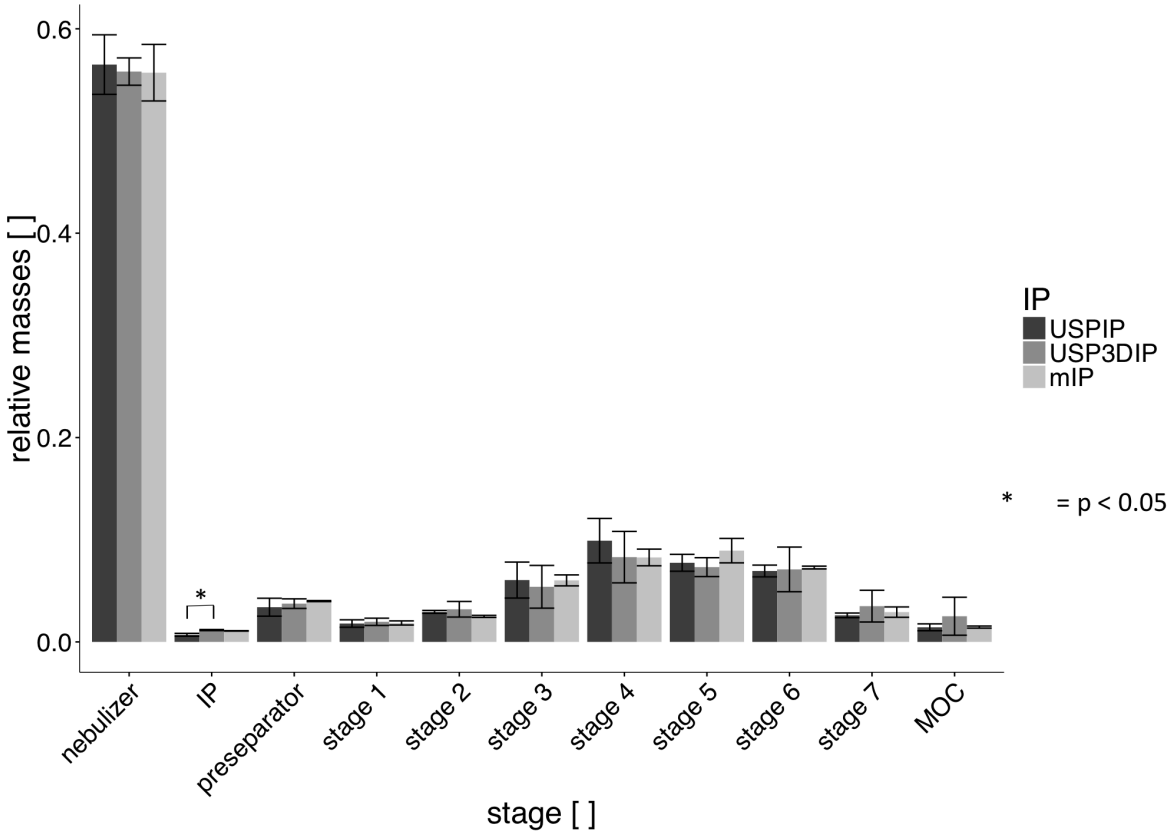


Figure 22. Results of NGI experiments analyzing the Sultanol nebulizer solution, comparing the USPIP, USP3DIP, and mIP.

To get a better understanding of the underlying mechanism we designed another IP with a surface area equivalent to the one of the trachea, still maintaining the basic geometry of the USPIP. Surface area of the USP3DIP and the mIP was calculated as 128.4 $cm^2$ and 201.3 $cm^2$ respectively. To generate the new model (USP3DSE), a cylinder with an inner surface of 72.9 $cm^2$ and an inner diameter equivalent to the USP IP was inserted into the lower segment of the USP3D model. Cascade impaction analysis of SAL formulated as pMDI showed statistical equivalence of deposition rates (Figure 23) and consequently of MMAD, GSD, and FPF (Table 11), when compared to the USPIP.

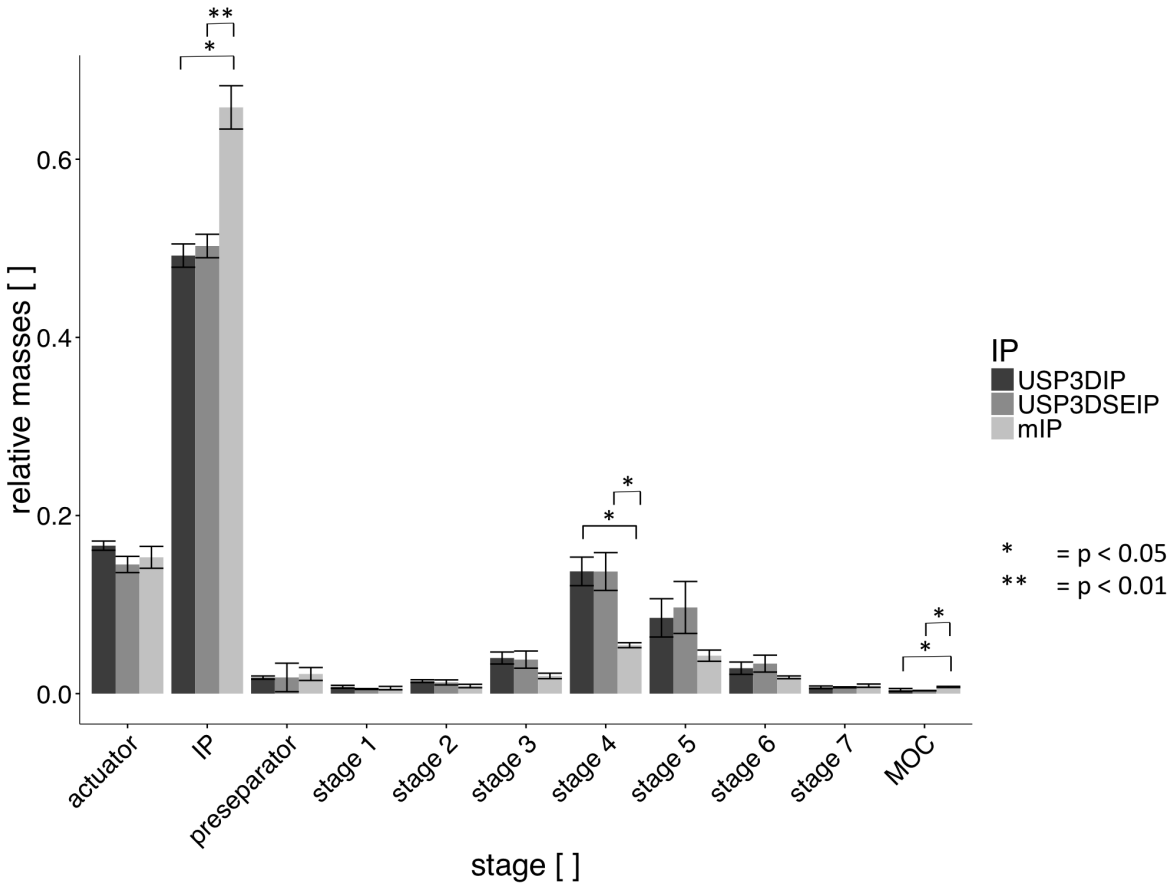


Figure 23. Results of NGI experiments using the Sultanol pMDI, comparing the USP3DSEIP, USPIP, and mIP.

### 3.1.1.2 CFD studies

To visualize the effect of different geometries of the USPIP and the trachea model on airflow velocities within the IPs, as occurring during assessment with the NGI, a CFD model was generated and evaluated. Figure 24 shows characteristic slices depicting the flow fields over the USPIP and the mIP. Intensity distributions of the flow velocity over planes normal to the flow vector were found to differ strongly.

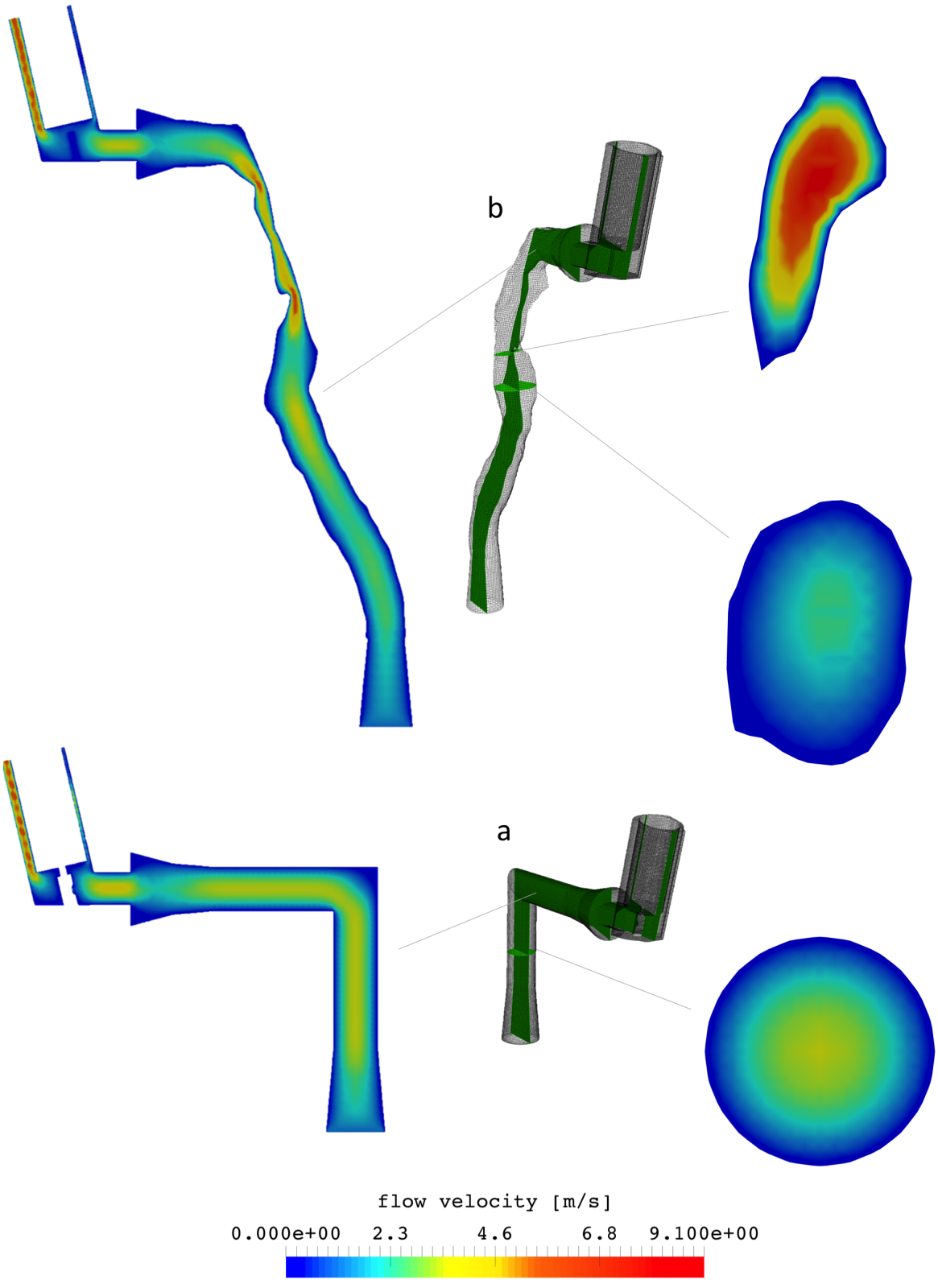


Figure 24. Results of CFD studies over the USPIP (a) and mIP (b). Heat maps show airflow velocities over charateristic slices.

### 3.1.1.3 Cascade impactor analysis using salbutamol pMDI formulation with VHC

The effect of a VHC device on particle deposition in the trachea model and its effect on PSD and lung deposition was investigated (see Figure 25). NGI experiments showed that adding a VHC to the assembly decreases IP deposition drastically as a large fraction was retained within the VHC. $F_{emitted}$ decreased significantly (p= 0.00007), whereas $FPF_{emitted}$ increased (p= 0.00087). MMAD, GSD, and $FPF_{total}$ were found to be statistically equivalent (see Table 11). Replacing the USPIP with the mIP was shown to increase IP deposition significantly. MMAD, GSD, $FPF_{total}$, $FPF_{emitted}$, and $F_{emitted}$ were found to be statistically equivalent, though a decrease in $FPF_{emitted}$ was observed.

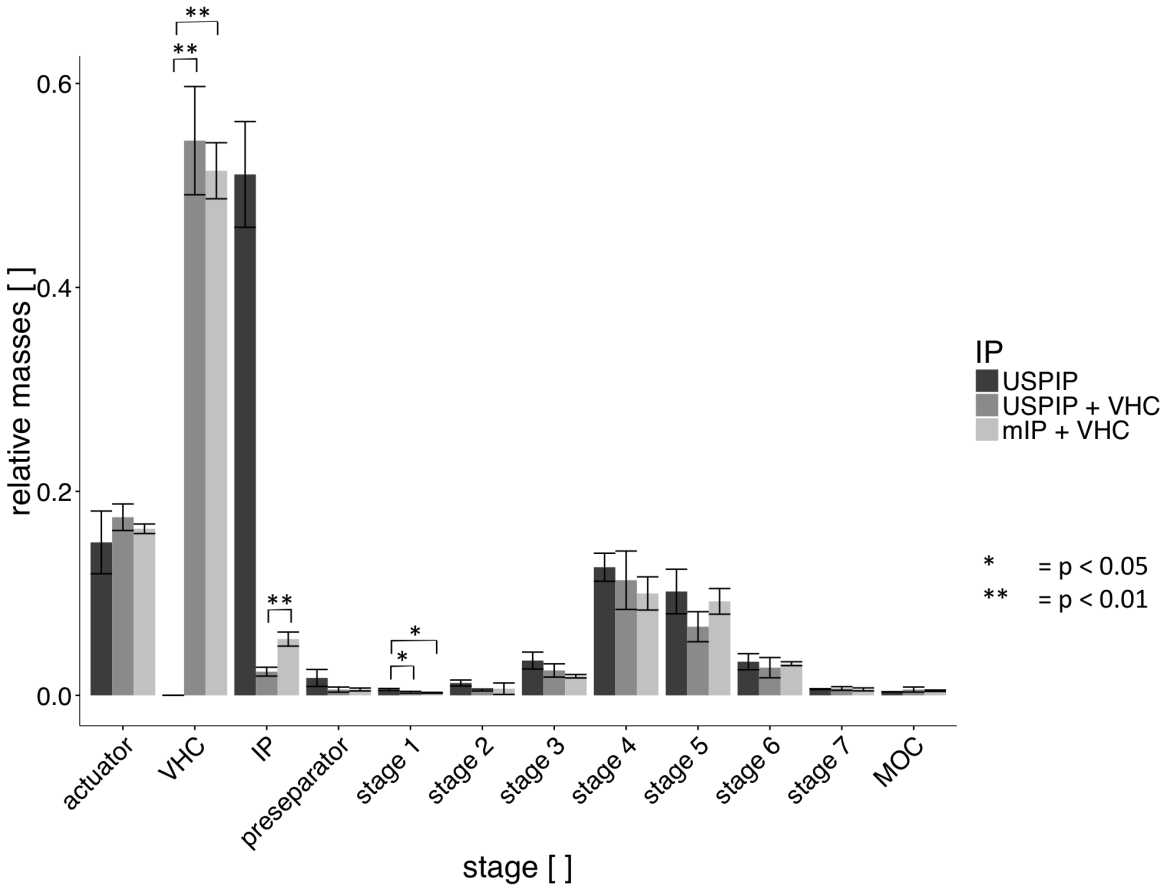


Figure 25. Results of NGI experiments using the Sultanol pMDI, analyzing the effect of adding a VHC to the USPIP and mIP.

### 3.1.2 **Discussion**

Since pressure drops generated using sealed 3D printed models were found comparable to the pressure drop achieved using the USPIP, air tightness of the printed models was found to be sufficient. Additionally, the quality of the joints connecting the test objects to the NGI and mouth piece adapters was assessed by determining deviations from the various flow rates adjusted using the USPIP. Since all test objects show no relevant intrinsic resistance, similar airflow rates can be expected when using set conditions (i.e. replacing the IP only). All deviations observed were found to be well below 5%, and therefore compliant with USP and Ph.Eur. requirements. Based on these observations it was concluded that the test objects are suitable for use in cascade impaction experiments using the NGI. Statistical equivalence of mIP deposition in an aNGI assessment of the pMDI formulation using three different copies of the mIP proves robustness of the manufacturing method. A 3D printed replica of the USPIP was generated and assessed, to evaluate the impact of using a different material (i.e. PLA instead of stainless steel) as well as the increase of surface roughness, which is a consequence of using FDM technique. In FDM, printouts are generated by stacking layers of extruded polymer filament generating a rougher surface, when compared to e.g. stainless steel. It was found that material and increased surface roughness have no significant effect on NGI experimental outcomes, when analyzing SAL formulated as pMDI or DPI. Thus, results of experiments using the USPIP and the mIP are comparable. The increase in IP deposition, as observed analyzing the pMDI, hypothetically can be explained by two different concepts. As aerosol particles dispensed from a suspension based pMDI are expected to interact (e.g. electrostatic interaction or capillary forces [8]) with surfaces to some extent, an increase of surface area exposed to the aerosol might lead to an increased deposition rate. Additionally, increased particle retention might be caused by alteration of the IP's geometry. This could lead to increased impaction or settling of the particles. So conclusively one must assume that both hypothetical interactions combined would explain the actual increase observed. Cascade impaction analysis showed statistically equivalent deposition, and consequently MMAD, GSD, and FPF, when determined using the USP3DSEIP (see Figure 23). Based on this observation one must conclude that the increase in deposition is solely caused by geometric factors. This conclusion is in good agreement with the statistical equivalence observed, when comparing the USP with USP3DIP, as increased surface roughness consequently demands an

increase in surface area, with constant object geometry. Apparently only a certain sub-population of aerosol particles are prone to surface interactions at given experimental parameters, and the surface area provided in the USP IP is sufficient for their deposition. This conclusion underlines that including physiological conditions in the design of an alternate IP, with the goal of better IVIVC is relevant, and is in good agreement with literature. Observation of the lack of a surface area related component, might be dose dependent though. Since the dose applied in this experimental setup already was the maximum dose monographed in USP and Ph.Eur. (i.e. 10 puffs), this can be evaluated as irrelevant, when USP/Ph.Eur. standards are applied. CFD simulations show that the trachea model generates sections with increased, as well as such with decreased airflow velocity, when compared to the USPIP. An increase in flow velocity leads to a higher acceleration of particles entrained by the air stream. Due to the increased momentum, this might cause separation from the stream, if particles undergo radial acceleration (i.e. a change in motion vector), and consequently impaction leading to an increase in overall particle deposition. Contrary, areas with lower velocities might facilitate settling of particles. Simulations show a consecutive cascade of high and low velocity sections in the trachea model, which might be causal for the increased particle deposition, as observed during NGI experiments. The increase in IP deposition causes a drop in FPF when determined with mIP. Interestingly, this correlates better to lung deposition, as reported in the product's prescribing information [158], compared to the one obtained using the USPIP. To date, no study available reports *in vivo* lung deposition of a SAL pMDI formulation, conducted after the transition from chlorofluorocarbon (CFC) to hydrofluoroalkane (HFA) propellants. Nevertheless, as *in vitro* assessment indicates equivalence of CFC and HFA formulations [159–163], a lung deposition of about 10-15%, as determined in scintigraphic studies [164,165] using aerodynamically equivalent $^{99m}$Tc-labelled teflon beads, appears reasonable. So, in this instance the 3D trachea model provides superior information to the formulation scientist, when compared to the USPIP. Much effort has already been made to investigate different approaches to improve IVIVC by replacing the USPIP with model IPs closer to physiological conditions. The MT model most intensely characterized and investigated was developed at the University of Alberta and became commercially available through Copley Scientific (Alberta idealized throat, AIT). Here, the investigators intended to generate a MT model representing the majority of individuals, showing no irregularities of the respiratory tract. Based on averaged observations made using CT and MRT imaging, as well as direct observations on hospitalized

patients, basic geometrical shapes were compiled into an idealized extrathoracic airways model [75]. A study published by Copley, Mitchell, and Solomon, investigating the effect of replacing the USPIP by the AIT when analyzing a commercial pMDI formulation of SAL reports a $FPF_{emitted}$ of 38.0 ±1.4 % and 33.4 ±1.3 % for the USP IP and the AIT respectively [73]. MMAD and GSD are reported as 2.5 ±0.1 µm and 1.9 ±0.2 µm respectively. Recalculating MMAD, GSD, and FPF from data provided there, but applying the data processing method used in this study, generates results comparable to those reported. Though the manufacturer of the pMDI used in this study is unclear and experimental setups differ slightly (i.e. no preseparator unit was used and stages were coated with silicone oil) a suitable level of comparability of both studies is observed. So it is reasonable to conclude that the 3D printed trachea model used in this study retains more particles dispensed from a SAL pMDI, thus generating a greater decrease in FPFs, when compared to the AIT. Additionally, results obtained here correlate better to *in vivo* data, so the trachea model provides not only a better IVIVC when compared to the USP IP, but also to the AIT. However, when evaluating the models one must be aware that our focus was on the prediction of lung deposition, whereas the AIT was designed and tested for MT IVIVC. Results of the present study are consistent with Copley, Mitchell, and Solomon, reporting differences in geometry to be more critical for particle deposition than surface related effects [73], which had been concluded from a previous study [166]. The main difference, between both MT models is that the developer of the AIT had put emphasis on modeling and idealizing the mouth cavity as well as the trachea, whereas the focus of this study was on the trachea only. Connection to the mouth piece adaptor here, was established through an element of the dimensions of the USP IP inlet, which is attached to the trachea at an angle of about 110°. Another important difference is the degree of idealization in the AIT that eventually might have caused a loss in geometry information, which has been shown to be causal for increased deposition rates in this study. Here, one might distinguish between geometries derived from physiological conditions, i.e. from CT scans, and artificial geometries, introduced to establish feasibility for the use with the NGI (e.g. with the addition of connectors). Experiments conducted using the DPI, as well as ones using the pMDI with the VHC indicate that when compared to the USP IP or AIT, the shortened distance from the valve to the 110° bend is not responsible for the increased deposition observed, since particle velocities (and consequently momentum) are dependent on the airflow velocity over the CI only. When compared to the USP IP, airflow velocities at the bend are lower, which in combination with the larger angle generates less radial acceleration.

Thus, less particle deposition is to be expected. Anyways, with this experimental setup it cannot be excluded that this mechanism might participate in the overall effect to a certain extent. The impact of the shortened distance from the pMDI nozzle orifice to the bend on aerosol characteristics could be assessed by adding further modifications e.g. an elongated IP inlet or an oral cavity to the model. These modifications were not yet included in this study as our primary aim is to demonstrate that FDM rapid prototyping using PLA filament is a suitable method to manufacture modified induction ports for NGI experiments and that results are responsive to alterations of the IP's geometry.

As the trachea shows the most complex geometry upstream from the bronchi it was chosen as critical physiological element to be investigated in this study. Though IVIVC already was found superior compared to the AIT it might be improved by assessing and taking into account the impact of e.g. the angle at which the aerosol plume enters the IP or, as mentioned, the absence of an oral cavity model, if found relevant. Besides in IVIVC to patient populations showing no irregularities of the respiratory tract the individual based approach of our model might be utilized to generate a platform technology to investigate particle deposition in special patient populations, or eventually be applied in a completely personalized approach. Here it could be e.g. utilized to generate a patient specific airways model to assess, which inhalable formulation would be most effective for the individual present. Another benefit of this method is that it can be rapidly adapted in case recommendations on how the pMDI is to be used are updated. E.g. Fadl et al. [167] showed that the angle at which the pMDI is applied has an impact on its performance. Anyways, as of now this observation has not been implemented into clinical practice but might eventually be incorporated into the respective guidelines. Another possible application might be to establish a better transferability of data generated in animal models. Further investigation is needed to evaluate if this finding can be confirmed with other pMDI formulations currently marketed and if different formulation strategies (e.g. formulating as solution or suspension) are critical to cascade impaction experiments when using the mIP. The VHC used in this study demonstrated a similar particle retention to that of the USPIP, but must be regarded to as part of the inhaler when processing the data. From a therapist's point of view this means reduced particle impaction in the upper airways, which is, besides omitting the need to perform pMDI actuation and inhalation maneuver simultaneously, the desired benefit of using a VHC/spacer. The impact of the reduction of particle velocities in the IP when adding a VHC has already

been discussed in the previous section. Due to the similarity of particle retention performance of both IPs to the VHC, the impact of replacing the USP IP with the mIP is marginal for overall formulation performance, though an increase in IP deposition was observed. Based on this dataset one must conclude that using the mIP instead of the USPIP does not provide additional information for pMDI assessment, when using a spacer device. Increased mIP deposition when analyzing a dry powder formulation of SAL was shown to be pronounced, but corresponded to a decrease in preseparator deposition. Cumulative IP and preseparator deposition was equivalent, showing 48.0 ±2.5% and 52.8 ±3.5% deposition for the USPIP and the mIP respectively. Thus, it can be concluded that the performance of the preseparator unit has a greater impact on PSD and FPF than the IP. Since all components upstream from S1 are excluded from the dataset when calculating the PSD, differentiation between deposition in the IP or preseparator does not offer additional information, especially because no size cut-offs can be attributed to any of the classes. So, in this specific case, replacing the USPIP by the mIP does not provide additional information for the researcher. This observation is contrary to the one made when analyzing the pMDI, where the impact of the preseparator was found negligible and unaffected from the IP performance. Higher preseparator deposition analyzing the DPI might be caused by incomplete de-agglomeration of the binary blend used in this formulation. Experimental behavior of a certain fraction of API particles (which have been traced in this study) might be strongly correlated to the behavior of the carrier lactose particles. Besides primary API particle size, density, shape, and de-agglomeration of the particles are critical parameters for their aerodynamic performance. When compared to suspension based pMDI formulations, DPI formulations must not only overcome interparticulate cohesive forces, but also adhesive forces to the carrier particle to de-agglomerate. So in this respect the suspension based pMDI can be understood as a border case of a hypothetical DPI using identical API particles, if alterations of the primary particles caused by e.g. the instability of suspension and effects caused by the increased exit velocity caused by evaporating propellant are ignored. So further investigation is needed to evaluate if conclusions drawn from experiments with this formulation are applicable to more modern formulation/inhaler systems as well, or if more sophisticated formulations behave more similar to pMDIs. The increase in IP deposition when comparing USPIP to USP3DIP analyzing a nebulized formulation indicates that data generated using the mIP might be compromised by material related effects. This might cause an underprediction of deposition in the lungs. Since deposition in the IP was found to be low (less than 2%) the impact of this

result is negligible. Due to their intrinsic aerosol characteristics, i.e. absence of agglomerates leading to a broad, monodisperse distribution, assessment of nebulized formulations does not benefit from modifications of the IP.

## 3.2 Results and discussion investigating cascade impactor performance of additional commercial pMDI formulations using modified induction ports

### 3.2.1 Results

#### 3.2.1.1 Induction ports assessed in this study

Figure 26 shows a photograph of induction ports assessed in this study. In addition to the USPIP, USP3DIP, and the mIP, another model (mIPext) was manufactured and assessed. This new model shows the trachea geometry investigated in the previous section (proximal section of the mIPext) merged with the MT region of the USPIP (distal section of the mIPext). This new model allows more differentiated investigation of the mechanisms, leading to increased mIP deposition, as reported in the previous section.

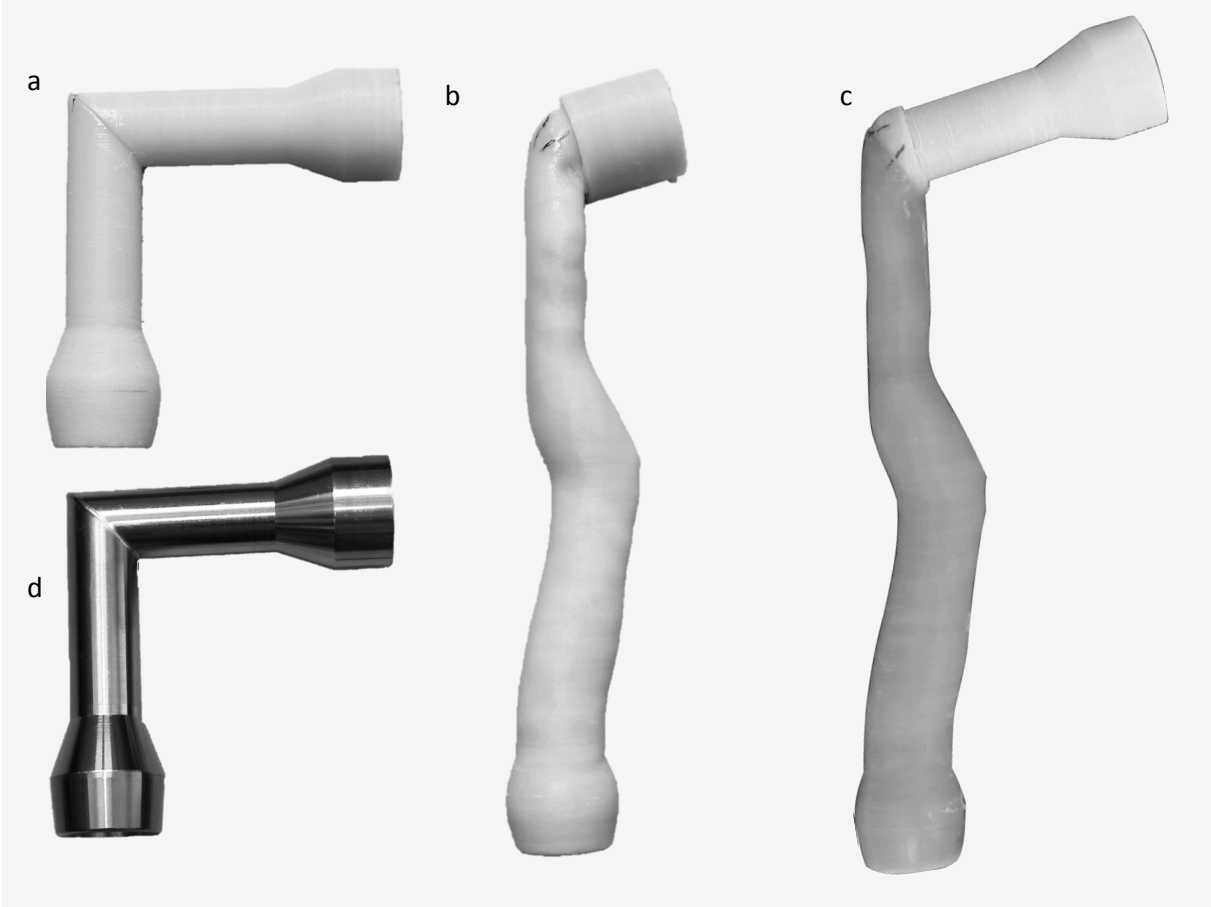


Figure 26. Photographs of the USP3DIP (a), mIP (b), mIPext (c), and USPIP (d).

### 3.2.1.2 Determination of valve diameter of pMDIs used

SEM images in Figure 27 show nozzles of actuators used in this study as well as nozzle diameters derived from the images.

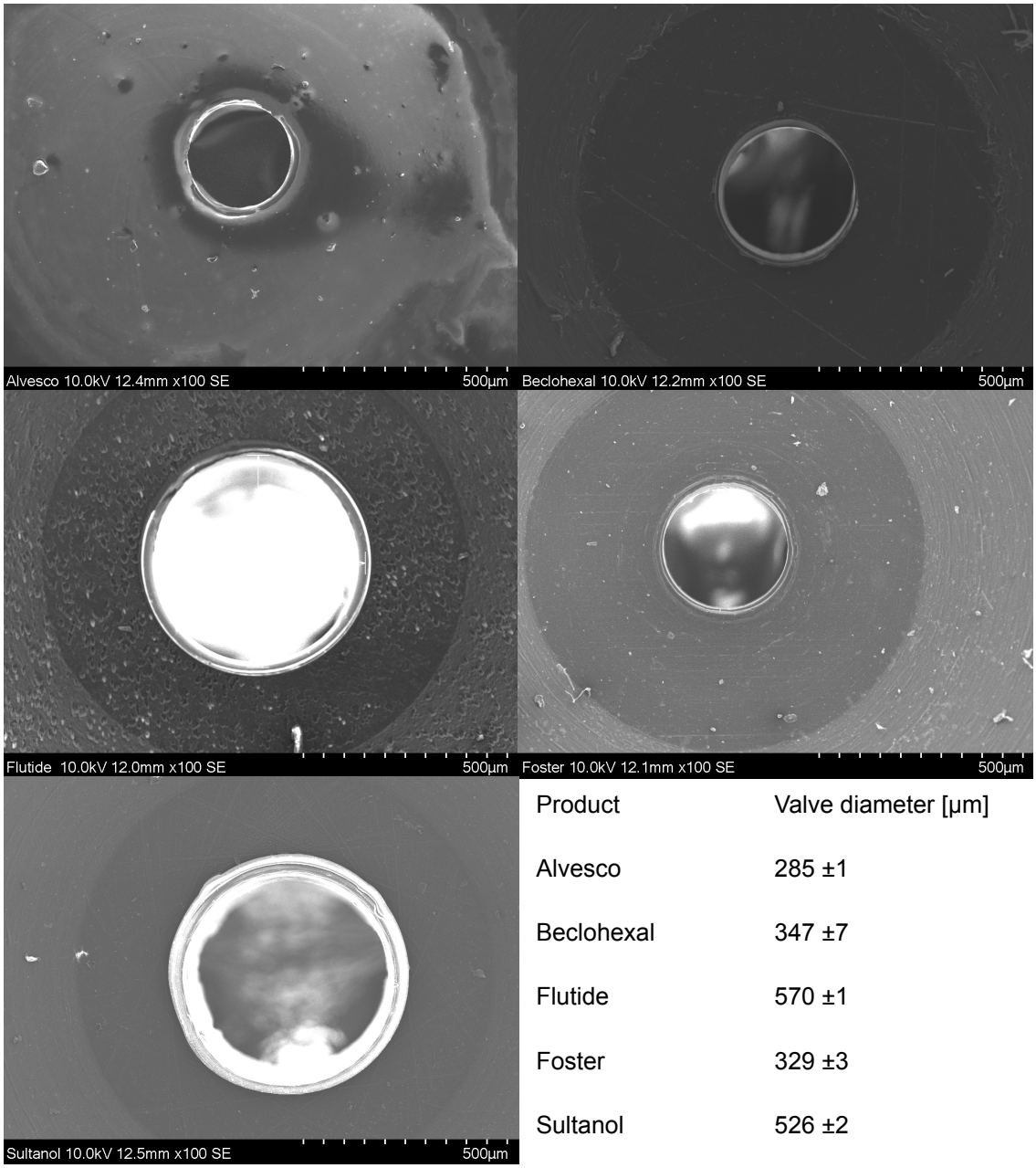


| Product | Valve diameter [µm] |
|---|---|
| Alvesco | 285 ±1 |
| Beclohexal | 347 ±7 |
| Flutide | 570 ±1 |
| Foster | 329 ±3 |
| Sultanol | 526 ±2 |

Figure 27. SEM images showing nozzles of actuators used in this study.

### 3.2.1.3 Cascade impactor analysis of Sultanol pMDI using the mIPext

Cascade impactor analysis of the Sultanol salbutamol pMDI formulation using the mIPext showed an increase in IP deposition, when compared to the USPIP, and a decreased IP deposition when compared to the mIP (see Figure 28). MMAD, $FPF_{total}$, and $FPF_{emitted}$ were found not significantly different (see Table 12), when compared to the USPIP.

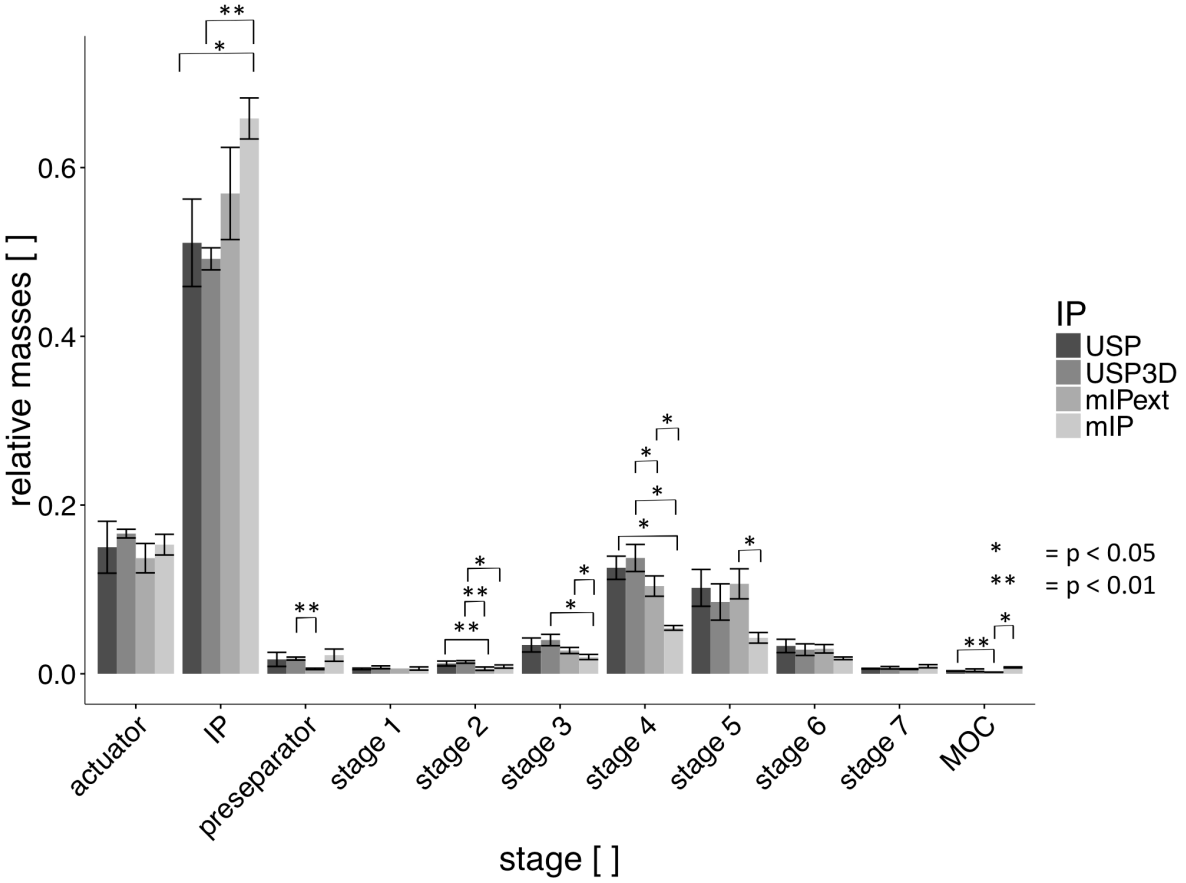


Figure 28. Results of NGI experiments using the sultanol pMDI formulation, analyzing the impact of the mIPext.

Table 12. Overview of aerosol characteristics for pMDI formulations and IPs tested.

| | | | IP tested | | |
|---|---|---|---|---|---|
| Formulation | | USPIP | USP3DIP | mIPext | mIP |
| Sultanol | **MMAD** [$\mu$m] | 2.47 ±0.12 | 2.58 ±0.11 | 2.37 ±0.16 | 2.32 ±0.08 |
| | **GSD** [] | 1.76 ±0.03 | 1.81 ±0.02 | 1.71 ±0.05 | 2.11 ±0.10 |
| | $\mathbf{FPF_{total}}$ [%] | 28.82 ±1.99 | 28.21 ±1.49 | 26.41 ±3.23 | 14.15 ±1.19 |
| | $\mathbf{FPF_{emitted}}$ [%] | 33.99 ±3.63 | 33.83 ±1.68 | 30.65 ±4.27 | 16.72 ±1.60 |
| | $\mathbf{F_{emitted}}$ [%] | 85.00 ±3.08 | 83.38 ±0.52 | 86.30 ±1.74 | 84.69 ±1.23 |
| Flutide | **MMAD** [$\mu$m] | 3.17 ±0.16 | 2.98 ±0.06 | 2.79 ±0.11 | 2.66 ±0.06 |
| | **GSD** [] | 1.80 ±0.04 | 1.77 ±0.01 | 1.77 ±0.01 | 1.75 ±0.03 |
| | $\mathbf{FPF_{total}}$ [%] | 38.29 ±3.18 | 35.99 ±1.50 | 30.21 ±2.88 | 25.84 ±1.45 |
| | $\mathbf{FPF_{emitted}}$ [%] | 42.08 ±3.16 | 39.44 ±0.83 | 32.74 ±2.47 | 27.96 ±1.58 |
| | $\mathbf{F_{emitted}}$ [%] | 91.44 ±1.67 | 91.23 ±2.10 | 92.21 ±2.49 | 92.41 ±0.15 |
| Beclohexal | **MMAD** [$\mu$m] | 1.18 ±0.06 | 1.12 ±0.02 | 1.08 ±0.00 | 0.98 ±0.01 |
| | **GSD** [] | 2.05 ±0.15 | 2.14 ±0.06 | 1.90 ±0.04 | 2.01 ±0.03 |
| | $\mathbf{FPF_{total}}$ [%] | 65.15 ±1.25 | 56.52 ±2.69 | 56.34 ±3.49 | 51.14 ±0.70 |
| | $\mathbf{FPF_{emitted}}$ [%] | 70.47 ±1.74 | 63.89 ±0.67 | 64.80 ±4.03 | 56.67 ±0.80 |
| | $\mathbf{F_{emitted}}$ [%] | 92.51 ±3.53 | 88.47 ±4.30 | 86.94 ±0.46 | 90.26 ±1.52 |
| Alvesco | **MMAD** [$\mu$m] | 1.38 ±0.06 | 1.26 ±0.01 | 1.22 ±0.01 | 1.21 ±0.02 |
| | **GSD** [] | 1.84 ±0.03 | 1.83 ±0.06 | 1.74 ±0.05 | 1.78 ±0.07 |
| | $\mathbf{FPF_{total}}$ [%] | 55.60 ±1.29 | 54.98 ±0.50 | 58.35 ±1.70 | 50.71 ±2.08 |
| | $\mathbf{FPF_{emitted}}$ [%] | 68.57 ±1.15 | 67.03 ±0.71 | 71.55 ±1.70 | 62.17 ±1.20 |
| | $\mathbf{F_{emitted}}$ [%] | 81.07 ±0.94 | 82.02 ±0.22 | 81.55 ±0.47 | 81.54 ±1.79 |
| Foster | **MMAD** [$\mu$m] | 1.21 ±0.02 | 1.15 ±0.02 | 1.14 ±0.06 | 1.02 ±0.03 |
| | **GSD** [] | 1.96 ±0.07 | 2.04 ±0.00 | 2.04 ±0.04 | 2.18 ±0.03 |
| | $\mathbf{FPF_{total}}$ [%] | 37.47 ±1.89 | 35.06 ±0.31 | 32.15 ±1.35 | 24.01 ±0.41 |
| | $\mathbf{FPF_{emitted}}$ [%] | 40.47 ±2.06 | 37.44 ±0.34 | 34.50 ±1.49 | 25.80 ±0.60 |
| | $\mathbf{F_{emitted}}$ [%] | 92.58 ±1.31 | 93.65 ±0.24 | 93.20 ±1.76 | 93.20 ±1.76 |

### 3.2.1.4 Cascade impactor analysis of the Flutide forte pMDI formulation

NGI analysis of the Flutide forte formulation using the USPIP showed a fairly high IP deposition (see Figure 29). S1, S2, S6, and S7 showed low particle deposition whereas S3-S5 contained the main fraction of the particles downstream from the IP. MOC and filter stages were found to show no particle deposition. USP3DIP was found to perform statistically equivalent to the USPIP. Contrary, mIPext, and mIP showed a statistically significant increase in IP deposition, when compared to the USPIP with the increase being more pronounced in the case of the mIP. MMAD, $FPF_{total}$, and $FPF_{emitted}$ were found to differ significantly (p= 0.03861, p= 0.03442, and p= 0.01811, respectively) when comparing the mIP to the USPIP. In the case of the mIPext, the increase in IP deposition did not result in significant differences in MMAD, $FPF_{total}$, $FPF_{emitted}$, or GSD, though a decrease in all parameters was observed (see Table12).

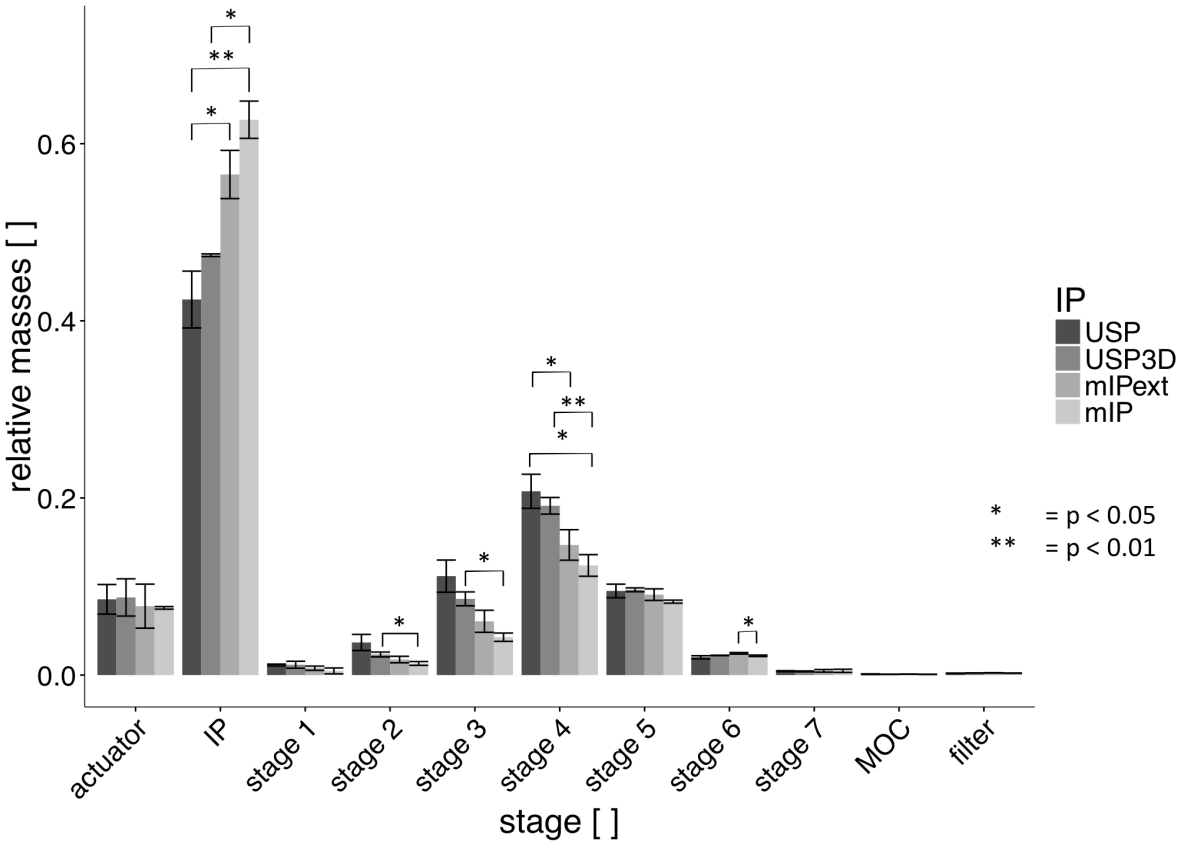


Figure 29. Results of NGI experiments using the Flutide forte formulation.

### 3.2.1.5 Cascade impactor analysis of the Beclohexal pMDI formulation

Analysis of the Beclohexal formulation using the NGI with the USPIP showed moderate IP deposition and a low particle deposition in S1-S4 as well as the filter stage. The main fraction of the sample recovered downstream from the IP was collected from S5-MOC (see Figure 30). When comparing the USPIP, USP3DIP, and mIPext, a slight but insignificant increase in IP deposition, which resulted in a statistically significant decrease in $FPF_{emitted}$ ($p= 0.03985$) in the case of USP3DIP, was seen. In contrast, the mIP showed a more pronounced and statistically significant increase in IP deposition, when compared to the USPIP. $FPF_{total}$ and $FPF_{emitted}$ were found to decrease significantly, when using the mIP. An overview of the aerosol characteristics that were determined can be found in Table 12.

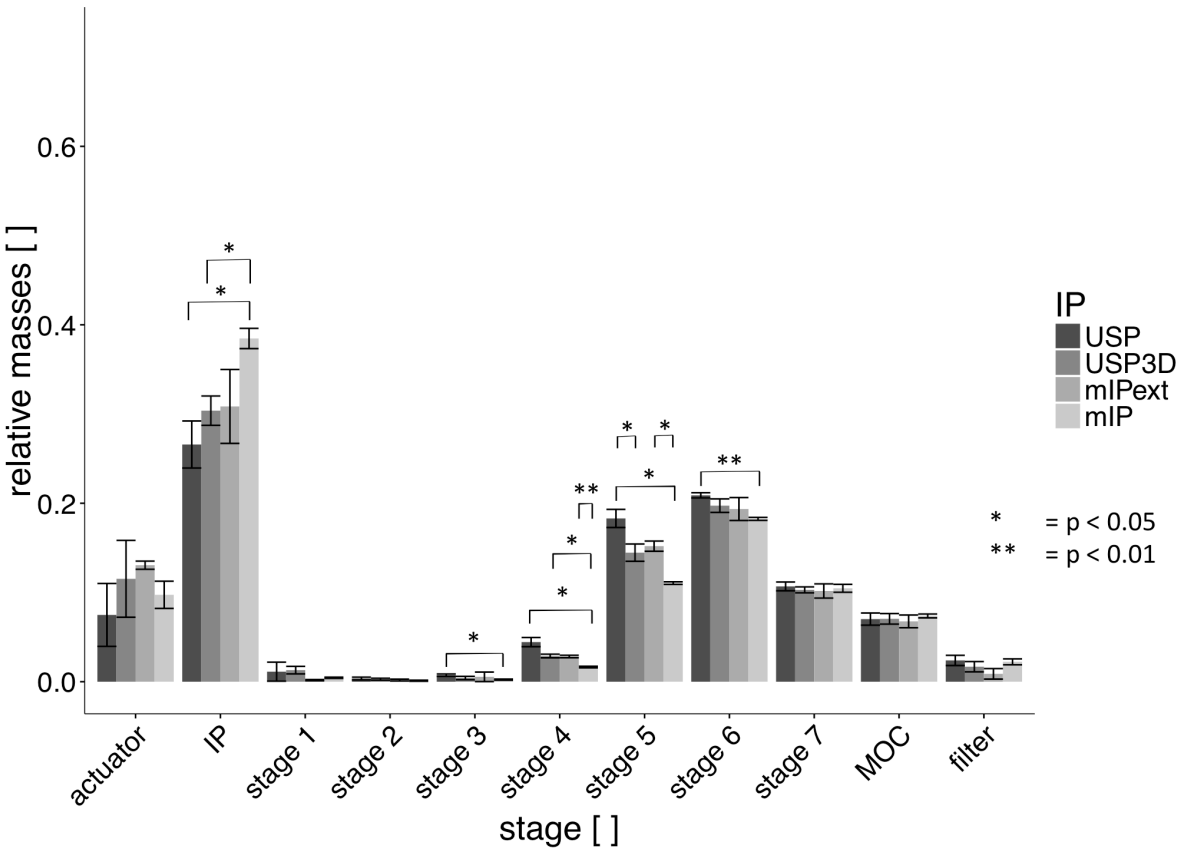


Figure 30. Results of NGI experiments using the Beclohexal formulation.

### 3.2.1.6 Cascade impactor analysis of the Alvesco pMDI formulation

Compared to the other formulations assessed, Alvesco ciclesonide showed an increased actuator deposition resulting in a $F_{emitted}$ of about 80% only (see Figure 31). NGI analysis using the USPIP showed fairly low IP deposition and little deposition in S1-S3. Apart from the actuator and IP stages, main particle deposition occurred in S4-filter stages. Aerosol characteristics that were determined are shown in Table 12. IP deposition, $FPF_{total}$, $FPF_{emitted}$, and GSD were found to be statistically equivalent when comparing USPIP and USP3DIP, though a slight increase in IP deposition was observed. S4 and S7 deposition was found to differ significantly. MIPext deposition was found to be lower, when compared to the USPIP and USP3DIP. When compared to the USPIP, mIP deposition was found to be significantly higher. $FPF_{total}$ was found to be insignificantly lower, whereas $FPF_{emitted}$ decreased to a statistically significant extent.

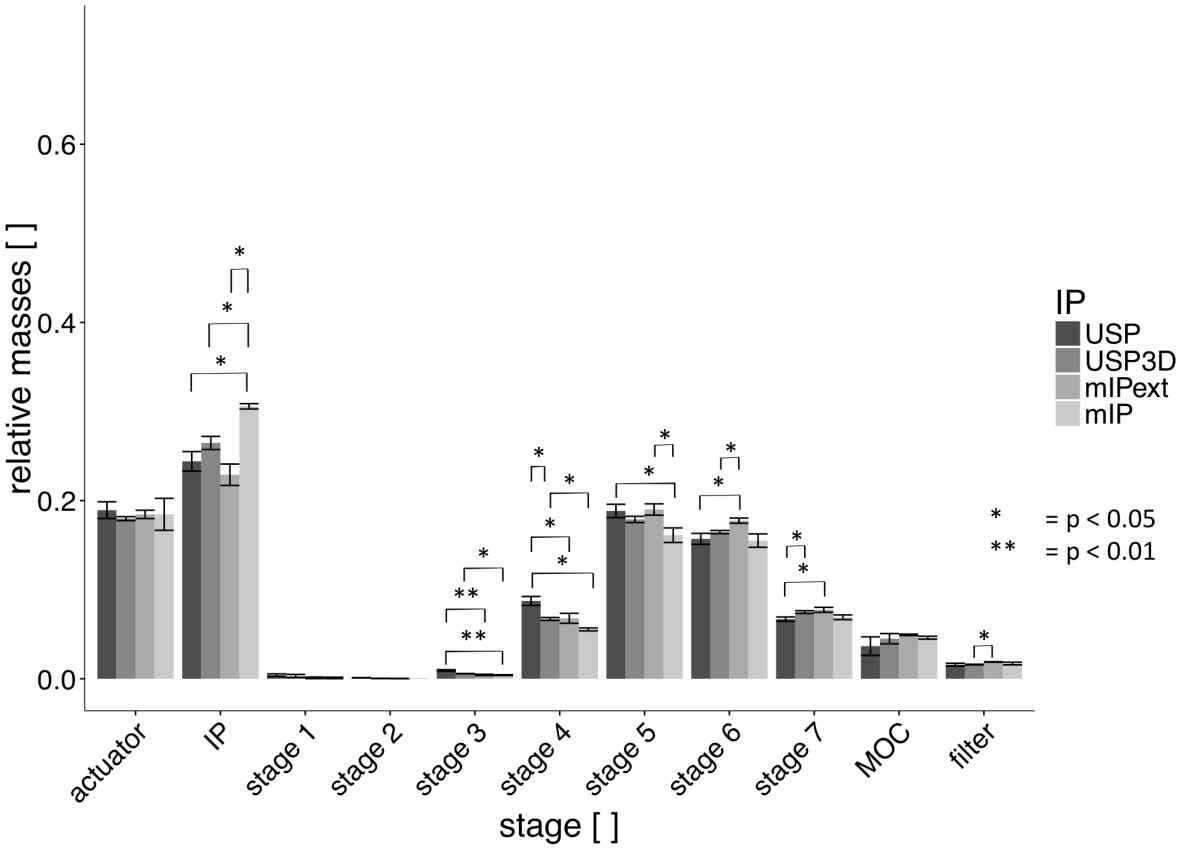


Figure 31. Results of NGI experiments using the Alvesco formulation.

### 3.2.1.7 Cascade impactor analysis of the Foster pMDI formulation

NGI assessment of the foster formulation using the USPIP showed little actuator deposition, high IP deposition, little deposition in S1-S3 and the filter stage and moderate deposition in S4-MOC (see Figure 32). Aerosol characteristics are summarized in Table 12. USPIP and USP3DIP were found to perform equivalently. Though not being statistically significant (p= 0.05734), mIPext showed an increase in deposition, when compared to the USPIP, resulting in an insignificant decrease in $FPF_{total}$ (p= 0.06067) and $FPF_{emitted}$ (p= 0.05477). In contrast, mIP showed a significant increase in IP deposition leading to a significant decrease in $FPF_{total}$ (p= 0.02221) and $FPF_{emitted}$ (p= 0.02931).

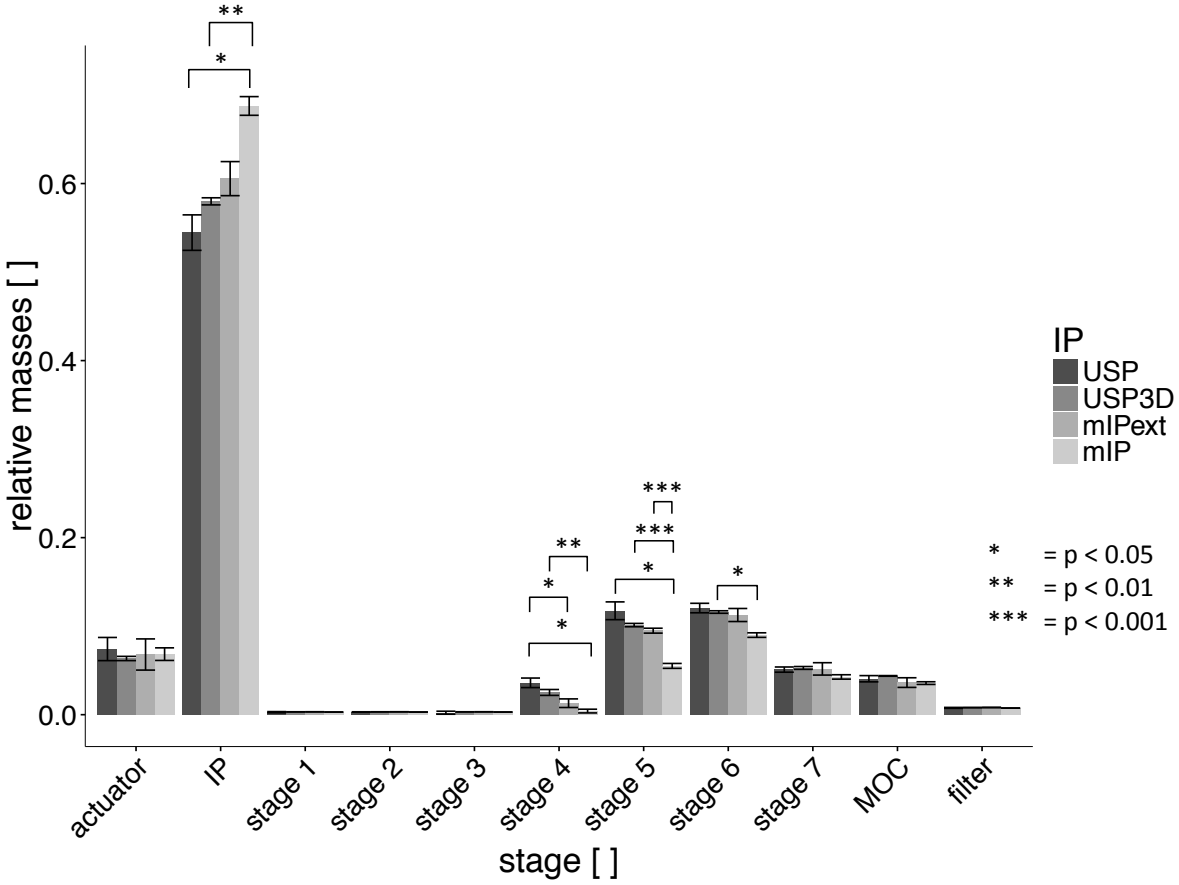


Figure 32. Results of NGI experiments using the Foster formulation.

### 3.2.1.8 IVIVC

Another aim of this study was to provide additional data on the correlation of particle deposition predicted to *in vivo* deposition, so formulations assessed were selected based on

availability of such data in literature. Table 13 gives an overview on sources included and lung depositions reported.

Table 13. Studies included for comparison of *in vitro* aerosol data with *in vivo* lung deposition from literature.

| | Formulation tested | Lung deposition [%] | Study |
|---|---|---|---|
| Salbutamol | Sultanol (GSK, London, UK) | 10-20 | [168] |
| Fluticasone propionate | Advair HFA (GSK, London, UK) | 16 (mild asthma) | [169] |
| | Flovent HFA (GSK, London, UK) | 24 (mild asthma) | [170] |
| Beclometasone dipropionate | Qvar (3M, St.Paul, MN, USA) | 53 ±7 | [171] |
| | Qvar (TEVA, Petach Tikwa, Israel) | 60 ±14 | [172] |
| | Qvar | 58 (mild asthma) | [169] |
| | Qvar | 55 (mild asthma) | [170] |
| | Foster (Chiesi, Parma, Italy) | 37 ±10 | [173] |
| Ciclesonide | n/r | 52 ±9 (mild asthma) | [174] |
| | n/r | 52 ±11 | [175] |

Figure 33 correlates $FPF_{emitted}$s determined using the USPIP, mIP, and mIPext and deposition data reported in literature. Diagonal lines indicate ideal correlation i.e. direct transferability of *in vitro* to *in vivo* data. It should be mentioned that the prescribing information of Sultanol reports a lung deposition of 10-20 %, which has been averaged, and so represents 15 ±5%. Additionally, data presented for the Foster formulation [173], was normalized to the emitted fraction. Figure 34 presents relative deviations of $FPF_{emitted}$ to lung deposition determined *in vivo*. Smaller deviations indicate better IVIVC and dashed lines depict the SD from data reported in the study. IVIVC using the mIP yielded good results for all except the Advair formulation and was found superior compared to the mIPext and USPIP in all cases except for the Foster formulation. IVIVC using the mIPext was found better to IVIVC using the USPIP in all cases but the ciclesonide formulation.

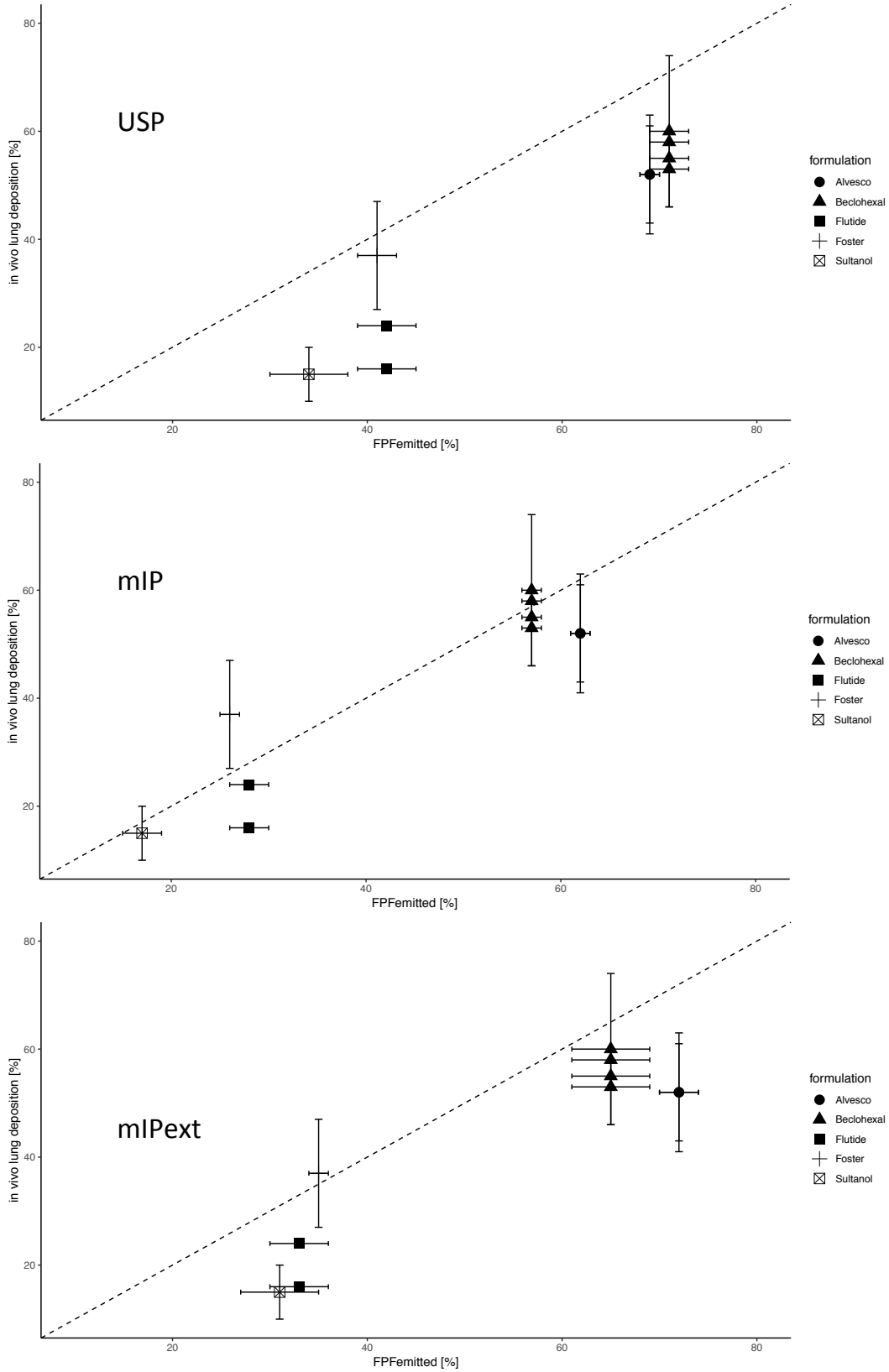


Figure 33. Comparison of *in vitro* prediction with *in vivo* lung deposition data from literature. Errorbars indicate one SD. The dashed line depicts ideal correlation.

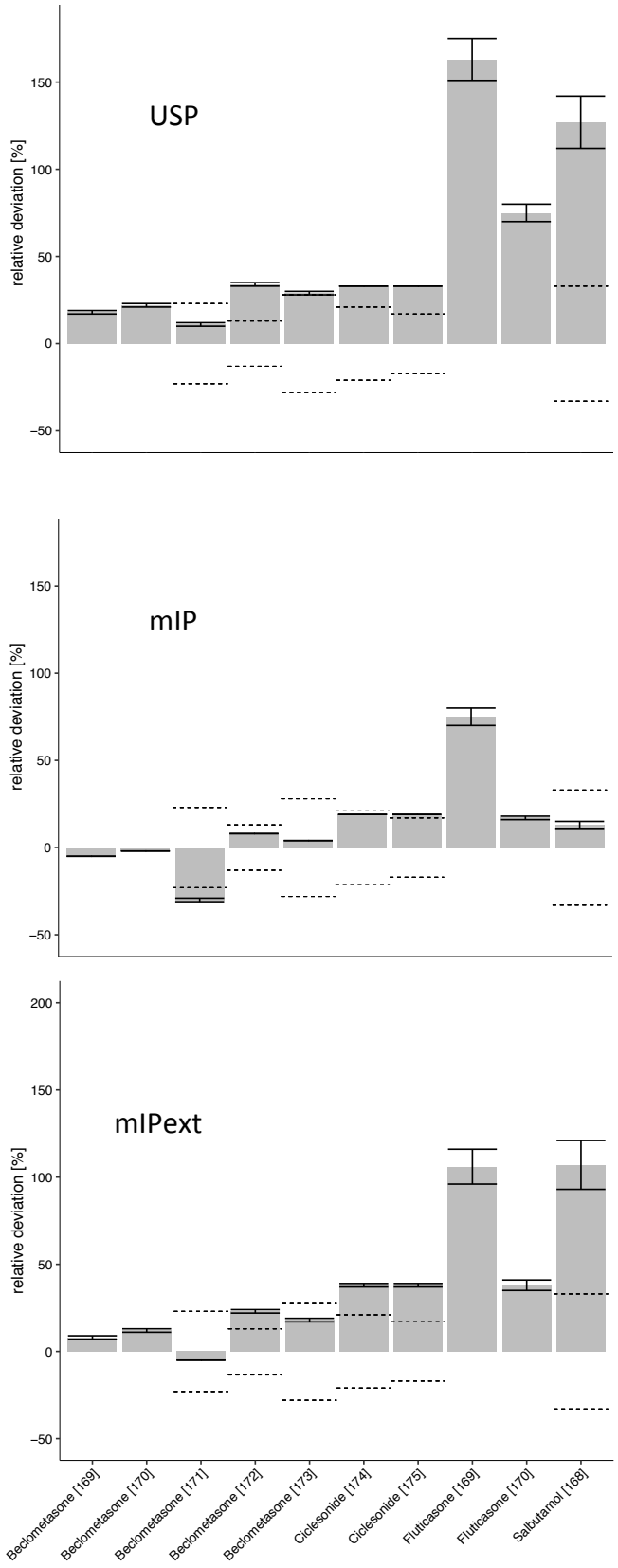


Figure 34. Deviations of predicted from *in vivo* depositions. Dashed lines indicate SD reported in studies, if applicable.

### 3.2.2 **Discussion**

In context of the previous chapter, the aim of this study was three-fold: a) to provide additional data supporting the observations made, b) to get a clearer idea which characteristics of pMDI formulations and actuator design trigger increased IP deposition, and c) to get a deeper understanding of which mechanisms are causal for any increased IP deposition observed. To address these issues, another set of four commercially available pMDI formulations was assessed using the USPIP, USP3DIP, and the mIP. Additionally, another modified IP (mIPext) was designed in a way that it would show the trachea geometry investigated in the previous chapter, but using the MT geometry of the USPIP, allowing plume expansion and deceleration of the aerosol particles before their transition into the proximal part of the IP.

Commercial formulations assessed show a broad range of aerosol characteristics and USPIP deposition ranging from about 25% in the Alvesco formulation up to more than 55% in the Foster formulation. Based on their IP deposition characteristics, products assessed can be classified into two groups. One group comprising of the Beclohexal and Alvesco formulations showing moderate IP deposition and another group, comprising of the Sultanol, Flutide, and Foster formulations, showing extensive IP deposition. Both pMDI formulations in the low deposition group are solution based, which presumably offers advantages for fine aerosol production, as no particles must be de-agglomerated. An interesting characteristic of the Alvesco formulation is the increased actuator deposition (in comparison to all formulations assessed) which is not easily understood as both formulations are qualitatively equivalent; i.e. API with HFA 134a and ethanol as solubility enhancer. This might be explained comparing the actuator nozzle diameters of both devices (see Figure 27). The slightly decreased nozzle orifice of the Alvesco pMDI might produce a wider spray cone (and hence increased actuator deposition [32]) which also reflects in the actuator design having a spherical mouthpiece whereas the mouthpiece of the Beclohexal pMDI is rather ellipsoid. Additionally, the ethanol content of the formulations might differ. A higher ethanol content would prolong the drying kinetics of the primary droplets produced, which also might trigger increased actuator deposition. However, since the quantitative composition is not reported, it would be speculative to draw any solid conclusions about this.

In contrast, preparations in the high deposition group are suspension based (Sultanol and Flutide), which also reflects in the actuator nozzle orifice diameters, which are significantly wider than their solution-based counterparts. An exception to this is the Foster pMDI, which

is solution based and shows an orifice diameter comparable to those found in the low deposition group, but shows increased IP deposition. An explanation for this can be found evaluating the formulation of the pMDI; besides ethanol and HFA 134a it also contains hydrochloric acid. Adding an acidic agent might have been necessary to solubilize the formoterol hemifumarate, which, along with beclometasone dipropionate, is also incorporated into the formulation. Though HCl is claimed on the label it is to be assumed that a solution of HCl in water was added. Due to its relatively low vapor pressure this would undoubtedly prolong the drying kinetics of the primary droplets produced, which, as discussed before, would act to reduce overall aerosol performance.

Though increased mIP deposition was observed for all formulations tested, high USPIP deposition was found to be indicative of increased mIPext deposition. Using the data discussed in the previous chapter, it was found that no valid quantitative assessment of the processes participating in the mechanism to cause an increase in observed IP deposition could be made. It should be noted that any increase in IP deposition may be a result of inertial impaction of particles in the IP bend as well as impaction/settling of particles caused by the trachea geometry, and pMDI with VHC and DPI experiments indicated relevance of the latter impaction/settling process. Cascade impactor analysis of the Sultanol pMDI formulation used in the previous chapter using the mIPext showed an increase in IP deposition when compared to the USP and USP3D IPs, but lower deposition when compared to the mIP. This is in good agreement with conclusions drawn from the previous study, as it could be interpreted that the increased deposition now found was caused by geometrical factors of the proximal part of the IP only, whereas the fraction differing from the mIP deposition was also related to increased inertial impaction in the bend of the IP, caused by the shortened distance from the pMDI device to the bend of the mIP. Similar results were obtained when analyzing the Flutide forte formulation. Here, a significant increase in IP deposition was observed for both mIPs, when compared to the USPIP. Additionally, the difference in deposition between the mIP and the mIPext was found to be less pronounced when compared to the Sultanol pMDI, indicating that inertial impaction in the bend of the IP here contributes to a lesser extent. The Foster pMDI behaved similar to the Sultanol formulation, so that conclusions drawn there are applicable.

Contrary, analysis of the Beclohexal and Alvesco formulations showed statistically increased mIP depositions, whereas the mIPext depositions were found statistically equivalent, when compared to the USPIP. So, it is to be concluded that for these formulations the increase in

mIP deposition observed, is solely caused by inertial impaction at the bend of the mIP; in contrast, increased impaction or settling in the proximal part of the mIP does not occur. Interestingly, mIPext deposition was found to be lower than USPIP deposition in the case of the Alvesco formulation. This might be correlated to the high actuator deposition, which can already retain the particles that would otherwise impact in the bend of the trachea. As discussed in the previous chapter the change in motion vector when transitioning from the distal to the proximal section of the mIP is less pronounced, when compared to the USPIP. This consideration also applies to the mIPext, as the angle connecting the two elements is identical to that of the mIP. So, this observation could be interpreted as evidence for the relevance of the head position of the patient when using a pMDI device, which is not reflected in the USPIP. As discussed in the previous chapter, this observation is in good agreement with literature. Nevertheless, this specific case might provide a suitable test system for future studies utilizing the 3D printed mIP model to investigate this effect more closely.

All pMDI formulations showing tracheal deposition are found in the high USPIP deposition group, whereas all low deposition group formulations investigated were not susceptible to that. As FPFs of low USPIP deposition pMDIs were found to be higher than ones of high IP deposition pMDIs, this finding might be attributed to the overall aerosol properties of these formulations, as apparently these pMDIs lack the fraction of aerosol particles that would be separated in the trachea. So, the ratio of both mechanisms participating in the overall effect is directly correlated to the overall aerosol performance, i.e. only formulations containing larger aerosol particles (or agglomerates) are susceptible to tracheal deposition. This finding is in good agreement with a study by Leach et al. conducted in 2012 [169]. Here, the authors compared *in vitro* and *in vivo* deposition of a HFA solution based pMDI formulation of beclometasone (QVAR, TEVA, Petach Tikwa, Israel) and a suspension based HFA formulation of Fluticasone (Advair, GSK, London, UK). The authors used radiolabelled aerosol particles to identify areas of deposition in the patients and quantify relative deposition. Radiolabelling was validated by cascade impaction assessment, allowing an estimate on how comparable findings of this study are to the present one. Unfortunately, some inconsistencies in the analytical method reported compromise detailed evaluation of the study. It is reported that aerosol characteristics were generated using the NGI, whereas deposition plots show a stage setup matching the ACI without terminal filter. Assuming that S0 and S7 reported in the plots correspond to S1 and MOC stages, which would be in that position in a regular NGI setup, data shows good agreement with results from this study. However, it must be noted that

the QVAR formulation shows higher actuator and consequently lower overall CI deposition, when compared to the Beclohexal formulation. It is unclear, how many actuations of the pMDI have been applied in each run but since the maximum number monographed in the USP and Ph.Eur. (i.e. n= 10) was applied in the present study, it is to be assumed that the number of actuations was equal, or less. As deposition in the actuator is likely to be a surface related effect this mechanism might be saturable, which would cause a decrease of relative actuator deposition at increased numbers of actuations. Anyways, as Leach et al. reported *in vivo* deposition data calculated as fractions *ex valve*, it is a valid assumption that data provided there is applicable to the formulations investigated here. Figure 35 shows γ-scintigraphic images of beclometasone and fluticasone deposition, as reported by Leach et al. The beclometasone formulation shows high deposition in the MT region and the lungs, whereas the fluticasone formulation shows deposition in the MT, trachea, and lungs. This finding supports the conclusion that tracheal deposition is relevant, though depending on the overall performance of the formulation, and that the proximal section of the mIP is related to physiological reality.

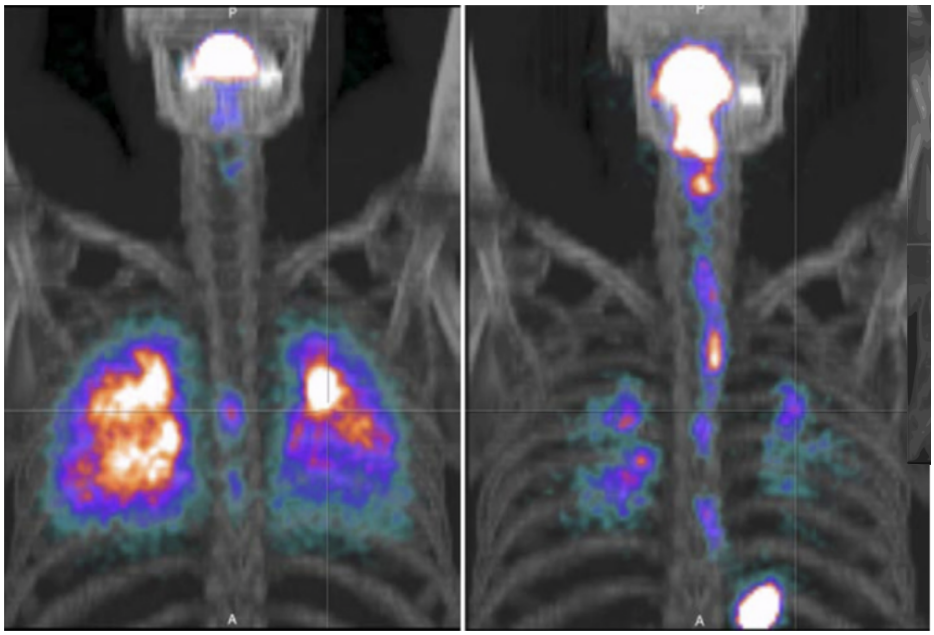

Figure 35. *In vivo* particle deposition of beclometasone (left) and fluticasone (right) pMDI formulations. Reproduced from [169] with kind permission from Elsevier.

.

Another aim of this study was to provide additional data on the correlation of particle deposition predicted to *in vivo* deposition, so formulations assessed were selected based on availability of appropriate data in the literature. Due to their limited availability, studies investigating lung deposition in mild asthmatic patients have also been included. In the case of pMDIs, comparative studies indicate that the impact of mild asthmatic symptoms on lung deposition is rather low [172,173], so in this context these groups might be treated equivalently.

In the case of salbutamol, $FPF_{emitted}$ determined using the mIP correlates well with *in vivo* deposition data reported in the product´s prescribing information. Comparability of this data set has already been discussed in the previous chapter. In contrast, the mIPext and USPIP rather overestimate lung deposition (see Figures 33 and 34). Similar results were observed in the case of the Flutide formulation, but IVIVC using the mIPext was found closer to that achieved with the mIP. And, predictions of lung deposition showed a greater deviation from *in vivo* deposition in the case of the Advair formulation. Advair is a combination preparation that includes fluticasone propionate and salmeterol xinafoate as a single dose formulation and as such, differs from the fluticasone propionate only formulation, assessed in this study. Nevertheless, as both formulations are formulated using the same approach it may be assumed that they perform similarly. The study presents cascade impactor data in order to validate the radio labeling technique applied, but fails to provide aerosol characterization of the test formulations. Comparability of data presented in that study to the *in vitro* performance reported in this study has already been discussed, in the previous paragraph. It was found that all IPs tested tended to overestimate the lung deposition that could be obtained. IVIVC of formulations containing beclometasone only, was found to be accurate within the precision range of the *in vivo* studies, whereas the USPIP rather over estimated its performance. In contrast, mIPext and USPIP provided good prediction in case of the Foster formulation, whereas the mIP underestimated *in vivo* performance, but not significantly. Comparing *in vivo* and *in vitro* data of the ciclesonide formulation shows that USPIP and mIPext overestimated lung deposition, whereas good IVIVC was achieved using the mIP.

Drawing conclusions from all the studies evaluated, NGI studies conducted using the mIPext tended to over predict lung deposition, whereas analysis with the mIP provided good IVIVC in most cases. Consequently, one must conclude that the distal section of the USPIP and the mIPext, which is supposed to mimic the MT region (see previous chapter), lacks physiological relevance. On the other hand, keeping in mind that the increase in mIP

deposition for many formulations was found to be caused by inertial impaction in the shortened MT region of the IP, these findings highlight the necessity to further investigate the exact mechanism that retains the particles in the MT region, and to incorporate these findings into the mIP. Thus, the next iteration of the mIP should include a biorelevant MT section.

# 4 Development of respirable, excipient free formulations of rifampicin

## 4.1 Results and discussion of the exploratory study

### 4.1.1 Results

#### 4.1.1.1 Manufacturing process

Solutions or suspensions of rifampicin, spray dried (SDr) from various solvents, was found to be a suitable method to produce dry powders that were appropriate for inhalation testing. Process yields were found to differ strongly among different formulations (Table 14). Lower process yields at higher solid content of formulations SDr from acetone was related to increased deposition in the column, rather than the product collection vessel of the spray drier. And only product collected from the collection vessel was included in this study.

In reference to Table 14 it should be noted that the formulation designated “RFDCMexp1” could not be manufactured, as the suspension was too viscous for atomization with the modified three fluid nozzle for the spray drier. Furthermore, spray freeze drying of the RFaqexp1 did not result in individual particles suitable for inhalation testing. And although spray freezing of the solution was found as suitable method to produce individual ice spheres, subsequent freeze-drying induced collapse and agglomeration of the particles. Recovery of the mass was possible only by scraping it off from the collection vessel, which eventually caused the formation of soft pellets. Due to this result, this formulation was omitted and no additional experiments were conducted. Similar results were obtained by consecutive spray and freeze drying of formulation RFaqexp2. Here, the collapse of the powder bed was not as pronounced as in the case of RFaqexp1, so soft pellets obtained were tested for their aerosol properties.

Table 14. Overview of manufacturing process during the exploratory study.

| Sample name | Solvent | Yield [%] | Approx. process time [h] |
|---|---|---|---|
| RFaqexp2 | | 23.0 | 12.5 |
| RFaqexp3 | | 29.9 | 12.5 |
| RFaqexp4 | | 13.9 | 8.3 |
| RFaqexp5 | | 26.2 | 4.1 |
| RFIPAexp1 | IPA | 39.7 | 1.8 |
| RFIPAexp2 | | 57.2 | 1.2 |
| RFIPAexp3 | | 55.1 | 0.6 |
| RFMeOHexp1 | MeOH | 36.1 | 2.0 |
| RFMeOHexp2 | | 36.5 | 1.3 |
| RFMeOHexp3 | | 67.5 | 0.7 |
| RFEtOHexp1 | EtOH | 14.5 | 31.7 |
| RFEtOHexp2 | | 17.4 | 21.0 |
| RFEtOHexp3 | | 32.2 | 10.5 |
| RFEtOHexp4 | | 36.8 | 0.6 |
| RFACexp1 | acetone | 43.0 | 3.0 |
| RFACexp2 | | 29.9 | 2.0 |
| RFACexp3 | | 19.4 | 1.0 |
| RFDCMexp2 | DCM | 12.0 | 0.1 |
| RFDCMexp3 | | 6.9 | 0.1 |

#### 4.1.1.2 Stability of aqueous solutions for the duration of the SDr process

Figure 36 shows process characteristics acquired during the manufacture of RFaqexp3, as well as concentrations of the feed solution and relative absorption at 334 nm and 475 nm for the duration of the acquisition. Concentration means are normally distributed, as indicated by the Shapiro-Wilk test ($p= 9.0 \times 10^{-10}$). Similarly, relative absorptions were also found to be normally distributed ($p= 3.5 \times 10^{-10}$).

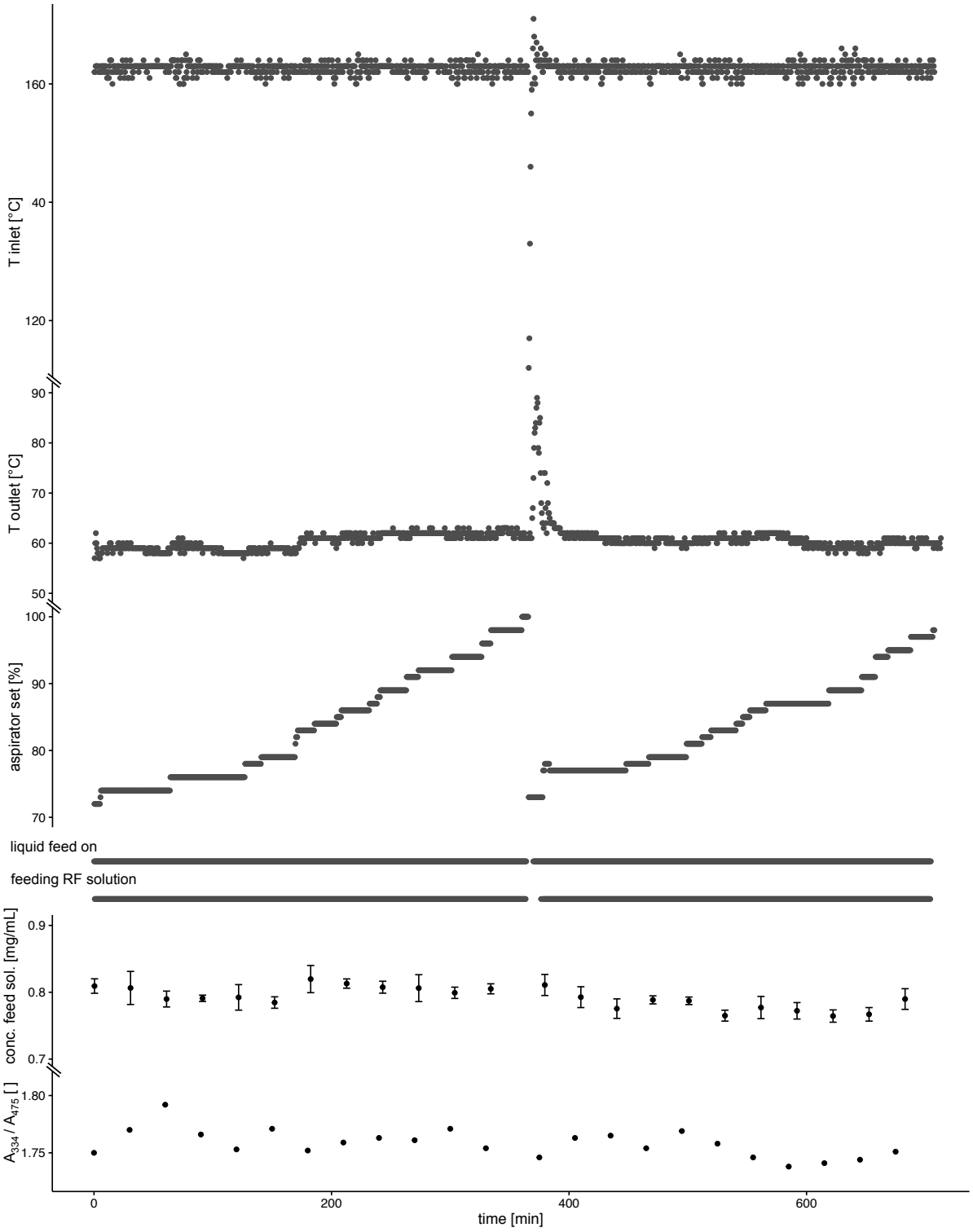


Figure 36. Process characteristics of RFaqexp3 showing in- and outlet temperature, aspirator set, and chemical stability of the RF feed solution.

#### 4.1.1.3 XRPD analysis of samples from the exploratory study

XRP diffractograms of samples manufactured are shown in Figure 37. XRP diffractograms of the individual samples were shifted on the y-axis for better comparability.

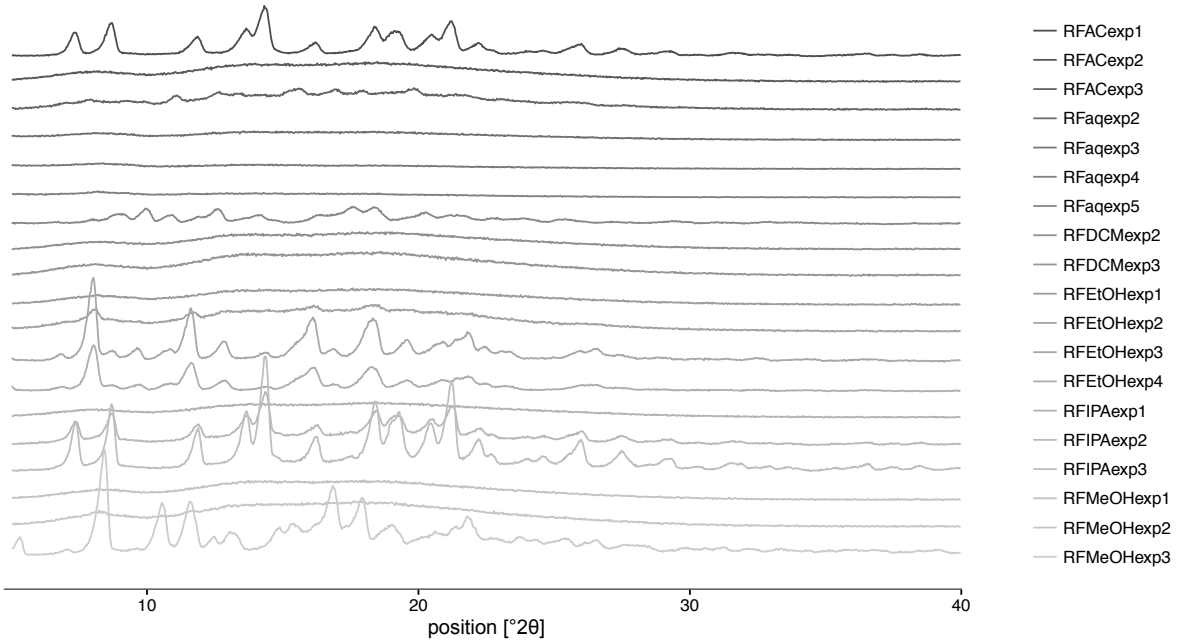


Figure 37. Results of XRPD analysis of samples from the exploratory study.

#### 4.1.1.4 Aerodynamic assessment of RF formulations using the Handihaler device

Aerosol characteristics of samples dispensed from the Handihaler device are shown in Table 15.

Table 15. Overview of aerosol characteristics of samples from the exploratory study.

| Sample name | FPF [%] | EF [%] | MMAD [$\mu$m] | GSD [ ] |
|---|---|---|---|---|
| RFaqexp2 | 47.92 ±4.12 | 97.89 ±1.67 | 1.70 ±0.19 | 3.21 ±0.07 |
| RFaqexp3 | 90.06 ±3.74 | 98.80 ±0.08 | 1.38 ±0.30 | 3.54 ±0.37 |
| RFaqexp4 | 78.02 ±0.32 | 97.92 ±0.16 | 1.82 ±0.13 | 3.21 ±0.08 |
| RFaqexp5 | 47.17 ±1.74 | 91.15 ±2.05 | 3.03 ±0.06 | 2.02 ±0.02 |
| RFIPAexp1 | 40.12 ±2.46 | 75.82 ±7.34 | 2.84 ±0.10 | 1.92 ±0.04 |
| RFIPAexp2 | 32.20 ±2.26 | 82.16 ±1.63 | 3.09 ±0.15 | 2.04 ±0.04 |
| RFIPAexp3 | 24.90 ±3.37 | 83.13 ±0.74 | 3.44 ±0.20 | 2.14 ±0.02 |
| RFMeOHexp1 | 23.27 ±2.06 | 72.47 ±3.20 | 2.96 ±0.14 | 2.09 ±0.06 |
| RFMeOHexp2 | 33.18 ±4.07 | 60.59 ±5.12 | 2.56 ±0.05 | 1.96 ±0.05 |
| RFMeOHexp3 | 31.04 ±1.13 | 81.51 ±2.53 | 3.91 ±0.01 | 2.08 ±0.03 |
| RFEtOHexp1 | 6.24 ±0.42 | 84.74 ±1.71 | 6.36 ±0.19 | 2.07 ±0.33 |
| RFEtOHexp2 | 13.28 ±1.17 | 74.46 ±2.29 | 3.00 ±0.07 | 2.07 ±0.12 |
| RFEtOHexp3 | 44.05 ±3.09 | 89.13 ±1.16 | 3.87 ±0.18 | 1.67 ±0.06 |
| RFEtOHexp4 | 43.70 ±3.52 | 88.48 ±1.57 | 3.83 ±0.16 | 1.91 ±0.02 |
| RFACexp1 | 7.07 ±1.92 | 83.99 ±2.32 | 2.96 ±0.21 | 1.89 ±0.02 |
| RFACexp2 | 28.30 ±2.74 | 61.22 ±1.78 | 2.52 ±0.05 | 2.02 ±0.02 |
| RFACexp3 | 32.20 ±2.26 | 82.16 ±1.63 | 3.09 ±0.15 | 2.04 ±0.04 |
| RFDCMexp2 | 37.00 ±1.00 | 79.31 ±2.56 | 3.41 ±0.25 | 2.23 ±0.05 |
| RFDCMexp3 | 35.29 ±3.53 | 69.31 ±4.37 | 3.00 ±0.09 | 2.09 ±0.04 |

#### 4.1.1.4.1 Samples SDr from water

Aerodynamic assessment of samples spray dried from watery solutions (RFaqexp2, RFaqexp3, and RFaqexp4) showed low to moderate inhaler and capsule deposition, moderate deposition over NGI stages S1-S7 and moderate to high deposition in the terminal filter (see Figure 38), which resulted in exceptionally high FPFs. As mentioned in the previous section, product recovery of RFaqexp2 from the vessel used for freeze drying facilitated the formation of soft pellets. NGI analysis of this formulation showed that a large fraction of the sample deposited in the preseparator stage. In contrast, RFaqexp3 and RFaqexp4 showed little preseparator deposition. Analysis of RFaqexp5 showed moderate inhaler, IP, and preseparator deposition, moderate deposition over S1-S6, and little or no deposition on S7, the MOC, or filter stages. Aerosol characteristics can be found in Table 15.

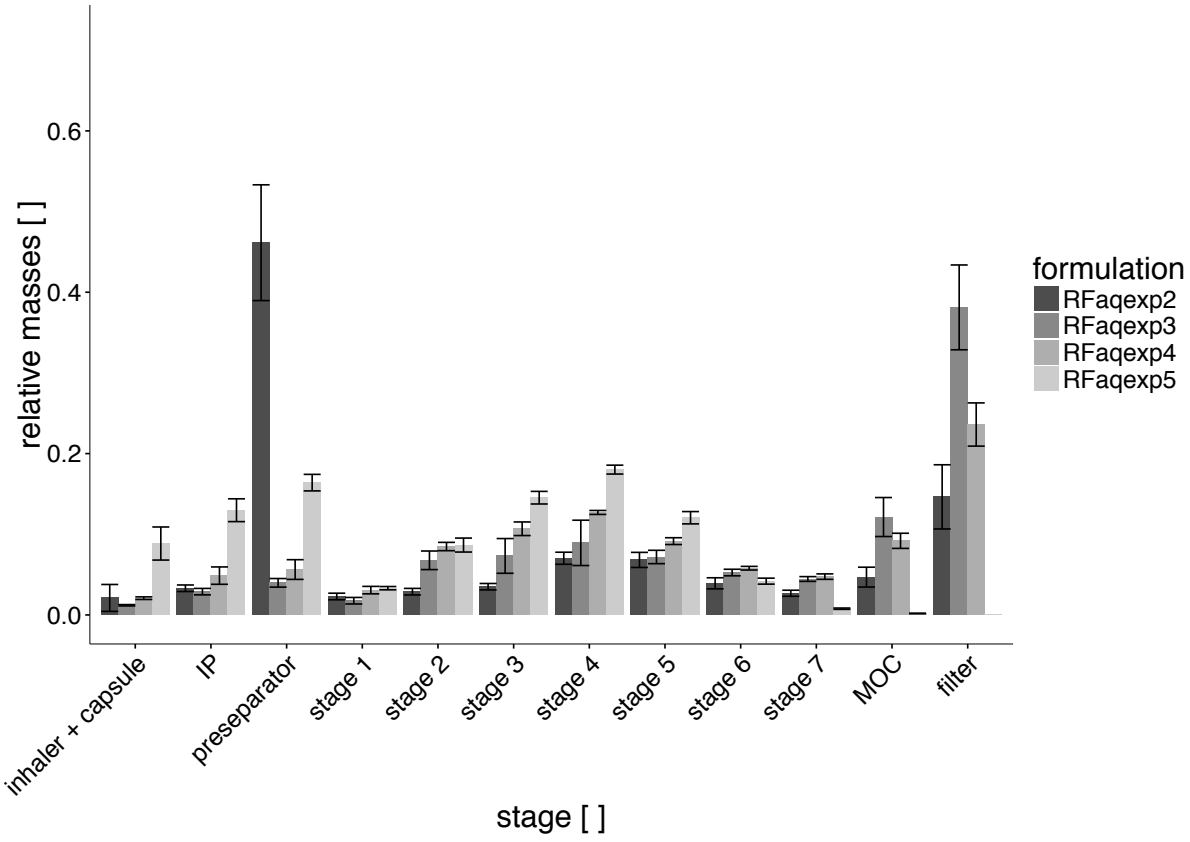


Figure 38. Results of cascade impactor experiments of samples SDr from water (exploratory study).

#### 4.1.1.4.2 Samples SDr from IPA

Cascade impactor analysis of samples SDr from IPA showed moderate to high inhaler, IP, and preseparator deposition (see Figure 39). S1-S6 deposition was found to be moderate. S7-filter stages showed little to no deposition. The highest FPF was observed for RFIPAexp1 (see Table 15).

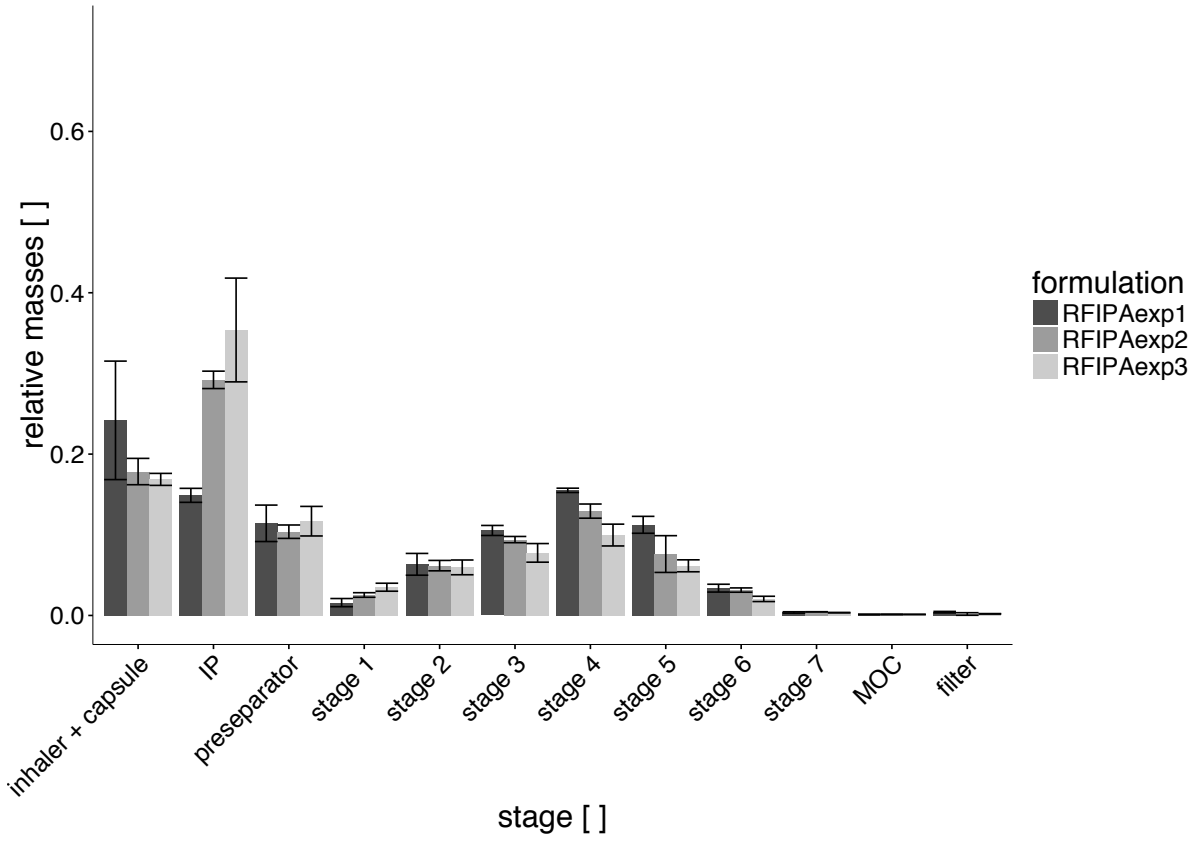


Figure 39. Results of cascade impactor experiments of samples SDr from IPA (exploratory study).

4.1.1.4.3 Samples SDr from MeOH

Cascade impactor analysis of solutions and suspensions SDr from MeOH showed moderate to high inhaler, IP, and preseparator deposition (see Figure 40). Deposition at S1-S6 was found to be moderate. All samples showed little deposition at S7-filter stages. The average FPF value obtained was found to be in an intermediate range (see Table 15).

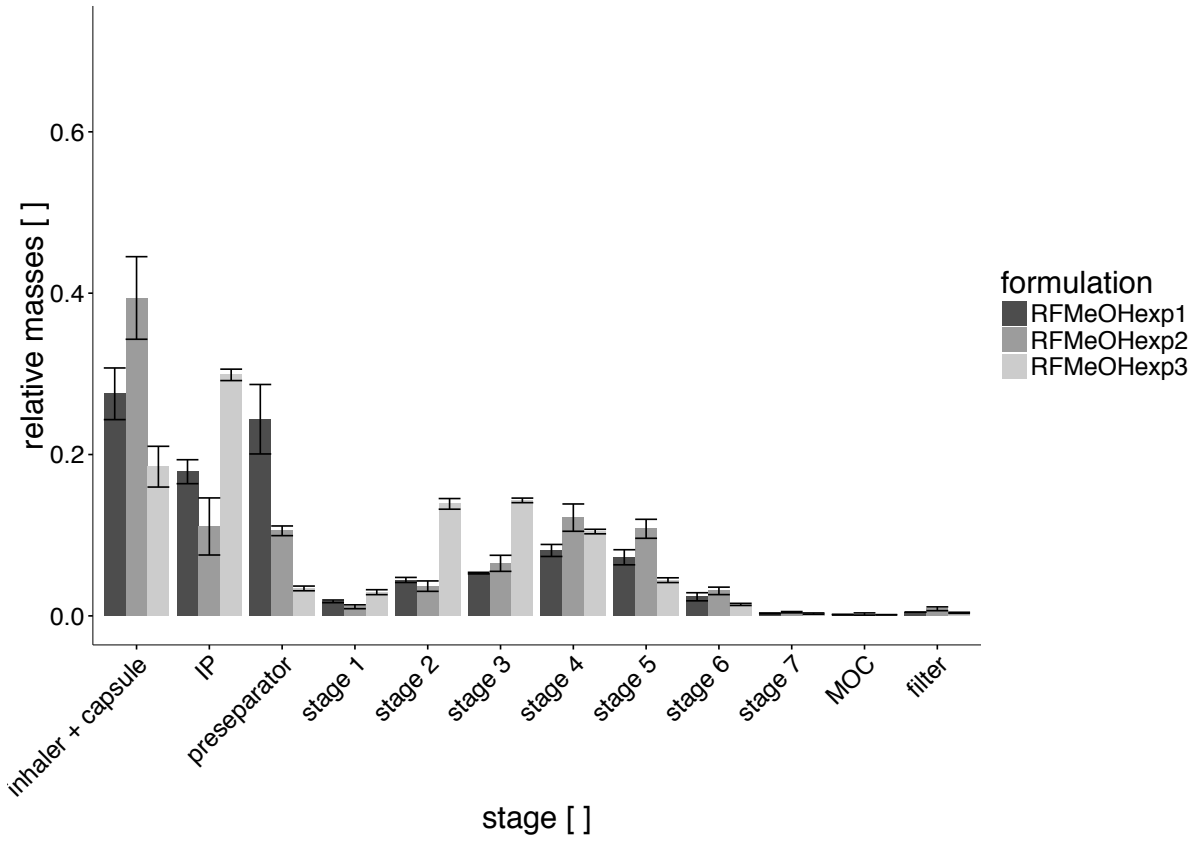


Figure 40. Results of cascade impactor experiments of samples SDr from MeOH (exploratory study).

#### 4.1.1.4.4 Samples SDr from EtOH

Samples SDr from ethanolic solutions (RFEtOHexp1) showed moderate to high inhaler and capsule deposition, high deposition at the IP and preseparator and little deposition at S1-S6 (see Figure 41). Downstream from S6, practically no deposition was observed. RFEtOHexp2 showed high inhaler and capsule, moderate IP, and high preseparator deposition. Similarly to RFEtOHexp1, deposition at S1-S6 was found to be very little; but the average MMAD (see Table 15) was shifted to a smaller diameter. RFEtOH3 and RFEtOH4 showed moderate deposition for the inhaler, capsule, and IP, and little deposition at the preseparator. Both formulations displayed moderate to high deposition at S2-S4, low to moderate deposition at S1, S5, and S6, and practically no deposition at S7-filter stages.

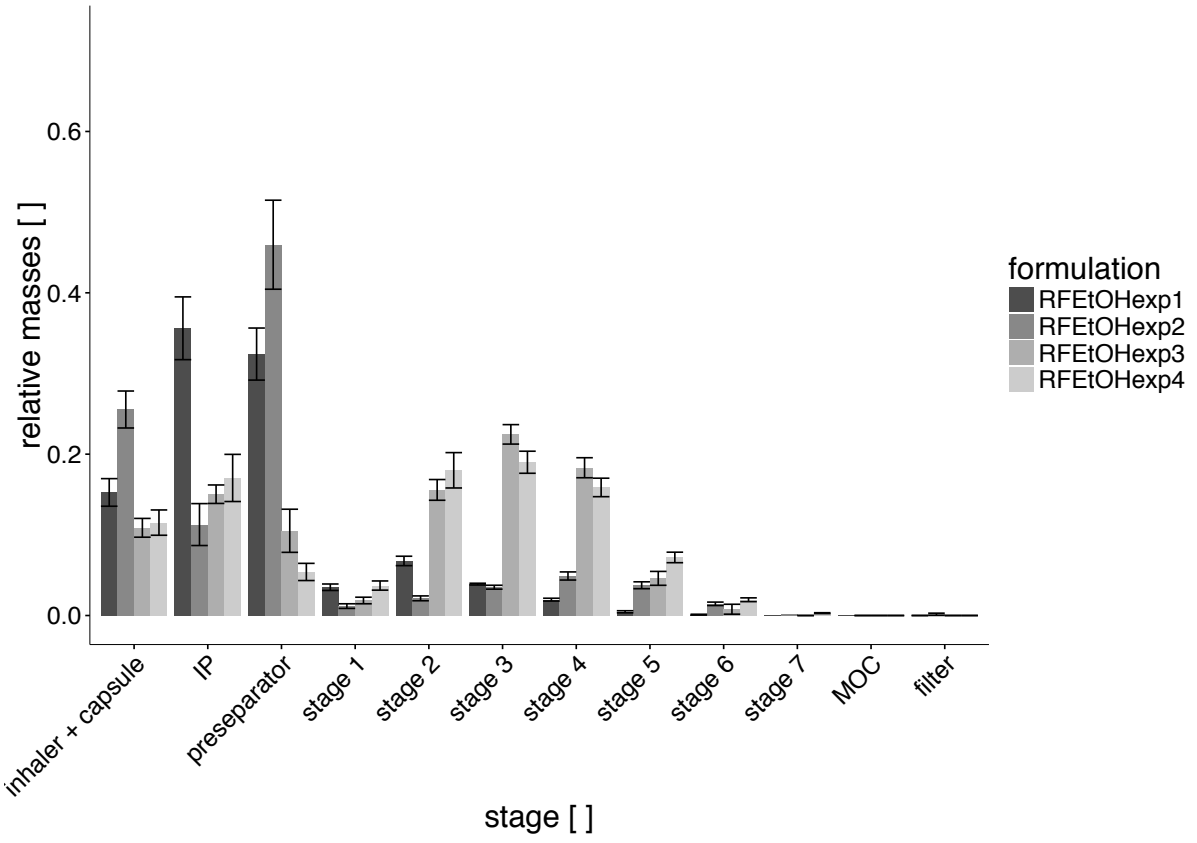


Figure 41. Results of cascade impactor experiments of samples SDr from EtOH (exploratory study).

4.1.1.4.5 Samples SDr from acetone

Samples SDr from acetone showed moderate to high inhaler, IP, and preseparator deposition (see Figure 42). Moderate deposition at S2-S6 was found in the case of RFACexp2 and RFACexp3. In contrast, RFACexp1 showed moderate deposition at S1-S3. All samples showed little S7, MOC, and filter deposition. Aerosol characteristics can be found in Table 15.

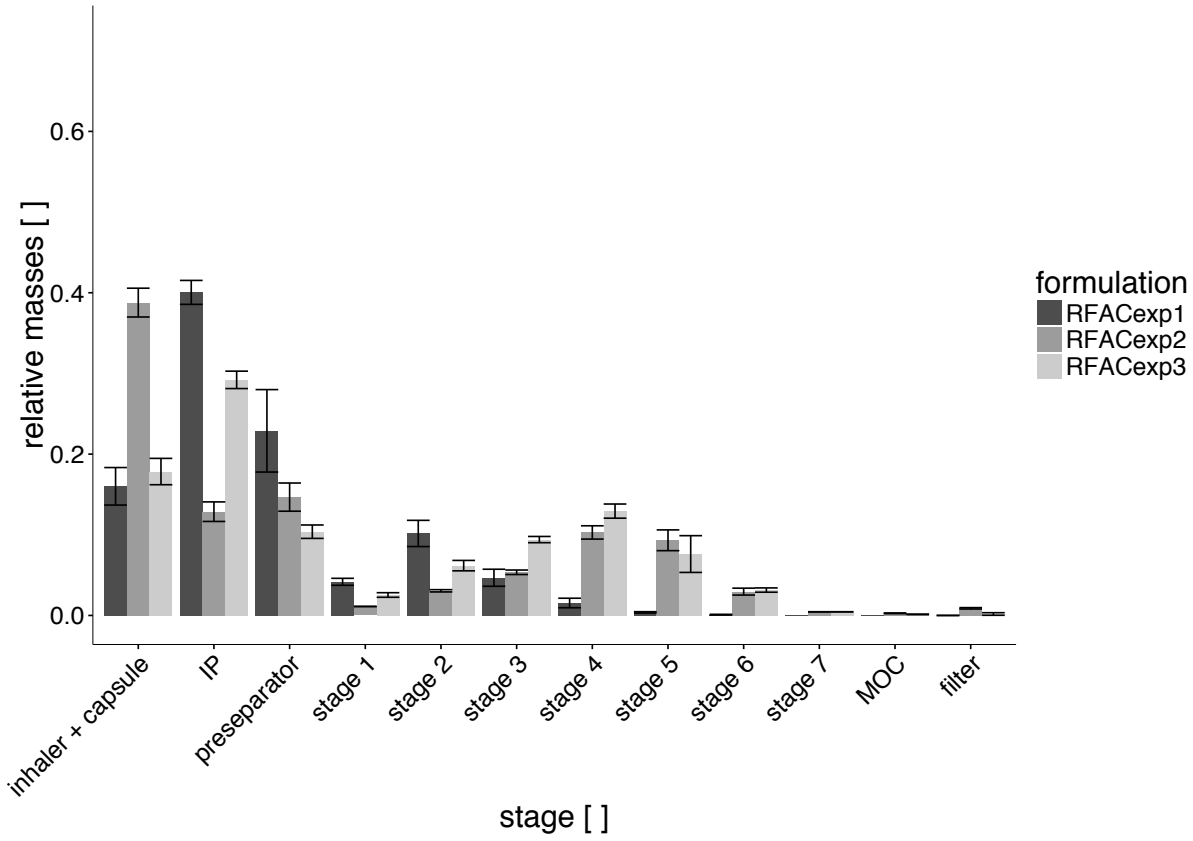


Figure 42. Results of cascade impactor experiments of samples SDr from acetone (exploratory study).

#### 4.1.1.4.6 Samples SDr from DCM

Samples SDr from DCM showed moderate to high inhaler and IP deposition and moderate deposition in S2-S5. Preseparator as well as S6-filter deposition was found to be low (see Figure 43). Aerosol characteristics are shown in Table 15.

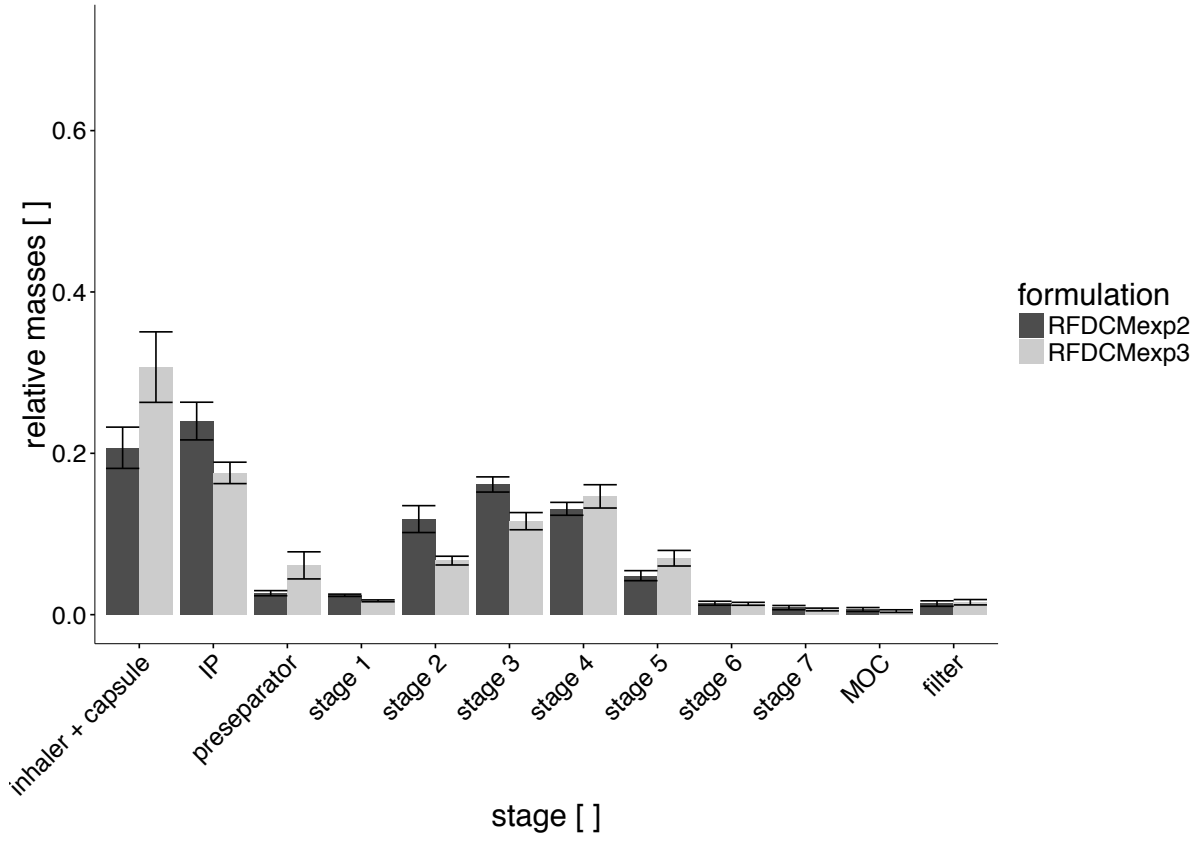


Figure 43. Results of cascade impator experiments of samples SDr from DCM (exploratory study).

### 4.1.2 **Discussion**

In the exploratory study trials, processability of solutions and suspensions of RF in various solvents, including standard organic solvents and water, was investigated and evaluated. As a secondary outcome parameter, suitability of formulations obtained for inhaler testing was assessed using the Next Generation Pharmaceutical Impactor. Additionally, XRPD analysis was utilized to discriminate between different (pseudo-) polymorphs of RF.

Stability of the manufacturing process was assessed analyzing both, stability of the process parameters as well as chemical stability of the feed solution. As RF is reported to show limited stability in aqueous solutions and process time of this batch was the longest in this study, RFaqexp3 was evaluated as most critical batch and was monitored in detail. The feed solution supplied was sampled and quantified at intervals of 30 minutes, over the period of the entire manufacturing process and concentration means were found to be normally distributed (Shapiro-Wilk test), indicating good stability. Additionally, a full UV-vis spectrum was recorded at each time point. According to the Ph.Eur. relative absorption of RF at 334 nm and 475 nm approximates as 1.75, so this method was used to verify chemical stability, in case the HPLC method used fails to separate degradation products (especially RF-quinone and desacetyl-RF) and RF. However, relative absorptions were found to comply with requirements and deviations were distributed evenly over the entire process.
It was concluded that RF remains stable in aqueous solution, for the duration of the process. Inlet and outlet temperatures were found to be stable over the entire process as well. During the process, the terminal filter unit became congested with product. As a result the aspirator set point was adjusted over time in order to maintain the pre-specified flow rate through the system of 15 NCMH. The terminal cloth filter had to be replaced with a clean one after approx. 360 minutes; reflecting in the interruption in the liquid feed, the drop in aspirator set point, and a temporary increase in outlet temperature (related to interrupted solvent atomization prior to switching off the aspirator). Decrease and subsequent overshooting of inlet temperature after exchanging the filter, was due to the heating interruption when replacing the filter, and consequent readjustment. The process presented is a representative example for all batches manufactured, but it should be noted, that inlet temperature, process duration, and number of filter bags used is dependent on the individual batch composition. Process parameters were recorded for all batches manufactured, but will not be discussed individually as it is very similar to what has already been presented earlier.

In the following section, all formulations that were manufactured in this study will be evaluated and discussed.

#### 4.1.2.1 RFaqexp1

It was found that spray freeze drying of aqueous solutions of RF did not result in a product suitable for inhalation testing. Manufacture of individual frozen spheres was found to be feasible, but subsequent freeze drying induced collapse of the particles, which was to be expected as the solid content of solutions sprayed was well below 0.2%$_{w/w}$, whereas a solid content of 1% is reported [176] as lower limit to generate structural intact lyophilisates. As equilibrium solubility was found to be 0.2 mg/mL (= 0.02%$_{w/v}$), a high degree of supersaturation would be necessary to provide concentrations high enough for the individual particles to remain structurally intact. Alternatively, incorporation of a matrix forming excipient (e.g. carbohydrate) might be suitable to produce intact spherical particles. But since the focus of this study was on the development of an excipient-free formulation, this was beyond the scope of these studies.

#### 4.1.2.2 RFaqexp2

Consecutive spray then freeze drying of aqueous, supersaturated solutions was found to be a feasible way to produce soft pellets, which generally demonstrated better flow properties than non-agglomerated dry powders. As this was not considered to be in the scope of the study, powder flow properties of the samples were not quantified. However, this advantage in formulation processability was achieved at the cost of a drastic reduction in aerosol performance, as soft pellets were not found to de-agglomerate easily following air entrainment, and thus impacted largely in the preseparator stage when analyzed using the NGI. A FPF of approximately 50% indicates superior performance to most commercially available DPI formulations. Nevertheless, this formulation shows a 50% lower FPF, when compared to equivalent formulations, which had not been subjected to the terminal freeze drying step (i.e. RFaqexp3 and RFaqexp4). Therefore, this manufacturing strategy was excluded from further investigation but might be continued at a later stage of development, if flow properties of non-agglomerated particles prove to be insufficient for processability during, for example scale up or production when automated filling is involved.

#### 4.1.2.3 RFaqexp3 and RFaqexp4

Spray drying of supersaturated aqueous solutions of RF resulted in easily aerosolized powders. This reflects in extraordinarily high FPFs, when analyzed using the NGI, which are at minimum comparable to high performance investigational DPI formulations and surpass commercial formulations available (also including pMDI and nebulized formulations), except of the Staccato (Alexza Pharmaceuticals, Mountain View, CA, USA), which performs equivalently well [8]. Thus, these formulations (as well as another RF concentration) were incorporated into the main study and will be discussed there in detail.

#### 4.1.2.4 RFIPAexp1

As expected, spray drying of solutions of RF in IPA yielded amorphous particles showing the characteristic collapsed spheres (‘donut shape’, data not shown), which is widely reported in literature. Aerosol performance of this formulation was found to be the best of all amorphous batches except RFaqexp3 and RFaqexp4. Hence, this formulation was included in the main study as reference formulation.

#### 4.1.2.5 RFIPAexp2 and RFIPAexp3

Spray drying of suspensions of RF in IPA yielded crystalline particles of the F-I polymorph. Aerosol assessment showed intermediate performance. As these formulations showed no special crystalline state, nor high aerosol performance, these formulations were not included into the main trials.

#### 4.1.2.6 RFMeOHexp1

Spray drying of solutions of RF in MeOH produced particles similar to RFIPAexp1. However, aerosol performance was found to be lower than RFIPAexp1. It may be assumed that reduced FPF is related to a lower geometrical diameter of the particles, which is probably due to a) the slightly lower solubility of RF in MeOH when compared to IPA and b) that RF has a higher tendency to supersaturate in MeOH, which facilitates protracted crust formation upon drying of the particles. Hypothesis b) is deduced from the observation that RF forms an unknown (pseudo-) polymorph when recrystallized from MeOH, which is hypothesized to require a certain degree of supersaturation in the solvent. As RFMeOHexp1 is equivalent to RFIPAexp1 but shows lower aerosol performance, this formulation was not further investigated.

#### 4.1.2.7 RFMeOHexp2

Despite the fact that this formulation is produced using a suspension, the spray dried product shows no distinct crystalline structure, which is probably related to the access amount of RF dissolved, dominating the overall solid state properties of the sample. Aerosol performance was found to be lower than RFIPAexp1, so this formulation was deemed to offer no benefit and was not further investigated.

#### 4.1.2.8 RFMeOHexp3

This formulation is similar to RFMeOHexp2 but with a higher solid fraction in the suspension, and yielded crystalline particles of an unknown (pseudo-) polymorph. Though the aerosol performance is intermediate only, this formulation demanded further investigation in the main study to clarify the solid state.

#### 4.1.2.9 RFEtOHexp1

Spray drying of ethanolic solutions of RF produced ultrafine amorphous particles, which is due to the low equilibrium solubility of RF in EtOH. Aerosol performance was low, as this formulation was extremely cohesive, due to its small geometric diameter (also see acoustic levitator experiments in 4.3.1.9). Though not being suitable for inhalation therapy, it is hypothesized that this formulation might provide a good testing system for DPI devices, as low aerosol performance is expected not to be related to inadequate geometry of the individual particles but rather incomplete de-agglomeration. De-agglomeration efficiency of the DPI would directly correlate to the aerosol performance. However, as of now this conclusion is speculative and should require further investigation in additional studies. Production costs of this formulation may be extremely high, as a large amount of EtOH (about 15 L) was needed to produce powder in a quantity sufficient for the tests in the main study. As the spray rate of the SDr was kept constant over all batches at 7.4 mL/min, this resulted in a spray process duration of more than 30 hours, which demanded the manufacture of three sub-batches. For these reasons it was excluded from the main study.

#### 4.1.2.10 RFEtOHexp2

XRPD analysis of this formulation showed that it has a significant degree of amorphous domains, though traces of an unknown (pseudo-) polymorph could be identified. As aerosol

performance was found to be low, this formulation was omitted in favor of RFEtOH3 and RFEtOH4.

#### 4.1.2.11 RFEtOHexp3 and RFEtOHexp4

Both formulations show the same (pseudo-) polymorph found in RFEtOHexp2 but at a higher degree of crystallinity. De-agglomeration of both formulations was easily achieved and overall aerosol performance was deemed good. Thus, and in order to clarify the solid state of the samples, RFEtOHexp 3 was included into the main study. Having a solid content of the spray solution identical to a formulation previously reported by Son and McConville [91], RFEtOHexp4 was included as a reference to assure comparability.

#### 4.1.2.12 RFACexp1

Unexpectedly, spray drying of solutions of RF in acetone yielded predominantly amorphous particles showing distinct traces of crystalline F-I domains. Two different mechanisms leading to this observation are imaginable. Either, particles crystallized from amorphous material after spray drying or crystalline nanoparticles passing the 0.22 µm filter were included in the feed solution prior to spray drying. Secondary recrystallization appears somewhat unlikely, as no other amorphous sample has shown such behavior so formation of nanocrystals is considered to be more likely. However, similarly to RFEtOHexp1, powders were very cohesive, demonstrating poor aerosol properties. Thus, this sample was excluded from further investigation.

#### 4.1.2.13 RFACexp2 and RFACexp3

Spray drying of suspensions of RF in acetone was found to yield amorphous particles showing aerodynamic properties comparable to RFIPAexp1, but at lower performance. During the spray drying process both batches showed high deposition in the spray cylinder. Product was collected from the collection vessel only. It was unexpected to find amorphous material, as spray drying of suspensions was expected to yield crystalline particles. This might be related to the high deposition of product in the spray cylinder. Only larger particles exceeding a certain aerodynamic diameter would impact in this site so particles suspended

might have been removed from the product collected. Even so, as these formulations offer no benefit over RFIPAexp1, they were excluded from further investigation.

#### 4.1.2.14 RFDCMexp2 and RFDCMexp3

Spray drying of solutions and suspensions of RF in DCM produced amorphous particles showing intermediate aerosol performance. It was unexpected that spray drying of suspensions would produce amorphous material. This observation may be explained by particle separation during the spray drying process. High spray column deposition was observed, so it may be assumed that, due to the high solubility (approx. 200 mg/mL), two distinct particle populations were formed. Recrystallization of RF in DCM presumably yields a suspension with larger primary particles, which is due to excessive particle growth that is related to high solubility. The larger, crystalline particles impacted in the spray column whereas the aerodynamically smaller amorphous particles, which formed from the material dissolved, were separated in the cyclone; where they were collected and analyzed. As these formulations offer no benefit over RFIPAexp1 they were excluded from additional investigation.

Table 16 gives an overview on key findings of the exploratory study and which batches were additionally investigated in the main study trials.

Table 16. Overview of key conclusions of the exploratory study.

| Sample name | Solvent | FPF [%] | Crystallinity [ ] | Polymorph [ ] | Incl. in main study? |
|---|---|---|---|---|---|
| RFaqexp2 | water | 47.92 ±4.12 | amorphous | | |
| RFaqexp3 | | 90.06 ±3.74 | amorphous | | x |
| RFaqexp4 | | 78.02 ±0.32 | amorphous | | x |
| RFaqexp5 | | 47.17 ±1.74 | crystalline | unknown I | x |
| RFIPAexp1 | IPA | 40.12 ±2.46 | amorphous | | x |
| RFIPAexp2 | | 32.20 ±2.26 | crystalline | F-I | |
| RFIPAexp3 | | 24.90 ±3.37 | crystalline | F-I | |
| RFMeOHexp1 | MeOH | 23.27 ±2.06 | amorphous | | |
| RFMeOHexp2 | | 33.18 ±4.07 | amorphous | | |
| RFMeOHexp3 | | 31.04 ±1.13 | crystalline | unknown II | x |
| RFEtOHexp1 | EtOH | 6.24 ±0.42 | amorphous | | |
| RFEtOHexp2 | | 13.28 ±1.17 | semi-crystalline | unknown III | |
| RFEtOHexp3 | | 44.05 ±3.09 | crystalline | unknown III | x |
| RFEtOHexp4 | | 43.70 ±3.52 | crystalline | unknown III | x |
| RFACexp1 | acetone | 7.07 ±1.92 | crystalline | F-I | |
| RFACexp2 | | 28.30 ±2.74 | amorphous | | |
| RFACexp3 | | 32.20 ±2.26 | amorphous | | |
| RFDCMexp2 | DCM | 37.00 ±1.00 | amorphous | | |
| RFDCMexp3 | | 35.29 ±3.53 | amorphous | | |

## 4.2 Results and discussion of the main study investigating manufacture of respirable rifampicin particles using organic solvents

### 4.2.1 Results

#### 4.2.1.1 Manufacture

Manufacture of formulations of RF recrystallized from organic solvents i.e. EtOH and MeOH investigated during the exploratory study was repeated successfully. RFIPAAm1 was manufactured as reference sample. Table 17 shows product yields and processing times from the manufacturing process.

Table 17. Product yields of SDr samples.

| Sample name | Solvent | Yield [%] | Approx. process time [h] |
|---|---|---|---|
| RFEtOHCryst1 | EtOH | 44.6 | 0.6 |
| RFEtOHCryst2 | | 58.8 | 8.4 |
| RFMeOHCryst1 | MeOH | 78.0 | 0.5 |
| RFIPAAm1 | IPA | 42.0 | 1.8 |

#### 4.2.1.2 Physicochemical characterization

##### 4.2.1.2.1 SEM images of particles obtained

SEM pictures (see Figure 44) of RFEtOHCryst1 and RFEtOHCryst2 showed particles of flake like shape in the size range around two to three µm. RFMeOHCryst1 showed two different particle populations of distinct morphology and size. One population showed larger particles of brick like shape, whereas the other displayed smaller particles of collapsed spherical shape similar to RFIPAAm1. RFIPAAm1 showed collapsed spheres as well and displayed the characteristic ‘donut shape’, typically known from spray dried solutions.

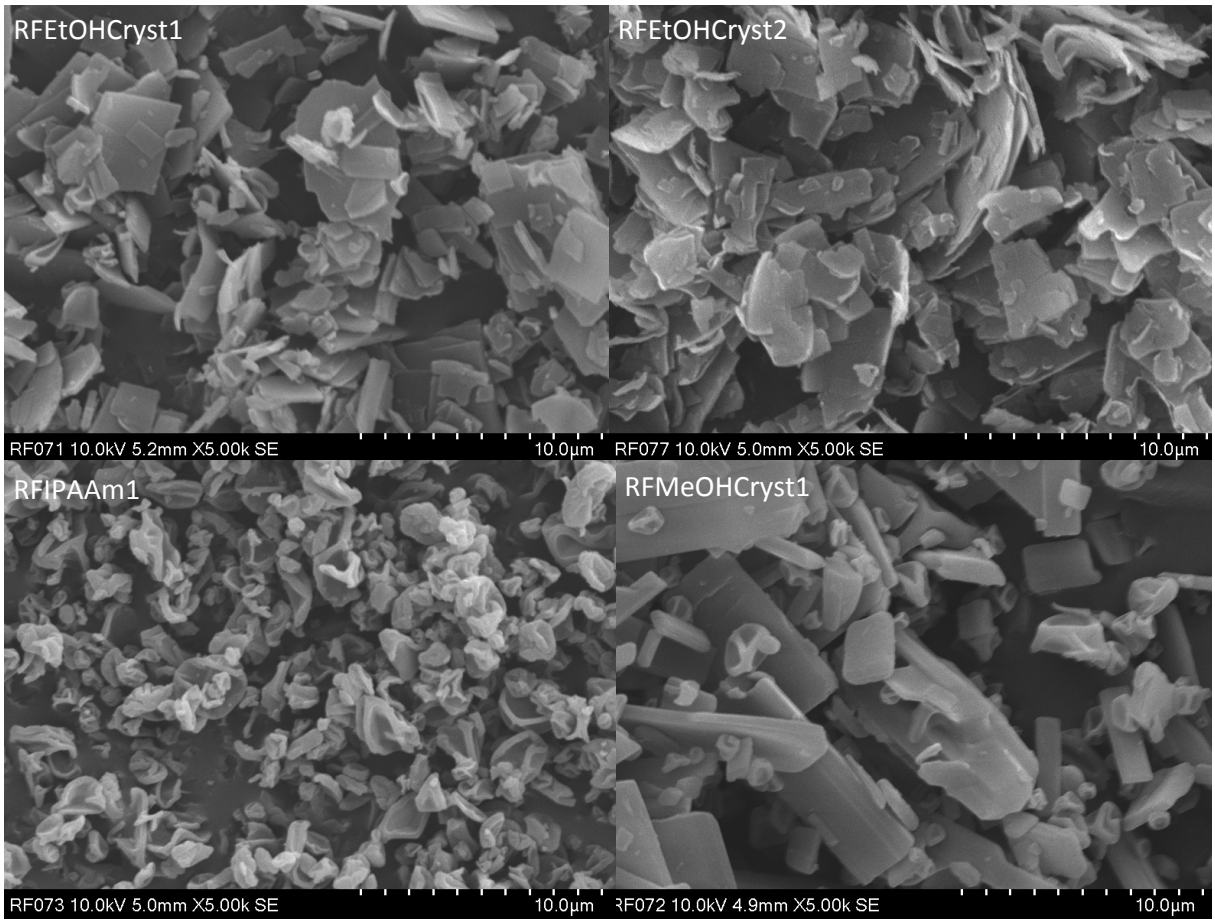


Figure 44. SEM images of RFEtOHCryst1 (top left), RFEtOHCryst2 (top right), RFMeOHCryst1 (bottom right), and RFIPAAm1 (bottom left).

#### 4.2.1.2.2 XRPD analysis of RF samples SDr from organic solutions or suspensions

XRPD analysis (see Figure 45) showed that spray drying of suspensions of RF in EtOH and MeOH produced crystalline particles. The x-ray diffractograms obtained are similar to F-II but present characteristic differences. Both samples recrystallized from EtOH are identical. RFIPAAm1 was found to be amorphous, which is consistent with results of the exploratory study. X-ray diffractograms of RFEtOHCryst1 exposed to different relative humidities (Figure 46) showed that particles decreased in crystallinity on drying by exposure to dry $N_2$ gas. Consecutive exposure to water vapor was found to induce irreversible peak shifts, indicating changes in the crystal composition of the particles, which was found terminated at 60% RH. Further increases in vapor saturation of the gas phase led to an increase in crystallinity, as indicated by an increase of absolute peak intensities. When exposed to lower vapor pressure, intensities were found to decrease and this process was found fully reversible.

RFMeOHCryst1 displayed similar behavior as RFEtOHCryst1 (Figure 47), but transition already occurred during the initial drying step. RFIPAAm1 was found to remain amorphous regardless at which RH it was being equilibrated (Figure 48). X-ray diffractograms of RFEtOHCryst1 and RFMeOHCryst1 exposed to increasing temperature showed that both samples decrease in crystallinity. RFMeOHCryst1 was found to be less thermo stable, showing mainly amorphous diffractograms at a temperature of 80 °C (Figure 50), whereas RFEtOHCryst1 (Figure 49) was found predominantly amorphous at a higher temperature of 100 °C. RFIPAAm1 remained amorphous at any temperature (Figure 51).

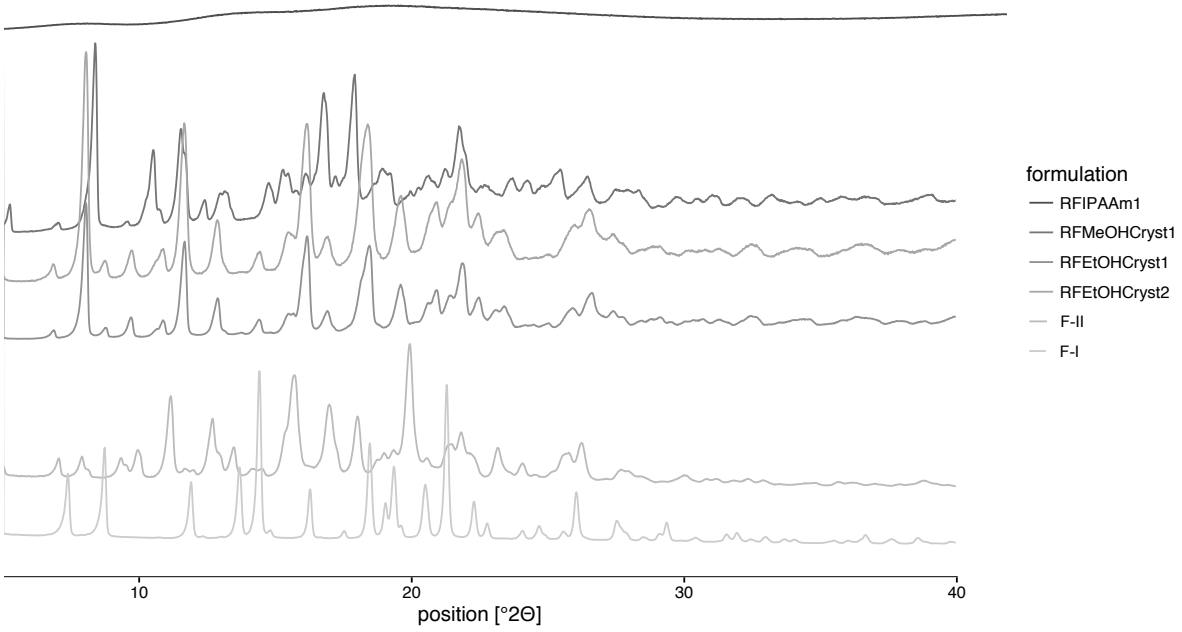


Figure 45. X-ray diffractograms of samples SDr from organic solvents.

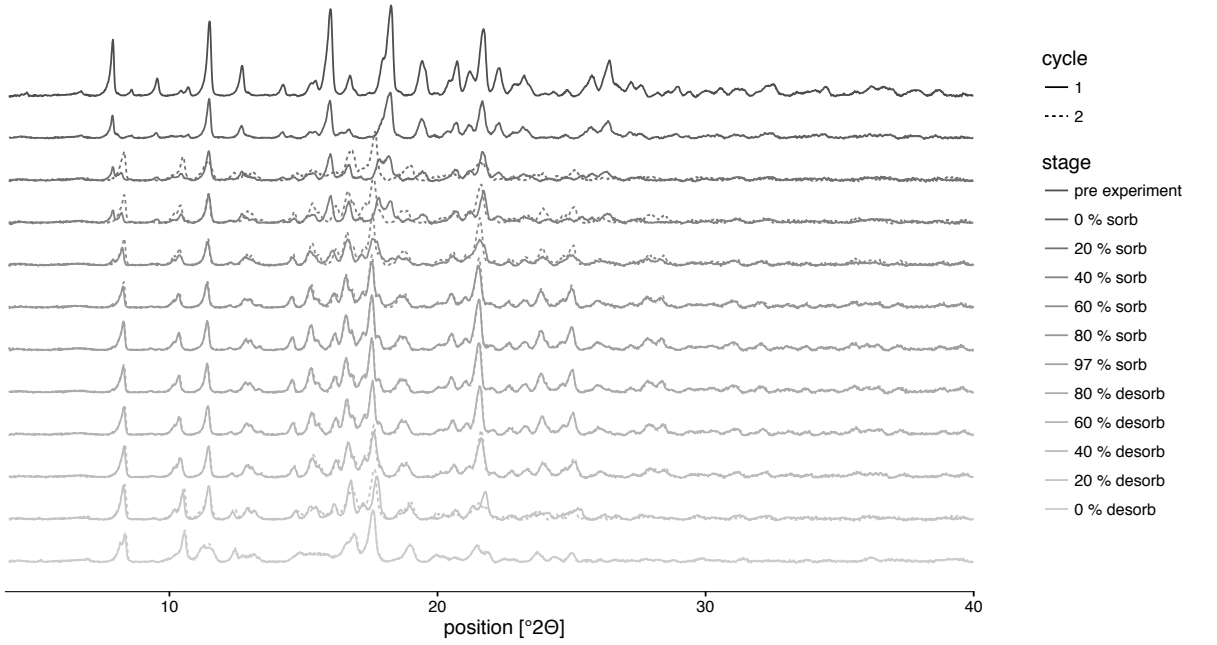


Figure 46. X-ray diffractograms of RFEtOHCryst1, equilibrated at different RF after initial drying.

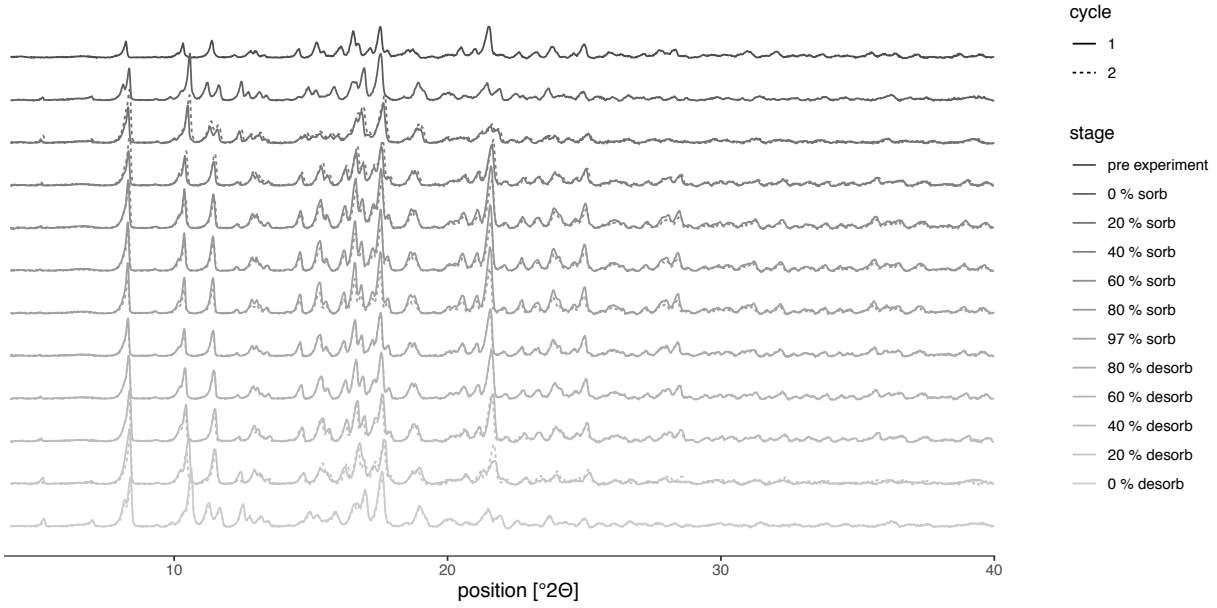


Figure 47. X-ray diffractograms of RFMeOHCryst1, equilibrated at different RH after initial drying.

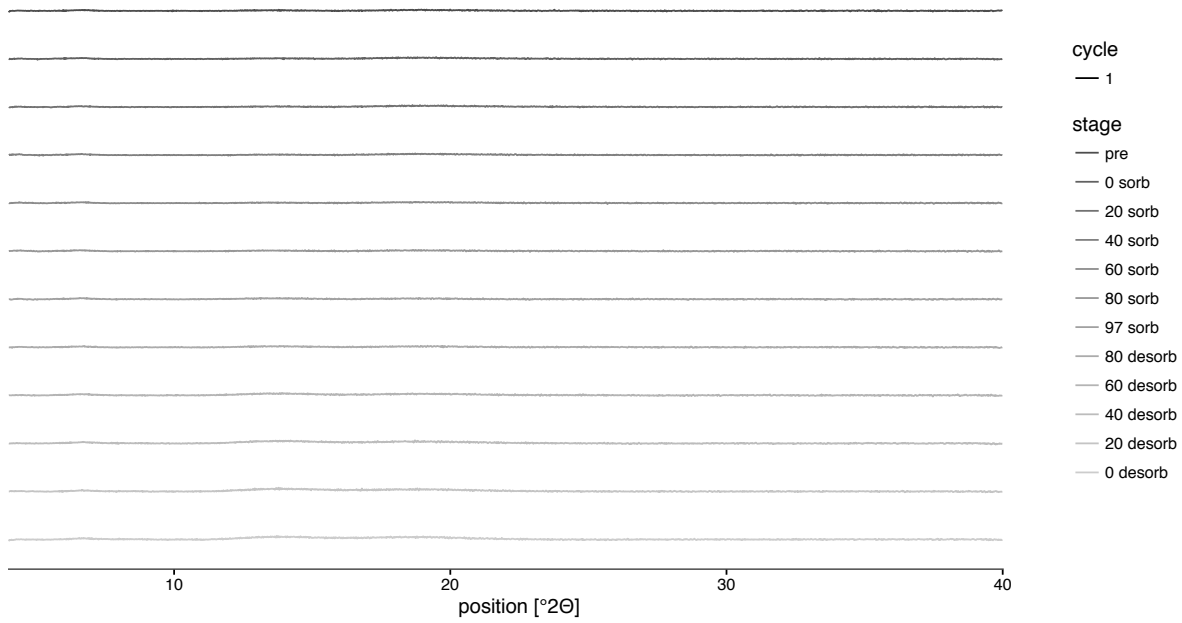


Figure 48. X-ray diffractograms of RFIPAAm1, equilibrated at different RH after initial drying.

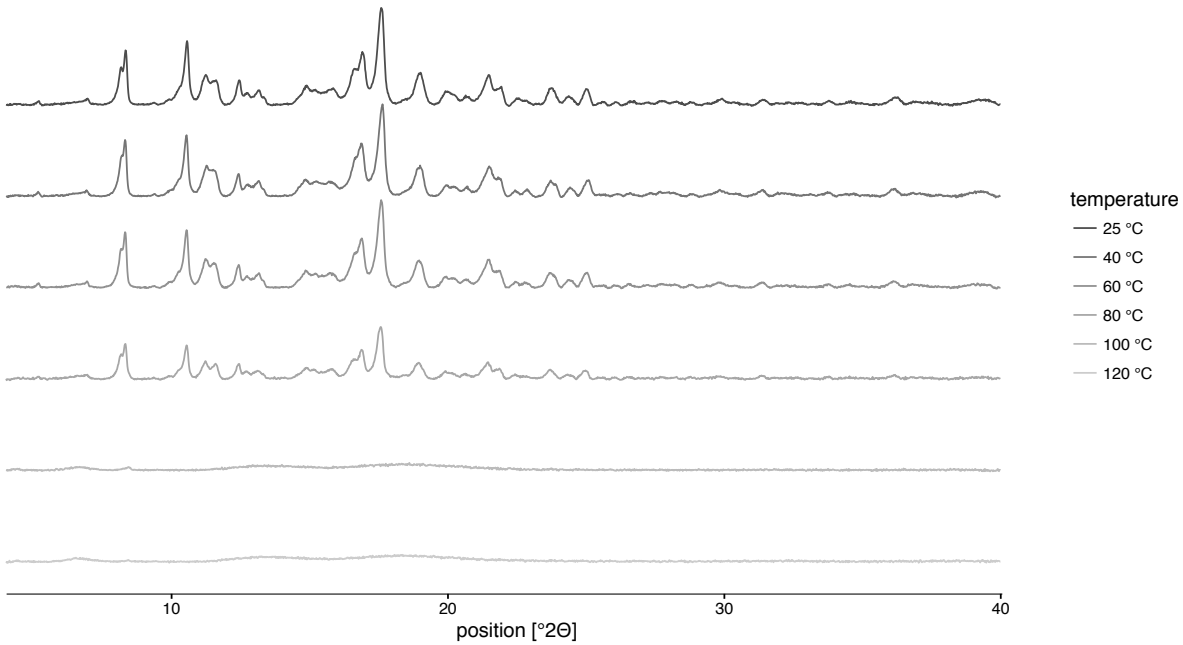


Figure 49. X-ray diffractograms of RFEtOHCryst1, equilibrated at different temperatures after initial drying.

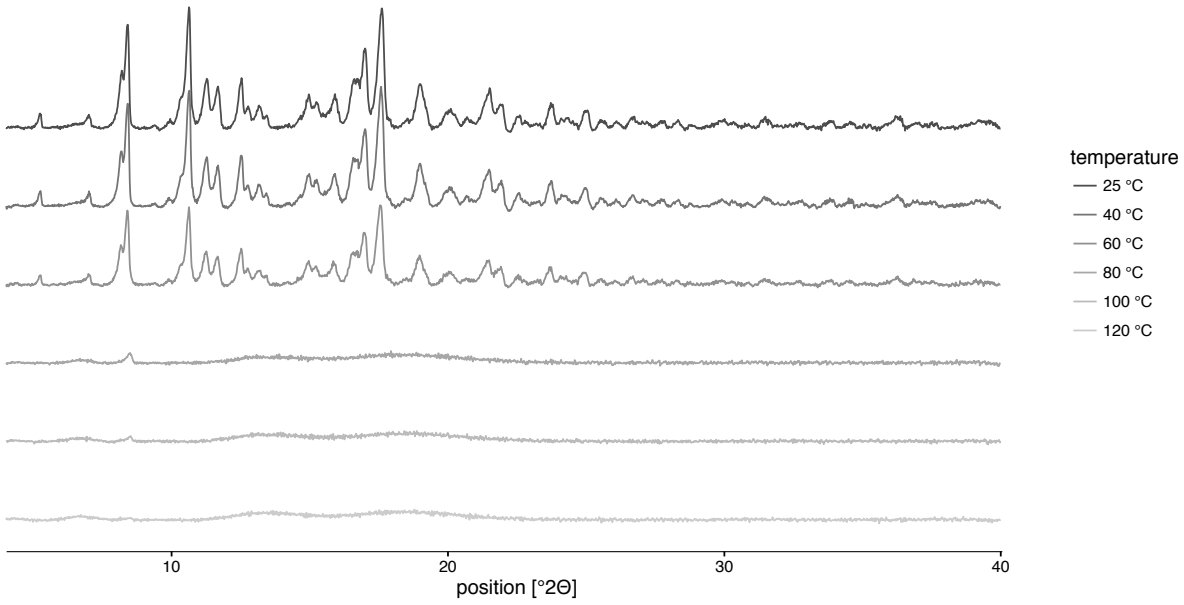


Figure 50. X-ray diffractograms of RFMeOHCryst1, equilibrated at different temperatures after initial drying.

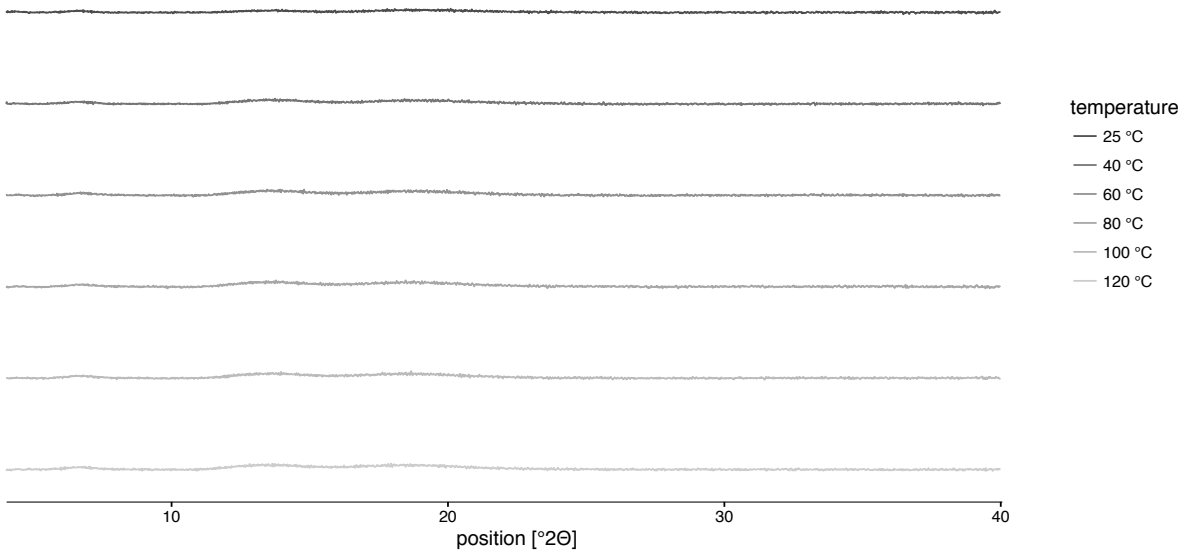


Figure 51. X-ray diffractograms of RFIPAAm1, equilibrated at different temperatures after initial drying.

#### 4.2.1.2.3 Analysis of residual solvents using the GC and Karl Fisher analysis

Analysis of residual solvents showed that RFEtOHCryst1 and RFEtOHCryst2 contain residual EtOH (Table 18). RFMeOHCryst1 was found to contain residual MeOH. Analysis of residual solvents showed that RFIPAAm1 contained residual isopropyl alcohol. All samples contained residual water.

Table 18. Overview of physical and chemical charaterization of RF samples.

| Sample name | Purity HPLC [%] | Water content [%] | Organic solvents [%] | TGA [%] |
|---|---|---|---|---|
| RFEtOHCryst1 | 91.0 ±0.2 | 0.6 ±0.3 | 8.4 ±0.1 (EtOH) | 90.6 ±0.2 |
| RFEtOHCryst2 | 90.3 ±1.9 | 1.3 ±0.2 | 7.9 ±0.7 (EtOH) | 90.3 ±0.2 |
| RFMeOHCryst1 | 95.3 ±0.6 | 1.8 ±0.1 | 5.8 ±0.6 (MeOH) | 94.5 ±0.2 |
| RFIPAAm1 | 97.6 ±1.5 | 1.1 ±0.2 | 2.9 ±0.2 (IPA) | 96.2 ±0.3 |

#### 4.2.1.2.4 DSC analysis of RF samples SDr from organic solutions or suspensions

Differential scanning calorimetry experiments of RFEtOHCryst1 and RFEtOHCryst2 showed broad desolvation peaks showing maxima at about 155 °C and 135 °C respectively (Figure 52), followed by a glass transition at 163 °C and an exothermic event starting from 180 °C. Results obtained from samples of RFMeOHCryst1 yielded similar results. The desolvation peak, that showed a maximum at about 130 °C, was less pronounced here. Also, peaks associated with decomposition are less pronounced. RFIPAAm1 showed an earlier desolvation peak (max= 68 °C). The glass transition, which was found at 163 °C, was followed by another exothermic peak.

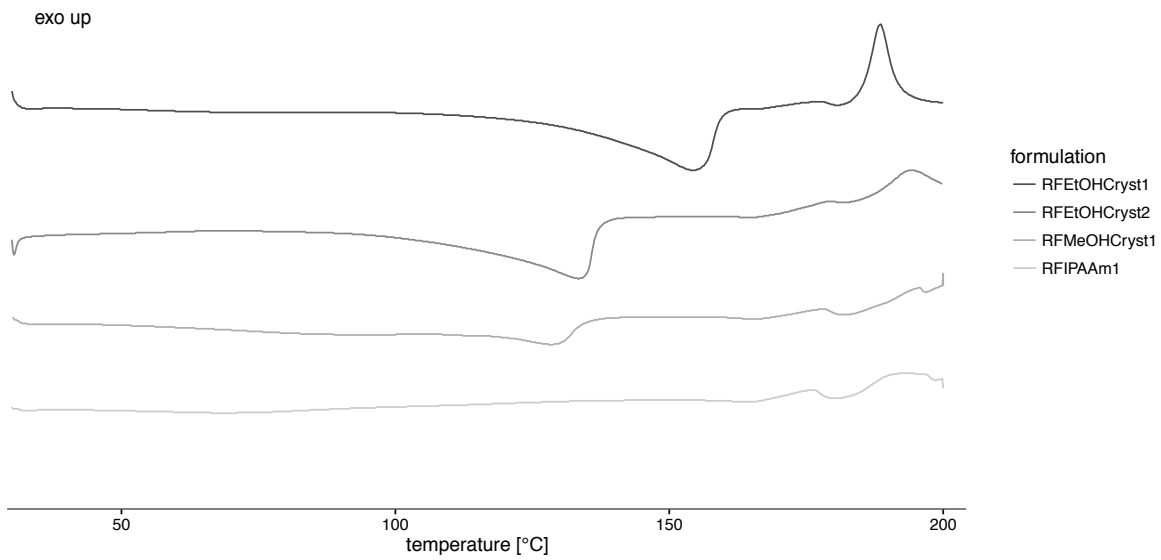


Figure 52. Results of DSC analyses of samples SDr from organic solvents.

#### 4.2.1.2.5 DVS analysis of RF samples SDr from organic solutions or suspensions

DVS analysis of RFEtOHCryst1 and RFEtOHCryst2 showed a loss in mass after exposure of one 0-97-0% RH cycle (see Figures 53 and 54). Desolvation isotherms of the first and second cycle were found to be congruent. Sorption/desorption isotherms of the second cycle showed characteristics identical to the isotherms obtained when analyzing RFMeOHCryst1. The isotherms differ in the extent of water uptake during the terminal equilibration step at 97% RH, which also is reflected in the extent of the hysteresis observed. RFMeOHCryst2 showed

three distinct sorption kinetics (Figure 55). The first and second displayed a sigmoidal transition with an inflection point at about 25% RH, and the second and third transitioned gradually one into the other. Extrapolated linear fits were found to intersect at 87.6% RH. Maximum water uptake at the equilibrated stage (Cycle 2) was found to be 9.9% w/w, 12.8% w/w, and 10.8% w/w for RFEtOHCryst1, RFEtOHCryst2, and RFMeOHCryst1 respectively. RFIPAAm (Figure 56) displayed a different sorption behavior, showing two distinct linear sorption kinetics and extrapolated linear fits intersected at 78.0% RH. Maximum water uptake was found to be 17.2% w/w.

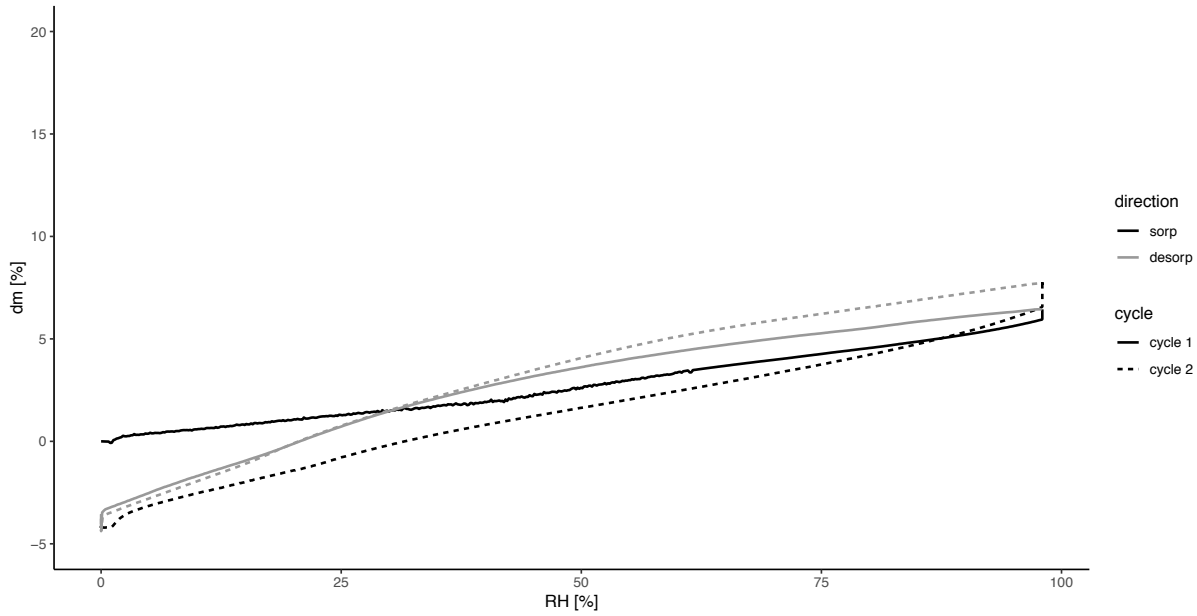


Figure 53. Results of DVS analysis of RFEtOHCryst1.

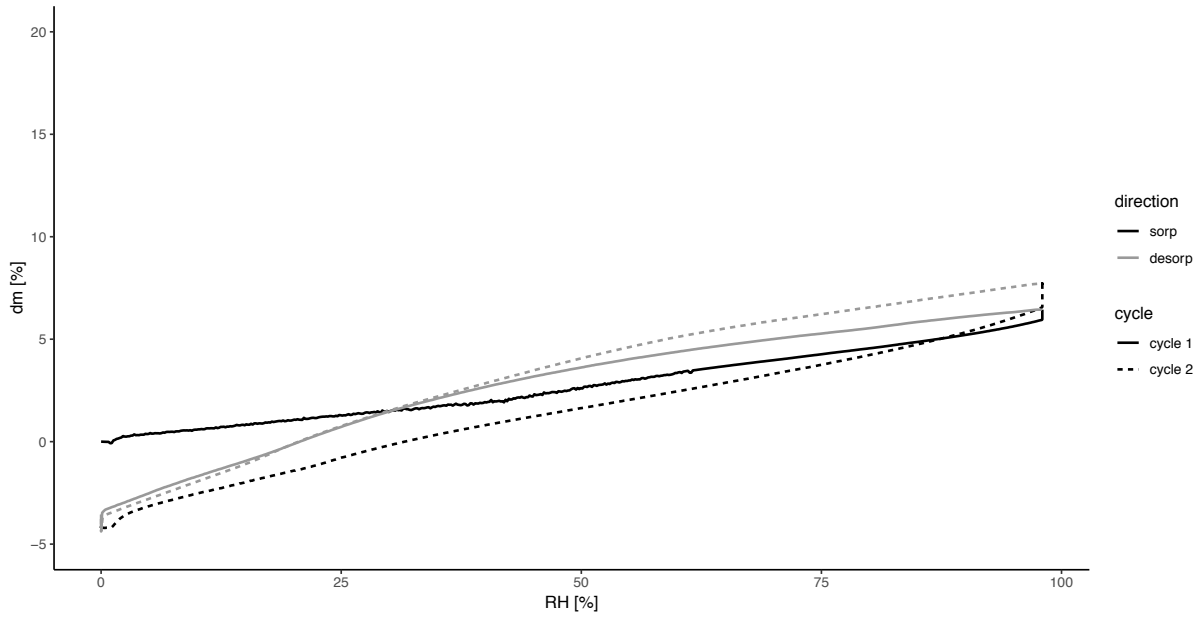


Figure 54. Results of DVS analysis of RFEtOHCryst2.

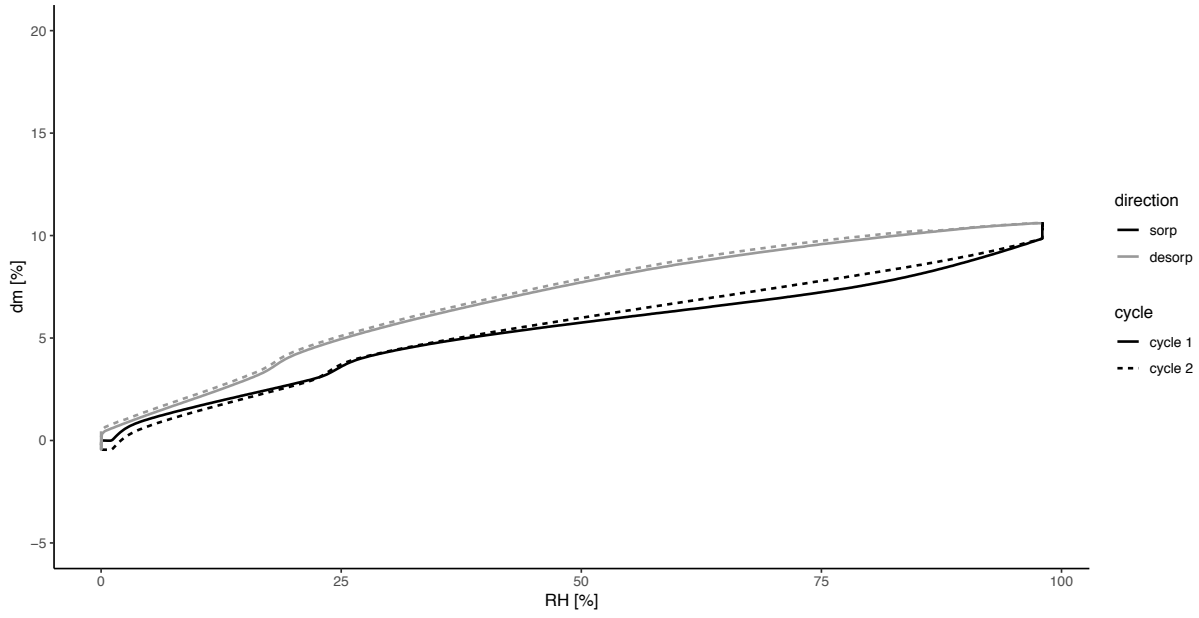


Figure 55. Results of DVS analysis of RFMeOHCryst1.

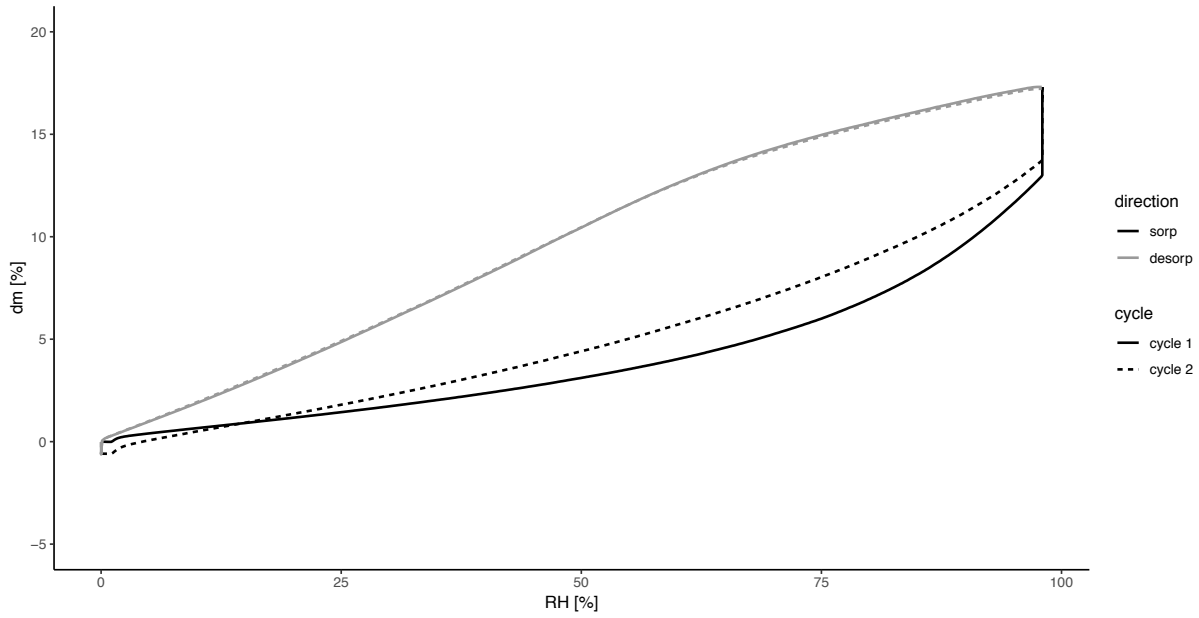


Figure 56. Results of DVS analysis of RFIPAAm1.

#### 4.2.1.3 Aerodynamic assessment of formulations using the Handihaler device

All formulations assessed showed good aerosol properties. Table 19 shows an overview on FPF, EF, MMAD, and GSD of the formulations tested. RFEtOHCryst2, was found to empty well from the capsule and showed moderate preseparator and low IP deposition respectively (Figure 57). In contrast, RFEtOHCryst1, RFMeOHCryst1, and RFIPAAm1 displayed extensive retention in device and capsule, which was found to reduce after storage in the case of RFEtOHCryst1 (as indicated in Section 4.2.1.6). IP deposition was found to be moderate, with RFIPAAm1 showing significantly lower deposition, when compared to the other formulations assessed. Preseparator deposition was found to be low for all formulations except RFIPAAm1, which showed moderate deposition. Particle size distributions of RFEtOHCryst1 and RFMeOHCryst1 were found to be similar, which was reflected in comparable MMAD and GSD values. In comparison, RFEtOHCryst2 showed a slight increase in MMAD, but GSD was found comparable. Conversely, MMAD of RFIPAAm1 was found to be lower and the GSD higher, when compared to the other formulations assessed. All samples showed little to no MOC and filter stage deposition.

Table 19. Aerodynamic characteristics of RF samples dispensed from the Handihaler device.

| Sample name | FPF [% ] | EF [% ] | MMAD [$\mu$m ] | GSD [ ] |
|---|---|---|---|---|
| RFEtOHCryst1 | 36.6 ±2.1 | 72.8 ±2.1 | 3.2 ±0.0 | 1.9 ±0.0 |
| RFEtOHCryst2 | 38.2 ±0.8 | 86.6 ±1.5 | 3.9 ±0.2 | 1.9 ±0.4 |
| RFMeOHCryst1 | 36.5 ±0.7 | 71.8 ±1.7 | 3.2 ±0.2 | 1.9 ±0.1 |
| RFIPAAm1 | 37.1 ±4.3 | 69.1 ±2.3 | 2.0 ±0.6 | 2.9 ±0.1 |

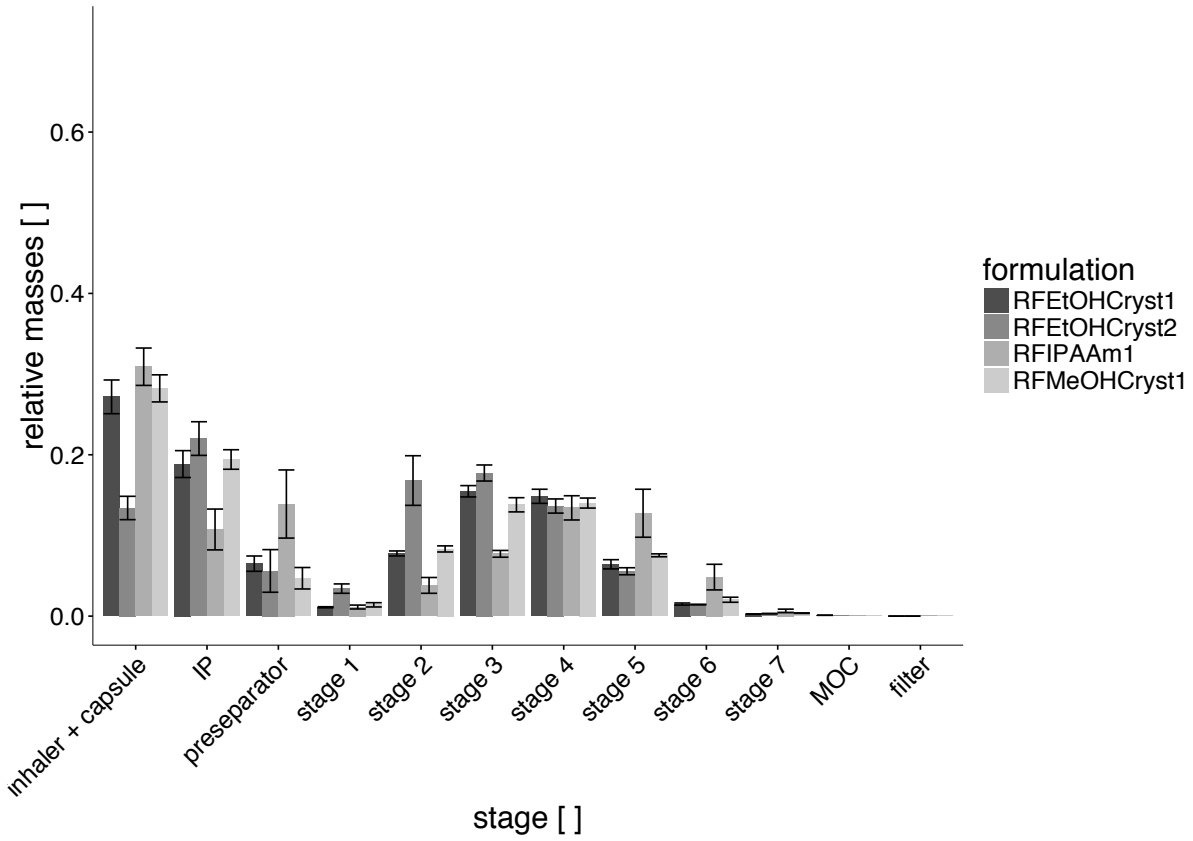


Figure 57. Results of cascade impactor experiments analyzing samples SDr from organic solvents, using the Handihaler device.

#### 4.2.1.4 Aerodynamic assessment of formulations using the Breezhaler device

Assessment of aerosol properties using the Breezhaler device (Figure 58) yielded better results when compared to the Handihaler. Inhaler and capsule depositions were found to be lower in all cases, but RFMeOHCryst1 showed an increased deposition. Cumulative IP and preseparator depositions were found to be reduced in all cases except RFIPAAm1, this translated into higher FPFs (Table 20). Overall performance of RFIPAAm1 was found to be similar with both devices, though an increase in MMAD was noted.

Table 20. Aerodynamic characteristics of RF samples dispensed from the Breezhaler device.

| Sample name | FPF [%] | EF [%] | MMAD [$\mu$m] | GSD [ ] |
|---|---|---|---|---|
| RFEtOHCryst1 | 54.5 ±6.8 | 80.3 ±1.6 | 2.7 ±0.4 | 2.4 ±0.1 |
| RFEtOHCryst2 | 50.1 ±2.6 | 87.1 ±1.1 | 3.3 ±0.2 | 2.5 ±0.0 |
| RFMeOHCryst1 | 52.2 ±1.3 | 61.4 ±2.7 | 1.6 ±0.1 | 2.2 ±0.1 |
| RFIPAAm1 | 35.91 ±1.5 | 73.7 ±4.6 | 3.0 ±0.2 | 2.8 ±0.2 |

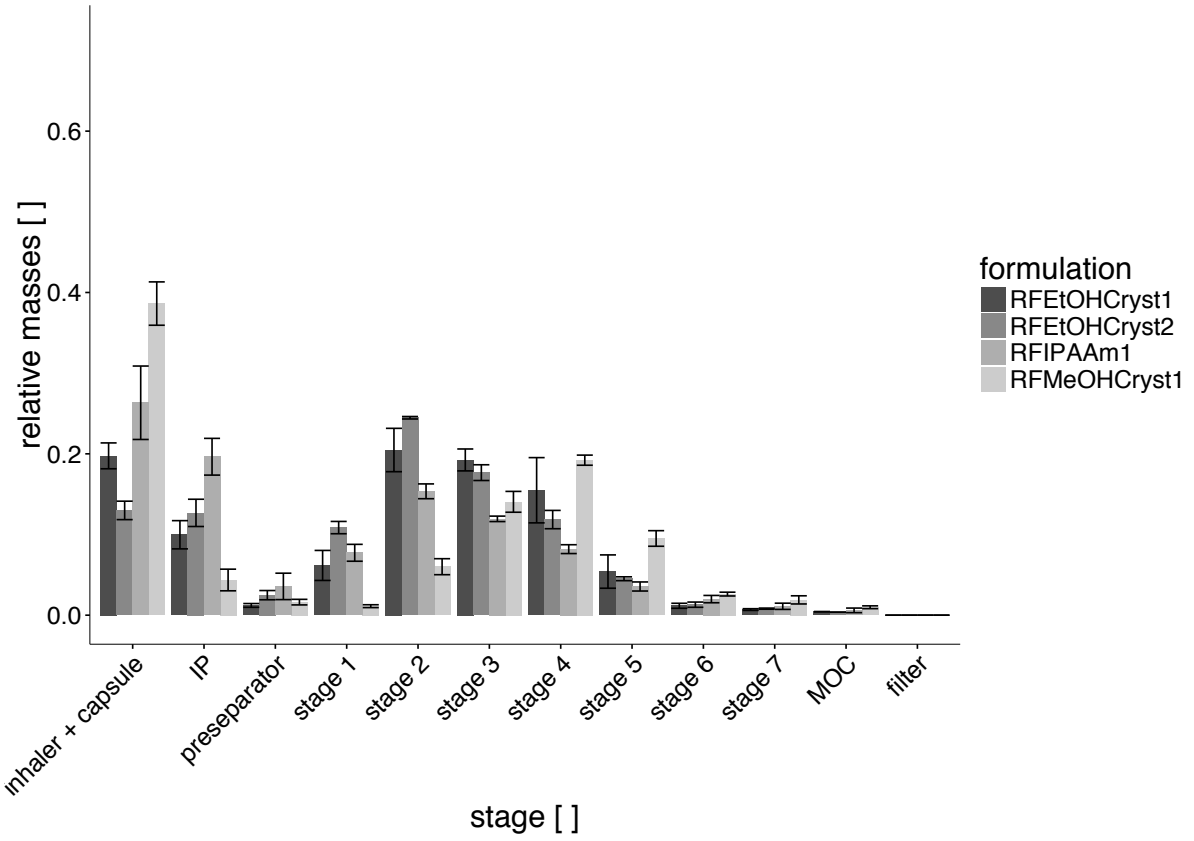


Figure 58. Results of cascade impactor experiments analyzing samples SDr from organic solvents, using the Breezhaler device.

#### 4.2.1.5 Aerodynamic assessment of formulations using the mIP

Samples were also investigated using a modified 3D printed induction port. The effect of material and surface properties on aerosol characteristics was assessed using a 3D printed copy of the USP IP. RFEtOHCryst1 was found to show statistically equivalent deposition on all stages (Figure 59), when comparing USPIP and USP3DIP. Using the mIP, a statistically significant increase in IP deposition was observed. Compared to the USPIP, S3 showed a statistically significant decrease in deposition. MMAD, GSD, and EF were found to be statistically equivalent for all IPs (Table 21). Though not being significant, $FPF_{total}$ showed a slight decrease. Analysis of RFMeOHCryst1 showed statistical equivalence when using the USPIP and USP3DIP (Figure 60). Significantly increased IP deposition was found using the mIP. GSD, $FPF_{total}$, and $FPF_{emitted}$ were found to be statistically equivalent in all cases. MMAD was found to be significantly different when comparing the USP3DIP to the mIP.

Aerosol analysis of RFIPAAm1 using the USPIP and USP3DIP showed statistical equivalence of deposition in all stages with the exception of S1, where deposition was found slightly increased in the case of the USP3DIP (Figure 61). MMAD, GSD, and FPFs were found statistically equivalent. In contrast, increased IP deposition was found using the mIP that corresponded to a significant decrease in preseparator deposition, when compared to the USP3DIP. MMAD, GSD, and FPFs were found statistically equivalent for all three IPs tested.

Table 21. Overview of aerosol characteristics of RF samples SDr from organic solvents, using the USPIP, USP3DIP, and mIP.

| | | IP tested | | |
|---|---|---|---|---|
| Sample name | | USPIP | USP3DIP | mIP |
| RFEtOHCryst1 | MMAD [$\mu$m] | 3.21 ±0.07 | 3.17 ±0.10 | 3.25 ±0.21 |
| | GSD [] | 1.90 ±0.02 | 1.90 ±0.02 | 1.96 ±0.03 |
| | $FPF_{total}$ [%] | 40.89 ±2.07 | 41.62 ±0.68 | 38.62 ±3.06 |
| | $FPF_{emitted}$ [%] | 52.57 ±1.05 | 54.06 ±1.28 | 47.52 ±3.31 |
| | $F_{emitted}$ [%] | 77.76 ±2.41 | 77.03 ±3.01 | 81.27 ±2.40 |
| RFMeOHCryst1 | MMAD [$\mu$m] | 3.14 ±0.14 | 3.36 ±0.07 | 3.02 ±0.05 |
| | GSD [] | 1.91 ±0.07 | 2.04 ±0.02 | 2.04 ±0.02 |
| | $FPF_{total}$ [%] | 36.46 ±0.66 | 37.03 ±2.15 | 34.05 ±3.09 |
| | $FPF_{emitted}$ [%] | 50.81 ±0.46 | 50.82 ±0.73 | 49.83 ±1.18 |
| | $F_{emitted}$ [%] | 71.77 ±1.68 | 72.88 ±4.34 | 68.29 ±5.41 |
| RFIPAAm1 | MMAD [$\mu$m] | 2.65 ±0.06 | 2.69 ±0.07 | 2.52 ±0.18 |
| | GSD [] | 1.98 ±0.04 | 1.99 ±0.02 | 2.03 ±0.05 |
| | $FPF_{total}$ [%] | 31.53 ±2.17 | 35.63 ±2.45 | 35.53 ±1.64 |
| | $FPF_{emitted}$ [%] | 43.33 ±3.52 | 46.14 ±2.77 | 47.35 ±2.64 |
| | $F_{emitted}$ [%] | 72.87 ±3.93 | 77.26 ±1.37 | 75.10 ±3.17 |

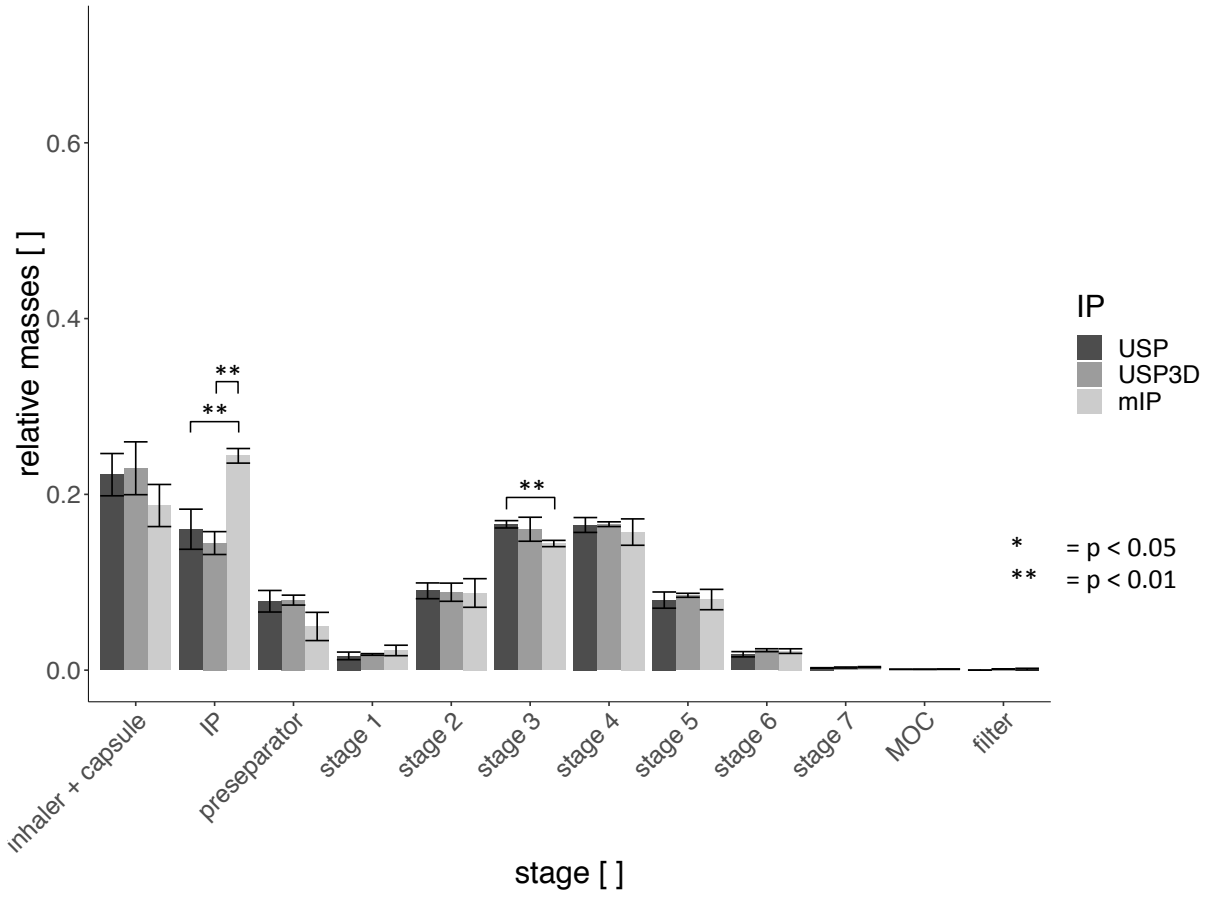


Figure 59. Results of cascade impactor analysis of RFEtOHCryst1, using the USPIP, USP3DIP, and mIP.

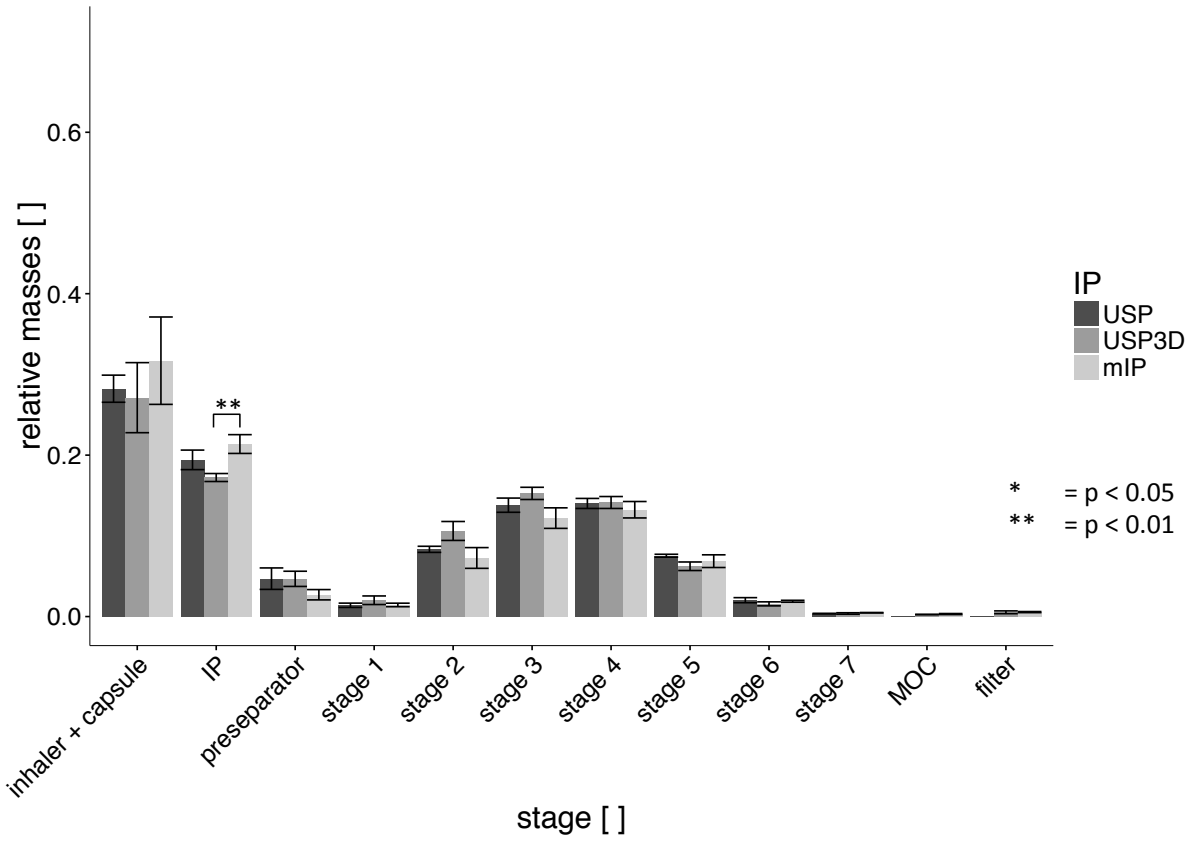


Figure 60. Results of cascade impactor analysis of RFMeOHCryst1, using the USPIP, USP3DIP, and mIP.

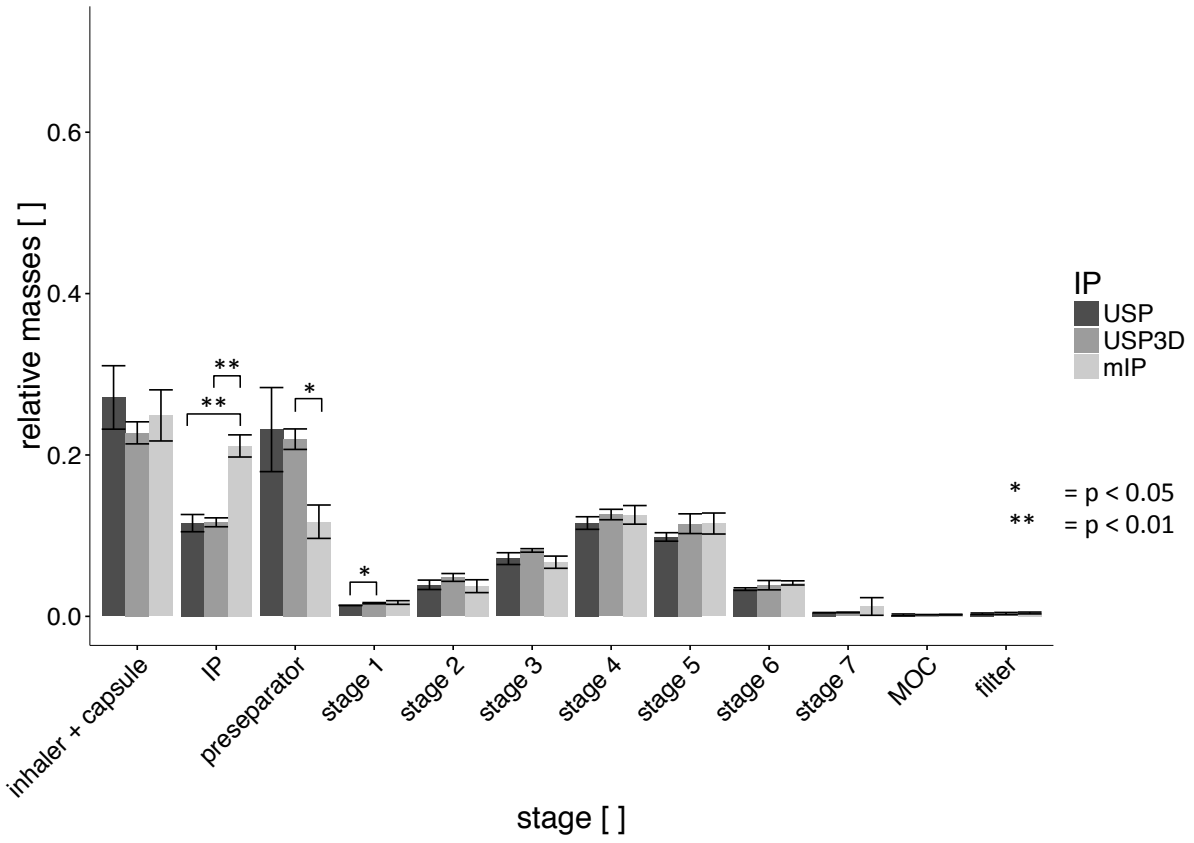


Figure 61. Results of cascade impactor analysis of RFIPAAm1, using the USPIP, USP3DIP, and mIP.

#### 4.2.1.6 Stability study

Table 22 shows sample content of RFEtOHCryst1, RFMeOHCryst1, and RFIPAAm1 as determined by HPLC after storage at ICH accelerated conditions as well as samples stored for six months at four °C. XRPD and DSC analyses results were consistent over the test period for all samples analyzed, indicating that no re-crystalization or polymorphic transformation occurred. RFEtOHCryst1 showed statistically significant changes in $F_{emitted}$ over time (p= 0.01972), which did not result in significantly increasing S4-filter stage deposition. Figure 62 shows the results of aNGI experiments.

Table 22. Content of samples SDr from organic solvents after storage.

| | | | | | HPLC [%] |
|---|---|---|---|---|---|
| Sample name | t= 0 months | t= 1 months | t= 3 months | t= 6 months | t= 6 months (fridge) |
| RFEtOHCryst1 | 90.8 ±0.5 | 91.0 ±0.2 | 89.3 ±1.6 | 89.9 ±1.3 | 89.5 ±1.7 |
| RFMeOHCryst1 | 95.0 ±0.9 | 95.3 ±0.6 | 69.0 ±1.8 | 81.5 ±2.6 | 94.4 ±0.9 |
| RFIPAAm1 | 97.6 ±1.5 | 91.6 ±0.4 | 67.8 ±4.5 | 60.2 ±2.8 | 96.2 ±0.3 |

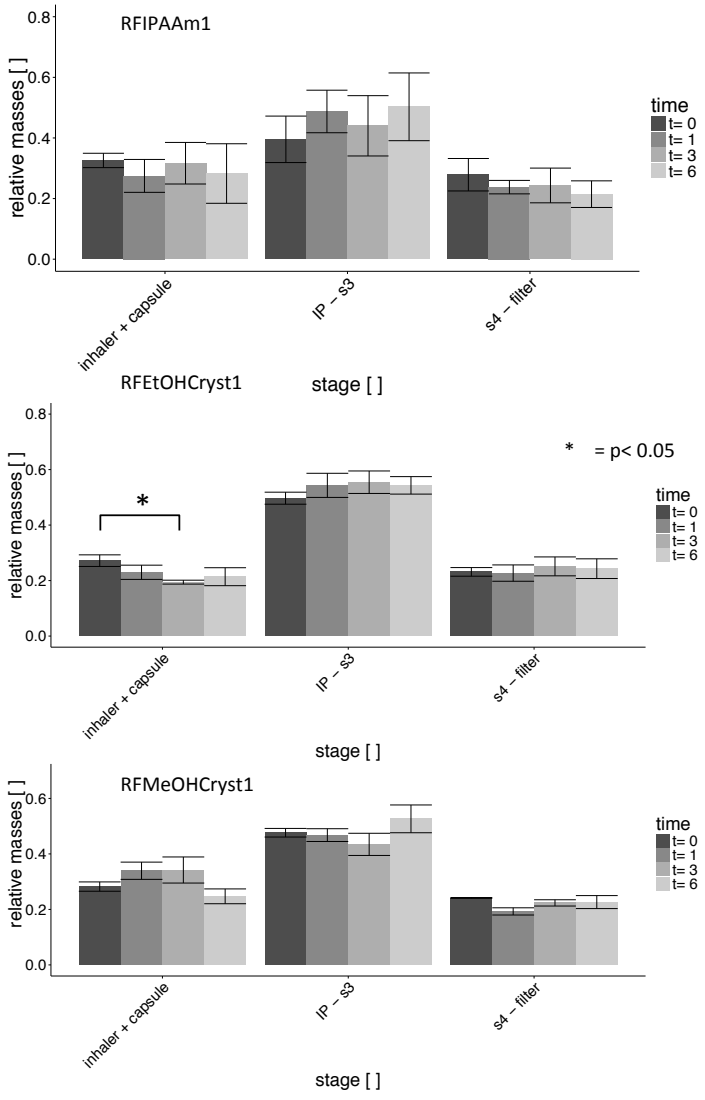


Figure 62. Results of aNGI experiments after one, three, and six months of storage at ICH accelerated conditions.

### 4.2.2 **Discussion**

Selected organic formulations investigated in the previous chapter were successfully repeated and process parameters as well as product properties were found in line with the exploratory study. Operational parameters were found comparable in terms of process time, process stability (data not shown) as indicated by outlet temperature, energy consumption, and product yield. Consistency of energy consumption was deduced from the rate of aspirator set [%] over time, necessary to maintain the specified system flow rate of 15 NCMH. As the terminal cloth filter became congested during the process, pressure drops over the filter unit increased as a function of process time. Aspirator levels were to be adjusted at certain intervals in order not to exceed the predefined operational specifications of the process. This also included timely exchange of the filter bag, when pressure drops exceeded a certain threshold value. Plots of aspirator set over time are expected to be characteristic for each formulation, which was found to be the case in these studies.

Also, solid state properties of the batches produced were consistent with ones of samples in the exploratory study. XRP diffractograms of RFEtOHCryst1 and RFEtOHCryst2 as well as RFMeOHCryst1 were found identical to RFEtOHexp3, RFEtOHexp4, and RFMeOHexp3 respectively. RFIPAAm1 showed a significant amount of residual isopropyl alcohol, which probably is easily reduced by adding an additional drying step. As samples were not intended for *in vivo* testing and as residual IPA at that quantity is not expected to diminish aerosol performance of the sample, no additional drying steps have yet been incorporated.

X-ray diffractograms of RFEtOHCryst1 and RFMeOHCryst1 were found to differ, indicating the formation of two distinct polymorphs or solvates. Analysis of residual solvents using gas chromatography and Karl Fisher analyses showed that large amounts of solvents, from which samples were recrystallized (being ethanol and methanol respectively), were retained within the powder. Additionally, both samples showed residual water at a lower quantity. TGA results were found in line with Karl Fisher and GC analyses so suitability of all methods applied can be assumed.

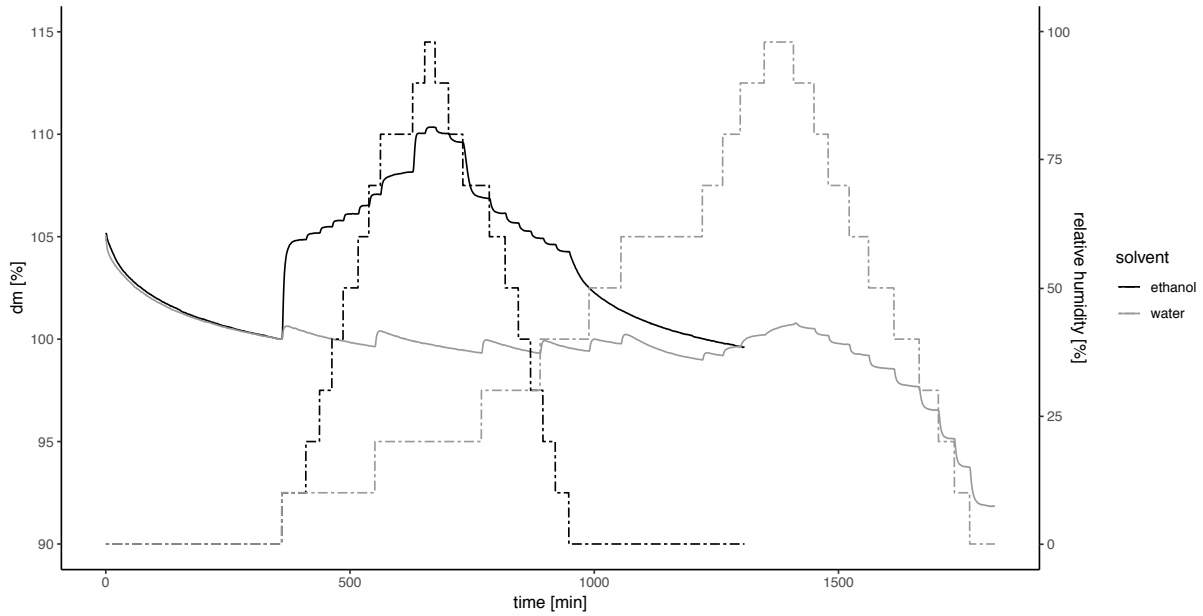


Figure 63. DVS isotherms of ethanol and water vapor, investigating a formulation manufactured by SDr a suspension of RF recrystallized from EtOH (redrawn from [177]).

DVS analysis of RFEtOHCryst1 showed a negative mass balance when equilibrated at 0% RH after subjecting the sample to one 0-97-0% RH cycle, which was shown to be related to the ethanol guest molecule exchange, earlier by this group (Figure 63) [177]. In that study, spray dried powder, similar to RFEtOHCryst1, was exposed to water and ethanol vapor respectively. The exposure to water vapor induced a loss in mass; conversely, exposure to ethanol vapor showed typical sorption behavior for a crystalline sample. It was concluded that ethanol was incorporated into the crystal lattice but might be replaced upon exposure to water vapor, which was thought indicative of a channel solvate mechanism. The results presented in those exposure studies demonstrate good agreement with x-ray trials that investigate changes in crystal structure of samples exposed to different RHs. In both cases, rearrangement of guest molecules was found to terminate at a RH of 60%. This hypothesis is also strongly supported by a study published by Li in 2011 [92] that investigated a different isostructural series of RF solvates. It was shown that guest solvent molecules found in samples recrystallized from different solvent mixtures were located in a solvent channel of indefinite extension along the α plane of the crystal lattice, and may be exchanged, depending on ambient conditions. A recent study published by Wicher et al. [95] reported similar results, but in samples recrystallized from different solvent mixtures. As previously mentioned, initial drying

followed by an exposure to high RH induced an irreversible change in the x-ray diffractograms obtained from RFEtOHCryst1. In contrast, RFMeOHCryst1 showed changes in the x-ray diffractograms when exposed to high RH that were found fully reversible (Figures 46 and 47). Additionally, x-ray data indicated that RFEtOHCryst1 converted into RFMeOHCryst1 after ethanol was ejected from the crystal lattice, since both formulations yielded identical x-ray diffractograms after being subjected to one cycle of 0-97-0% RH (Figure 64). Based on this observation one must conclude that RFEtOHCryst1 and RFMeOHCryst1 belong to an isostructural group of RF solvates.

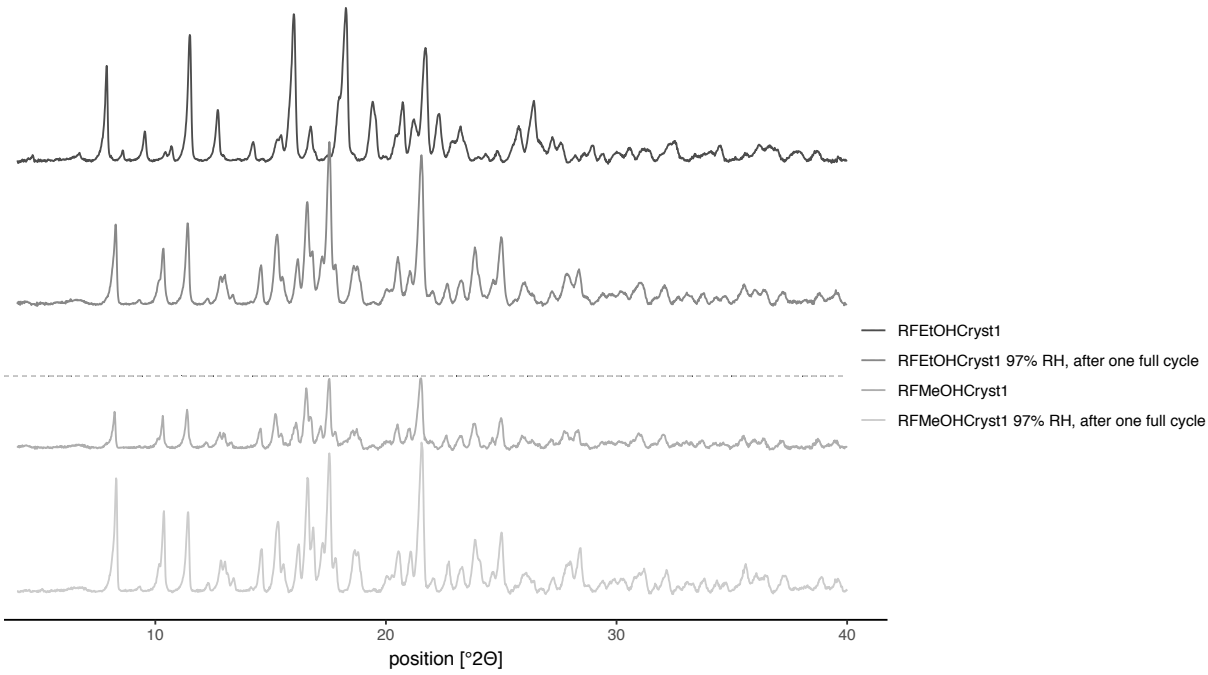


Figure 64. Comparison of x-ray diffractograms of RFEtOHCryst1 and RFMeOHCryst1 after exposure to one 0-97-0% RH cycle.

Interestingly, DVS analyses of both samples show a sigmoidal transition from one sorption kinetic to another, taking place at about 20% RH, which was also reflected in the x-ray pattern obtained. This might be interpreted in a way that exposure to this relative humidity induces slight changes in the lattice that might be associated with early rehydration. Thus, water uptake observed prior to this threshold would be surface bound only. It is to be mentioned though, that this effect is more pronounced in the case of RFMeOHCryst1. SEM and XRPD

data showed that RFMeOHCryst1 contains a second population of amorphous particles, so this effect might also be related to a rearrangement of easily accessible water, adsorbed to the amorphous particles into the desolvated channel solvate. It was shown that both samples increase in crystallinity, when exposed to higher RH, which might be explained by more complete rehydration of the channels. Slight and reversible shifts in the x-ray diffractograms observed when (de-) hydrating the samples are attributed to differences in the channel geometry, when comparing the desolvated and hydrated state, as different guest molecules occupy different volumes. RFEtOHCryst1 and RFMeOHCryst1 were found to decrease in crystallinity, when exposed to higher temperatures (Figures 49 and 50). Interestingly, RFMeOHCryst1 turned amorphous at a lower temperature than RFEtOHCryst1, which is in good agreement with the channel solvate concept, as methanol has a higher vapor pressure than ethanol at a given temperature, and is thus expected to be more easily replaced in the channel. This observation is also in line with DSC experiments conducted, showing an earlier onset and maximum of the desolvation peak in the case of RFMeOHCryst1. It was observed that temperatures in DSC and x-ray experiments do not match, as applying a heating rate is not feasible in XRPD due to the time required to record the x-ray diffractograms. As Samples were equilibrated at the respective temperatures during the x-ray trials, lower desolvation temperatures were observed in both cases. As already mentioned, this is a heating rate related phenomena and DSC and x-ray experiments are expected to match at infinitely low heating rates in the DSC. Observation of a glass transition during the DSC experiments was also in good agreement with the XRPD trials. DSC thermograms recorded are in good agreement with ones reported in literature, and show desolvation peaks of differing extent, followed by the aforementioned glass transition. Interestingly RFEtOHCryst1 shows a pronounced exothermic event at about 180 °C that is less pronounced in RFEtOHCryst2, RFMeOHCryst1, and RFIPAAm1 samples. Commonly, this event is interpreted as “melting” of the desolvated crystals [91,96], which was based on hot stage microscopic observations. This sharp exothermic peak could be interpreted differently, and is more likely associated to oxygen dependent degradation, which was reported earlier by this group [177]. In that study, the degradation process was assessed by heating up samples to the respective temperature using the DSC under $N_2$ and $O_2$ purges respectively, followed by HPLC assessment of the recovered sample and it was shown that an $O_2$ purge induced complete degradation of the sample while degradation was found less complete under a $N_2$ purge. Thus, this exothermic

event should be evaluated as artifact introduced during sample preparation and in fact it was no longer observed during the stability studies.

Several polymorphs, hydrates, and solvates of RF have already been reported in literature [90,92–96,178]. X-ray diffractograms obtained have been compared to relevant data provided in the respective publications and Figure 65 provides an overview on diffraction patterns reported. It should be noted that Li identified the RF pentahydrates reported by Pelizza et al. as members of one isostructural series, which was based on single crystal x-ray data. Comparing XRPD data provided in both studies shows that RF • 0.54 EtOH • 3.92 $H_2O$ bears characteristics of both pentahydrates proposed.

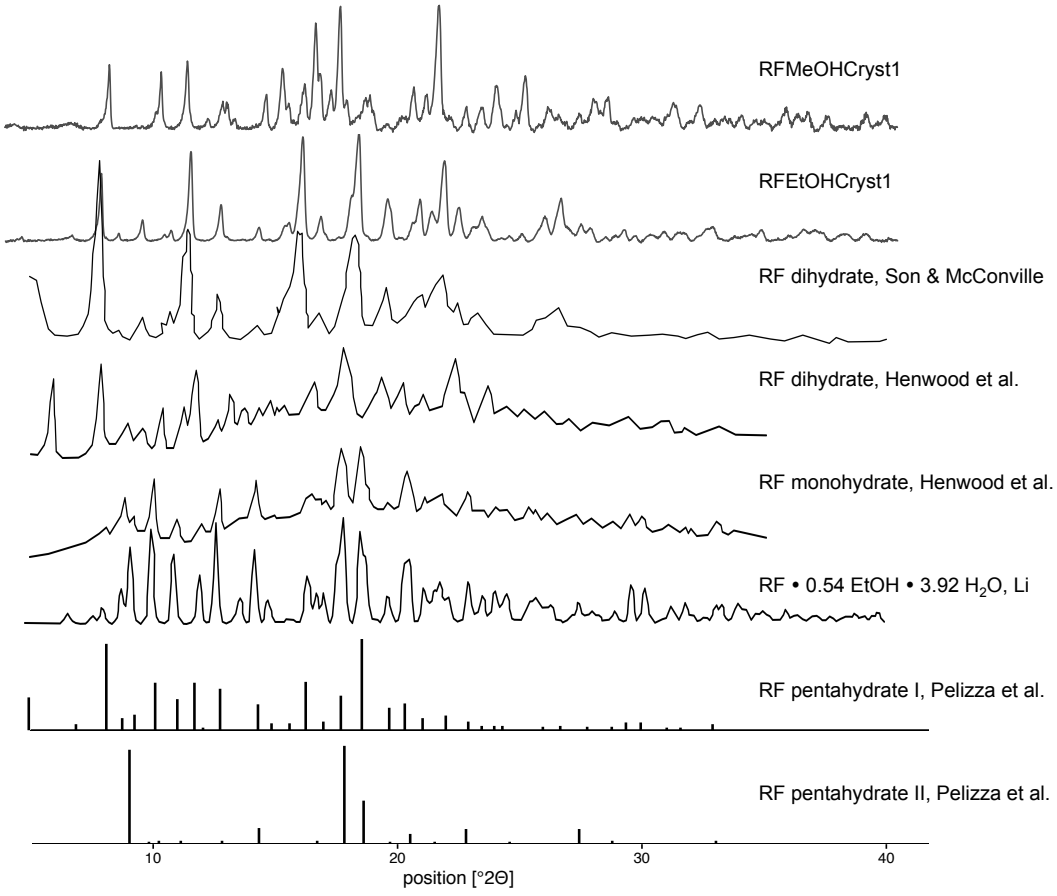


Figure 65. X-ray diffractograms of several RF hydrates reported in literature (redrawn from [90–92]).

Comparison of x-ray diffraction patterns shows that RFEtOHCryst1 (and RFEtOHCryst2) are identical to a RF dihydrate, proposed by Son and McConville, which was to be expected as

manufacturing procedure reported there was also applied in this study, though minor alterations (e.g. different temperature for recrystallization, different outlet temperature) have been introduced. Interestingly, Henwood et al. reported [90] XRPD data obtained from a series of RF solvates characterized as dihydrate that show a higher degree of similarity to the one obtained from the RFMeOHCryst1 sample. It was also found to bear strong similarity to x-ray diffractograms of vacuum dried RF dihydrate, reported by Son and McConville [91], strengthening the hypothesis that these RF dihydrates as well as RFEtOHCryst1 and RFMeOHCryst1 belong to one isostructural group. Taking into account that samples reported by Henwood et al. were recrystallized from a variety of solvents including benzene, tetrahydrofuran, dimethylformamide, and ethyl acetate, this is quite remarkable as these solvents provide fundamentally different hydrogen bond acceptor and donor properties when compared to ethanol or methanol, which Li described as essential for intermolecular interaction and crystal formation. Additionally, Li and Wicher et al. [92,95] reported that RF crystallizes in a zwitterionic state, when crystallized from protic solvents whereas recrystallization from aprotic solvents promotes the non-ionic state. Thus, one might hypothesize that the initial polymorph obtained after recrystallization was lost during the (vacuum) drying step applied and that polymorphic transition occurred upon rehydration. Anyways, it is to be mentioned that the sample reported (only one diffractogram stated as representative for the entire series was provided) also shows additional peaks, but as calculated and measured diffractograms from the pentahydrate isostructural family published by Li show, multiple similar x-ray diffractograms can be characteristic for one isostructural series.

Stoichiometries reported are not instantly brought in line with results of the present study. As both solvates were reported to have incorporated water only, one must assume that at the stage of determination all guest molecules (which are expected to be initially present) already had been exchanged. LOD determined in the respective studies were expected to agree with maximum differences in mass observed in the DVS experiments, especially in the case of RFEtOHCryst2, which had the same solvent/RF ratio as the RF dihydrate reported by Son and McConville, thus assuming amorphous content might be comparable. Comparing DVS and TGA data of the amorphous reference formulation provided there, indicates that samples had been stored under moisture protective conditions, as the LOD of 0.94% would be expected for sample equilibration at a RH lower than 30%, which might have been a result of storage in a closed container, creating a rather dry microenvironment. Anyways, this hypothesis is only

valid assuming that additional drying had occurred, which has not been reported. As significant differences were observed here and water content of the samples was shown to alter as a function of RH, one might hypothesize that the dihydrate reported might have been analyzed at an incomplete state of hydration. It was also noted that content of RF slightly decreased during stability testing, whereas it was found statistically equivalent in this study, so decrease observed might be associated with a higher degree of rehydration occurring over time, rather than chemical degradation. Similar considerations apply comparing data presented here to the study published by Henwood et al. In this case, samples were vacuum dried so complete removal of guest molecules prior to hydration can be assumed. As samples have not been equilibrated to a specific RH, nor DVS data was presented, incomplete rehydration appears plausible. DVS results from this study showed maximum water uptake determined during the second cycle of 9.9% 12.1%, and 10.8% for RFEtOHCryst1, RFEtOHCryst2, and RFMeOHCryst1 respectively, which would be equivalent to a molar RF/water ratio of 1:4.8, 1:5.8, and 1:5. Even so, completeness of solvent exchange was not verified after DVS experiments so a non removable fraction of solvent might still be present (under the given experimental conditions). Also, it is to be assumed that a certain fraction of the water adsorbed is surface bound and might have a measurable, though probably not pronounced, effect, especially considering that primary particle sizes of the samples were small, which consequently demands a high surface area. Additionally, one needs to keep in mind that RFMeOHCryst1 displays a certain fraction of amorphous particles that tend to incorporate bulk water at higher RH. For this particle collective, behavior similar to RFIPAAm1 showing extensive water uptake and swelling, is to be expected. It is to be mentioned that non-congruence of sorption isotherms of RFIPAAm1 is to be attributed to mechanical rearrangement of the sample and sorption kinetics were found slower during the first cycle, which might be explained by the higher vapor pressure required to provide energy needed for the rearrangement. Though RF/water ratios derived from DVS data might be interpreted in a way that they indicate formation of another pentahydrate, several observations contradict this hypothesis. It is to be mentioned that XRP diffractograms of RFEtOHCryst1 and RFEtOHCryst2 as well as RFMeOHCryst1 differed from all powder x-ray data provided on the pentahydrate series. Also RFaqCryst1, which will be presented in the next chapter, was identified as member of the pentahydrate family and shows fundamentally different water sorption behavior, requiring an extensive amount of time to equilibrate at 0% RH so apparently guest molecules are bound more tightly, or solvate channels are more narrow in

this family (see [95]). In contrast, samples investigated in this chapter require more time to equilibrate at higher RH, but were found to de-solvate readily. And though this study provides valuable information on macroscopic behavior and stability of this isostructural family, crystallographic assessment would be needed to clarify if samples presented in this chapter are another permutation of one of the isostructural families already reported, or if they belong to an individual class.

Assessment of aerosol properties using the Handihaler device showed good performance for all formulations. All formulations except RFEtOHCryst2 showed extensive retention within inhaler and capsule, which is to be attributed to the conservative storage conditions applied; so as not to alter the initial solid state obtained after spray drying. Especially in the case of spray dried samples, it is advisable to equilibrate samples intended for dry powder aerosolization at higher RH, in order to reduce electrostatic charges introduced during the manufacturing process. In this study, samples were collected in the container intended for storage being a screw cap glass vial that was attached to the high-performance cyclone of the spray drier, and sample manipulation afterwards was reduced to a minimum. Prior to separation from the air stream, powders were found to propagate in a vortical motion along the walls of the vessel, which leads to triboelectric charging. Before further use, all samples were equilibrated at 32% RH, which in an earlier study was found to maintain the solid state of RFEtOHCryst samples, but might not be sufficiently high to efficiently remove electrostatics at the given timeframe (data not shown). Samples analyzed in the exploratory study (see previous chapter) were treated less solid-state conservatively and showed better emptying (i.e. they were exposed to ambient conditions before equilibration to 32% RH). One exception was RFEtOHexp2, but this formulation consisted of extremely fine particles and was not easily de-agglomerated, so low ejection rate was attributed to that. Better ejection of RFEtOHCryst2 might be explained by the higher water content (Section 4.3.1.2.3) of the sample, indicating that it might have been exposed to higher RH during manufacture or sample handling. RFIPAAm1 showed lower IP and correspondingly higher preseparator deposition, which is to be attributed to incomplete powder de-agglomeration. RFEtOHCryst2 was found to have a larger MMAD when compared to RFEtOHCryst1, which is expected to reflect larger geometric diameters of the primary particles. Due to the higher solid content of the suspension that was spray dried, a larger diameter of the primary particles was in line with expectations. Existence of a second particle population observed (SEM) in the case of

RFMeOHCryst1 was not reflected in cascade impactor data, as overall content of that population may have been too low to be detected at the level of precision of the impactor, or incomplete de-agglomeration of this fraction from the other particles may have been a factor. In light of the aforementioned considerations, it is to be concluded that samples assessed were not tested under conditions optimized for aerosol performance, hence the potential performance of the formulations might actually be higher than reflected in these studies. Comparing results obtained here to those reported with similar formulations by Son and McConville [91], overall performance reported in this study was found to be lower. Apart from reasons already mentioned, this might be attributed to application of non-standard conditions during inhalation testing in that study, as the NGI was operated at a flow rate of 60 L/min, which generates a higher pressure drop than 4 kPa over the Handihaler, and might result in better, though less biorelevant powder de-agglomeration.

Aerosol properties of samples have also been investigated using the Breezhaler device. Here, aerosol performance of all crystalline samples was found to be better, as indicated by higher FPFs, smaller MMADs, and larger GSDs. Though not being immediately obvious, larger GSD in this case might be indicative of better particle de-agglomeration, since agglomerates, which had impacted in earlier stages using the Handihaler, partially de-agglomerated and impacted in later stages using the Breezhaler; becoming accessible for determination of the aPSD. This is an interesting case, highlighting the necessity to evaluate aPSDs in context of the entire experimental setup and one needs to keep in mind that aPSDs reported might not reflect the entire particle population of the bulk powder, unless a suitable method (e.g. pressure titration) is being performed. Better performance of the crystalline samples assessed may likely be attributed to a higher degree of de-agglomeration achieved by the Breezhaler device. This could be related to the lower intrinsic resistance (Section 1.4.1.2.1) of the device, demanding a higher system flow rate to achieve the required $\Delta p$ of 4 kPa. In this specific case this demanded operation of the NGI at 100.0 L/min, as the flow rate actually required is beyond the calibrated range of the NGI. Thus, more energy per unit time is introduced into the system, which is expected to aid better de-agglomeration. Interestingly, RFIPAAm1 showed comparable performance for both inhalers. At first glance, this observation is in good agreement with data published by Son and McConville [91], where performance of the amorphous reference formulation was even found lower when investigated using an Aerolizer (compared to the Handihaler) type device. As already mentioned (Section 1.4.3.3), one needs to keep in mind that CI analysis was performed at 60 L/min, so the Aerolizer might not have

de-agglomerated the powder properly, which also is reflected by the extensive retention within the capsule reported there, and it is to be assumed that this mechanism is not responsible for the performance observed here. Comparing IP depositions of all formulations on both devices shows that all crystalline formulations demonstrate lower IP deposition when using the Breezhaler. This is understandable, as larger agglomerates are expected to be broken up more efficiently, and thus not impacting in the bend of the IP. In the case of RFIPAAm1 an apparently higher degree of de-agglomeration came at the cost of higher triboelectric charging, leading to higher adherence to the IP walls, especially at the inlet section. This hypothesis is also supported by the increase in MMAD observed. Smaller particles, especially, are expected to show increased adherence due to triboelectric charging, so it should be assumed that a certain fraction of fine particles was removed by this mechanism, consequently leading to an increase in MMAD. Based on these observations, one can conclude that the different inhalers investigated have device specific, balanced, and geometry derived properties. In this case the ability to more efficiently de-agglomerate at the cost of triboelectric induction of the powders, and depending on the properties of powders to be aerosolized, different inhalers are expected to be more suitable for the given formulation than others. As a consequence, triboelectric charging of the powder could prove to be an intrinsic limit to performance of de-agglomeration units, if traditional approaches in DPI design, involving kinetic de-agglomeration, are applied. On the other hand, triboelectric charges are expected to rapidly dissipate upon exposure to high RH as occurring in biological systems, so this consideration might be limited to the device itself, lowering its overall impact.

Aerodynamic properties of RFEtOHCryst1, RFMeOHCryst1, and RFIPAAm1 have also been investigated using the modified IP, presented in Chapter 3. To show independence from the manufacturing method, a copy of the USPIP was 3D printed and assessed. As all formulations except RFIPAAm1 showed statistically equivalent deposition in the USPIP and USP3DIP, it should be assumed that manufacturing technique and materials used have no influence on outcome of these experiments. RFEtOHCryst1 showed a significant increase in IP deposition that corresponded to a decrease in preseparator and S3 deposition. MMAD and GSD were found to be unaffected. The FPF showed a decrease by approximately 5%, which was not statistically significant. Due to the low extent of this effect its therapeutic impact would be expected to be low, and such differences in lung deposition are certainly hard to assess in an *in vivo* setting. Similar results were obtained analyzing the RFMeOHCryst1 formulation.

MMADs of RFMeOHCryst1 determined using the USP3DIP and the mIP respectively, demonstrated a significant difference of about 0.3 µm, but the impact of this observation must be evaluated as little. It is to be concluded that all formulations assessed are not suspected to perform significantly different, when tested in an *in vivo* setting. RFaqAm1 showed statistically insignificant increase in the mIP only but also slight increase in preseparator deposition was observed. Cumulative IP and preseparator deposition differed significantly ($p= 0.01653$) comparing USP and USP3D IP as well as USPIP and mIP ($p= 0.00294$). It is to be assumed that in this case we see a slight influence of the material used, causing increased adherence/retention. As a consequence a statistically decreased deposition in S5 was observed that also translated in statistically significant decrease in FPFs, in the case of the mIP. Anyways, though mIP and USP3D perform statistically equivalent, it is to be assumed that the USPIP overestimates lung deposition in this case. It is to be mentioned that the effect is as low as about 6% in predicted deposition so in an IVIVC this effect is hardly expected to be traceable.

Stability testing of formulations assessed showed good chemical stability of samples recrystallized from ethanol. The amorphous sample spray dried from IPA was found to be chemically unstable, which is in line with literature [91]. Surprisingly, RFMeOHCryst1 showed certain degradation, which was not expected as crystalline samples were deemed to be stable. Interestingly, content determined after three months of storage was found lower than the one determined after six months. Repetition of the experiments at both time points (t= 3 months was already repeated as content determined differed from expectation) verified correctness of the analytical method used. A possible explanation for this might be separation of the two particle populations found in this formulation. For stability testing, powder aliquots were prepared reflecting each time point and stored in a separate vial, so that manipulation of the samples during analysis at the respective time points would not affect the results obtained. As one population was found fully amorphous, they are expected to show different degradation kinetics so differences found here might actually reflect the extent of amorphous content in the respective samples. Anyways, all samples assessed were found to be chemically stable at refrigerated conditions. During the entire test period, no recrystallization or amorphization occurred, as indicated by XRPD and DSC measurements. Aerosol performance was found to be stable for all samples over the entire test period. Only RFEtOHCryst1

showed a slight increase in $F_{emitted}$, which did not translate into higher deposition lower than S3.

## 4.3 Results and discussion of the main study investigating manufacture of respirable rifampicin particles using water

### 4.3.1 Results

#### 4.3.1.1 Manufacture

Manufacture of aqueous formulations described in chapter 4.1. was repeated successfully. One formulation spray dried from an isopropyl alcoholic solution of RF was successfully manufactured as reference formulation. Table 23 shows product yields from the manufacturing process.

Table 23. Product yields of samples SDr from water.

| Sample name | Solvent | Yield [%] | Approx. process time [h] |
|---|---|---|---|
| RFaqCryst1 | water | 27.6 | 4.1 |
| RFaqAm1 | | 27.8 | 12.5 |
| RFaqAm2 | | 25.4 | 12.5 |
| RFaqAm3 | | 30.3 | 8.3 |
| RFIPAm1 | IPA | 42.0 | 1.8 |

#### 4.3.1.2 Physicochemical characterization

##### 4.3.1.2.1 SEM images of particles obtained

SEM pictures (see Figure 66) of RFaqCryst1 showed micro particles of brick like shape, displaying different axis ratios and sizes. Contrary, images of RFaqAm1, RFaqAm2, and RFaqAm3 showed highly collapsed, thin walled microspheres. RFIPAAm1 was already discussed in the previous chapter.

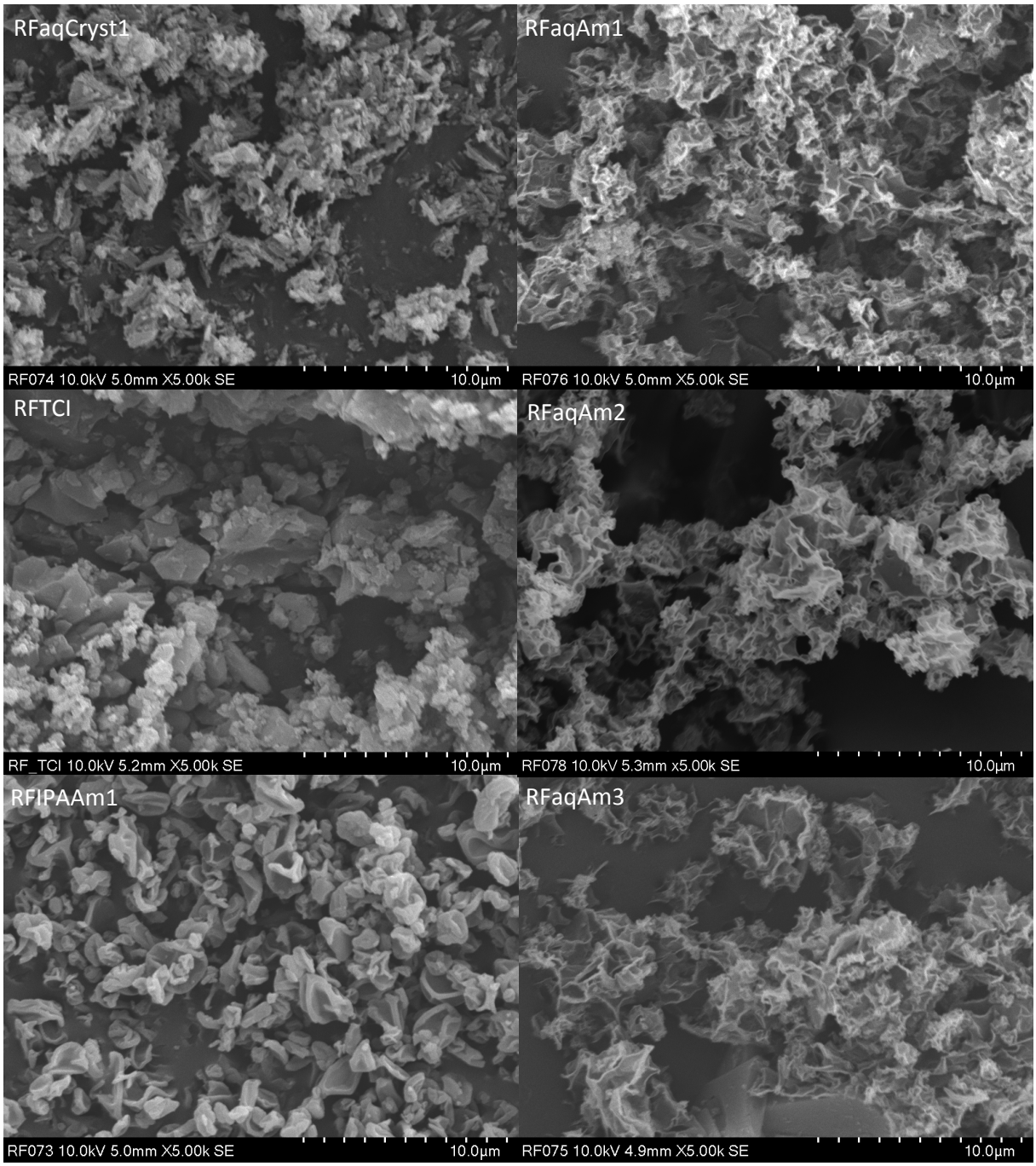


Figure 66. SEM images of RFaqCryst1, RFaqAm1, RFaqAm2, RFaqAm3, RFIPAAm1, and the starting material obtained from TCI.

4.3.1.2.2 XRPD analysis of RF samples SDr from aqueous solutions or suspensions

XRPD analysis (see Figure 67) showed that spray drying of an aqueous suspension (RFaqCryst1) generates crystalline particles, whereas all other samples were found to be amorphous. No sample showed polymorphic transition or recrystallization upon exposure to

different RH (see Figures 68 and 69). Exposure to higher temperatures induced a decrease in crystallinity in the case of RFaqCryst1 and RFaqAm1 remained amorphous (see Figures 70 and 71).

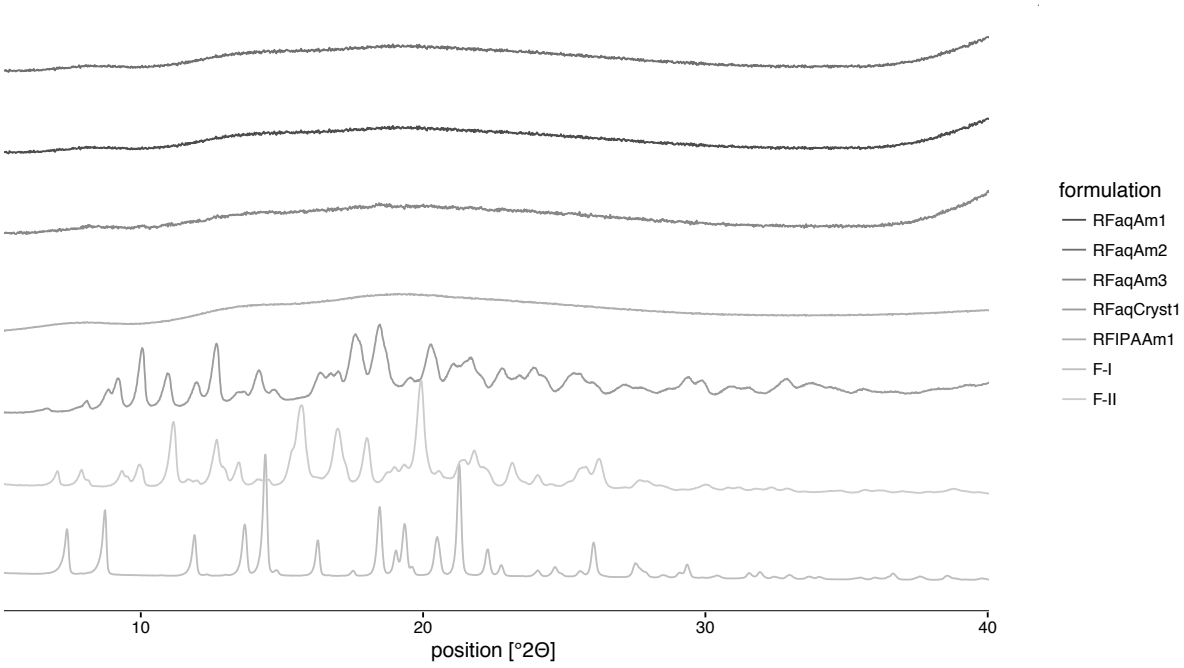


Figure 67. X-ray diffractograms of samples SDr from water.

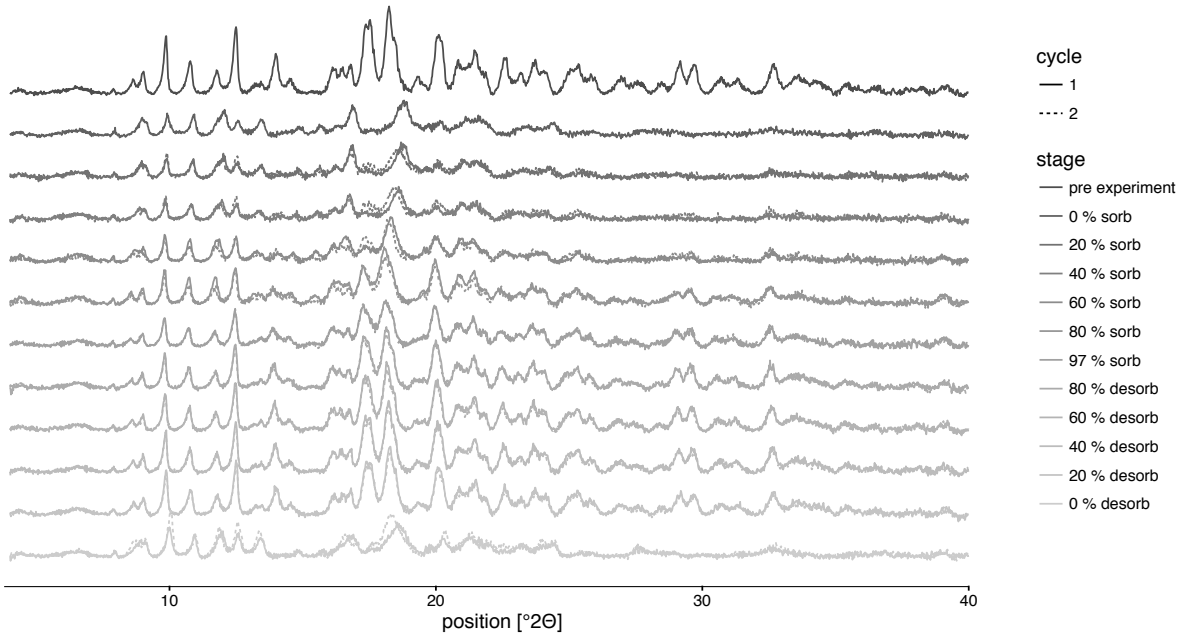


Figure 68. X-ray diffractograms of RFaqCryst1, equilibrated at different RH.

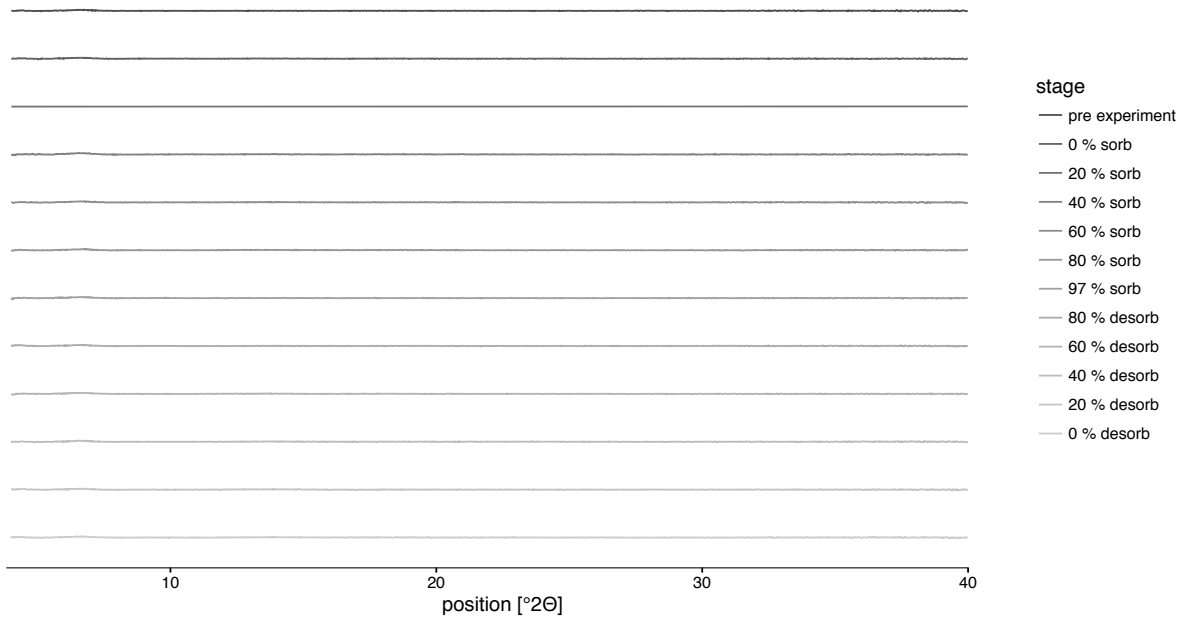


Figure 69. X-ray diffractograms of RFaqAm1, equilibrated at different RH.

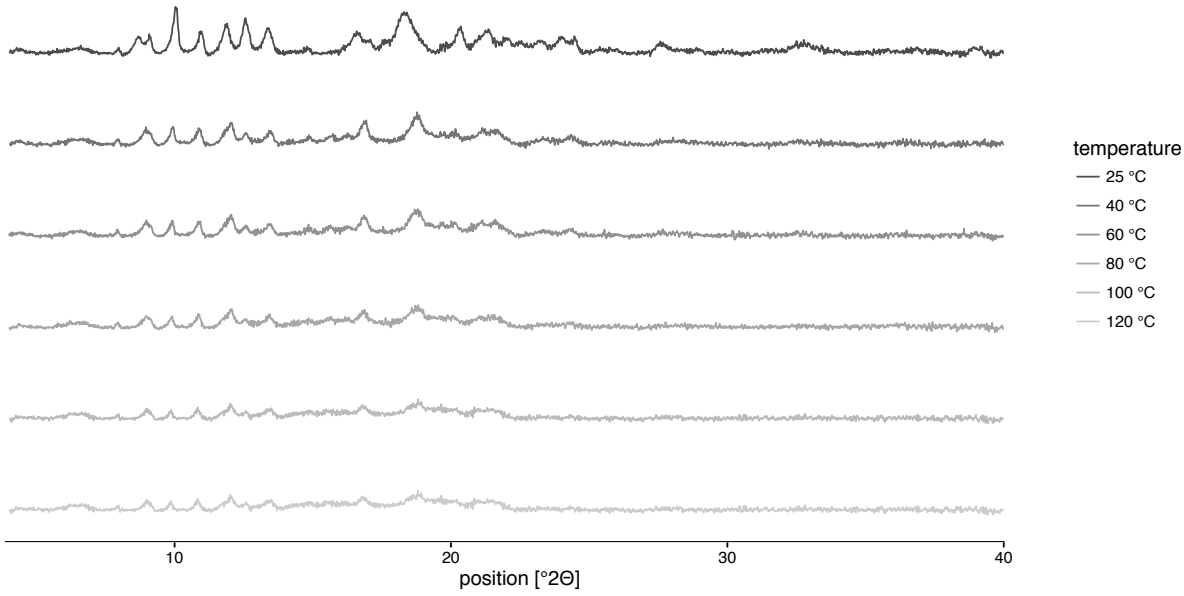


Figure 70. X-ray diffractograms of RFaqCryst1, equilibrated at different temperatures.

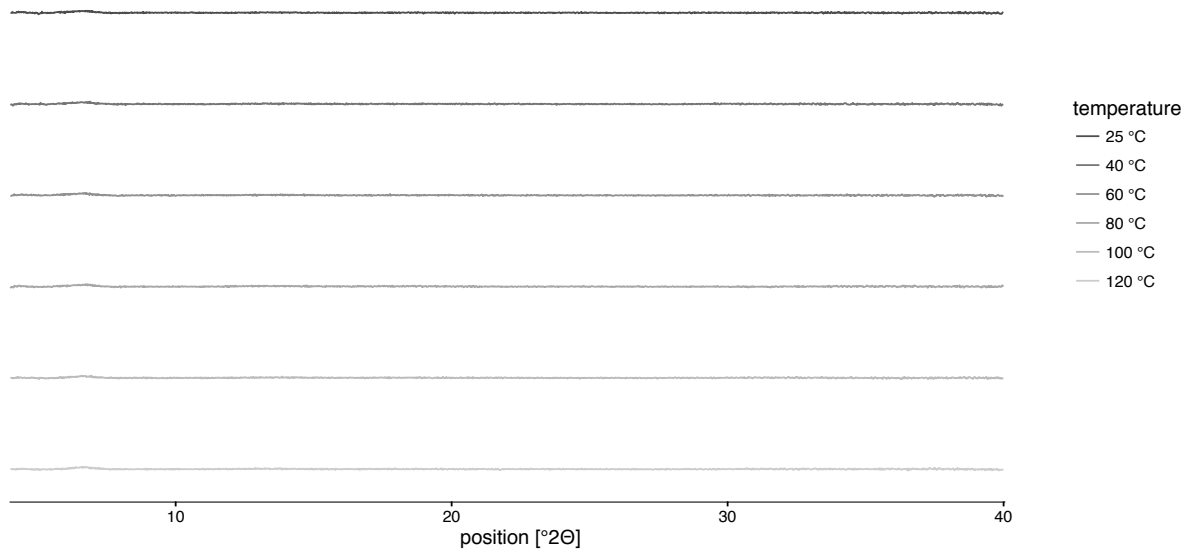


Figure 71. X-ray diffractograms of RFaqAm1, equilibrated at different temperatures.

4.3.1.2.3 Analysis of residual solvents using the GC

Analysis of residual solvents showed that RFIPAAm1 contained residual isopropyl alcohol (see Tab 2) (also see previous chapter).

Table 24. Overview of physical and chemical characterization of RF samples.

| Sample name | Purity HPLC [%] | Water content [%] | Organic solvents [%] | TGA [%] |
|---|---|---|---|---|
| RFaqCryst1 | 91.7 ±1.3 | 7.0 ±0.3 | 0.0 | 92.5 ±0.0 |
| RFaqAm1 | 94.1 ±0.1 | 5.7 ±0.2 | 0.0 | 95.1 ±0.7 |
| RFaqAm2 | 93.5 ±0.9 | 4.3 ±0.9 | 0.0 | 94.9 ±0.3 |
| RFaqAm3 | 93.3 ±0.7 | 6.0 ±0.1 | 0.0 | 93.0 ±0.0 |
| RFIPAAm1 | 97.6 ±1.5 | 1.1 ±0.2 | 2.9 ±0.2 (IPA) | 96.2 ±0.3 |

4.3.1.2.4 DSC analysis of RF samples SDr from aqueous solutions or suspensions

DSC thermograms (see Figure 72) of RFaqAm1, RFaqAm2, and RFaqAm3 showed broad desolvation peaks of residual solvent from about 40-100 °C, followed by a glass transition at 164 °C. RFIPAAm1 showed a less pronounced desolvation peak, followed by a glass transition at the same temperature. RFaqCryst1 showed two overlaying desolvation endotherms, peaking at 100 °C and 113 °C respectively. Similar to the amorphous samples investigated, RFaqCryst1 showed a glass transition at 164 °C.

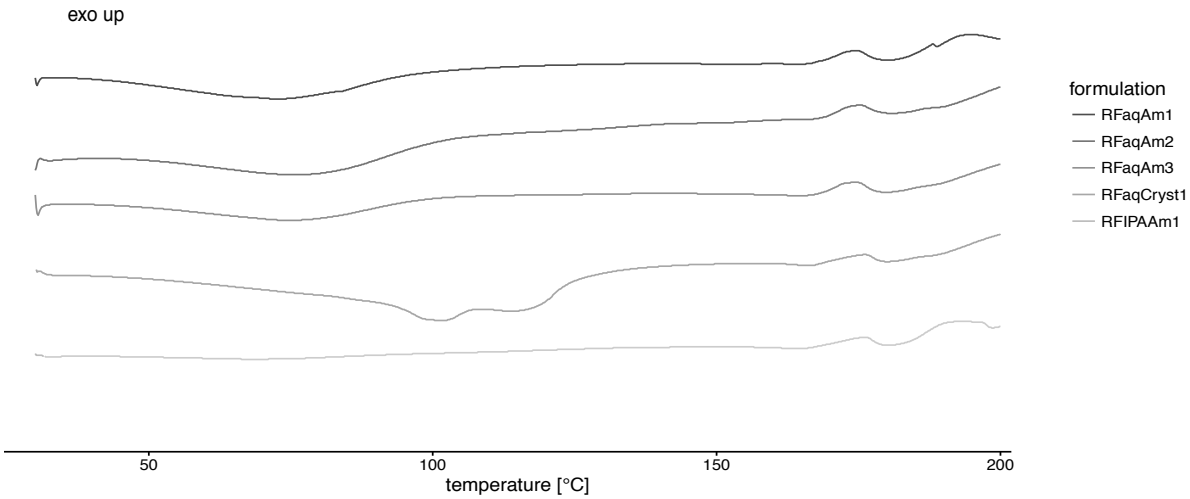


Figure 72. Results of DSC analysis of samples SDr from water.

4.3.1.2.5 DVS analysis of RF samples SDr from aqueous solutions or suspensions

DVS analysis of samples spray dried from water showed two distinguishable sorption patterns. RFaqAm1, RFaqAm2, and RFaqAm3 showed biphasic sorption kinetics with terminal linearity and intersections ($2^{nd}$ cycle) at 80.2% RH, 79.0% RH, and 77.2% RH respectively. Samples showed accelerated uptake at higher RH. Maximum water uptake observed for amorphous samples was found at approximately $15\%_{w/w}$ (Figures 73-75). At lower RH the physisorbed water was found to be easily liberated, and samples were found to equilibrate before terminal drying. It should be noted that sorption isotherms of cycles one and two are not in agreement, as samples swell at higher RH. RFaqCryst1 was less distinguishable for the individual sorption kinetics, and the intersection point was found at 30.1% RH (Figure 76). Equilibration at 97% RH led to a lower increase in mass, when compared to RFaqAm1, RFaqAm2, and RFaqAm3. RFaqCryst1 showed pronounced desorption upon drying at 0% RH. All samples showed pronounced hysteresis. (Note: DVS data of RFIPAAm1 was already presented and discussed in 4.2.1.2.5).

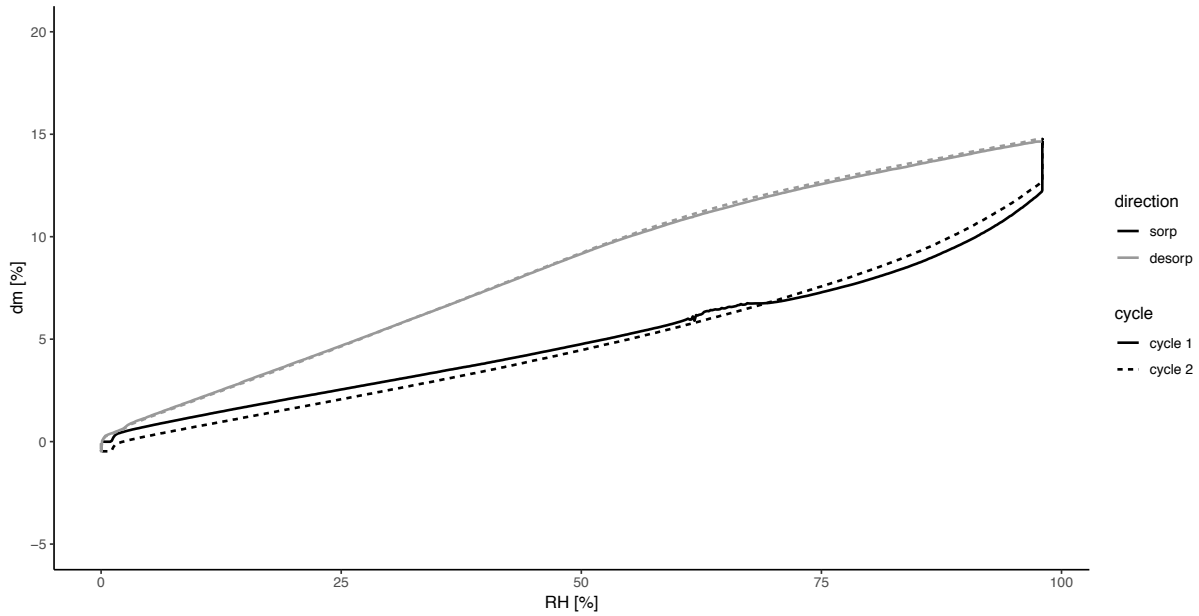


Figure 73. Results of DVS analysis of RFaqAm1.

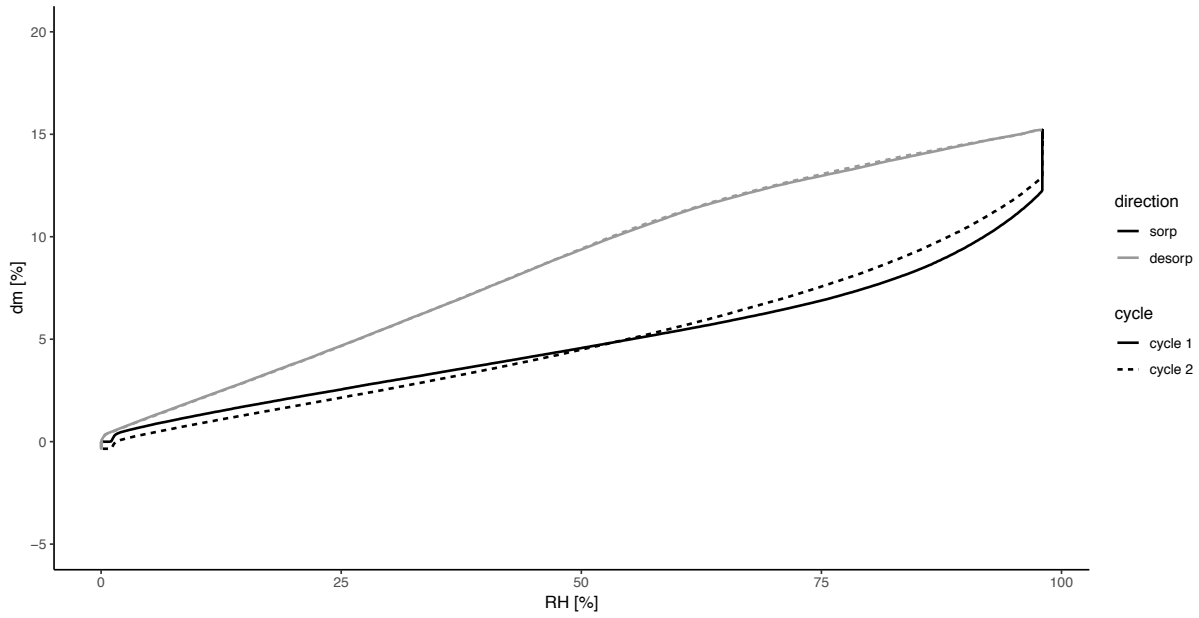


Figure 74. Results of DVS analysis of RFaqAm2.

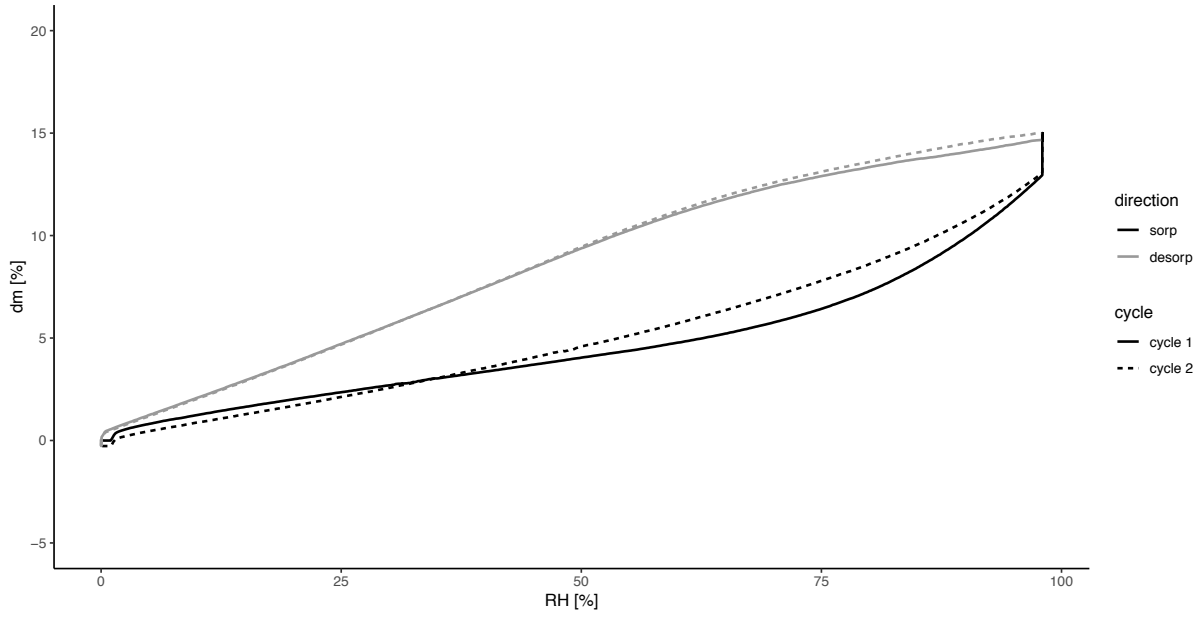


Figure 75. Results of DVS analysis of RFAqAm3.

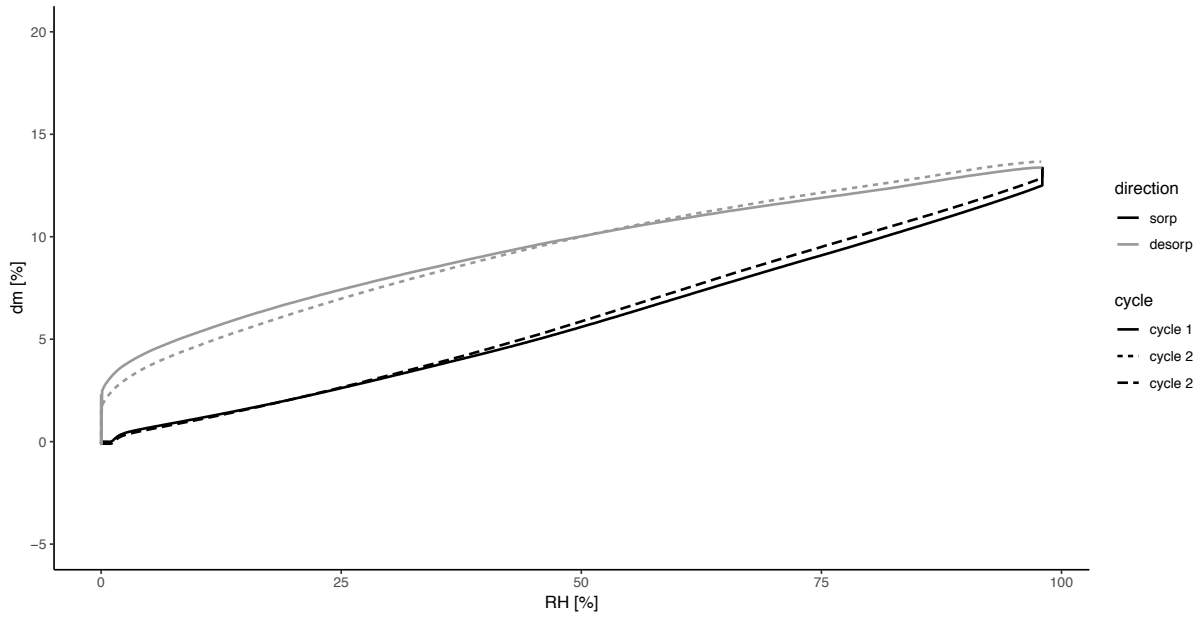


Figure 76. Results of DVS analysis of RFAqCryst1.

#### 4.3.1.3 Aerodynamic assessment of formulations using the Handihaler device

All formulations assessed showed good to excellent aerosol properties. Table 25 provides an overview on FPF, EF, MMAD, and GSD of the formulations tested. RFaqCryst1 was found to empty well from the capsule and showed low and moderate IP and preseparator deposition, respectively (Figure 77). In contrast, RFIPAAm1 displayed extensive retention in the device and capsule, which was observed to reduce slightly after storage (Section 4.2.1.7). Both IP and preseparator depositions were found to be similar, leading to an overall performance comparable to that of RFaqCryst1 (Table 25). All three formulations that were spray dried from aqueous solutions (RFaqAm1, RFaqAm2, and RFaqAm3) demonstrated excellent aerosol properties, with powder retention within the device and capsule combined, well below 5%. Both IP and preseparator deposition values were found to be low. And these formulations showed high deposition in the MOC and the terminal glass fiber filter.

Table 25. Aerodynamic characteristics of RF samples SDr from water, dispensed from the Handihaler device.

| Sample name | FPF [%] | EF [%] | MMAD [$\mu$m] | GSD [ ] |
|---|---|---|---|---|
| RFaqCryst1 | 41.0 ±3.6 | 88.7 ±1.1 | 2.9 ±0.1 | 2.1 ±0.0 |
| RFaqAm1 | 88.7 ±2.0 | 98.0 ±0.2 | 1.4 ±0.2 | 3.2 ±0.1 |
| RFaqAm2 | 81.8 ±0.9 | 98.4 ±0.2 | 1.6 ±0.1 | 3.0 ±0.1 |
| RFaqAm3 | 80.0 ±0.4 | 98.1 ±0.2 | 1.6 ±0.1 | 3.4 ±0.1 |
| RFIPAAm1 | 37.1 ±4.3 | 69.1 ±2.3 | 2.0 ±0.6 | 2.9 ±0.8 |

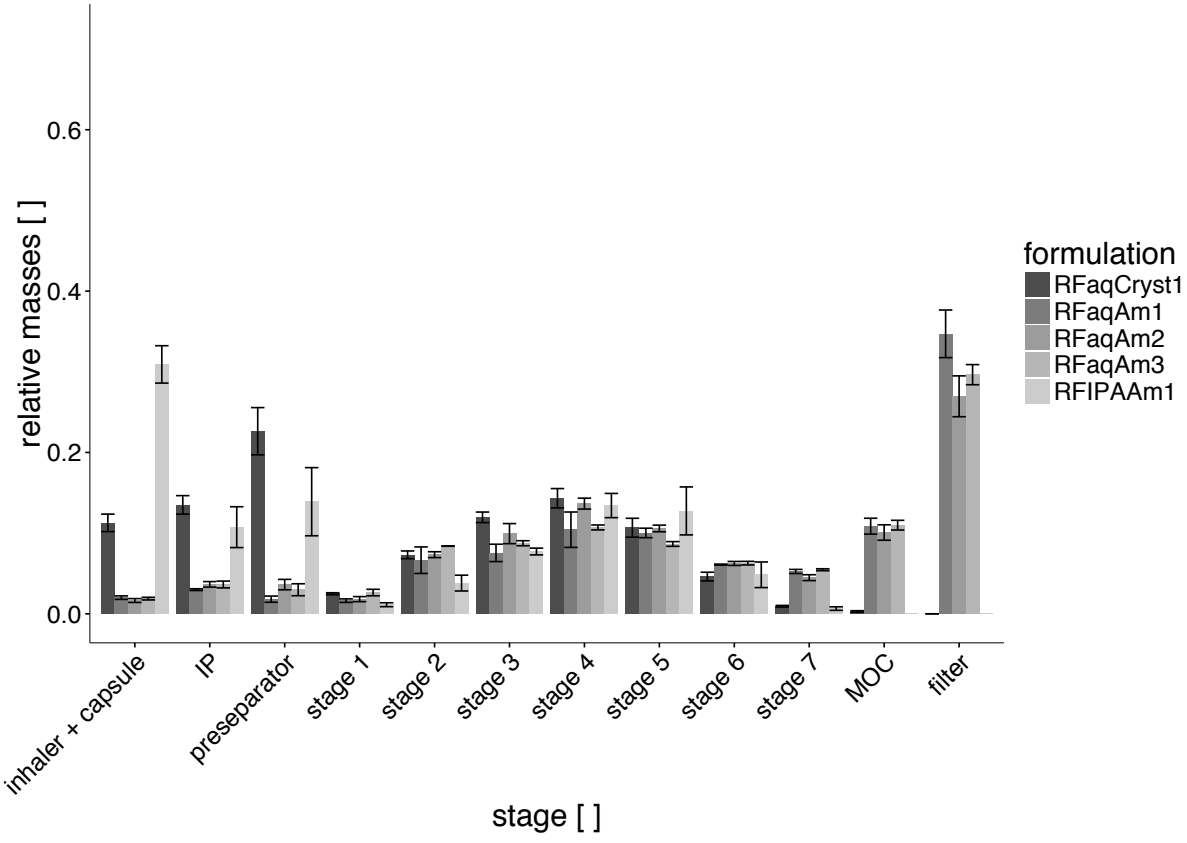


Figure 77. Results of cascade impactor experiments analyzing samples SDr from water, using the Handihaler.

#### 4.3.1.4 Characterization of the ACT

In order to assess if formulations investigated would be suitable for application by a single use, disposable DPI, they were also analyzed for their aerosol properties using a low cost,

disposable DPI surrogate (ACT). The model was chosen to provide little de-agglomeration efficiency only and based on a charcoal filter unit that originally consisted of a cardboard tube of uniform diameter, which was filled with charcoal pellets and capped with one perforated ceramic and plastic stopper, respectively. In this study, the charcoal pellets were removed and replaced with the test formulation. Modified (charcoal pellets were removed) Actitubes showed high airflow resistance of $1.1 \times 10^{-1}(\sqrt{kPa} * min)/L$ (Figure 78) creating a pressure drop of 4 kPa over the inhaler at a flow rate of 19.2 ±0.3 L/min. The average orifice diameter in the caps was determined to be 0.92 ±0.2 mm. Figure 76 shows results of the CFD study, as well as SEM images of the end caps and a photograph of the entire Actitube and components. The CFD study showed that high airflow velocities were generated inside the inlet and outlet channels, while low velocities are maintained inside the cardboard tube that holds the bulk powder prior to aerosolization (Figure 79). The inside of the plastic cap shows slightly increased velocities, when compared to the tube body.

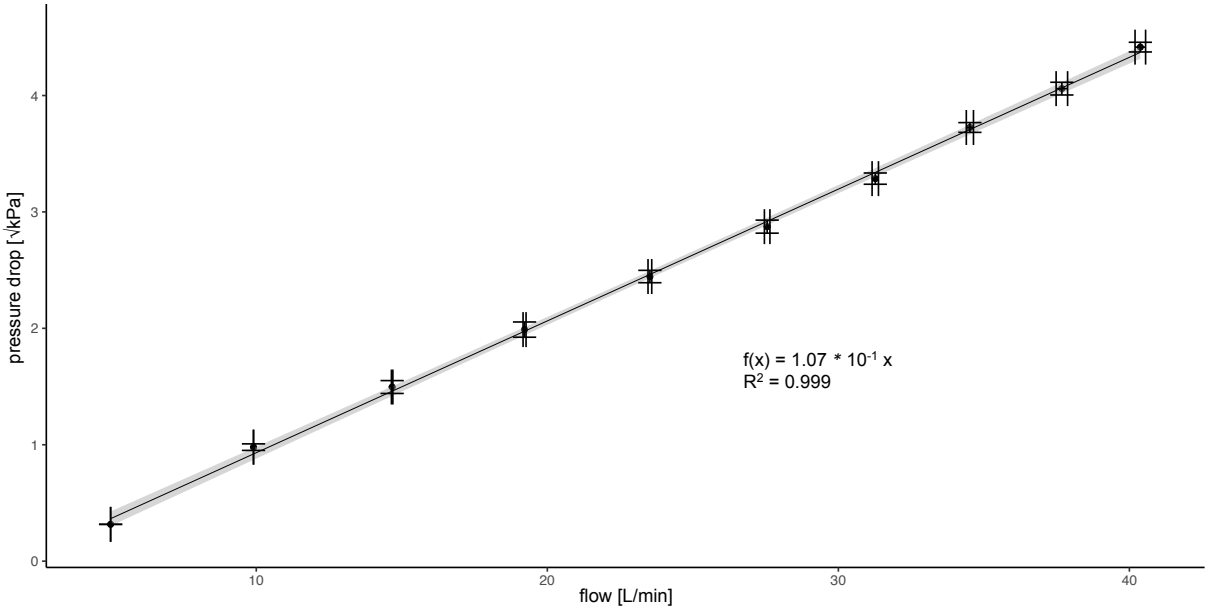


Figure 78. Pressure drop of modified Actitube charcoal filters over flow rate.

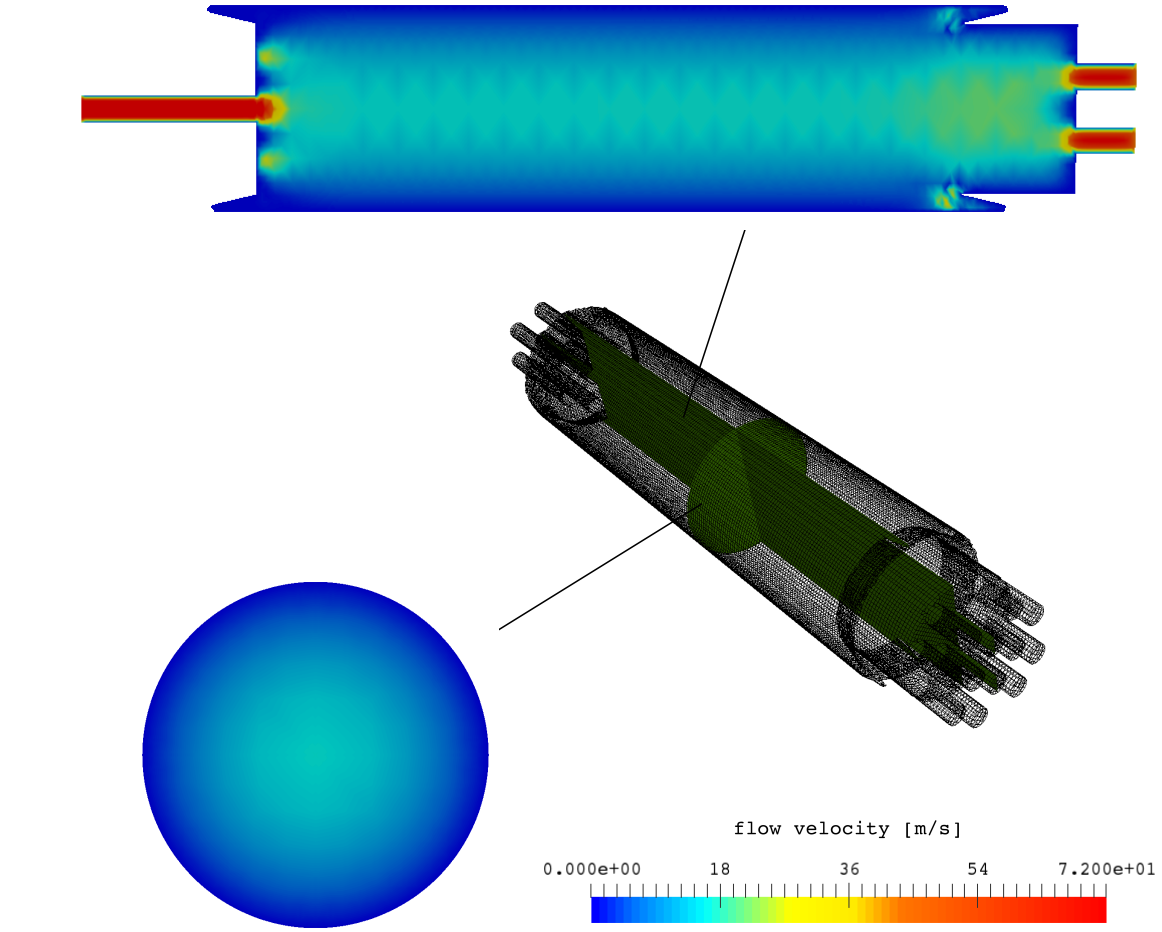


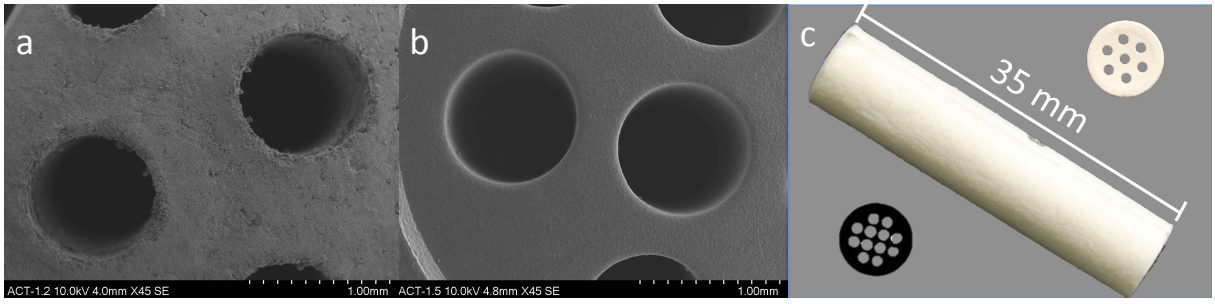


Figure 79. Top: results of CFD study. Characteristic slices depict flow velocity fields over the Actitubes. Bottom: SEM images of the ceramic end cap (a), plastic end cap (b), and a photograph of the Actitube (c).

#### 4.3.1.5 Aerodynamic assessment of formulations of RF SDr from watery solutions or suspensions, using the ACT

RFaqCryst1 and RFIPAAm1 were found to perform poorly when dispensed from the ACT, showing FPFs well below 10% (Table 26). In contrast, RFAqAm1, RFAqAm2, and RFAqAm3 showed FPFs higher than 10%, with RFAqAm1 exhibiting the highest FPF. Figure 80 provides an overview for cascade impactor experiments using the ACT.

Table 26. Aerodynamic characteristics of RF samples dispensed from the ACT.

| Sample name | FPF [%] | EF [%] | MMAD [$\mu$m] | GSD [ ] |
|---|---|---|---|---|
| RFaqCryst1 | 5.8 ±2.3 | 51.0 ±16.7 | 4.6 ±0.4 | 2.1 ±0.1 |
| RFaqAm1 | 33.6 ±3.0 | 90.3 ±0.2 | 3.9 ±1.4 | 3.9 ±0.6 |
| RFaqAm2 | 17.3 ±2.8 | 99.6 ±0.0 | 4.7 ±0.5 | 3.1 ±0.4 |
| RFaqAm3 | 11.8 ±3.4 | 99.2 ±0.0 | 5.3 ±1.2 | 2.5 ±0.1 |
| RFIPAAm1 | 7.2 ±4.3 | 66.7 ±9.9 | 3.7 ±0.2 | 2.0 ±0.0 |

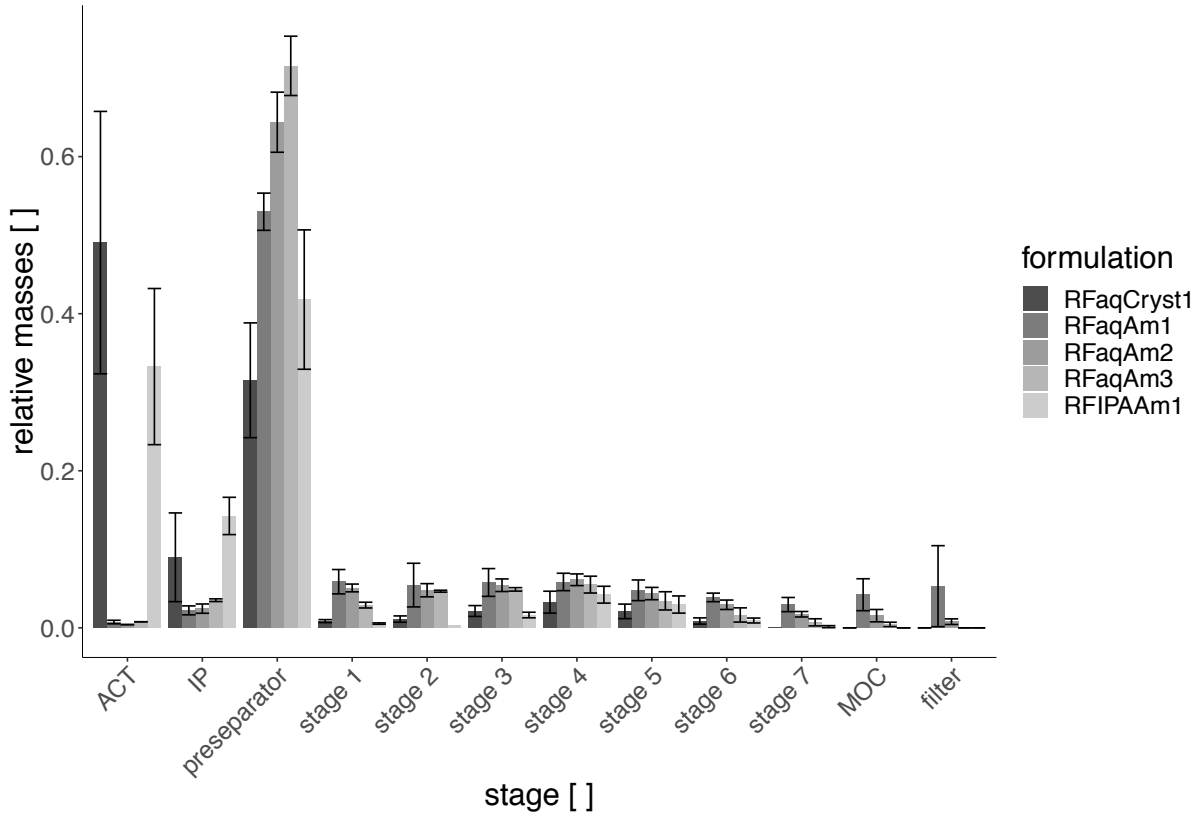


Figure 80. Results from cascade impactor experiments analyzing samples SDr from water, using the ACT.

#### 4.3.1.6 Aerodynamic assessment of formulations of RF SDr from watery solutions or suspensions using a modified induction port

Aerosol characteristics of RFaqCryst1, RFaqAm1, and RFIPAAm1 investigated using a modified induction port are shown in Table 27. RFaqCryst1 showed increased deposition in the mIP when compared to the USPIP (Figure 81), corresponding to a lower deposition in the preseparator unit, with no significant difference in aerosol characteristics. Additionally, USPIP and USP3DIP yielded statistically equivalent results.

In the case of RFaqAm1, a slight but significant increase in preseparator deposition was found when the USP3D was used (Figure 82). Deposition in the mIP was found to be increased, but not significantly. Additionally, USP3DIP and the mIP showed statistically lower deposition

on S5. Increased mIP deposition resulted in a statistical decrease in $FPF_{total}$ (p= 0.02819) and $FPF_{emitted}$ (p= 0.01763).

Table 27. Aerodynamic characteristics of RF samples SDr from water, using the USPIP, USP3DIP, and mIP.

| | | IP tested | | |
|---|---|---|---|---|
| Sample name | | USPIP | USP3DIP | mIP |
| RFaqCryst1 | **MMAD** [$\mu$m] | 2.85 ±0.07 | 2.70 ±0.15 | 2.92 ±0.17 |
| | **GSD** [] | 2.08 ±0.02 | 2.09 ±0.01 | 2.09 ±0.00 |
| | $\mathbf{FPF_{total}}$ [%] | 42.55 ±1.75 | 45.57 ±5.23 | 41.39 ±4.11 |
| | $\mathbf{FPF_{emitted}}$ [%] | 48.22 ±2.02 | 51.34 ±6.22 | 45.77 ±5.35 |
| | $\mathbf{F_{emitted}}$ [%] | 88.26 ±1.42 | 88.80 ±1.44 | 90.55 ±1.66 |
| RFaqAm1 | **MMAD** [$\mu$m] | 1.44 ±0.18 | 1.59 ±0.01 | 1.51 ±0.08 |
| | **GSD** [] | 3.14 ±0.08 | 3.32 ±0.01 | 3.34 ±0.13 |
| | $\mathbf{FPF_{total}}$ [%] | 88.71 ±2.04 | 85.31 ±2.16 | 81.99 ±1.89 |
| | $\mathbf{FPF_{emitted}}$ [%] | 90.52 ±1.89 | 86.86 ±2.37 | 83.29 ±2.47 |
| | $\mathbf{F_{emitted}}$ [%] | 98.00 ±0.22 | 98.21 ±0.26 | 98.44 ±0.19 |

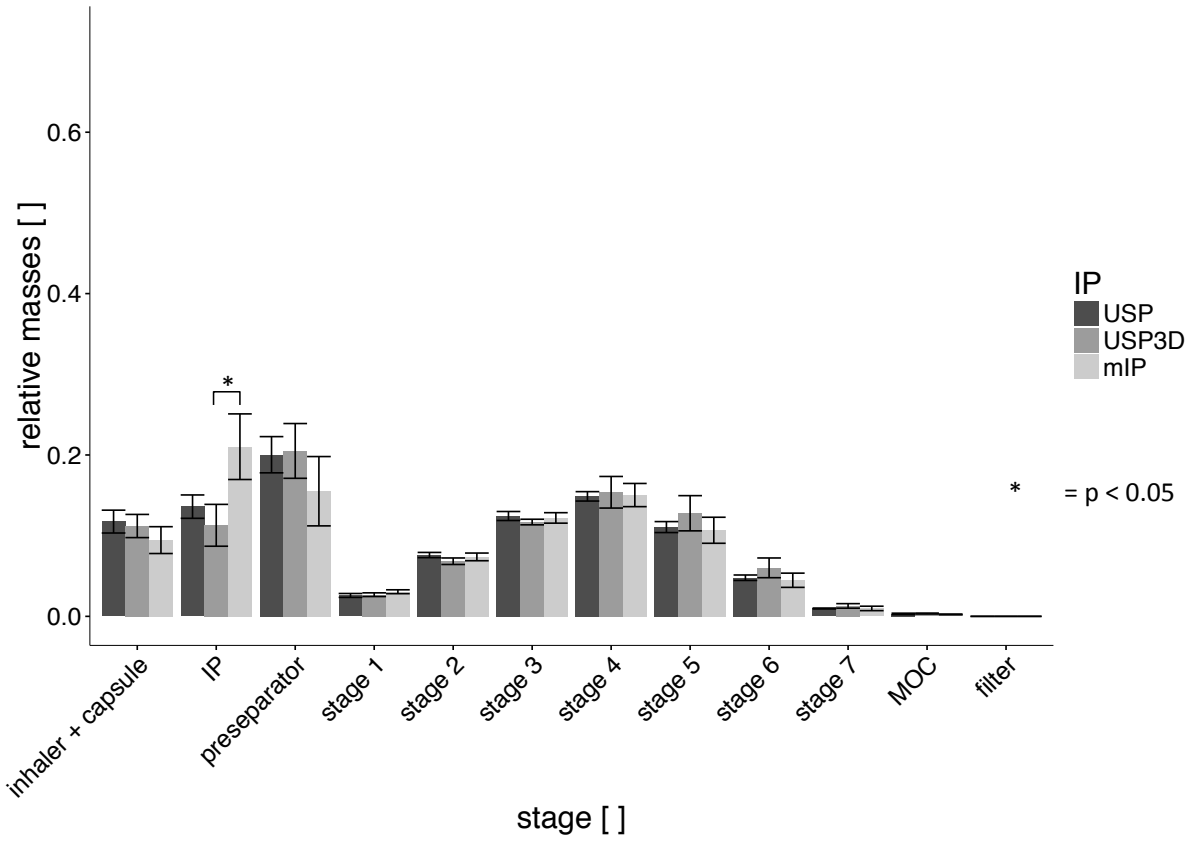


Figure 81. Results of cascade impactor analysis of RFaqCryst1, using the USPIP, USP3DIP, and mIP.

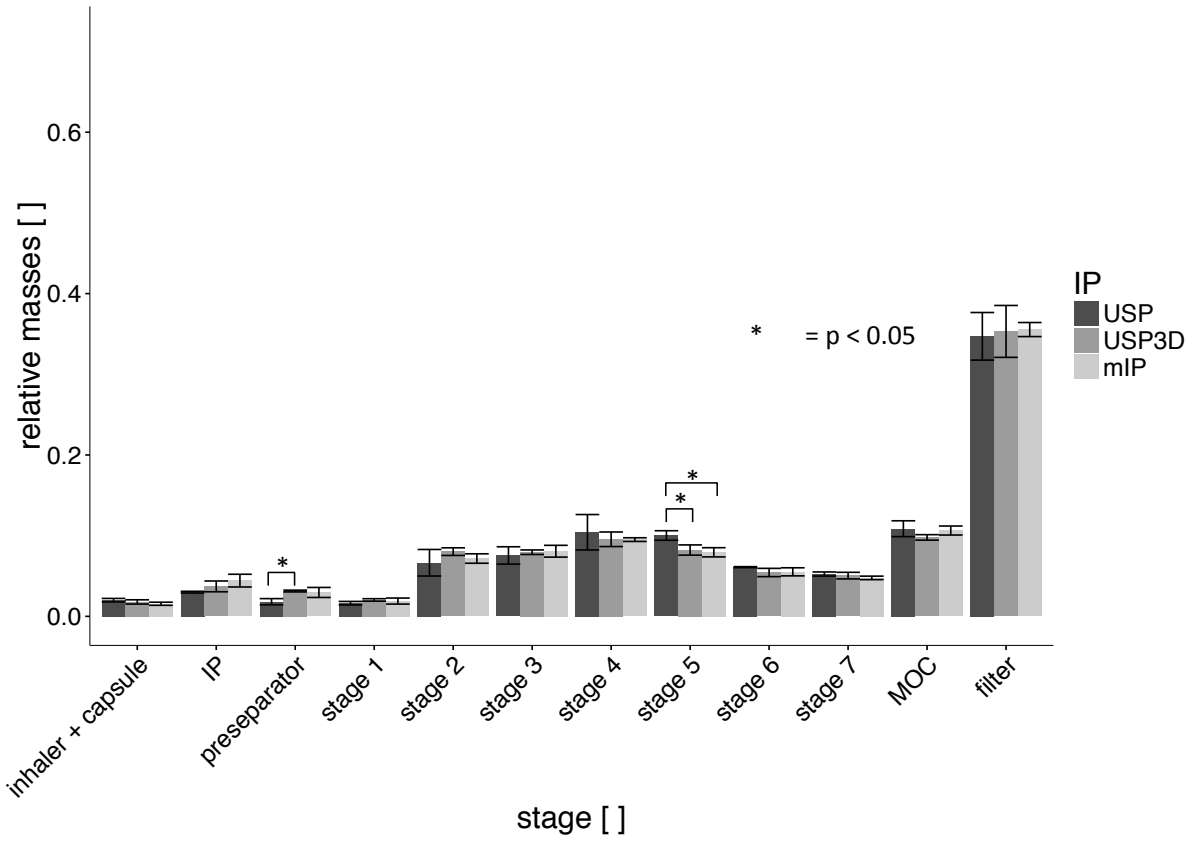


Figure 82. Results of cascade impactor analysis of RFaqAm1, using the USPIP, USP3DIP, and mIP.

#### 4.3.1.7 Investigation of particle formation using the acoustic levitator

##### 4.3.1.7.1 Rheological properties of liquids and solutions used

Physicochemical characteristics of liquids used are shown in Table 28.

Table 28. Physicochemical characteristics of liquids used in the levitator experiments.

| Solvent | $C_{RF}$ [mg/mL] | $\rho$ [g/cm$^3$] | $\gamma$ [ g/s$^2$] | $\nu$ [mm$^2$/s] |
|---|---|---|---|---|
| $H_2O$ | 1.5 ±0.06 | 1.00 ±0.00 | 46.8 ±0.5 | 0.95 ±0.01 |
| EtOH | 1.4 ±0.01 | 0.79 ±0.00 | 23.1 ±0.5 | 1.37 ±0.00 |
| IPA | 1.5 ±0.00 | 0.78 ±0.00 | 21.5 ±0.6 | 2.65 ±0.02 |
| $H_2O$ | 0 | 1.00 ±0.00 | 70.2 ±0.2 | 0.92 ±0.01 |
| EtOH | 0 | 0.79 ±0.00 | 22.1 ±0.7 | 1.37 ±0.00 |
| IPA | 0 | 0.78 ±0.00 | 22.8 ±0.5 | 2.65 ±0.01 |

##### 4.3.1.7.2 Determination of contact angle of plain solvents by DSA

Figure 83 shows images of the DSA. Uneven surfaces seen in the images of EtOH and IPA are due to the material, which had been dissolved and then re-solidified. Droplets of EtOH and IPA were found to spread entirely. The contact angle for water was determined to be 95.9 ±3.1°.

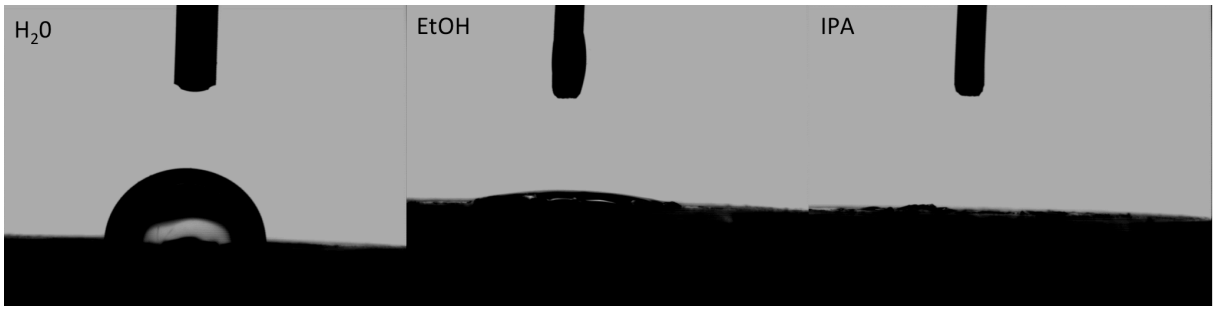


Figure 83. Images of droplets of water, EtOH, and IPA on compacted RFIPAAm1.

##### 4.3.1.7.3 Acoustic levitator experiments

Droplets of pure IPA or EtOH were found to show reduced drying times to that of water. It

was noted that pure IPA, EtOH, and aqueous solutions of RF show a greater droplet deformation at a set energy input, which consequently demanded adjustment of the driving voltage of the piezo and droplet repositioning relative to the nodes, so as to stay within the pre-specified range for the axis ratio. Drying of droplets of pure solvents (IPA, EtOH, or $H_2O$) in the acoustic field showed a steady reduction of relative $d_{eq}$(area). It was observed that $\Delta d_{eq}(area)/\Delta t$ developed in a nonlinear manner (Figure 84), increasing slightly over time. Axis ratios of pure solvent droplets were found to decrease slightly over time. After reaching a critical mass threshold, all solvents showed an increase of variability in the length of the major axis, which is correlated to ghosting of the image, caused by an increase in x-position instability of the droplet in the acoustic field. Evolution of the axis ratio over time, when adding RF to the solvent, was found to be equivalent to the plain solvent in the case of EtOH and IPA (Figure 84). Rel. $d_{eq}$(area) evolution of pure EtOH and a ethanolic RF solution were found to be identical. Rel. $d_{eq}$(area) evolution of solutions of RF in IPA were initially aligned to the ones of pure solvent, but eventually a plateau was reached with no further change over time (Figure 84, top right panel). Axis ratio evolution of aqueous solutions of RF were found to differ strongly, steadily increasing over time until a plateau was reached, before abruptly changing. Rel. $d_{eq}$(area) evolution over time of aqueous RF solutions initially showed congruence with the pure solvent droplets, but after reaching a critical point, relative $d_{eq}$(area) abruptly dropped to a plateau; eventually changing its level, as observed with the axis ratio. Figure 85 shows characteristic pictures of different stages of the drying process for solutions of RF, as well as SEM images of the resulting particles, recovered from the levitator. In the case of EtOH, no particles could be recovered.

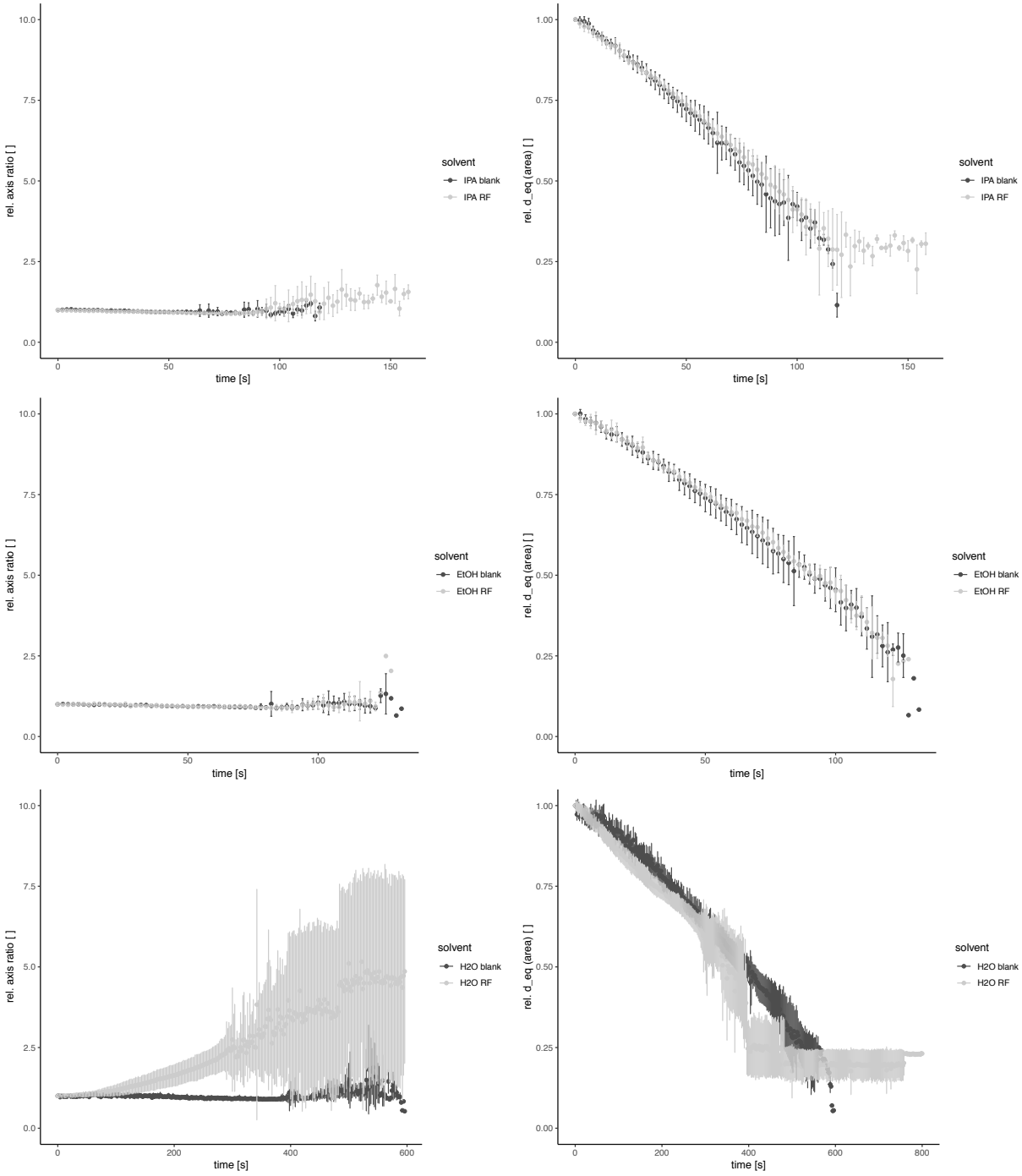


Figure 84. Results of levitation experiments: evolution of rel. axis ratio and $d_{eq}$(area) over time (left and right panel series respectively).

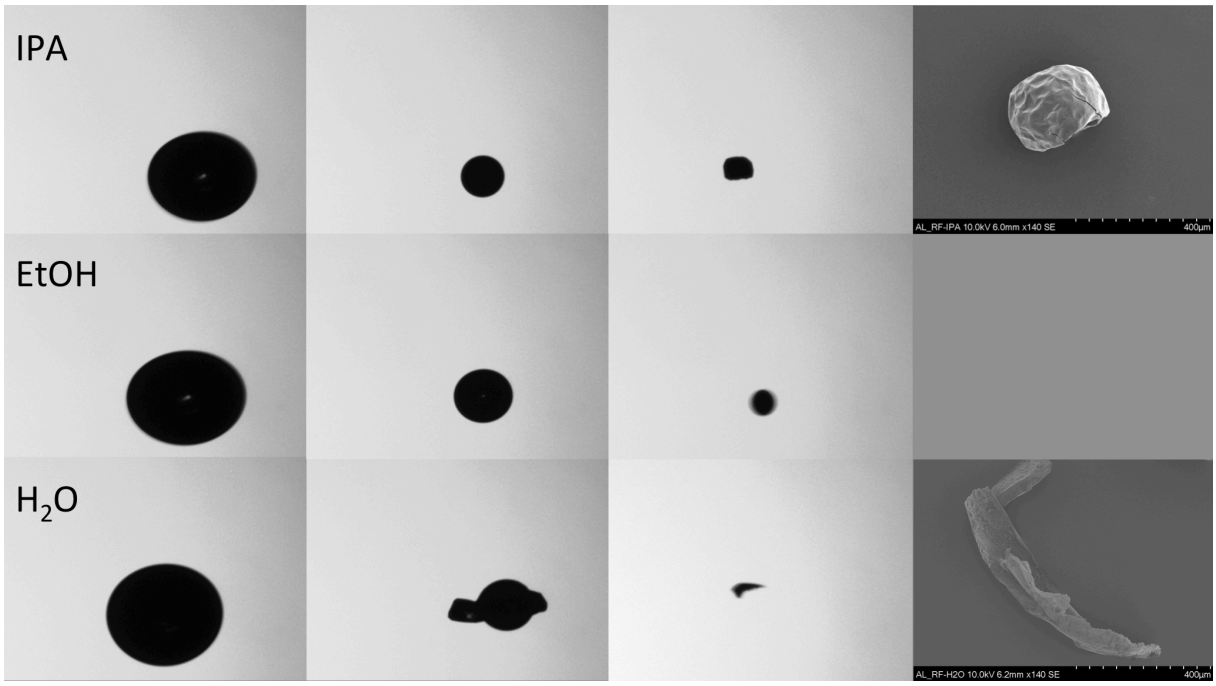


Figure 85. Characteristic backlight pictures, depicting the evolution of RF solutions from droplet to particle (first three columns). SEM images (last column) of particles obtained from drying IPA (top) and $H_2O$ (bottom).

#### 4.3.1.8 Stability study

Table 29 shows drug content of RFaqCryst1, RFaqAm1, and RFIPAAm1 as determined by HPLC, after storage at ICH accelerated conditions as well as samples stored for six months at four °C. XRPD and DSC analysis results were consistent over the test period for all samples analyzed, indicating that no re-crystalization or polymorphic transformation occurred. Figure 86 shows the results of aNGI experiments.

Table 29. Content of RF samples SDr from water after storage.

| | HPLC [%] | | | | |
|---|---|---|---|---|---|
| Sample name | t= 0 months | t= 1 months | t= 3 months | t= 6 months | t= 6 months (fridge) |
| RFaqCryst1 | 91.7 ±1.3 | 91.0 ±1.7 | 80.1 ±0.4 | 80.4 ±1.6 | 92.5 ±0.0 |
| RFaqAm1 | 94.1 ±0.1 | 87.7 ±5.5 | 65.1 ±0.7 | 59.8 ±1.4 | 95.1 ±0.7 |
| RFIPAAm1 | 97.6 ±1.5 | 91.6 ±0.4 | 67.8 ±4.5 | 60.2 ±2.8 | 96.2 ±0.3 |

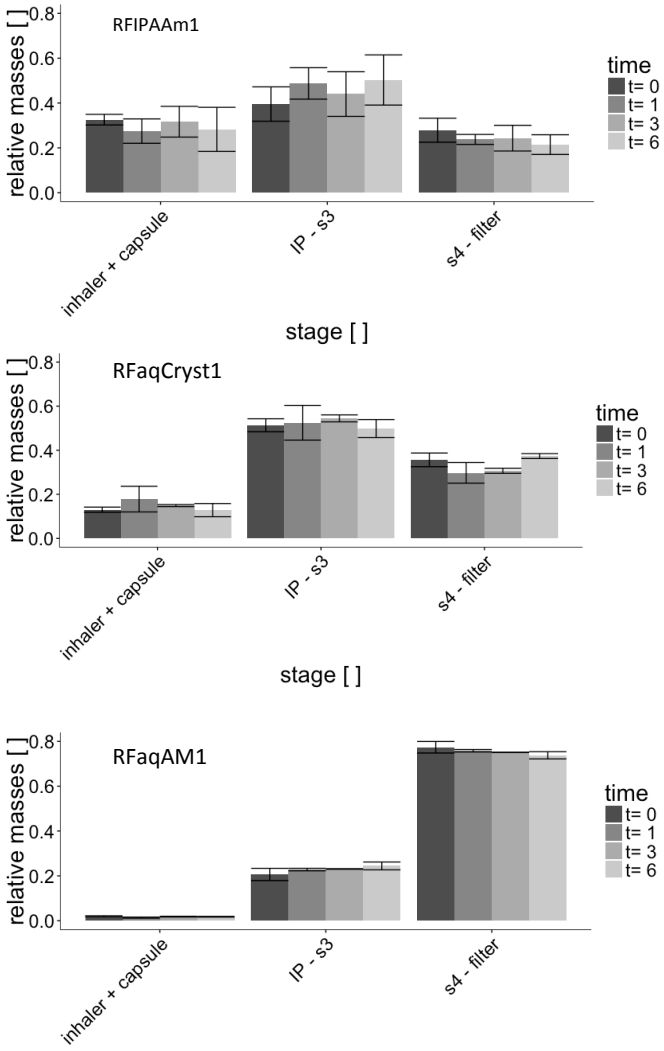


Figure 86. Results of aNGI experiments after one, three, and six months of storage at ICH accelerated conditions.

### 4.3.2 **Discussion**

Manufacture and testing of formulations investigated in the exploratory study was successfully repeated, demonstrating consistent product and process properties. Solid state properties of the batches produced, were consistent with the results of the exploratory study. Compositions of formulations spray dried from aqueous solutions were slightly modified to include an additional concentration, in order to estimate how robust these formulations are, when aerosol performance is evaluated (in the context of solid content of the feed solutions). XRP diffractograms of RFaqCryst1 were found to be identical to RFaqexp5, and all other samples were consistently amorphous. RFIPAAm1 showed a significant amount of residual isopropyl alcohol (as discussed in the previous section, 4.2.1.2.3). Samples spray dried from water had significant amounts of residual water, but preliminary studies investigating a similar formulation showed that FPFs drop, when the powders are kept over a drying agent such as silica (data not shown). Furthermore, as already mentioned, formulation batches produced in this study were not intended for *in vivo* testing, and, as residual solvents at that quantity were not expected to fundamentally influence aerosol properties, samples were processed in accordance with the other formulation test batches.

Aerodynamic testing showed that all amorphous formulations spray dried from water have excellent aerosol properties. FPFs were found to be extremely high so effective lung targeting is to be expected. High deposition in the terminal filter unit indicated that a major fraction of these formulations was in the aerodynamic nm range; providing a suitable tool to test the hypothesis that particles showing an aerodynamic diameter lower than one µm are not expected to persist within the lungs, but rather are exhaled, which was based on investigations using inert standard particles [12]. Due to the high surface area associated with the low aerodynamic diameter (also see next paragraph for the mechanism of particle formation) and the high capacity of incorporating water as shown in DVS experiments, one might hypothesize that this type of particle would alter its aerodynamic properties (i.e. settling velocity) as a function of time, when in a biorelevant environment. However, this hypothesis is not easily tested *in vitro*, since the residence time of the particles expected *in vivo* is not reflected in the cascade impactor experiment.

Spray drying of suspensions of RF recrystallized from water yielded a formulation with good aerosol properties, which was indicated by fine particle fractions comparable to 'state of the art' commercially available formulations. This type of formulation performed slightly better than particles spray dried from suspensions of RF in EtOH or MeOH, which had been discussed in the previous section (4.2.1.3). But it should be anticipated, that this formulation has potential for improvement in its performance by optimization of composition, and/or process parameters, as well as storage conditions. In this set of studies, manufacturing parameters were chosen so as to be suitable for processing with a greater variety of solvents, but each solvent of course, demands for specific optimization. Also, storage conditions were selected in a conservative way, and the focus was on chemical and thermodynamic stability, rather than optimization of aerosol performance. RFaqCryst1 was also found to be superior to RFIPAAm1, an amorphous reference formulation spray dried from IPA, by displaying higher FPFs and improved long-term stability.

Since it was found that powders spray dried from aqueous solutions of RF were easily de-agglomerated with high FPFs, these formulations should be considered as interesting candidates for application with a low cost, disposable DPI device. It was concluded that these formulations demand little performance from the DPI's de-agglomeration unit to perform properly, so no complex geometries or intricate flow paths need to be incorporated into their design. To verify this hypothesis, aerosol characterization was also performed using a low performance, low cost DPI surrogate (ACT). Consisting of a simple cardboard tube that is sealed with two perforated stoppers that create a high intrinsic resistance, the low-cost disposable inhaler model was designed to reflect a worst case scenario inhalation device. CFD simulations showed that little impartment of energy into the powder bed is expected, since flow velocities of a non-turbulent current within the device are limited by a high pressure drop, generated at the inlet of the device. The low aerosol performance of RFaqCryst1 and RFIPAAm1 is in good agreement with the CFD study conducted. As a consequence, RFaqCryst1 and RFIPAAm1 showed pronounced retention of the powder within the DPI model, with the emitted fraction having a high degree of agglomeration; as indicated by high IP and preseparator deposition values. Conversly, RFaqAm1, RFaqAm2, and RFaqAm3 were found to empty well from the device. Nevertheless, these formulations also showed high preseparator deposition indicating that samples were not fully de-agglomerated. The FPFs recorded were found to be in the range of 10-30%, indicating acceptable aerosol properties in the case of RFaqAm1. These powders were found to empty easily from the device, with little

IP deposition. The major fraction of the particles was deposited in the preseparator stage, so incomplete de-agglomeration is to be assumed. Even so, it was confirmed that powders designed using this formulation strategy could be manufactured in a way that they do not demand high performance devices to aerosolize properly, which leaves more room to focus on patient and product safety as well as cost and material efficiency, when developing such a delivery system. As an additional benefit, using the ACT offered a more discriminative test system for high performance formulations. Using the Handihaler device, RFaqAm1, RFaqAm2, and RFaqAm3 yielded similar FPFs of 88.7 ±2.0%, 81.8 ±0.9%, and 80.0 ±0.4% respectively, whereas analysis using the ACT yielded FPFs of 33.6 ±2.3%, 17.3 ±2.8%, and 11.8 ±3.4% respectively. Interestingly, FPFs determined using the ACT were found to be negatively correlated to the concentrations of the spray dried solutions, which is good agreement with our expectations (also see Equation 1) but the Handihaler device failed to resolve these intricate differences. So the concept of aerosol testing using a low performance device might offer additional information for the formulation scientist.

Aerodynamic properties of RFaqCryst1 and RFaqAm1 were investigated using a more bio-relevant, 3D printed induction port, which was developed earlier by this group. Also, the effect of material properties on IP deposition was investigated using a 3D-printed copy of the USPIP. RFaqCryst1 showed statistically equivalent IP deposition and overall performance when investigated with the USPIP and USP3DIP respectively, so it can be concluded that material and surface properties were irrelevant here, which is in good agreement with literature and in line with results presented in Chapter three. MIP deposition was found to be increased when compared to the USPIP and USP3DIP but corresponded to a drop in preseparator deposition, so consequently cumulative IP and preseparator deposition of 33.6 ±2.3% and 36.5 ±5.7 for the USPIP and the mIP, respectively were found to be statistically equivalent ($p= 0.47997$). Also, MMAD, GSD, and additionally FPFs were found to be statistically equivalent. This is in good agreement with literature and confirms observations made during the initial assessment of the mIP using a DPI formulation (Cyclocaps Cyclohaler). RFaqAm1 showed insignificantly increased IP deposition in the case of the USP3DIP and mIP, when compared to the USPIP. Also, deposition in the preseparator stage was found to be slightly increased, which was significant in the case of the USP3DIP. Correspondingly, a significant decrease in deposition was found in S5, which resulted in significantly lower FPFs, when comparing the USPIP and mIP. This finding could be indicative that actual *in vivo* performance might be over predicted, using the USPIP, but it is

unclear, if the predicted relative reduction of 8% would be traceable *in vivo*. Though not being significant, a slight reduction in FPFs was observed comparing the USPIP and the USP3DIP, which could be indicative of a material related effect observed. So, in this case the model would erroneously under predict the actual lung deposition. Due to the low difference in predicted lung deposition and the uncertainty associated with the possible influence of the material, it is to be assumed that in this case using the mIP offers no additional information. Results from cascade impactor analysis of RFIPAAm1 using the mIP were discussed in the previous section.

Aerosol properties of formulations spray dried from aqueous solutions were found to be consistently high. To understand the mechanism leading to the extraordinary aerosol characteristics observed for this type of formulation, the process of particle formation was investigated using an acoustic levitator. Due to the low solid content of the solutions, these formulations were expected to show spherical, amorphous particles of fairly low geometric diameter, which would result in rather low aerosol performance, as these powders would not be easily de-agglomerated. The acoustic levitator provides a suitable tool to investigate the mechanism of particle formation during the spray drying process. A droplet of one µL of the test solution is kept in constant levitation in an acoustic field, while being exposed to a steady nitrogen flow at a pre-specified flow rate and temperature. Mass transfer from the droplet is measured indirectly by determining geometries from backlight images of the droplet. The evolution of droplet diameter over time is indicative for the mass transfer rate, if constant droplet geometry is being assumed. The droplet's shape deviates from the ideal sphere as, in order to overcome gravity, the acoustic force is applied. In reality, interactions of the droplet with the acoustic field are more complex, as also frequency of the signal as well as the position of the droplet relative to the acoustic output nodes influences the overall extent and geometry of the force applied to the droplet. If transducer frequency and transducer/reflector geometries are kept constant, comparable deformation is expected, if the liquids used show similar rheological properties [179,180]. In the case of the aqueous solutions of RF it was found that particle deformation (i.e. ratio of the major and minor axis of the ellipsoid at set conditions) was more pronounced than the one observed for pure water, so viscosity, density, and surface tension values were estimated to investigate those differences in rheology. Density was found to be identical when comparing plain solvents to solutions of RF in the respective solvent, which was to be expected at solid content as low as 0.15%$_{w/v}$. Viscosity

was found to be equivalent in the case of EtOH and IPA, whereas a decrease in viscosity was observed for aqueous solutions of RF. But, given the precision of the experimental setup and control of environmental conditions, this result was considered to be insignificant. In contrast, aqueous solutions of RF showed a significant and pronounced decrease in surface tension, when compared to water. Based on this finding one must conclude that RF shows interfacial activity and so must be regarded as a surfactant. Solutions of RF in organic solvents showed no difference in surface tension, indicating a higher degree of solubilization of the drug molecules. As reduced surface tension (being the amount of energy required to magnify a surface by one unit) at given energy input must result in a larger surface, deviation from the ideal sphere must occur, as this geometrical shape minimizes the surface area to volume ratio.
In order to increase the comparability of samples with different deformation behavior, droplet diameters were reported as the diameter of a backlight image area equivalent sphere (= $d_{eq}$(area)). Plots of $d_{eq}$(area) over time can be used to visualize at what relative droplet volume crust formation of the material dissolved occurs. It is expected that the concentration of the material dissolved, increases over the period of the drying process, as solvent is being constantly removed from the system. When reaching a specific threshold value, the solvent/solute system transforms from a liquid into a semi-solid state, and the overall geometry of the particle becomes dominated by the solidified material. This hypothetically occurs in two different ways: (i) either the solidified material is evenly distributed throughout the droplet, or (ii) phase separation occurs, facilitating formation of a shell of solid material and incorporating a liquid core. If additional solvent is removed, this is expected to lead to the formation of solid or hollow particles respectively. Depending on the wall thickness and viscoelastic behavior at given temperature of the shell, it either collapses upon removal of the core liquid and forms characteristic ‘donut shaped’ particles, or forms microspheres, if the walls withstand the forces occurring. One needs to keep in mind that during the drying process additional processes such as diffusion of solvent from the core into the shell occur, which might have a different kinetic rather than mass transfer from the particle surface, which also changes over time as it is surface area dependent. As experiments in the acoustic levitator were conducted at a lower temperature, and at different mass flow rates of the drying gas than occurring during the spray drying process, no quantitative predictions on, for example, kinetics during spray drying can be made. This method provides fundamental information, helping to distinguish between different mechanisms of particle formation and is therefore suitable for use when investigating the mechanism responsible for the different particle

properties observed, comparing particles from spray dried solutions from water to ones from IPA or EtOH. Droplet diameter evolution upon drying of solutions of RF in IPA occurred as expected, based on aforementioned considerations. When compared to the plain solvent, initially, both droplets show congruent diameter evolution. At a characteristic time point (i.e. at a specific concentration of the solute) the diameter remained constant in the case of the solution, whereas there was a steady decreases in the case of the pure solvent until complete evaporation of the droplet occurred, or the droplet was ejected from the system. At the end of the drying phase standard deviations were found to increase, which is related to increasing instability of the droplet in the acoustic field, which often times was found to increase to the extent whereby the droplet was ejected from the acoustic field. Aqueous based solutions initially showed congruent drying curves when compared to the plain solvent. In contrast to the solutions with IPA, evolution of the diameter did not transit smoothly into a plateau phase indicating crust formation, but exhibited an abrupt change in particle diameter, which remained constant upon additional drying. This can be interpreted as rapid re-arrangement of the particle's basic geometry (i.e. particle collapse). It was observed that in some cases another re-arrangement event occurred, which became obvious by a shift in plateau level. Also, evolution of the droplet/particle axis ratio over time was found to differ significantly when comparing watery solutions of RF to solutions in IPA, or pure solvents. Solutions of RF in IPA or EtOH, as well as the pure solvents, show little changes in droplet geometry over time. It was noted that droplets became more spherical at lower volumes, which is in good agreement with our expectations, as forces applied to the droplet are expected to be lower at lower volumes, which is due to the lower mass experiencing gravitational pull, as well as smaller a volume available for interactions with the acoustic field. So cohesive forces at the droplet's surface (i.e. surface tension) become dominant, leading to an increase in sphericity. In contrast, droplets of aqueous solutions of RF showed a constant change in axis ratio, which is of increasing deviance from the ideal sphere. This behavior is not readily understood, but becomes comprehensible upon evaluation of backlight pictures of the droplet at characteristic time points. The first picture (Figure 85, bottom panel series), which was taken at the beginning of the drying process, shows droplet morphology comparable to the ones found for pure solvent droplets. The second picture, taken at about half of the time of the process duration, could be interpreted to show that after early crust formation the core droplet partly detached from the shell, which is subsequently deformed by the acoustic field, as the droplet in the core decreases in diameter. It should be assumed that initially the shell might be

stabilized by vapor pressure, created by the evaporating core droplet. Thus, at this stage the particle would form a ternary system consisting of the liquid core, a gas phase consisting of water vapor, and the semi-solid shell. It was noted that some particles show early collapse, whereas others maintain the ellipsoid shape longer. This might be related to early rupture of the shell, due to the vapor pressure inside. In this scenario the shell would no longer be stabilized, collapsing around the liquid core, as observed in the figure. However, it is to be highlighted that this was not occurring in all cases and that this picture was chosen, as it clearly shows detachment of the liquid core from the shell, which is not easily visible if early collapse does not occur. The third picture, taken at the end of the process, shows a particle that has lost its liquid core and comprises of the shell only. Interestingly, standard deviations of the particle´s axis ratio increased earlier in the case of the aqueous solution of RF, when compared to the plain solvent. The images taken during the study were compiled into a video sequence that indicated that the droplet was moving individually within the shell. It was also found that in some cases, multiple droplets occur in one shell. Interaction with the shell apparently shifts the center point of rotation of the particle outside the latter, as mass distribution within the system shifts upon drying of the core, and core-shell interactions become more dominant. Additionally, the images indicate that the core-forming droplet was ejected from the system, when a critical mass was reached, while the shell (or fragments of it) often times remain within the acoustic field. To exit from the shell, the droplet must penetrate the crust; this destroys it and induces collapse of the now evacuated shell. This eventually leads to the highly collapsed particles observed in the acoustic levitator, as well as in the spray drying trials. It was also observed that in some cases (Figure 85) the shell is ripped apart and only fragments of it remain in the field. This process was interpreted as a cause for the drastic and sudden change in axis ratio observed, analyzing the axis ratio evolution of droplets of aqueous solutions of RF. Multiple re-arrangements observed would thus be associated with the consecutive ejection of multiple droplets from the shell. To support the hypothesis that the core droplet detaches early from the shell, contact angle measurements of IPA, EtOH, and aqueous droplets on RFIPAAm1 compressed to a disk were conducted. It was assumed that the angle between the inner surface of the shell and the liquid core must exceed a certain threshold, for detachment to occur, so fundamental differences in the contact angle were expected, when comparing the organic solvents to water. Experiments conducted were found to support this hypothesis as water showed a contact angle greater than 90°, whereas ethanol and IPA were found to spread entirely on the surface. Figure 87 depicts different mechanisms

of particle formation from solutions of RF in IPA (top series) and water (bottom series), as proposed based on results of this study. It should be mentioned that formation of only one core droplet is depicted here.

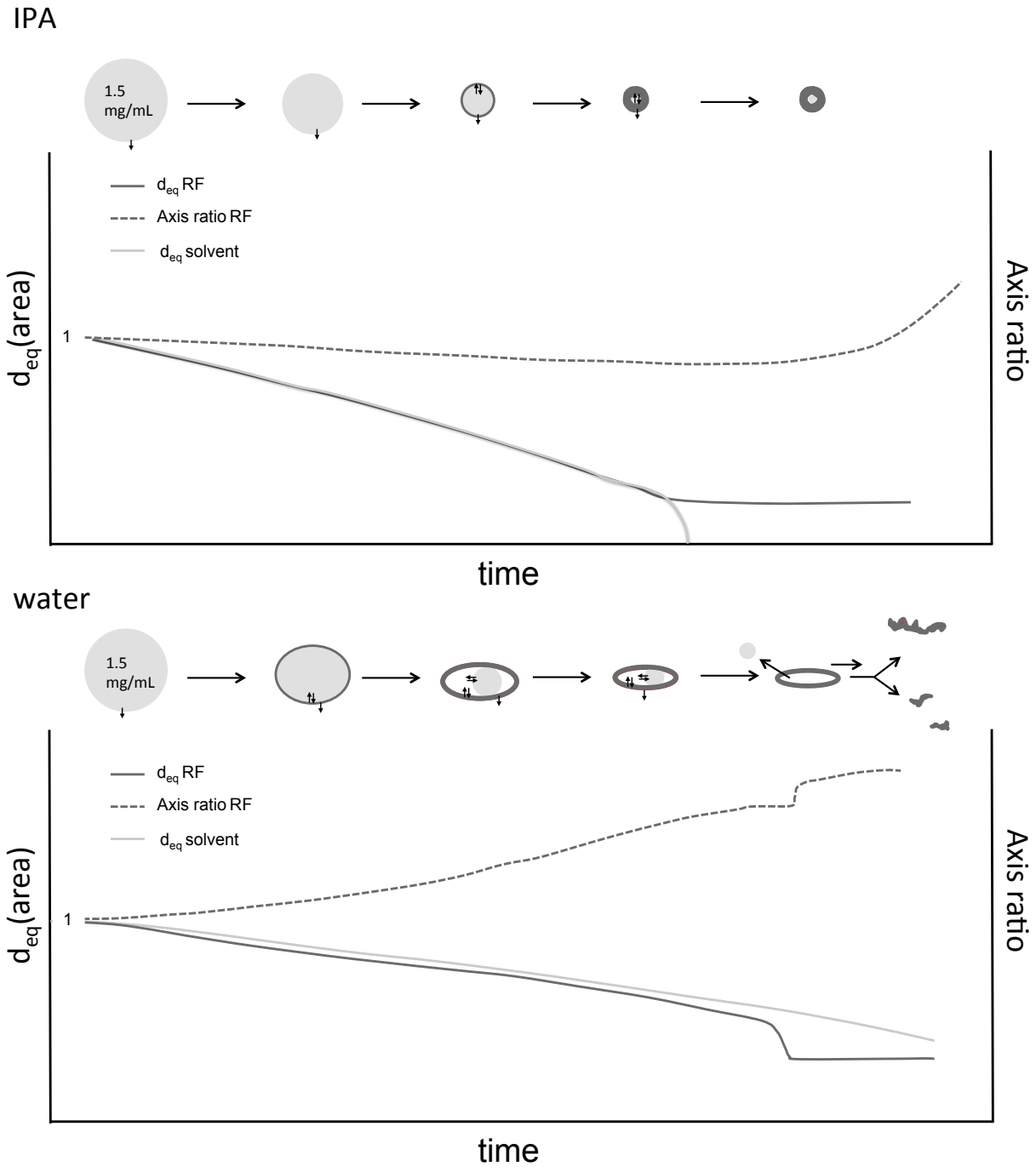


Figure 87. Schematic overview on particle formation mechanisms proposed.

As already mentioned, drying kinetics observed in the acoustic levitator are not comparable to ones occurring upon spray drying. Reducing the temperature and therefore the velocity of the process is necessary to more closely investigate its distinct phases. It is to be assumed, that during the spray drying process crust formation might occur in a similar way as found in the acoustic levitator, but the shell would be subjected to increased vapor pressure, causing the shell to burst. Induced by the drop in pressure associated with that, the solvent core might flash evaporate, causing the shell to collapse. Assuming this, onset time of crust formation, properties of the solvent-shell interface, and shell thickness when collapsing would mainly influence the morphological properties of the resultant particle. Also, during spray drying obviously no force from the acoustic field is imparted, this leads to less asymmetric particles. Comparing both processes investigated and applying aforementioned considerations for applicability of this model to spray drying, it was concluded that aqueous samples of RF show: a) an earlier onset in solid crust formation, b) that the shape of the shell early decouples from the shape of the liquid core, which c) results in a more voluminous shell with lower wall thickness, that d) produces highly collapsed, low apparent density particles after solvent evaporation.

Conclusions drawn from these experiments are in good agreement with literature. In 2013, Chan et al. published a study incorporating a reference formulation of RF spray dried from EtOH/water 50/50 [138], yielding particles showing shape and performance similar to RFaqAm1, RFaqAm2, and RFaqAm3 . This as well as several follow up publications focused on the manufacture of combined antibiotic formulations incorporating RF ([139], [140], [141], [143]). It was found that presence of RF was the key factor for aerosol performance for these formulations and from this observation the hypothesis was derived that RF must be the factor responsible for basic particle geometry and that accumulation of RF in the particles' surface was to be expected. In order to test this hypothesis, particle surface composition was analyzed using XPS and ToF-SIMS (Section 1.5) and the predominance of RF in the shell was confirmed. Accumulation of RF in the shell was attributed to the hydrophobicity of RF. Interestingly, Chan et al. also report increased relative deposition of RF to other drugs incorporated in the lower stages of the cascade impactor, which was attributed to inhomogenous drug distribution and fragmentation of the particle. Both observations made are in good agreement with the model of particle formation presented in this study as predominance of RF in combined antibiotic particles at the particle surface is to be expected, assuming interfacial accumulation of RF leading to shell formation as proposed here.

Separation of more hydrophilic drugs incorporated appears reasonable, as they are expected to dissolve in the liquid core, which was shown to separate from the shell. Also flash evaporation of the core material would presumably lead to separation of drugs incorporated.

Being produced by spray drying aqueous suspensions of RF, RFaqCryst1 shows a distinct x-ray diffraction pattern that differs from both solvent free polymorphic forms of RF. XRP diffractograms recorded after exposure to different RH show that it became more amorphous upon drying but increased in crystallinity when being exposed to higher RH, which was not only associated with an increase of intensity of the diffractogram but also with slight and reversible alterations in the x-ray reflection pattern (Figure 68). RFaqCryst1 further decreased in crystallinity upon solvent removal by thermal drying, as indicated by XRPD and DSC. Showing two overlapping desolvation peaks, DSC experiments indicate two distinct types of water. First desolvation peak (max.≈ 100 °C) is likely to be associated with physisorbed or bulk water, whereas the second desolvation peak (max.≈ 115 °C) is attributed to the removal of crystal water that is more tightly bound thus exiting at temperatures higher than its boiling point. A Tg at approximately 165 °C is indicative of amorphous material in the sample. This hypothesis is also supported by DVS results that indicated a minimum of two different sorption kinetics. Being relatively slow, desolvation kinetic observed upon terminal drying at 0% RH (end of cycle) is indicative for the removal of more tightly bound crystal water. This is in good agreement with the more rapid water uptake at higher RH, as indicated by the short time needed to fully equilibrate at 97% RH (about 90 minutes). As this process was found to be fully reversible, one might hypothesize that solvent molecules are located inside a channel within the crystal lattice. Conversly, RFIPAAm1 requires a longer period of time (about 330 min) to fully equilibrate at 97% RH, which probably is related to the necessity to displace RF molecules, as macroscopically observed by swelling of the sample. And in contrast, RFaqCryst1 shows no extensive swelling, which becomes accessible by the higher congruence of sorption isotherms of Cycle 1 and 2. So one must conclude that mechanisms of water incorporation differ.

Comparison of x-ray diffractograms obtained with ones reported in literature showed a high similarity with a rifampicin RF • 0.54 EtOH • 3.92 $H_2O$ solvate reported by Li in 2010 [92] (see Figure 88). This solvate was identified as member of an isostructural series of RF solvates that feature highly similar host conformations. In this isosctructural family, guest molecules (EtOH, MeOH, and water) were found to be interchangeable and are located within

a solvent channel along the α plane of the crystal lattice. Li also identified RF pentahydrate, which was published earlier by Gadret et al. [93], as member of this isostructural group and verified that samples with mixed guest populations subsequently transform into RF pentahydrate, when exposed to ambient humidity. Given the congruence of the XRPD pattern as well as conclusions drawn from DVS and DSC results, it is to be assumed that RFaqCryst1 is another member of this isostructural group. Additionally, x-ray diffractograms of RFaqCryst1 also show high similarity with a RF monohydrate, reported by Henwood et al. in 2001 [90]. In this study, RF was recrystallized from EtOH and vacuum dried. Unfortunately, storage conditions of the samples are not reported. So, based on findings of the present study (also see previous section), one might assume that solvent of crystallization was removed during the drying step and crystals were later re-hydrated, incorporating water from ambient humidity. The exact experimental procedure remains unclear, as it was stated that the monohydrate became fully amorphous upon drying, which is not in line with the manufacturing method reported. Also, identification of the solvate as monohydrate is not easily understood, based on TGA/DSC data presented. No effort was made to confirm this hypothesis by qualitative solvent analysis (e.g. Karl Fisher analysis). However, in light of the manufacturing method and x-ray data presented it is to be assumed that this RF species might be another member of this isostructural group.

Incorporation of water into the crystal lattice was found to vary as a function of ambient vapor pressure, which might correspond to different degrees of saturation of positions for solvent molecules available in the channel. Loss on initial drying during the DVS experiment (data not shown) is in good agreement with loss on drying determined by TGA, so complete removal of water from the sample can be assumed. Maximum water uptake determined at 97% RH was found to be 13.37 % w/w which is equivalent to a molar ratio of RF:$H_2O$ of 1:6.1. But, given the small particle size and corresponding large surface area of the sample, it is to be assumed that a certain fraction of this is rather physisorbed than crystal water. Thus, RFaqCryst1 could be identical to RF pentahydrate proposed by Gadret et al. Unfortunately, the original publication provides single crystal x-ray data only, so direct comparability is somewhat limited.

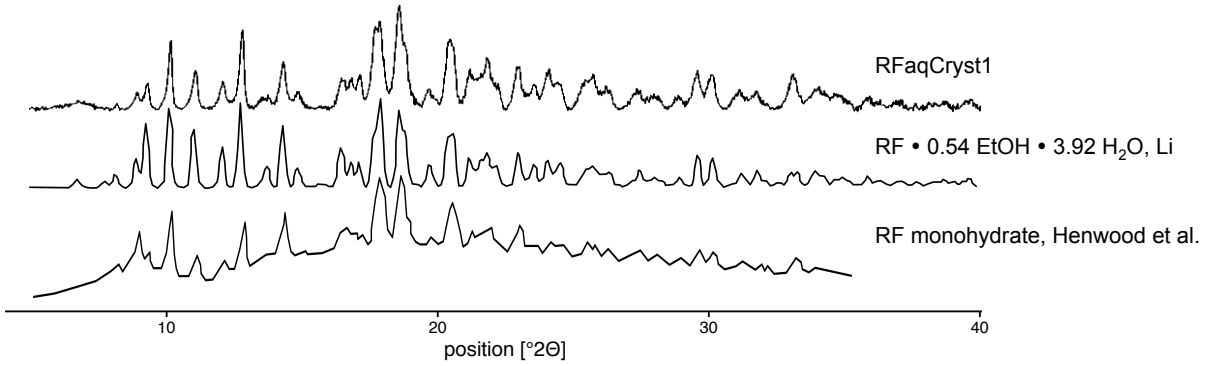


Figure 88. X-ray powder diffractograms of RFaqCryst1, RF • 0.54 EtOH • 3.92 $H_2O$ (redrawn from [92]), and RF monohydrate (redrawn form[90]).

Stability studies at accelerated ICH conditions showed that all samples investigated show stability of their aerodynamic properties over the entire range of the study. In this study, an abbreviated NGI setup, where a glass fiber filter was inserted upstream of S4, was used. S4 was selected as size cut off, since, starting from this stage, all particles collected are expected to be in the $d_{ae} \leq$ five µm range. Additionally, it was expected that smaller particles are more prone to undergo processes triggering particle growth, so excluding the fraction of the FPF that would impact in S3, was found to be the more conservative approach than also including S3.

Chemical stability of all powder samples was found insufficient under conditions applied. Interestingly, RFaqAm1, which was expected to be the most sensitive batch from that series, did not show a higher degree of degradation than RFIPAAm1. It is well known that amorphous SDr samples of rifampicin undergo degradation [91], so a decrease in RF content was to be expected. However, as specific surface areas are expected to be higher in the samples spray dried from water and as oxidation to RF-quinone is reported as one of the major routes of degradation [89], a more rapid degradation was expected. Also, RFaqCryst1 showed significant degradation over the six months period of storage. This was unexpected as it was assumed that crystalline samples would be stable. As no further characterization of the degradation products was performed, the mechanism of degradation remains unclear. One might hypothesize that $O_2$ triggered oxidation, or hydrolysis to 3-formyl Rifamycin SV might have occurred [89]. As all samples contained significant amounts of water and were not stored under an inert atmosphere, it is possible that this might have created a microenvironment facilitating both routes of degradation. Ambient air not only provides $O_2$ for oxidation, but

also $CO_2$, which might have interacted with the water, providing protons for acid catalyzed hydrolyzation. As FPFs of samples spray dried from aqueous solutions were shown to be fairly robust to the solid content of the feed solution, it is expected to be feasible to incorporate antioxidizing or buffering excipients into the formulation, without decreasing its aerosol performance. Especially as it is assumed that, due to the high molecular weight of RF, already small amounts might be effective. But, one must keep in mind that during the manufacturing process phase separation (RF and antioxidizing agent) might occur, limiting the protective effect. It was shown that storage at low temperatures successfully protects all formulations from degradation. However, it is not desirable to keep the potential product refrigerated, as countries with the highest demand for improved TB therapy often lack suitable infrastructure to ensure product stability upon transport and storage (also see introduction, 1.4.1). Another approach to prevent degradation would be to keep the dry powders protected from ambient gases using inert atmosphere packing. As these formulations are intended for use in single use, disposable low cost DPIs, these could be individually blistered, and could provide sufficiently high protection of the product.

To summarize, formulations investigated in this section show excellent aerosol properties, making them interesting candidates for application using a low-cost disposable DPI. In anti-infective airways therapy, single use devices are preferred as they minimize the risk of infections of medicinal staff, family members, or other groups of persons possibly exposed to contaminated inhalers. As of now, the formulations suffer from chemical instability, but different approaches have been discussed to optimize either the formulation itself or storage conditions applied in a way that would provide a higher stability. The following studies on these formulations should focus on improvement of the chemical stability, as well as characterization of aerosol performance from devices with dose compartments of higher volumes, to investigate what the maximal applicable dose of this formulation is. It is also of interest to investigate *in vivo* deposition of the particles. This is not only relevant in the context of developing a novel inhalable TB therapy but also because formulations described in this chapter offer an excellent system to test the hypothesis that particle showing a $d_{ae}$ lower than one µm are being exhaled, which is generally assumed.

# 5 General discussion and outlook

The present work touches on two distinct, but related topics i.e. the development of an improved *in vitro* model to predict aerosol lung deposition *in vivo,* and the development of a particle engineered, excipient free formulation of rifampicin to be used in the context of tuberculosis therapy. Aerosol analysis using the improved model was eventually applied to formulation candidates investigated, providing more biorelevant assessment of their aerodynamic properties. Following, both topics will be discussed separately including a discussion of the main findings, their context in literature as well as an outlook.

## 5.1 Development of a novel, 3D printed induction port for use in cascade impactor analysis

Analysis using cascade impaction devices is the most relevant method to describe pharmaceutical aerosols. Knowledge of the aerodynamic properties of a formulation is not only important in the context of reproducible manufacture, but can also be utilized to predict aerosol deposition *in vivo*. Particles of different aerodynamic diameter, deposit in anatomically different locations of the human respiratory system. It is widely accepted that particles showing an aerodynamic diameter of one to five µm effectively target the lungs. Larger particles are likely to impact in the upper respiratory system, whereas smaller particles might be exhaled [16]. The Next Generation Pharmaceutical Impactor is a cascade impaction device that was distinctively designed in the early 2000s to meet the needs associated with aerosol analysis of pharmaceutical aerosols. Nevertheless, the main focus of the developing consortium was on providing highly standardized testing equipment for QC and industrial manufacture. As a consequence, the NGI as monographed in USP and Ph.Eur. lacks physiological accuracy, which compromises its ability to be used as predictive tool in IVIVC [72]. Especially its induction port, which is a tube of uniform cross sectional diameter, a 90° bend and tapered ends, is seen as one of the major issues of the NGI, when IVIVC is desired. Consequently, much effort has been made to develop more realistic mouth/throat models and geometries utilized have been derived from MRT/CT images, observations on patients, or

casts [74–78]. Advanced MT models have been prepared using resin, rubber, or fiber glass [75-77], as well as rapid prototyping techniques, such as fused deposition modeling (FDM) [78]. Main focus of these studies was on MT deposition, rather than its impact on the aerodynamic particle size distribution and the models often times were tested individually, i.e. not using the NGI, or another CI. Contrary, the most extensively studied MT model (Alberta idealized throat, AIT) is commercially available as a substitute induction port for use with the NGI. This model is based on patient data, which have been idealized and compiled into an extrathoracic mouth/throat model, based on simple, geometries. It is available in two different versions, representing the averaged adult and the averaged child respectively. These models are manufactured from stainless steel, and are not intended to be modified in order to adapt for pathophysiological alterations of the respiratory tract, special patient populations e.g. pre-school children, or a completely individualized approach.

In the present work we presented a novel, modified induction port (mIP) that was based on a computer tomographic scan of a trachea that was obtained from an open access database. FDM 3D printing technique, which, in context of personalized medicine, had gained a lot of attention over the past few years, was used as rapid prototyping technique. It has been shown that FDM 3D printing using PLA filament is a suitable technique to produce modified induction port models that were found to fully comply with USP and Ph.Eur. requirements in terms of air tightness and flow stability. Also it was shown that FDM 3D printing produces the models in a reproducible quality. To assess the impact of the material used, all formulations investigated were also tested on a 3D printed copy of the regular USPIP, and only the nebulized formulation (Sultanol forte) showed a statistically significant increase in deposition. Conclusively, it was found that surface properties in this experimental setup play a minor role only, which is in good agreement with a study conducted using the AIT, where coating the IP's walls with different materials had been shown to not affect the outcome of the aerosol analysis [73]. In order to understand which formulation strategy produces aerosols showing increased tracheal deposition, commercial preparations of salbutamol formulated as pMDI (with and without VHC), DPI, and solution for nebulization were assessed using the novel IP. DPI and nebulized formulations, as well as the pMDI with VHC were found not to benefit from alterations of the IP. In the case of the DPI this was due to a decrease in preseparator deposition that corresponded to an increase in IP deposition. So, though increased IP deposition was observed, cumulative IP and preseparator deposition was found unaffected which consequently translated into equivalence of the aerosol characteristics

determined, using the USPIP and the mIP respectively. In the case of the nebulized formulation, IP deposition was found to be low in all cases, so that the impact of modifying the IP was found to be irrelevant in a therapeutic context. Contrary, the pMDI formulation assessed showed increased IP deposition using the mIP, which translated into lower fine particle fractions (being the fraction of the dose with an aerodynamic diameter ≤ five µm). CFD studies confirmed that basing the IP model on physiologically relevant geometries produces significantly different airflow patterns, when compared to the regular USP IP, which can aid to explain the increased deposition observed. In order to distinguish between increased deposition caused by physiological relevant and artificial geometries respectively, another modified induction port was designed. This model shows a greater distance of the actuator valve from the 90° bend and allows plume expansion. Tests with additional, commercially available pMDI formulations showed that different particle populations tend to impact in different areas of the MT and that pMDI formulation performance is negatively correlated to MT deposition. A specific pMDI formulation strategy - suspending the API particles in the propellant - was shown to be more susceptible to MT deposition than solution based pMDIs, which show a higher performance in general.

To assess the suitability of the novel IP model for IVIVC, additional pMDI formulations were selected based on availability of *in vivo* deposition data in literature, and assessed using the mIP as well as the mIPext (mIP with USP distal part). It was found that IVIVC is superior using the mIP instead of the USPIP. Interestingly, it was also found superior to the one achieved using the mIPext, highlighting the need to include an (more sophisticated) oral cavity model into the future makes of the model. IVIVC was also found superior, to one achieved using the AIT but as this conclusion was based on literature review it must be evaluated as indicative only.

As already mentioned, as a next step in the development of this model, an oral cavity model is to be included. Geometries should be derived from CT scans as well, but it is also to be investigated if exact geometries of the individual patient are as critical as it was found in the case of the trachea, or if an idealized geometry offers the same information for the researcher. In later studies the model could be utilized to investigate aerosol deposition in special patient populations e.g. children of different age, the elderly, or patients showing pathophysiological alterations of the respiratory tract. Additionally, it could also be used to optimize device use in clinical practice, as e.g. the effect of different head positions on aerosol deposition could easily be investigated without the need to perform clinical trials. As literature e.g. indicates a

strong impact of the pMDI spray angle on particle deposition [167], a certain relevance is to be expected here.

## 5.2 Development of excipient free dry powder formulations of RF

Despite all efforts, tuberculosis infection is still one of the leading causes of death in the world. It is caused by the gram-negative bacterial species *M.tuberculosis* and primarily infects the lungs, though secondary systemic infections may occur. In routine therapy, four first line antibiotics, namely rifampicin, ethambutol, pyrazinamide, and isoniazid are applied and the standard therapy includes per oral administration of aforementioned substances over a period of at least 26 weeks. In the case of RF, it is often accompanied with unwanted side effects, which is related to the high daily doses needed to achieve suitable drug concentrations at the site of infection i.e. the lungs. In order to decrease systemic exposure - which is expected to limit side effects and increase patients' adherence - a respirable dosage form of RF is desirable. Development of particle engineered dry powder formulations for pulmonary therapy started in the early 2000s. Since then, numerous studies have been published focusing on different aspects of a potential therapeutic strategy. One approach that has been widely investigated is the formulation of micro- and nanoparticulate systems to proactively target alveolar macrophages, which host the bacteria in infected tissue. Different classes of excipients including PLGA, lipids, chitosan, or modified carbohydrates have been investigated as potential matrix forming system but in most cases issues with aerosol performance, drug loading, or drug stability are potential drawbacks. Another approach is the development of high drug load, excipient free formulations. This approach aims to provide high concentrations of the API in the lungs, as the maximum dose applicable using traditional formulation strategies, i.e. formulating as interactive blend, is limited to a few mg. Contrary, particle engineered formulations can be optimized in a way that delivery of up to about 50 mg (and maybe more) per dose becomes accessible. In 2011, Son and McConville had reported a first formulation strategy for the manufacture of a high drug load, excipient free formulation [91]. In this approach, RF was recrystallized from ethanol and subsequently spray dried, which yielded a RF solvate of unique, flake like shape that was characterized as dihydrate and showed excellent aerosol properties and good stability. Anyways, from that publication it was

unclear how the dihydrate was formed and at which step the water was introduced into the system. Two solvent free polymorphs, as well as numerous hydrates and solvates of RF are reported in literature and it was hypothesized that recrystallizing RF from other solvents might produce particles with enhanced aerosol properties. Thus, one aim of the present work was a) to explore, if other common solvents could be utilized in a similar manner as ethanol and b) clarify the solid state characteristics of the RF dihydrate. Suitable candidates for investigation were screened in an exploratory study, in which RF was recrystallized from ethanol, methanol, IPA, acetone, DCM, and water at two API to solvent ratios. Additionally, equilibrium saturated solutions of RF in all solvents mentioned were spray dried, as a control. Distinct polymorphs (XRPD) were found for samples recrystallized from ethanol, methanol, and water. Except of samples spray dried from water, all solutions yielded amorphous, spherical, slightly collapsed particles. Contrary, spray drying of watery solutions of RF yielded highly collapsed, amorphous particles of exceptionally high fine particle fractions, when dispensed from common inhalation devices. Best performing (NGI) formulations showing distinct X-ray pattern as well as the best performing amorphous formulations were repeated and investigated more detailed.

DVS, GC, KF, and XRPD experiments revealed that RF samples recrystallized from ethanol as well as ones recrystallized from methanol belong to one isostructural series of solvato polymorphs, in which guest molecules were found to be inter-changable, depending on the ambient conditions applied. This was found in good agreement with literature. In a study published by Li [92], RF was recrystallized from several mixtures of solvents and it was shown to form different channel solvates. This result has recently been confirmed and extended by Wicher et al. [95]. Application of these finding on results obtained investigating the samples recrystallized from methanol and ethanol yielded a good model to explain the observations made. Based on the results presented in this work in context of the literature available, one must conclude that the solvent gravimetrically quantified in the study by Son and McConville might be ethanol, water, or - most likely - a mixture thereof. Ethanol would be present from the manufacturing process, whereas the water would have been introduced from ambient moisture, subsequently replacing the ethanol molecules. Samples recrystallized from water were identified as member of another isostructural group of RF solvates and were found to be related to a RF • 0.54 EtOH • 3.92 $H_2O$ solvate reported by Li [92], a RF pentahyhdrate reported by Gadret et al. [93], and a RF monohydrate reported by Henwood et al. [90]. All formulations showed good aerosol properties yielding FPFs from 30 - 40%. It is

to be mentioned though that samples were treated in a conservative way in order to maintain their original solid state and formulations have not been optimized for aerosol properties, so it appears reasonable to assume that significantly higher FPFs could be achieved using this formulation strategy. Amorphous control formulations manufactured by spray drying solutions of RF in IPA yielded FPFs in the same range. Contrary, spray drying of solutions of RF in water produced ultra fine powders, yielding FPFs of up to 90%, using the Handihaler DPI. These formulations were also tested using a low cost, low performance, disposable DPI surrogate, in order to investigate what minimal requirements are to be met by the DPI, in order for these formulations to display acceptable performance. It was shown, that this type of formulation demands little performance of the DPIs de-agglomeration engine, supporting the hypothesis that it is suitable for application using a low cost, low performance device. Additionally, it was found that using this model offered a higher degree of discriminability in that high FPF range, when compared to the Handihaler. A similar type of particles had already been reported by Chan et al., who spray dried a hydroalcoholic solution of RF. To understand why spray drying from water yielded drastically different particles, when compared to e.g. ones spray dried from ethanolic solutions of about the same concentration, the mechanism of particle formation was investigated using an acoustic levitator. It was found, that in this system RF forms a shell at an early stage of droplet evolution that decouples from the liquid core and eventually collapses into a highly corrugated, low density particle. The mechanism proposed is in good agreement with data published by Chan et al. and other groups using the same approach, which had, based on ToF - SIMS and XPS experiments, concluded that RF accumulates at the particle surface. Due to their excellent aerosol properties, these particles are good candidates for use in a single use disposable DPI product. Additionally, this mechanism could be exploited in a platform technology to produce high efficiency aerosols, if a physiologically neutral excipient showing similar interfacial behavior could be found. Anyways, stability studies revealed that all formulations except the one recrystallized from ethanol show limited chemical stability only, though stability of the aerosol performance was found to be good. In the case of the amorphous formulations, incorporating protective agents might increase their chemical stability. In the case of crystalline formulations, suitable storage conditions i.e. refrigerated storage under $N_2$ atmosphere could increase the shelf life of these powders. As formulations recrystallized from MeOH or water offer no benefits over formulations recrystallized from ethanol but show impaired stability, the RF ethanol/water

solvate would be the polymorph of choice to proceed with. Future studies could include optimiziation of the particles in terms of aerosolizability and macrophage uptake.

# 6 References

[1] K.E. Barrett, W.F. Ganong, Ganong's review of medical physiology., McGraw-Hill Medical, New York, 2010. http://site.ebrary.com/id/10326225 (accessed April 22, 2018).
[2] P. Vaupel, H.-G. Schaible, E. Muschler, Anatomie, Physiologie, Pathophysiologie des Menschen, 7th ed., WVG, 2015.
[3] National Heart, Lung, and Blood Institute, Guidelines for the Diagnosis and Management of Asthma (EPR-3), (2007). https://www.nhlbi.nih.gov/health-topics/guidelines-for-diagnosis-management-of-asthma.
[4] Global Initiative for Chronic Obstructive Lung Disease, Pocket guide to COPD diagnosis, management, and prevention, (2017). http://goldcopd.org (accessed May 30, 2018).
[5] Global Initiative for Chronic Obstructive Lung Disease, Global strategy for the diagnosis, management, and prevention of chronic obstructive pumonary disease (2018 report), (2018). http://goldcopd.org (accessed May 30, 2018).
[6] B.S. Quon, C.H. Goss, B.W. Ramsey, Inhaled Antibiotics for Lower Airway Infections, Ann. Am. Thorac. Soc. 11 (2014) 425–434. doi:10.1513/AnnalsATS.201311-395FR.
[7] A.J. Hickey, Back to the future: Inhaled drug products, J. Pharm. Sci. 102 (2013) 1165–1172. doi:10.1002/jps.23465.
[8] K. Berkenfeld, A. Lamprecht, J.T. McConville, Devices for Dry Powder Drug Delivery to the Lung, AAPS PharmSciTech. (2015) 479–490. doi:10.1208/s12249-015-0317-x.
[9] D.A. Edwards, A. Ben-Jebria, R. Langer, Recent advances in pulmonary drug delivery using large, porous inhaled particles, J. Appl. Physiol. 85 (1998) 379–385.
[10] V.A. Marple, D.L. Roberts, F.J. Romay, N.C. Miller, K.G. Truman, M. Van Oort, B. Olsson, M.J. Holroyd, J.P. Mitchell, D. Hochrainer, Next Generation Pharmaceutical Impactor (A New Impactor for Pharmaceutical Inhaler Testing). Part I: Design, J. Aerosol Med. 16 (2003) 283–299. doi:10.1089/089426803769017659.
[11] D.L. Morris, L. Hannon, A.L. Garcia, Slip length in a dilute gas, Phys. Rev. A. 46 (1992) 5279–5281. doi:10.1103/PhysRevA.46.5279.
[12] J. Heyder, J. Gebhart, G. Rudolf, C.F. Schiller, W. Stahlohofen, Deposition of particles in the human respiratory tract in the size range 0.005 - 15 μm, J. Aerosol Sci. 17 (n.d.) 811–825.
[13] W. Stahlhofen, J. Gebhart, J. Heyder, Experimental determination of the regional deposition of aerosol particles in the human respiratory tract, Am. Ind. Hyg. Assoc. J. 41 (1980) 385-398a. doi:10.1080/15298668091424933.
[14] M. Lippmann, Regional Deposition of Particles in the Human Respiratory Tract, in: R. Terjung (Ed.), Compr. Physiol., John Wiley & Sons, Inc., Hoboken, NJ, USA, 2011: pp. 213–232. doi:10.1002/cphy.cp090114.
[15] J. Heyder, Deposition of Inhaled Particles in the Human Respiratory Tract and Consequences for Regional Targeting in Respiratory Drug Delivery, Proc. Am. Thorac. Soc. 1 (2004) 315–320. doi:10.1513/pats.200409-046TA.
[16] J. Meier, H. Rettig, H. Hess, Biopharmazie. Theorie und Praxis der Pharmakokinetik, Thieme Verlag, 1981.
[17] N.R. Labiris, M.B. Dolovich, Pulmonary drug delivery. Part I: Physiological factors affecting therapeutic effectiveness of aerosolized medications: Physiological factors affecting the effectiveness of inhaled drugs, Br. J. Clin. Pharmacol. 56 (2003) 588–599. doi:10.1046/j.1365-2125.2003.01892.x.

[18] R. Vanbever, J.D. Mintzes, J. Wang, J. Nice, D. Chen, R. Batycky, R. Langer, D.A. Edwards, Formulation and physical characterization of large porous particles for inhalation, Pharm. Res. 16 (1999) 1735–1742.
[19] M.J. Telko, A.J. Hickey, Dry Powder Inhaler Formulation, Respir. CARE. 50 (2005) 19.
[20] C. Dunbar, A.J. Hickey, P. Holzner, Dispersion and characterization of pharmaceutical dry powders, KONA Powder Part J. (1998) 7–45.
[21] P.M. Young, A. Sung, D. Traini, P. Kwok, H. Chiou, H.-K. Chan, Influence of Humidity on the Electrostatic Charge and Aerosol Performance of Dry Powder Inhaler Carrier based Systems, Pharm. Res. 24 (2007) 963–970. doi:10.1007/s11095-006-9218-8.
[22] A.H.L. Chow, H.H.Y. Tong, P. Chattopadhyay, B.Y. Shekunov, Particle Engineering for Pulmonary Drug Delivery, Pharm. Res. 24 (2007) 411–437. doi:10.1007/s11095-006-9174-3.
[23] A. Voss, W.H. Finlay, Deagglomeration of dry powder pharmaceutical aerosols, Int. J. Pharm. 248 (2002) 39–50. doi:10.1016/S0378-5173(02)00319-8.
[24] A.R. Clark, A.M. Hollingworth, The relationship between powder inhaler resistance and peak inspiratory conditions in healthy volunteers--implications for in vitro testing, J. Aerosol Med. Off. J. Int. Soc. Aerosols Med. 6 (1993) 99–110. doi:10.1089/jam.1993.6.99.
[25] H.A. Tiddens, D.E. Geller, P. Challoner, R.J. Speirs, K.C. Kesser, S.E. Overbeek, D. Humble, S.B. Shrewsbury, T.A. Standaert, Effect of Dry Powder Inhaler Resistance on the Inspiratory Flow Rates and Volumes of Cystic Fibrosis Patients of Six Years and Older, J. Aerosol Med. 19 (2006) 456–465. doi:10.1089/jam.2006.19.456.
[26] M.R. Feddah, K.F. Brown, E.M. Gipps, N.M. Davies, In-vitro characterisation of metered dose inhaler versus dry powder inhaler glucocorticoid products: influence of inspiratory flow rates, J. Pharm. Pharm. Sci. Publ. Can. Soc. Pharm. Sci. Soc. Can. Sci. Pharm. 3 (2000) 318–324.
[27] J.G.Y. Chan, J. Wong, Q.T. Zhou, S.S.Y. Leung, H.-K. Chan, Advances in Device and Formulation Technologies for Pulmonary Drug Delivery, AAPS PharmSciTech. 15 (2014) 882–897. doi:10.1208/s12249-014-0114-y.
[28] M.P. Timsina, G.P. Martin, C. Marriott, D. Ganderton, M. Yianneskis, Drug delivery to the respiratory tract using dry powder inhalers, Int. J. Pharm. 101 (1994) 1–13.
[29] B.J. O'Connor, The ideal inhaler: design and characteristics to improve outcomes, Respir. Med. 98 (2004) 10–16. doi:10.1016/j.rmed.2004.02.006.
[30] H. Bisgaard, Delivery of Inhaled Medication to Children, J. Asthma. 34 (1997) 443–467. doi:10.3109/02770909709055389.
[31] C. Friebel, H. Steckel, Single-use disposable dry powder inhalers for pulmonary drug delivery, Expert Opin. Drug Deliv. 7 (2010) 1359–1372. doi:10.1517/17425247.2010.538379.
[32] S.P. Newman, Principles of Metered-Dose Inhaler Design, Respir Care. 50 (2005) 1177–1190.
[33] T. Noakes, Medical aerosol propellants, J. Fluor. Chem. (2002) 35–45.
[34] K.J. McDonald, G.P. Martin, Transition to CFC-free metered dose inhalers—into the new millennium, Int. J. Pharm. 201 (2000) 89–107.
[35] C. Vervaet, P.R. Byron, Drug-surfactant-propellant interactions in HFA-formulations, Int. J. Pharm. 186 (1999) 13–30.
[36] H.D.C. Smyth, The influence of formulation variables on the performance of alternative propellant-driven metered dose inhalers, Adv. Drug Deliv. Rev. 55 (2003) 807–828. doi:10.1016/S0169-409X(03)00079-6.

[37] Inhalation delivery of therapeutic peptides and proteins / edited by Akwete Lex Adjei, Pramod K. Gupta., New York: M. Dekker, 1997.
[38] S. Stein, B.R. Forsyth, J.S. Stefely, J.D. Christensen, T.D. Alband, P.A. Jinks, Expanding the dosing range of metered dose inhalers through formulation and hardware optimization, Respir Drug Deliv. 1 (2004) 125–134.
[39] S.W. Stein, P. Sheth, P.D. Hodson, P.B. Myrdal, Advances in Metered Dose Inhaler Technology: Hardware Development, AAPS PharmSciTech. 15 (2014) 326–338. doi:10.1208/s12249-013-0062-y.
[40] A.R. Clark, MDIs: Physics of Aerosol Formation, J. Aerosol Med. 9 (1999) 19–26.
[41] Y.-J. Son, J.T. McConville, Advancements in Dry Powder Delivery to the Lung, Drug Dev. Ind. Pharm. 34 (2008) 948–959. doi:10.1080/03639040802235902.
[42] J.P. Mitchell, M.W. Nagel, Valved holding chambers (VHCs) for use with pressurised metered-dose inhalers (pMDIs): a review of causes of inconsistent medication delivery, Prim. Care Respir. J. 16 (2007) 207–215. doi:10.3132/pcrj.2007.00034.
[43] P. l. Marshik, J. s. Larsen, C. l. Leach, P. c. Halverson, B. p. Ekholm, M. h. Amies, H. b. Kaiser, S. c. Weisberg, J. a. Sellers, A Novel Breath Actuated Device (Autohaler$^{TM}$) Consistently Actuates During the Early Phase of Inspiration, J. Aerosol Med. 8 (1995) 187–195. doi:10.1089/jam.1995.8.187.
[44] M. Dahlbäck, Behavior of Nebulizing Solutions and Suspensions, J. Aerosol Med. 7 (1994) 13–18. doi:10.1089/jam.1994.7.Suppl_1.S-13.
[45] P.P.H.L. Brun, A.H. de Boer, H.W. Frijlink, H.G.M. Heijerman, A review of the technical aspects of drug nebulization, Pharm. World Sci. 22 (2000) 75–81. doi:10.1023/A:1008786600530.
[46] Labiris N. R., Dolovich M. B., Pulmonary drug delivery. Part II: The role of inhalant delivery devices and drug formulations in therapeutic effectiveness of aerosolized medications, Br. J. Clin. Pharmacol. 56 (2003) 600–612. doi:10.1046/j.1365-2125.2003.01893.x.
[47] V. Knight, N.V. Koshkina, E. Golunski, L.E. Roberts, B.E. Gilbert, Cyclosporin a aerosol improves the anticancer effect of Paclitaxel aerosol in mice., Trans. Am. Clin. Climatol. Assoc. 115 (2004) 395–404.
[48] Y.K. Lentz, T.J. Anchordoquy, C.S. Lengsfeld, Rationale for the selection of an aerosol delivery system for gene delivery, J. Aerosol Med. Off. J. Int. Soc. Aerosols Med. 19 (2006) 372–384. doi:10.1089/jam.2006.19.372.
[49] E. Köhler, V. Sollich, R. Schuster-Wonka, J. Hühnerbein, Lung deposition in cystic fibrosis patients using an ultrasonic or a jet nebulizer, J. Aerosol Med. Off. J. Int. Soc. Aerosols Med. 16 (2003) 37–46. doi:10.1089/089426803764928347.
[50] A. Elhissi, K.M.G. Taylor, Delivery of liposomes generated from proliposomes using air-jet, ultrasonic, and vibrating-mesh nebulisers, J. Drug Deliv. Sci. Technol. 15 (2005) 261–265. doi:10.1016/S1773-2247(05)50047-9.
[51] A.B. Watts, J.T. McConville, R.O. III Williams, Current Therapies and Technological Advances in Aqueous Aerosol Drug Delivery, Drug Dev. Ind. Pharm. 34 (2008) 913–922. doi:10.1080/03639040802144211.
[52] O. Selroos, A. Pietinalho, H. Riska, Delivery Devices for Inhaled Asthma Medication, Clin. Immunother. 6 (1996) 273–299. doi:10.1007/BF03259089.
[53] A.P. Roth, C.F. Lange, W.H. Finlay, The Effect of Breathing Pattern on Nebulizer Drug Delivery, J. Aerosol Med. 16 (2003) 325–339. doi:10.1089/089426803769017677.
[54] K. Nikander, J. Denyer, M. Everard, G.C. Smaldone, Validation of a new breathing simulator generating and measuring inhaled aerosol with adult breathing patterns, J.

Aerosol Med. Off. J. Int. Soc. Aerosols Med. 13 (2000) 139–146. doi:10.1089/089426800418668.

[55] K. Leung, E. Louca, A.L. Coates, Comparison of breath-enhanced to breath-actuated nebulizers for rate, consistency, and efficiency, Chest. 126 (2004) 1619–1627. doi:10.1378/chest.126.5.1619.

[56] J. Denyer, T. Dyche, The Adaptive Aerosol Delivery (AAD) Technology: Past, Present, and Future, J. Aerosol Med. Pulm. Drug Deliv. 23 (2010) 1–10. doi:10.1089/jamp.2009.0791.

[57] C. O'Callaghan, P.W. Barry, The science of nebulised drug delivery, Thorax. 52 (1997) 31–44.

[58] Medizinische Medien Informations GmbH, Gelbe Liste Pharmindex, Gelbe Liste Pharmindex. (2018). https://www.gelbe-liste.de (accessed April 24, 2018).

[59] J.P. Mitchell, M.W. Nagel, Improved laboratory test methods for orally inhaled products, Ther. Deliv. 4 (2013) 1003–1026. doi:10.4155/tde.13.66.

[60] R. Dimmick, M. Hatch, J. Ng, A particle-sizing method for aerosols and fine powders, AMA Arch Indust Health. (1959) 23–29.

[61] A.A. Andersen, New sampler for the collection, sizing, and enumeration of viable airborne particles, J Bacteriol. (1958) 471–484.

[62] G.P. Polli, W.M. Grim, F.A. Bacher, M.H. Yunker, Influence of Formulation on Aerosol Particle Size, J. Pharm. Sci. 58 (1969) 484–486. doi:10.1002/jps.2600580422.

[63] V.A. Marple, A fundamental study of inertial impactors, University of Minnesota, 1970.

[64] V.A. Marple, K. Willeke, Impactor design, Atmos. Environ. 10 (n.d.) 891–896.

[65] D.J. Rader, V.A. Marple, Effect of Ultra-Stokesian Drag and Particle Interception on Impaction Characteristics, Aerosol Sci. Technol. 4 (1985) 141–156. doi:10.1080/02786828508959044.

[66] C. Fang, V. Marple, K. Rubow, Influence of cross-flow on particle collection characteristics of multi-nozzle impactors, J. Aerosol Sci. 22 (1991) 403–415. doi:10.1016/0021-8502(91)90001-X.

[67] EDQM, European Pharmacopoeia 9.0, (2017).

[68] United states pharmacopoeial convention inc., 2018 US Pharmacopoeia-National Formulary [USP 41 NF 36], Rockville, MD, 2018.

[69] J.P. Mitchell, J. Suggett, M. Nagel, Clinically Relevant In Vitro Testing of Orally Inhaled Products—Bridging the Gap Between the Lab and the Patient, AAPS PharmSciTech. 17 (2016) 787–804. doi:10.1208/s12249-016-0543-x.

[70] A.S. Melani, M. Bonavia, V. Cilenti, C. Cinti, M. Lodi, P. Martucci, M. Serra, N. Scichilone, P. Sestini, M. Aliani, M. Neri, Inhaler mishandling remains common in real life and is associated with reduced disease control, Respir. Med. 105 (2011) 930–938. doi:10.1016/j.rmed.2011.01.005.

[71] T.G. Dzubay, L.E. Hines, R.K. Stevens, Particle bounce errors in cascade impactors, Atmospheric Environ. 1967. 10 (1976) 229–234. doi:10.1016/0004-6981(76)90095-0.

[72] A.R. Clark, S.P. Newman, N. Dasovich, Mouth and oropharyngeal deposition of pharmaceutical aerosols, J. Aerosol Med. 11 (1998) 116–121.

[73] M. Copley, J. Mitchell, D. Solomon, Evaluating the Alberta throat: an innovation to support the acquisition of more clinically applicable aerosol aerodynamic particle size distribution (APSD) data in oral inhaled product (OIP) de- velopment, Inhalation. 5 (2011).

[74] K.-H. Cheng, Y.-S. Cheng, H.-C. Yeh, D.L. Swift, Measurements of Airway Dimensions and Calculation of Mass Transfer Characteristics of the Human Oral Passage, J. Biomech. Eng. 119 (1997) 476–482. doi:10.1115/1.2798296.

[75] K.W. Stapleton, E. Guentsch, M.K. Hoskinson, W.H. Finlay, On the suitablility of k-ε turbulence modeling for aerosol deposition in the mouth and throat: a comparison with experiment, J. Aerosol Sci. 31 (2000) 739–749.
[76] Y. Zhou, J. Sun, Y.-S. Cheng, Comparison of Deposition in the USP and Physical Mouth–Throat Models with Solid and Liquid Particles, J. Aerosol Med. Pulm. Drug Deliv. 24 (2011) 277–284. doi:10.1089/jamp.2011.0882.
[77] P.K.P. Burnell, L. Asking, L. Borgström, S.C. Nichols, B. Olsson, D. Prime, I. Shrubb, Studies of the Human Oropharyngeal Airspaces Using Magnetic Resonance Imaging IV—The Oropharyngeal Retention Effect for Four Inhalation Delivery Systems, J. Aerosol Med. 20 (2007) 269–281. doi:10.1089/jam.2007.0566.
[78] B. Grgic, W. Finlay, P. Burnell, A. Heenan, In vitro intersubject and intrasubject deposition measurements in realistic mouth–throat geometries, J. Aerosol Sci. 35 (2004) 1025–1040. doi:10.1016/j.jaerosci.2004.03.003.
[79] A.H. de Boer, D. Gjaltema, P. Hagedoorn, H.W. Frijlink, Characterization of inhalation aerosols: a critical evaluation of cascade impactor analysis and laser diffraction technique, Int. J. Pharm. 249 (2002) 219–231. doi:10.1016/S0378-5173(02)00526-4.
[80] M.A. Alhnan, T.C. Okwuosa, M. Sadia, K.-W. Wan, W. Ahmed, B. Arafat, Emergence of 3D Printed Dosage Forms: Opportunities and Challenges, Pharm. Res. 33 (2016) 1817–1832. doi:10.1007/s11095-016-1933-1.
[81] S.T. Cole, R. Brosch, J. Parkhill, T. Garnier, C. Churcher, D. Harris, S.V. Gordon, K. Eiglmeier, S. Gas, C.E.B. III, F. Tekaia, K. Badcock, D. Basham, D. Brown, T. Chillingworth, R. Connor, R. Davies, K. Devlin, T. Feltwell, S. Gentles, N. Hamlin, S. Holroyd, T. Hornsby, K. Jagels, A. Krogh, J. McLean, S. Moule, L. Murphy, K. Oliver, J. Osborne, M.A. Quail, Deciphering the biology of Mycobacterium tuberculosis from the complete genome sequence, Nature. 396 (1998) 537–544.
[82] P. Tattevin, E. Casalino, L. Fleury, G. Egmann, M. Ruel, E. Bouvet, The Validity of Medical History, Classic Symptoms, and Chest Radiographs in Predicting Pulmonary Tuberculosis, Chest. 115 (1999) 1248–1253. doi:10.1378/chest.115.5.1248.
[83] World Health Organization, Global tuberculosis report 2017, World health organization, S.l., 2017.
[84] P. Nahid, S.E. Dorman, N. Alipanah, P.M. Barry, J.L. Brozek, A. Cattamanchi, L.H. Chaisson, R.E. Chaisson, C.L. Daley, M. Grzemska, J.M. Higashi, C.S. Ho, P.C. Hopewell, S.A. Keshavjee, C. Lienhardt, R. Menzies, C. Merrifield, M. Narita, R. O'Brien, C.A. Peloquin, A. Raftery, J. Saukkonen, H.S. Schaaf, G. Sotgiu, J.R. Starke, G.B. Migliori, A. Vernon, Executive Summary: Official American Thoracic Society/Centers for Disease Control and Prevention/Infectious Diseases Society of America Clinical Practice Guidelines: Treatment of Drug-Susceptible Tuberculosis, Clin. Infect. Dis. 63 (2016) 853–867. doi:10.1093/cid/ciw566.
[85] Riemser Pharma GmbH, Fachinformation Eremfat, (2015).
[86] K.R. Page, F. Sifakis, R.M. de Oca, W.A. Cronin, M.C. Doherty, L. Federline, S. Bur, T. Walsh, W. Karney, J. Milman, Improved adherence and less toxicity with rifampin vs isoniazid for treatment of latent tuberculosis: a retrospective study, Arch. Intern. Med. 166 (2006) 1863–1870.
[87] R.O. Watson, P.S. Manzanillo, J.S. Cox, Extracellular M. tuberculosis DNA Targets Bacteria for Autophagy by Activating the Host DNA-Sensing Pathway, Cell. 150 (2012) 803–815. doi:10.1016/j.cell.2012.06.040.
[88] M. Hoppentocht, P. Hagedoorn, H.W. Frijlink, A.H. de Boer, Developments and strategies for inhaled antibiotic drugs in tuberculosis therapy: A critical evaluation, Eur. J. Pharm. Biopharm. 86 (2014) 23–30. doi:10.1016/j.ejpb.2013.10.019.

[89] N. Maggi, C.R. Pasqualucci, R. Ballotta, P. Sensi, Rifampicin: A New Orally Active Rifamycin, Chemotherapy. 11 (1966) 285–292. doi:10.1159/000220462.

[90] S.Q. Henwood, W. Liebenberg, L.R. Tiedt, A.P. Lötter, M.M. de Villiers, Characterization of the Solubility and Dissolution Properties of Several New Rifampicin Polymorphs, Solvates, and Hydrates, Drug Dev. Ind. Pharm. 27 (2001) 1017–1030. doi:10.1081/DDC-100108364.

[91] Y.-J. Son, J.T. McConville, A new respirable form of rifampicin, Eur. J. Pharm. Biopharm. 78 (2011) 366–376. doi:10.1016/j.ejpb.2011.02.004.

[92] J. Li, Supramolecular modification of selected antitubercular drugs [dissertation], Cape town: University of cape town; 2010.

[93] M. Gadret, M. Goursolle, J.M. Leger, J.C. Colleter, Structure cristalline de la rifampicine C43N4O12H58.5H2O, Acta Crystallogr. B. 31 (1975) 1454–1462. doi:10.1107/S0567740875005407.

[94] M.M. de Villiers, M.R. Caira, J. Li, S.J. Strydom, S.A. Bourne, W. Liebenberg, Crystallization of Toxic Glycol Solvates of Rifampin from Glycerin and Propylene Glycol Contaminated with Ethylene Glycol or Diethylene Glycol, Mol. Pharm. 8 (2011) 877–888. doi:10.1021/mp100459y.

[95] B. Wicher, K. Pyta, P. Przybylski, M. Gdaniec, Solvates of Zwitterionic Rifampicin: Recurring Packing Motifs via Nonspecific Interactions, Cryst. Growth Des. 18 (2018) 742–754. doi:10.1021/acs.cgd.7b01121.

[96] G. Pelizza, M. Nebuloni, P. Ferrari, G. Gallo, Polymorphism of rifampicin, Il Farm. 32 (1977) 471–480.

[97] S.Q. Henwood, M.M. de Villiers, W. Liebenberg, A.P. Lötter, Solubility and Dissolution Properties of Generic Rifampicin Raw Materials, Drug Dev. Ind. Pharm. 26 (2000) 403–408. doi:10.1081/DDC-100101246.

[98] National Library of Medicine, PubMed, (2018). https://www.ncbi.nlm.nih.gov/pubmed/.

[99] D. Moher, A. Liberati, J. Tetzlaff, D.G. Altman, Preferred Reporting Items for Systematic Reviews and Meta-Analyses: The PRISMA Statement, PLoS Med. 2009 Jul; 6(7)

[100] M. Thorpe, Delivery characteristics and patients; handling of two single-dose dry-powder inhalers used in COPD, Int. J. Chron. Obstruct. Pulmon. Dis. (2011) 353–363. doi:10.2147/COPD.S18529.

[101] H. Mohammed, J. Arp, F. Chambers, M. Copley, V. Glaab, M. Hammond, D. Solomon, K. Bradford, T. Russell, Y. Sizer, S.C. Nichols, D.L. Roberts, C. Shelton, R. Greguletz, J.P. Mitchell, Investigation of Dry Powder Inhaler (DPI) Resistance and Aerosol Dispersion Timing on Emitted Aerosol Aerodynamic Particle Sizing by Multistage Cascade Impactor when Sampled Volume Is Reduced from Compendial Value of 4 L, AAPS PharmSciTech. 15 (2014) 1126–1137. doi:10.1208/s12249-014-0111-1.

[102] plastiape, Single-dose inhalers for capsules: a consolidated tradition with ample growth prospects, OnDrug Deliv. (2012) 26–27.

[103] Cipla, Cipla product brochure, (n.d.). www.ciplamed.com (accessed May 15, 2018).

[104] K. Ikegami, Y. Kawashima, H. Takeuchi, H. Yamamoto, N. Isshiki, D. Momose, K. Ouchi, Improved Inhalation Behavior of Steroid KSR-592 in Vitro with Jethaler® by Polymorphic Transformation to Needle-Like Crystals (ᴺᴸ-Form), (n.d.) 7.

[105] J.H. Bell, P.S. Hartley, J.S.G. Cox, Dry Powder Aerosols I: A New Powder Inhalation Device, J. Pharm. Sci. 60 (1971) 1559–1564. doi:10.1002/jps.2600601028.

[106] H. Schiavone, S. Palakodaty, A. Clark, P. York, S.T. Tzannis, Evaluation of SCF-engineered particle-based lactose blends in passive dry powder inhalers, Int. J. Pharm. 281 (2004) 55–66. doi:10.1016/j.ijpharm.2004.05.029.

[107] C.E. Astete, C.M. Sabliov, Synthesis and characterization of PLGA nanoparticles, J. Biomater. Sci. Polym. Ed. 17 (2006) 247–289. doi:10.1163/156856206775997322.

[108] J.M. Anderson, M.S. Shive, Biodegradation and biocompatibility of PLA and PLGA microspheres, Adv. Drug Deliv. Rev. 28 (1997) 5–24.

[109] Y. Pathak, D. Thassu, Drug delivery nanoparticles formulation and characterization, Informa Healthcare, New York, 2009.

[110] V.V. Sethuraman, A.J. Hickey, Powder properties and their influence on dry powder inhaler delivery of an antitubercular drug, AAPS PharmSciTech. 3 (2002) 7–16. doi:10.1208/pt030428.

[111] I. Coowanitwong, V. Arya, P. Kulvanich, G. Hochhaus, Slow Release Formulations of Inhaled Rifampin, AAPS J. 10 (2008) 342–348. doi:10.1208/s12248-008-9044-5.

[112] J.C. Sung, D.J. Padilla, L. Garcia-Contreras, J.L. VerBerkmoes, D. Durbin, C.A. Peloquin, K.J. Elbert, A.J. Hickey, D.A. Edwards, Formulation and Pharmacokinetics of Self-Assembled Rifampicin Nanoparticle Systems for Pulmonary Delivery, Pharm. Res. 26 (2009) 1847–1855. doi:10.1007/s11095-009-9894-2.

[113] K. Ohashi, T. Kabasawa, T. Ozeki, H. Okada, One-step preparation of rifampicin/poly(lactic-co-glycolic acid) nanoparticle-containing mannitol microspheres using a four-fluid nozzle spray drier for inhalation therapy of tuberculosis, J. Controlled Release. 135 (2009) 19–24. doi:10.1016/j.jconrel.2008.11.027.

[114] Y.-J. Son, J.T. McConville, Preparation of sustained release rifampicin microparticles for inhalation: Sustained-release inhaled rifampicin, J. Pharm. Pharmacol. 64 (2012) 1291–1302. doi:10.1111/j.2042-7158.2012.01531.x.

[115] W. Mehnert, K. Mäder, Solid lipid nanoparticles: Production, characterization and applications, Adv. Drug Deliv. Rev. 47 (2001) 165–196. doi:10.1016/S0169-409X(01)00105-3.

[116] A. Samad, Y. Sultana, M. Aqil, Liposomal Drug Delivery Systems: An Update Review, Curr. Drug Deliv. 4 (2007) 297–305.

[117] N. Changsan, H.-K. Chan, F. Separovic, T. Srichana, Physicochemical characterization and stability of rifampicin liposome dry powder formulations for inhalation, J. Pharm. Sci. 98 (2009) 628–639. doi:10.1002/jps.21441.

[118] N. Changsan, A. Nilkaeo, P. Pungrassami, T. Srichana, Monitoring safety of liposomes containing rifampicin on respiratory cell lines and *in vitro* efficacy against *Mycobacterium bovis* in alveolar macrophages, J. Drug Target. 17 (2009) 751–762. doi:10.3109/10611860903079462.

[119] G.S.V. Kumar, M. Varghese, Annapoorna, Sivakumar, S. Mundayoor, Dry powder cationic lipopolymeric nanomicelle inhalation for targeted delivery of antitubercular drug to alveolar macrophage, Int. J. Nanomedicine. 8 (2013) 2871–2885. doi:10.2147/IJN.S47456.

[120] M.L. Manca, D. Valenti, O.D. Sales, A. Nacher, A.M. Fadda, M. Manconi, Fabrication of polyelectrolyte multilayered vesicles as inhalable dry powder for lung administration of rifampicin, Int. J. Pharm. 472 (2014) 102–109. doi:10.1016/j.ijpharm.2014.06.009.

[121] J. Patil, Vk. Devi, K. Devi, S. Sarasija, A novel approach for lung delivery of rifampicin-loaded liposomes in dry powder form for the treatment of tuberculosis, Lung India. 32 (2015) 331–338. doi:10.4103/0970-2113.159559.

[122] C. Singh, L.V.S.K. Koduri, V. Dhawale, T.D. Bhatt, R. Kumar, V. Grover, K. Tikoo, S. Suresh, Potential of aerosolized rifampicin lipospheres for modulation of pulmonary pharmacokinetics and bio-distribution, Int. J. Pharm. 495 (2015) 627–632. doi:10.1016/j.ijpharm.2015.09.036.

[123] E. Maretti, C. Rustichelli, M. Romagnoli, A.G. Balducci, F. Buttini, F. Sacchetti, E. Leo, V. Iannuccelli, Solid Lipid Nanoparticle assemblies (SLNas) for an anti-TB inhalation treatment - A Design of Experiments approach to investigate the influence of pre-freezing conditions on the powder respirability, Int. J. Pharm. 511 (2016) 669–679. doi:10.1016/j.ijpharm.2016.07.062.

[124] E. Maretti, L. Costantino, C. Rustichelli, E. Leo, M.A. Croce, F. Buttini, E. Truzzi, V. Iannuccelli, Surface engineering of Solid Lipid Nanoparticle assemblies by methyl α- d -mannopyranoside for the active targeting to macrophages in anti-tuberculosis inhalation therapy, Int. J. Pharm. 528 (2017) 440–451. doi:10.1016/j.ijpharm.2017.06.045.

[125] T. Srichana, C. Ratanajamit, S. Juthong, T. Suwandecha, N. Laohapojanart, P. Pungrassami, A.R. Padmavathi, Evaluation of Proinflammatory Cytokines and Adverse Events in Healthy Volunteers upon Inhalation of Antituberculosis Drugs, Biol. Pharm. Bull. 39 (2016) 1815–1822. doi:10.1248/bpb.b16-00354.

[126] R.C. Rowe, P.J. Sheskey, S.C. Owen, American Pharmacists Association, Handbook of pharmaceutical excipients / edited by Raymond C. Rowe, Paul J. Sheskey, Siân C. Owen., Pharmaceutical Press ; American Pharmacists Association, London; Greyslake, IL; Washington, DC, 2006.

[127] A. Kundawala, Preparation, In Vitro Characterization, and In Vivo Pharmacokinetic Evaluation of Respirable Porous Microparticles Containing Rifampicin, Sci. Pharm. 82 (2014) 665–681. doi:10.3797/scipharm.1307-03.

[128] R.V. Pai, R.R. Jain, A.S. Bannalikar, M.D. Menon, Development and Evaluation of Chitosan Microparticles Based Dry Powder Inhalation Formulations of Rifampicin and Rifabutin, J. Aerosol Med. Pulm. Drug Deliv. 29 (2016) 179–195. doi:10.1089/jamp.2014.1187.

[129] T. Rawal, R. Parmar, R.K. Tyagi, S. Butani, Rifampicin loaded chitosan nanoparticle dry powder presents an improved therapeutic approach for alveolar tuberculosis, Colloids Surf. B Biointerfaces. 154 (2017) 321–330. doi:10.1016/j.colsurfb.2017.03.044.

[130] T. Mizoe, T. Ozeki, H. Okada, Application of a Four-fluid Nozzle Spray Drier to Prepare Inhalable Rifampicin-containing Mannitol Microparticles, AAPS PharmSciTech. 9 (2008) 755–761. doi:10.1208/s12249-008-9109-x.

[131] M.V. Vadakkan, S.S. Binil Raj, C.C. Kartha, G.S. Vinod Kumar, Cationic, amphiphilic dextran nanomicellar clusters as an excipient for dry powder inhaler formulation, Acta Biomater. 23 (2015) 172–188. doi:10.1016/j.actbio.2015.05.019.

[132] A.K. Goyal, T. Garg, G. Rath, U.D. Gupta, P. Gupta, Development and Characterization of Nanoembedded Microparticles for Pulmonary Delivery of Antitubercular Drugs against Experimental Tuberculosis, Mol. Pharm. 12 (2015) 3839–3850. doi:10.1021/acs.molpharmaceut.5b00016.

[133] A.K. Goyal, T. Garg, G. Rath, U.D. Gupta, P. Gupta, Chemotherapeutic Evaluation of Guar Gum Coated Chitosan Nanoparticle Against Experimental Tuberculosis, J. Biomed. Nanotechnol. 12 (2016) 450–463. doi:10.1166/jbn.2016.2180.

[134] T. Garg, G. Rath, A.K. Goyal, Inhalable chitosan nanoparticles as antitubercular drug carriers for an effective treatment of tuberculosis, Artif. Cells Nanomedicine Biotechnol. (2015) 1–5. doi:10.3109/21691401.2015.1008508.

[135] M. Mohseni, K. Gilani, Z. Bahrami, N. Bolourchian, S.A. Mortazavi, Preparation and In-vitro Evaluation of Rifampin-loaded Mesoporous Silica Nanoaggregates by an Experimental Design, (2015) 359–371.
[136] R. Parikh, L. Patel, S. Dalwadi, Microparticles of rifampicin: comparison of pulmonary route with oral route for drug uptake by alveolar macrophages, phagocytosis activity and toxicity study in albino rats, Drug Deliv. 21 (2014) 406–411. doi:10.3109/10717544.2013.851302.
[137] T. Rawal, L. Kremer, I. Halloum, S. Butani, Dry-Powder Inhaler Formulation of Rifampicin: An Improved Targeted Delivery System for Alveolar Tuberculosis, J. Aerosol Med. Pulm. Drug Deliv. 30 (2017) 388–398. doi:10.1089/jamp.2017.1379.
[138] J.G.Y. Chan, H.-K. Chan, C.A. Prestidge, J.A. Denman, P.M. Young, D. Traini, A novel dry powder inhalable formulation incorporating three first-line anti-tubercular antibiotics, Eur. J. Pharm. Biopharm. 83 (2013) 285–292. doi:10.1016/j.ejpb.2012.08.007.
[139] Q. Zhou, T. Gengenbach, J.A. Denman, H.H. Yu, J. Li, H.K. Chan, Synergistic Antibiotic Combination Powders of Colistin and Rifampicin Provide High Aerosolization Efficiency and Moisture Protection, AAPS J. 16 (2014) 37–47. doi:10.1208/s12248-013-9537-8.
[140] W. Wang, Q.T. Zhou, S.-P. Sun, J.A. Denman, T.R. Gengenbach, N. Barraud, S.A. Rice, J. Li, M. Yang, H.-K. Chan, Effects of Surface Composition on the Aerosolisation and Dissolution of Inhaled Antibiotic Combination Powders Consisting of Colistin and Rifampicin, AAPS J. 18 (2016) 372–384. doi:10.1208/s12248-015-9848-z.
[141] S.H. Lee, J. Teo, D. Heng, W.K. Ng, Y. Zhao, R.B.H. Tan, Tailored Antibiotic Combination Powders for Inhaled Rotational Antibiotic Therapy, J. Pharm. Sci. 105 (2016) 1501–1512. doi:10.1016/j.xphs.2016.02.007.
[142] K. Kadota, A. Senda, H. Tagishi, J.O. Ayorinde, Y. Tozuka, Evaluation of highly branched cyclic dextrin in inhalable particles of combined antibiotics for the pulmonary delivery of anti-tuberculosis drugs, Int. J. Pharm. 517 (2017) 8–18. doi:10.1016/j.ijpharm.2016.11.060.
[143] M.A.M. Momin, I.G. Tucker, C.S. Doyle, J.A. Denman, S.C. Das, Manipulation of spray-drying conditions to develop dry powder particles with surfaces enriched in hydrophobic material to achieve high aerosolization of a hygroscopic drug, Int. J. Pharm. 543 (2018) 318–327. doi:10.1016/j.ijpharm.2018.04.003.
[144] M.A.M. Momin, I.G. Tucker, C.S. Doyle, J.A. Denman, S. Sinha, S.C. Das, Co-spray drying of hygroscopic kanamycin with the hydrophobic drug rifampicin to improve the aerosolization of kanamycin powder for treating respiratory infections, Int. J. Pharm. 541 (2018) 26–36. doi:10.1016/j.ijpharm.2018.02.026.
[145] W. Rasband, ImageJ, National Institutes of Health, n.d. https://imagej.nih.gov/ij/ (accessed July 24, 2015).
[146] M. Doube, M.M. Kłosowski, I. Arganda-Carreras, F.P. Cordelières, R.P. Dougherty, J.S. Jackson, B. Schmid, J.R. Hutchinson, S.J. Shefelbine, BoneJ: Free and extensible bone image analysis in ImageJ, Bone. 47 (2010) 1076–1079. doi:10.1016/j.bone.2010.08.023.
[147] M. Kintel, OpenSCAD, n.d. http://www.openscad.org (accessed June 8, 2015).
[148] The Blender Foundation, Blender, 2015. https://www.blender.org (accessed July 25, 2015).
[149] A. Ranellucci, Slic3r, 2016. http://slic3r.org.
[150] The OpenFOAM Foundation, OpenFoam, OpenCFD Ltd, n.d. http://www.openfoam.com (accessed November 5, 2016).

[151] E.A. Matida, W.H. Finlay, C.F. Lange, B. Grgic, Improved numerical simulation of aerosol deposition in an idealized mouth–throat, J. Aerosol Sci. 35 (2004) 1–19. doi:10.1016/S0021-8502(03)00381-1.

[152] S.N. Eggerstedt, M. Dietzel, M. Sommerfeld, R. Süverkrüp, A. Lamprecht, Protein spheres prepared by drop jet freeze drying, Int. J. Pharm. 438 (2012) 160–166. doi:10.1016/j.ijpharm.2012.08.035.

[153] G. Murtaza, M. Ahmad, M.A. Madni, M.W. Asghar, A new reverse phase hplc method with fluorescent detection for the determination of salbutamol sulfate in human plasma, Bull. Chem. Soc. Ethiop. 23 (2009) 1–8.

[154] N. Redman-Furey, K. Poiesz, J. Miller, C. Grundner, An evaluation of primary water standards by TG/DTA and vapor sorption analysis, J. Therm. Anal. Calorim. 102 (2010) 633–639. doi:10.1007/s10973-010-0943-1.

[155] B. Al Zaitone, A. Lamprecht, Single droplet drying step characterization in microsphere preparation, Colloids Surf. B Biointerfaces. 105 (2013) 328–334. doi:10.1016/j.colsurfb.2013.01.021.

[156] U.D. of Health, H.S.F.C. for D. Evaluation, Guidance for Industry Q1A(R2) Stability Testing of New Drug Substances and Products, Health Qual. Life Outcomes. 4 (2003) 1–20.

[157] The R Foundation for Statistical Computing, R, Vienna, Austria, n.d. https://www.r-project.org (accessed August 17, 2015).

[158] GSK, Fachinfo Sultanol pMDI, (2013). www.fachinfo.de (accessed August 8, 2016).

[159] A. Cripps, M. Riebe, M. Schulze, R. Woodhouse, Pharmaceutical transition to non-CFC pressurized metered dose inhalers, Respir. Med. 94 (2000) 3–9. doi:10.1016/S0954-6111(00)80143-2.

[160] C.L. Leach, The CFC to HFA Transition and Its Impact on Pulmonary Drug Development, Respir. Care. 50 (2005) 1201–1208.

[161] P.W. Barry, C. O'Callaghan, In vitro comparison of the amount of salbutamol available for inhalation from different formulations used with different spacer devices, Eur. Respir. J. 10 (1997) 1345–1348.

[162] D.L. Ross, B.J. Gabrio, Advances in Metered Dose Inhaler Technology with the Development of a Chlorofluorocarbon-Free Drug Delivery System, J. Aerosol Med. 12 (1999) 151–160. doi:10.1089/jam.1999.12.151.

[163] K.J. McDonald, G.P. Martin, Transition to CFC-free metered dose inhalers - into the new millennium, Int. J. Pharm. 201 (2000) 89–107. doi:10.1016/S0378-5173(00)00401-4.

[164] B.M. Zainudin, M. Biddiscombe, S.E. Tolfree, M. Short, S.G. Spiro, Comparison of bronchodilator responses and deposition patterns of salbutamol inhaled from a pressurised metered dose inhaler, as a dry powder, and as a nebulised solution., Thorax. 45 (1990) 469–473. doi:10.1136/thx.45.6.469.

[165] S.P. Newman, A.R. Clark, N. Talaee, S.W. Clarke, Pressurised aerosol deposition in the human lung with and without an" open" spacer device., Thorax. 44 (1989) 706–710.

[166] Y. Zhang, K. Gilbertson, W.H. Finlay, *In Vivo–In Vitro* Comparison of Deposition in Three Mouth–Throat Models with Qvar ® and Turbuhaler ® Inhalers, J. Aerosol Med. 20 (2007) 227–235. doi:10.1089/jam.2007.0584.

[167] A. Fadl, J. Wang, Z. Zhang, Y. Sung Cheng, Effects of MDI spray angle on aerosol penetration efficiency through an oral airway cast, J. Aerosol Sci. 38 (2007) 853–864. doi:10.1016/j.jaerosci.2007.06.002.

[168] GSK, Fachinfo Sultanol forte, (2014).

[169] C.L. Leach, P.J. Kuehl, R. Chand, L. Ketai, J.P. Norenberg, J.D. McDonald, Characterization of respiratory deposition of fluticasone-salmeterol hydrofluoroalkane-134a and hydrofluoroalkane-134a beclomethasone in asthmatic patients, Ann. Allergy. Asthma. Immunol. 108 (2012) 195–200. doi:10.1016/j.anai.2012.01.010.

[170] C.L. Leach, P.J. Kuehl, R. Chand, J.D. McDonald, Respiratory Tract Deposition of HFA–Beclomethasone and HFA–Fluticasone in Asthmatic Patients, J. Aerosol Med. Pulm. Drug Deliv. 29 (2016) 127–133. doi:10.1089/jamp.2014.1199.

[171] C.L. Leach, P.J. Davidson, B.E. Hasselquist, R.J. Boudreau, Lung deposition of hydrofluoroalkane-134a beclomethasone is greater than that of chlorofluorocarbon fluticasone and chlorofluorocarbon beclomethasone*: A cross-over study in healthy volunteers, Chest. 122 (2002) 510–516. doi:10.1378/chest.122.2.510.

[172] C.L. Leach, P.J. Davidson, R.J. Boudreau, Improved airway targeting with the CFC-free HFA-beclomethasone metered-dose inhaler compared with CFC-beclomethasone, Eur. Respir. J. 12 (1998) 1346–1353.

[173] W. De Backer, A. Devolder, G. Poli, D. Acerbi, R. Monno, C. Herpich, K. Sommerer, T. Meyer, F. Mariotti, Lung Deposition of BDP/Formoterol HFA pMDI in Healthy Volunteers, Asthmatic, and COPD Patients, J. Aerosol Med. Pulm. Drug Deliv. 23 (2010) 137–148. doi:10.1089/jamp.2009.0772.

[174] S. Newman, A. Salmon, R. Nave, A. Drollmann, High lung deposition of 99mTc-labeled ciclesonide administered via HFA-MDI to patients with asthma, Respir. Med. 100 (2006) 375–384. doi:10.1016/j.rmed.2005.09.027.

[175] C.L. Leach, T.D. Bethke, R.J. Boudreau, B.E. Hasselquist, A. Drollmann, P. Davidson, W. Wurst, Two-Dimensional and Three-Dimensional Imaging Show Ciclesonide Has High Lung Deposition and Peripheral Distribution: A Nonrandomized Study in Healthy Volunteers, J. Aerosol Med. 19 (2006) 117–126. doi:10.1089/jam.2006.19.117.

[176] E.C. To, J.M. Flink, 'Collapse', a structural transition in freeze dried carbohydrates, Int. J. Food Sci. Technol. 13 (1978) 567–581.

[177] K. Berkenfeld, Lamkin, Lessel Kybran, Lamprecht, Alf, McConville, Jason T, Determination of thermodynamic properties of a rifampicin solvate recrystallized from ethanol, in: Albuquerque, 2013.

[178] B. Wicher, K. Pyta, P. Przybylski, E. Tykarska, M. Gdaniec, Redetermination of rifampicin pentahydrate revealing a zwitterionic form of the antibiotic, Acta Crystallogr. C. 68 (2012) 209–212. doi:10.1107/S0108270112015296.

[179] Y. Tian, R.G. Holt, R.E. Apfel, A new method for measuring liquid surface tension with acoustic levitation, Rev. Sci. Instrum. 66 (1995) 3349–3354. doi:10.1063/1.1145506.

[180] E. Trinh, P. Marston, J. Robey, Acoustic measurement of the surface tension of levitated drops, J. Colloid Interface Sci. 124 (1988) 95–103. doi:10.1016/0021-9797(88)90329-3.

# 7 Publications

In scientific journals:

K. Berkenfeld, M. Bernauer, J.T. McConville, A. Lamprecht, Investigating cascade impactor performance using a modified 3D printed induction port, International Journal of Pharmaceutics. 535 (2018) 402-409. doi:10.1016/j.ijpharm.2017.10.039.

K. Berkenfeld, A. Lamprecht, J.T. McConville, Devices for Dry Powder Drug Delivery to the Lung, AAPS PharmSciTech. (2015). doi:10.1208/s12249-015-0317-x.

Conference participations:

K. Berkenfeld, J.T. McConville, A. Lamprecht, Manufacture and Characterization of Inhalable Rifampicin Crystals, PBP world meeting in: Granada, Spain, 2018

K. Berkenfeld, M. Bernauer, J.T. McConville, A. Lamprecht, Investigating ACI Performance of a Salbutamol pMDI Formulation Using Modified 3D printed Induction Port, AAPS annual meeting and exposition in: San Diego, CA, USA, 2017

K. Berkenfeld, M. Bernauer, A. Lamprecht, J.T. McConville, Manufacture and Assessment of a Novel 3D Printed Induction Port for Cascade Impactor Analysis, Excipient Fest in: Providence, RI, USA, 2017

K. Berkenfeld, J.T. McConville, A. Lamprecht, Manufacture and Characterization of Rifampicin Particles for Aerosolization, AAPS annual meeting and exposition in: Orlando, FL, USA, 2015.

A.-D. Le, J.O. Morales, K. Berkenfeld, A. Elmaoued, J.T. McConville, Core Forming Antisolvent Co-precipitation of Protein Loaded Crystals, AAPS annual meeting and exposition in: Orlando, FL, USA, 2015

A.-D. Le, J.O. Morales, K. Berkenfeld, A. Elmaoued, J.T. McConville, Antisolvent Co-Precipitation Synthesis of D,L-Valine/Lysozyme,Excipient Fest in: Raleigh, NC, USA 2014

K. Berkenfeld, L.K. Lamkin, A. Lamprecht, J.T. McConville, Preformulation Development Studies of Respirable Rifampicin Particles through Crystal Modification, AAPS annual meeting and exposition in: San Antonio, TX, USA 2013

K. Berkenfeld, L.K. Lamkin, A. Lamprecht, J.T. McConville, Preformulation development of polymorphic rifampicin particles for pulmonary delivery, ACCP annual meeting in: Albuquerque, NM, USA, 2013

K. Berkenfeld, L.K. Lamkin, A. Lamprecht, J.T. McConville, Determination of Thermodynamic Properties of a Rifampicin Solvate Recrystallized From Ethanol, in: MWSOT regional chapter annual meeting in: Albuquerque,NM, USA, 2013

# 8 Addendum

## 8.1 List of mathematical and physical descriptors

| Descriptor | Explanation | Unit |
|---|---|---|
| $C_{ae}$ | Cunningham slip correction factorreference | [] |
| $C_p$ | Cunningham slip correction factor sample | [] |
| $d_{ae}$ | Aerodynamic diameter | µm |
| $d_{eq}$(area) | Diameter of a sphere with equivalent backlight image area as the particle of interest. | µm |
| $d_{geo}$ | Geometric diameter | µm |
| EF | Emitted fraction | % |
| $FEV_1$ | Forced expiratory volume in one second | L/s |
| FPF | Fine particle fraction | % |
| $FPF_{emitted}$ | Fine particle fraction of the emitted dose | % |
| $FPF_{total}$ | Fine particle fraction of the total dose | % |
| FVC | Forced vital capacity | L |
| GSD | Geometric standard deviation | [] |
| KGBW | Kilogram bodyweight | kg |
| LOD | Loss on drying | % |
| MMAD | Mass median aerodynamic diameter | µm |
| NCMH | Normal cubic meter per hour | $m^3/h$ |
| RH | Relative humidity | % |
| $\rho_{ae}$ | Density (reference) | $g/cm^3$ |
| $\rho_p$ | Density (particle) | $g/cm^3$ |
| $\chi$ | Shape correction factor | [] |

Please note that units presented are not necessarily compliant with the SI system and reflect their use in context of this work.

## 8.2 List of abbreviations

| | |
|---|---|
| ACI | Andersen cascade impactor |
| ACT | Disposable inhaler model |
| AL | Acoustic levitation |
| aNGI | Abbreviated NGI |
| API | Active pharmaceutical ingredient |
| aPSD | Aerodynamic PSD |
| CFC | Chlorofluorocarbon |
| CFD | Computational fluid dynamics |
| CI | Cascade impactor |
| CLSM | Confocal laser scanning microscopy |
| COPD | Chronic obstructive pulmonary disease |
| CT | Computer tomography |
| CYP | Cytochrome P-450 |
| DSA | Drop shape analysis |
| DCM | Dichloromethane |
| DPI | Dry powder inhaler |
| DSC | Differential scanning calorimetry |
| DVS | Dynamic vapor sorption |
| EtOH | Ethanol |
| FDA | US food and drug administration |
| FDM | Fused deposition modeling |
| FI | RF form I |
| FII | RF form II |
| HBβCD | Highly branched β-cyclodextrin |
| HFA | Hydrofluoroalkane |
| HPLC | High performance liquid chromatography |
| ICH | International Conference on Harmonization |
| IgE | Immunoglobulin E |
| INH | Isoniazid |

| | |
|---|---|
| IP | Induction port |
| IPA | Isopropyl alcohol |
| IVIVC | *In vitro* / *in vivo* correlation |
| MeOH | Methanol |
| mIP | Modified IP |
| MOC | Micro orifice collector |
| MP | Microparticle |
| MRT | Magnetic resonance tomography |
| MSLI | Multi stage liquid impinger |
| MT | Mouth/throat |
| NCMH | Normal cubic meters per hour |
| NGI | Next Generation Pharmaceutical Impactor |
| NP | Nanoparticle |
| Ph.Eur. | European pharmacopoeia |
| PLA | Poly - (D,L-lactic acid) |
| PLGA | Poly - (D,L-lactic-co-glycolic acid) |
| pMDI | Pressurized metered dose inhaler |
| PSD | Particle size distribution |
| PVA | Polyvinylalcohol |
| QC | Quality control |
| RF | Rifampicin |
| Sx | Stage x of the NGI |
| SAL | Salbutamol |
| SDr | Spray dried |
| SEM | Scanning electron microscope |
| TB | Tuberculosis |
| TGA | Thermogravimetric analysis |
| ToF - SIMS | Time of flight – secondary ion mass spectrometry |
| USP | United states pharmacopoeia |
| VHC | Valved holding chamber |
| XPS | X-ray photoelectron spectroscopy |
| XRPD | X-ray powder diffractometry |

## 8.3 List of Figures

## 8.4 List of tables